



Leeds Liverpool Newcastle Sheffield

MRC DiMeN Doctoral Training Partnership

Discovery Medicine North

Find me and eat me: understanding how signals from dying cells regulate macrophage behaviour

Olivier Ryan Tardy

A thesis submitted in partial fulfilment of the requirements for the
degree of Doctor of Philosophy

The University of Sheffield
Faculty of Medicine, Dentistry and Health
Department of Infection, Immunity and Cardiovascular Disease (IICD)
Submitted October 2021



The
University
Of
Sheffield.



Acknowledgements

I want to dedicate this thesis to my family. Both my mum and dad, Janys & Yvan Tardy, have always been there for me during this journey and without their love and support, I would not be where I am today. I want to especially mention my brother, Luc, for his advice, friendship, and comradery throughout our lives.

I want to thank both my supervisors, Dr Lynne L Prince and Dr Iwan R Evans for their support and advice over the course of my PhD. They not only taught me how to conduct research but allowed me to take control of my project while showing great compassion, patience and offering guidance whenever needed. The woods are still a little blurred at times, but I can at least tell them apart from the trees now. I also must acknowledge all those past and present members of the Evans and Prince groups who welcomed me into academia and helped teach me what it is to be a researcher: of note, I would thank Dr Hannah Roddie, Dr Jonny Coates and Emma Armitage who were indispensable to me reaching this point, and it is with great confelicity that I see them continue to do great things. I would especially acknowledge Elliot Brooks for being a stalwart companion throughout our studies together as someone I could confide in and discuss not just science, but life. In addition, I would thank Dr Yin Xin Ho, Kimberly Herman and Rebecca Dowey for their help with experiments and for making the Prince group a great lab to work in.

I would like to extend my gratitude to the medical research council and discovery medicine north doctoral training partnership (DiMeN-DTP) for their financial support, training courses and for providing a network of colleagues. The events and networking sessions have truly helped me develop as a collaborative researcher and opened my eyes to scientific opportunities, especially outside academia. Dr Emily Goodall has earned the admiration and respect of all of us through her dedication to building DiMeN into the success it has become and will continue to be. I would also like to mention the Bateson centre, the department of infection, immunity, and cardiovascular disease (IICD) and the university of Sheffield for providing the environment for scientific research and personal development. I must also acknowledge the support given to me by the disability and dyslexia support services (DDSS)

and Hayley Rennie for her mentoring and for reminding me that life is wonderful, even if experiments aren't working.

I would like to thank all the technical and support staff who were critical to every experiment presented in this thesis: I would like to make special mention of Dr Darren Robinson and the Wolfson light microscopy facility and Dr Kath Whitley along with the rest of the fly facility team as well as Dr Colin Gray and Benjamin Durham.

Finally, While I would thank all those who have shown me friendship these past four years, I would be remiss to not give special mention to Dr Daniel Bennison, Ffion Hammond, Jacqueline Chalakova, Elliot Brooks, and Jacob Rudman for the joy they have brought me: together we have slayed dragons, watched **many** terrible movies, and have grown as both scientists and people.

Abstract

How multifunctional cells such as macrophages interpret the different cues within their environment and undertake an appropriate response is a key question in developmental biology. Understanding how cues are prioritised is critical to answering this – both the clearance of apoptotic cells (efferocytosis) and the migration towards damaged tissue is dependent on macrophages being able to interpret and prioritise multiple chemoattractants, polarise, and then undertake an appropriate migratory response. Herein, I have used *Drosophila melanogaster* as a model to assess the dynamics of efferocytosis *in vivo* using live-caspase fluorophores and examine the role of Spitz, the cardinal *Drosophila* epidermal growth factor ligand, in regulation of macrophage behaviour in the developing fly embryo. In addition, I have also used *ex vivo* human macrophages to assay the chemotactic potential of apoptotic find-me cues in a novel adaption of the Ibidi μ -slide migration system. The results show that misexpression of activated Spitz can impact embryonic macrophage polarity, distribution, migration and perturb apoptotic cell clearance. Imaging of apoptosis and efferocytosis during *Drosophila* embryogenesis has revealed that caspase activity and clearance by immune cells is not an exclusive pathway, and that apoptotic recruitment appears to be more context and range dependent than previously thought. I have also been able to show that monocyte derived macrophages can be successfully used in the 2D Ibidi μ -slide assay and that signals derived from apoptotic cells are able to interfere with normal chemotactic responses in a localised fashion. Taken together, these results present several important conclusions: Spitz regulates macrophage migration and may operate as a chemoattractant in certain context, information which may help us to understand the role EGF ligands play in immune cell recruitment during development and at sites of disease pathology; exposure to apoptotic-cell derived find-me cues are able to inhibit macrophage chemotaxis towards the pro-inflammatory chemokine C5a; and efferocytosis *in vivo* occurs in a more rapid fashion than that observed *in vitro*, with clearance being only one fate for apoptotic cells.

Abbreviation list

Adenosine tri-phosphates – ATP
Anti-microbial peptides – AMP
Anti-Nuclear Antigen Immunoglobulin-G – ANA-IgG
Apoptotic null supernatant – ANN
Apoptotic protease activating factor 1 – APAF-1
Apoptotic supernatant – ASN
Aspect ratio – AR
Biological Dynamic Modeller – BioDynaMo
Blc-2 domain – BH
by National Research Ethics Service – NRES
C-Jun N-terminal Kinase – JNK
C-Mer Tyrosine Kinase – MerTK
Calcium-independent phospholipase A₂ – iPLA₂
Cell-mediated immunity – CMI
Chronic obstructive pulmonary disease – COPD
Cleaved DCP-1 – cDCP-1
Complement 5a receptor – C5aR
Complement protein fragment 5a – C5a
Damage-Associated Molecular Patterns – DAMPs
Death inducing signalling complex – DISC
Deleted in colorectal cancer – DCC
Deoxyribose nucleic acid – DNA
Di-phospho ERK – dpERK
Direct Inhibitor of Apoptosis-Binding protein with LOW pl – DIABLO
Drosophila Epidermal growth factor receptor – DER
Endothelial Monocyte Activating Polypeptide 2 – EMAP-II
Epidermal growth factor – EGF
Epidermal growth factor receptor – EGFR
Erythropoietin – Epo
Ethylenediaminetetraacetic acid – EDTA
Extracellular matrix – ECM
FAS-Associated Death Domain containing protein – FADD
Foetal Bovine Serum – FBS
Förster resonance energy transfer – FRET
Forward migration index – FMI
Forward migration index parallel to the gradient – FMI_{||}
Forward migration index perpendicular to the gradient – FMI_⊥
G-protein coupled receptor – GCPR
Green fluorescent protein – GFP
Growth arrest-specific gene 6 – Gas6
Glutathione S-transferase – GST
Hanks Balanced Salt Solution – HBBS
Hs-hid – heat shock hid
Immune deficiency pathway – Imd

Immunoglobulin-G – IgG
Inhibitor of apoptosis proteins – IAPs
Laplacian of Gaussian – LoG
Larval proventriculus – PV
LC3-Associated Phagocytosis – LAP
Local excitation, global inhibition – LEGI
Lysophosphatidylcholine – LPC
Milk fat globule-EGF factor 8 protein – MGF-E8
Mitochondrial membrane permeabilization – MMP
Mitochondrial outer membrane permeabilization – MOMP
Mitogen activated protein kinase – MAPK
Monocyte chemoattractant protein-1 – MCP-1
Monocyte-derived macrophages – MDMs
N-formyl-Met-Leu-Phe – fMLP
Nitrogen oxide – NO
Non-hydrolysable ATP – ATP_γs
Nucleotide tri-phosphates – NTPs
Patatin-like phospholipase A2 – PLA₂
Pathogen-associated molecular pattern – PAMPs
PDGF/VEGF family of growth factor – Pvf
PDGF/VEGF family of growth factor receptor – Pvr
Peptidoglycan protein recognition – PGPR
Peripheral blood mononuclear cells – PBMC
Phosphatase and Tensin homolog deleted on chromosome 10 – PTEN
Phosphate buffered solution – PBS
Phosphatidylcholine – PC
Phosphatidylinositol 3,4,5-trisphosphate – PIP₃
Phosphatidylinositol 3,5-bisphosphate – PIP₂
Phosphatidylinositol-3-kinase – PI3K
Phosphatidylserine – PS
Platelet-derived growth factor – PDGF
Platelet-poor plasma - PPP
Platelet-rich plasma – PRP
Polymerase chain reaction – PCR
Programmed cell death – PCD
Reactive oxygen species – ROS
Reaper, Grim, hid – RGH
Ribose nucleic acid – RNA
Ribosomal protein S19 – RPS-19
Second Mitochondria-derived Activator of Caspase – Smac
Six microns under – Simu
Soluble guanylyl cyclase – sGC
Sphingosine Kinase 2 – SphK2
Sphingosine-1-phosphate – S1P
Systemic Lupus Erythematosus – SLE
T cell immunoglobulin and mucin domain – Tim-4
Target of rapamycin complexes – TORC

Terminal deoxynucleotidyl transferase-mediated dUTP nick end-labelling – TUNEL
Macrophage Migration Inhibitory Factor - MIF
Transforming growth factor beta – TGF- β
Tumour necrosis factor alpha – TNF- α
Tyrosyl tRNA synthetase – TyrRS
Uridine tri-phosphates – UTP
Vascular endothelial growth factor – VEGF
Vascular endothelial growth factor family of growth factor – VEGF
Ventral midline – VML
Ventral nerve cord – VNC

Table of Contents

Title page	1
Acknowledgements	2
Abstract	4
Abbreviation list	5
Table of Contents	8
Table of Figures	11
Table of Tables	12
Chapter 1 - Introduction	13
1.1 Introduction	13
1.2 Innate immunity in vertebrates and <i>Drosophila</i>	14
1.2.1 <i>Drosophila</i> as a model organism for the study of innate immunity	14
1.2.1.1 Why learn how to fly? Advantages of <i>Drosophila</i> as a model system	14
1.2.1.2 <i>Drosophila</i> embryogenesis as a model of innate immunity	14
1.2.1.3 <i>Drosophila</i> embryonic haematopoiesis and immune competence	15
1.2.2 Macrophage functions	17
1.2.2.1 Macrophage polarisation and sub-types	17
1.2.2.2 Macrophage recognition receptors and chemotaxis mechanisms	18
1.2.2.3 Mechanisms of immune cell migration and chemotaxis	20
1.2.2.4 Inflammatory wound responses	22
1.2.2.5 Mechanisms of macrophage phagocytosis	23
1.3 Apoptosis and efferocytosis	24
1.3.1 Functions and mechanisms of programmed cell death (PCD)	24
1.3.1.1 Extrinsic and intrinsic apoptosis in mammals	25
1.3.1.2 Regulation of apoptosis in <i>Drosophila</i>	26
1.3.2 Taking cells to the grave – efferocytosis and the role of macrophages	29
1.3.3 Find-me cues: multifunctional pro-efferocytosis molecules	31
1.3.3.1 Sending out an S.O.S – find-me cue variation and identity	31
1.3.3.2 Apoptotic generation of find-me cues	32
1.3.3.3 Signal propagation and gradient formation	34
1.3.3.4 Find-me cue signalling outcomes	35
1.3.3.5 Implications of efferocytosis on health	38
1.3.4 Find-me cues in <i>Drosophila</i> : evidence and potential candidates	39
1.3.4.1 <i>Drosophila</i> epidermal growth factor signalling	40
1.3.4.2 Potential role of EGF in <i>Drosophila</i> efferocytosis	42
1.4 Experimental aims and hypothesis	43
Chapter 2 - Materials and methods	45
2.1 Fly husbandry and genetics	45
2.1.1 Fly stocks and transgenic constructs	45
2.1.2 Transgene recombination and Polymerase Chain Reaction (PCR) validation	45
2.1.3 Transgenesis of apoptotic sensors	47
2.2 Microscopy and imaging	47
2.2.1 Imaging and wounding of <i>Drosophila</i> embryos	47
2.2.1.1 Preparation of embryos for live imaging and fixation	47
2.2.1.2 Imaging of immunostained embryos	48
2.2.1.3 Imaging of <i>ex vivo</i> adult flies	48

2.2.2 Imaging of Ibidi μ -slides and MDM migration.....	48
2.3 Immunofluorescence and staining methods	49
2.3.1 LysoTracker Red staining of live embryos.....	49
2.3.2 Acridine orange staining of live embryos.....	49
2.3.3 Immunostaining of <i>Drosophila</i> embryos.....	49
2.4 Image processing and analysis of <i>Drosophila</i> phenotypes	50
2.4.1 Post-capture processing of raw microscopy files.....	50
2.4.2 Quantification of macrophage morphology and migration	51
2.4.3 Assessment of adult fly eye phenotypes.....	51
2.4.4 Quantification of vital dye staining and immunostaining in embryos	51
2.4.5 Quantification of macrophage recruitment to specific tissues.....	52
2.4.6 Apoptotic induction methods and quantification	52
2.4.7 Tracking and quantification of caspase activation events	53
2.4.8 Quantification of macrophage wound responses	53
2.5 Preparation of human blood cells and derivatives	54
2.5.1 Ethical approval.....	54
2.5.2 Isolation of whole blood peripheral blood mononuclear cells (PBMCs)	54
2.5.2.1 Purification and culture of monocyte-derived macrophages (MDMs)	55
2.5.3 Generation of cell supernatants.....	55
2.6 Cell migration assay methods	55
2.6.1 Principles of the Ibidi® μ -slide chemotaxis chamber	55
2.6.2 MDM culture methods and preparation for chemotaxis assays.....	56
2.6.3 Chemotaxis slide workflow and experimental set-up.....	57
2.6.4 Processing and analysis of MDM chemotaxis in μ -slides.....	58
2.7 Data tabulation and statistical analyses	59
Chapter 3: Investigating the dynamics of efferocytosis during <i>Drosophila</i> embryogenesis 60	
3.1 Introduction	60
3.1.1 Apoptosis in mammals and <i>Drosophila</i>	60
3.1.2 Assaying apoptosis via non-genetic methods	61
3.1.3 Genetically-encoded apoptosis reporters.....	61
3.1.4 Assaying efferocytosis during <i>Drosophila</i> embryogenesis	64
3.2 Results	65
3.2.1 Development and validation of ubiquitous embryonic GC3Ai recombinants.....	65
3.2.2 Embryonic GC3Ai accurately reports developmental apoptosis compared to cDCP-1.....	68
3.2.3 Embryonic GC3Ai outperforms other live-apoptosis tracking tools.....	71
3.2.4 Efferocytosis dynamics can be accurately studied <i>in vivo</i> using GC3Ai	74
3.2.5 Optimisation of induced apoptosis models to study efferocytosis.....	83
3.2.6 Tissue-specific apoptotic induction can be used to study find-me cue dynamics	85
3.3 Discussion	88
3.3.1 GC3Ai accurately reports embryonic apoptosis in <i>Drosophila</i> and is beneficial compared to contemporary methods	88
3.3.2 GC3Ai can be used to study the efferocytosis process in real-time.....	90
3.3.3 Apoptosis can be artificially induced to study efferocytosis.....	93
3.3.4 Future work and COVID-19 impact	94
3.3.5 Concluding remarks.....	95
Chapter 4: Assessing chemotactic competition using a 2D ex vivo cell model	96
4.1 Introduction	96
4.2 Results	98
4.2.1 MDMs undergo chemotaxis towards C5a using the Ibidi μ -slide chemotaxis	98

4.2.1.1	Optimisation of MDM transfer conditions for migration assays.....	98
4.2.1.2	MDMs undergo chemotaxis towards C5a using the Ibidi μ -slide chemotaxis	99
4.2.1.3	Optimisation of MDM chemotaxis tracking and quantification	103
4.2.1.4	MDMs did not chemotax towards fMLP or MCP-1 using the Ibidi μ -slide	105
4.2.2	MDMs do not respond to long-range apoptotic signal gradients in 2D chemotaxis experiments ..	108
4.2.3	Local apoptotic supernatant partially inhibits the migration of MDMs towards a defined source of C5a	110
4.2.4	The pan-caspase inhibitor Q-VD-OPh reduces MDM migration towards C5a	115
4.3	Discussion	118
4.3.1	MDMs can undergo chemotaxis in response to 2D chemokine gradients.....	118
4.3.2	Apoptotic-derived signals are short range and can inhibit chemotaxis towards C5a	119
4.3.3	Pan-caspase inhibition can perturb macrophage motility	121
4.3.4	COVID-19 impact statement and future work	122
4.3.5	Concluding remarks.....	123
Chapter 5: The epidermal growth factor ligand Spitz modulates macrophage efferocytosis, wound responses and migration dynamics during <i>Drosophila</i> embryogenesis		124
5.1	Introduction	124
5.1.1	<i>Drosophila</i> immunity, apoptosis and efferocytosis.....	124
5.1.2	Epidermal growth factor signalling in <i>Drosophila</i>	125
5.2	Results	126
5.2.1	Screening for EGF activity using disruption of eye development	126
5.2.2	Spitz alters the morphology and migration dynamics of <i>Drosophila</i> embryonic macrophages	129
5.2.3	Cleavage is necessary for Spitz-mediated regulation of macrophage behaviour	135
5.2.4	Macrophages express EGFR and show increased ERK activity in the presence of Spitz	138
5.2.5	Tissue-specific release of Spitz alters macrophage localisation and vacuolation	141
5.2.6	Spitz exposure reduces efferocytic capacity of macrophages	147
5.2.7	Spitz exposure dampens wound responses in macrophages in a distance-dependant manner	151
5.3	Discussion	154
5.3.1	Spitz as a chemoattractant and its possible mechanisms of action	155
5.3.2	Spitz as a potential apoptotic-derived find-me cue	156
5.3.4	Effect of post-translational modification on Spitz function	157
5.3.5	Future work and COVID-19 impact	158
5.3.6	Conclusions	159
Chapter 6 - Final discussion.....		160
6.1	Project summary and discussion	160
6.1.1	Live imaging of caspase dynamics underlines the complexity of efferocytosis in <i>Drosophila</i>	160
6.1.2	<i>Ex vivo</i> migration chambers can be used to investigate how macrophages prioritise apoptotic cell signals.....	163
6.1.3	Epidermal growth factor as an immuno-chemoattractant in <i>Drosophila</i>	165
6.1.4	Perspectives for future work.....	167
6.1.5	Limitations and caveats of this study	168
6.1.6	Conclusion	169
Appendix.....		170
References.....		171

Table of Figures

FIGURE 1.1 – MACROPHAGE DISPERSAL DURING DROSOPHILA EMBRYOGENESIS.....	17
FIGURE 1.2 – BASIC APOPTOTIC PATHWAYS IN MAMMALS AND DROSOPHILA	28
FIGURE 1.3 – THE STAGES OF EFFEROCTOSIS	29
FIGURE 1.4 – CASPASE-MEDIATED FIND-ME CUE RELEASE	34
FIGURE 1.5 – PROCESSING AND RELEASE OF SPITZ IN DROSOPHILA	42
FIGURE 2.1 – SCHEMATIC AND DIMENSIONS OF THE IBIDI® μ -SLIDE CHAMBER	56
FIGURE 3.1 – GENETIC METHODS FOR ASSAYING APOPTOSIS IN VIVO	64
FIGURE 3.2 – CONFOCAL CONFIRMATION OF EMBRYONIC XC3AI EXPRESSION	67
FIGURE 3.3 – GC3AI ACCURATELY REPORTS DROSOPHILA EMBRYONIC APOPTOSIS COMPARED TO CDCP-1 STAINING	71
FIGURE 3.4 – COMPARISON OF GC3AI, APOLINER AND AO LABELLING DURING DROSOPHILA EMBRYOGENESIS	74
FIGURE 3.5 – CASPASE ACTIVATION LEADING TO APOPTOTIC CELL FRAGMENTATION.....	76
FIGURE 3.6 – TRANSIENT CASPASE ACTIVITY IN NON-MACROPHAGE EFFEROCTOSED CELLS	78
FIGURE 3.7 – VISUALISATION OF EFFEROCTIC PROCESSES IN REAL-TIME.....	80
FIGURE 3.8 – SUMMARY OF APOPTOTIC CASPASE DYNAMICS	82
FIGURE 3.9 – FREQUENCY OF APOPTOSIS DURING DEVELOPMENTAL AND INDUCED APOPTOTIC SYSTEMS	85
FIGURE 3.10 – OPTIMISATION OF INDUCED APOPTOTIC MODELS IN DROSOPHILA EMBRYOS	88
FIGURE 4.1 – OPTIMISATION OF CELL CULTURE TRANSFER CONDITIONS	99
FIGURE 4.2 – IBIDI μ -SLIDE EXPERIMENTAL SET UP FOR SINGLE CHEMOATTRACTANTS	100
FIGURE 4.3 – C5A STIMULATES MDM CHEMOTAXIS USING THE IBIDI μ -SLIDE.....	102
FIGURE 4.4 – OPTIMISATION OF CELL CULTURE TRANSFER CONDITIONS	104
FIGURE 4.5 – MCP-1 DID NOT INDUCE MIGRATION OF MDMS IN THE IBIDI M-SLIDE SYSTEM	106
FIGURE 5.6 – FMLP DID NOT INDUCE MIGRATION OF MDMS IN THE IBIDI M-SLIDE SYSTEM	107
FIGURE 4.7 – APOPTOTIC SUPERNATANT DOES NOT INDUCE MDM MIGRATION AT LONG RANGE	109
FIGURE 4.8 – IBIDI μ -SLIDE EXPERIMENTAL SET UP FOR MDM SATURATION WITH ASN	110
FIGURE 4.9 – EXPOSURE TO ASN INHIBITS MDM MIGRATION TOWARDS C5A.....	113
FIGURE 4.10 – NECROTIC SUPERNATANT DOES NOT ALTER MDM MIGRATION TOWARDS C5A.....	115
FIGURE 4.11 – TREATMENT WITH Q-VD-OPH REDUCES THE CHEMOTACTIC RESPONSE OF MDMS TO C5A.....	118
FIGURE 5.1 – IDENTIFICATION OF ACTIVE UAS LINES THROUGH EYE-SPECIFIC PROLIFERATION ASSAY.....	129
FIGURE 5.2 – MACROPHAGE-SPECIFIC EXPRESSION OF SPITZ DOES NOT ALTER DEVELOPMENTAL DISPERSAL OR TOTAL NUMBERS OF MACROPHAGES IN THE EMBRYO	131
FIGURE 5.3 – SPITZ STIMULATES MACROPHAGE ELONGATION, IMPAIRS EFFEROCTOSIS AND ALTERS MIGRATION DYNAMICS	134
FIGURE 5.4 – EXPRESSION OF A MEMBRANE-BOUND FORM OF SPITZ FAILS TO INDUCE CHANGES IN EMBRYONIC MACROPHAGE BEHAVIOUR	136
FIGURE 5.5 – EXPRESSION OF A REGULATED EGF LIGAND KEREN INCREASES MACROPHAGE CLUSTERING BUT DOES NOT ALTER OTHER BEHAVIOUR DURING EMBRYOGENESIS.....	138
FIGURE 5.6 – EMBRYONIC MACROPHAGES EXPRESS EGFR AND EXOGENOUS SPITZ ACTIVATES ERK SIGNALLING	141
FIGURE 5.8 – SPITZ SECRETION FROM THE SALIVARY GLAND AND ANAL PAD DOES NOT AFFECT MACROPHAGE DISPERSAL	147
FIGURE 5.9 – SPITZ IMPAIRS MACROPHAGE-MEDIATED APOPTOTIC CELL CLEARANCE	149
FIGURE 5.10 – SPITZ DOES NOT ALTER PHAGOSOME VOLUME IN MACROPHAGES	150
FIGURE 5.11 – SPITZ IMPAIRS MACROPHAGE WOUND RESPONSES	154

Table of Tables

TABLE 1.1 – SUMMARY OF KNOWN FIND-ME CUES	37
TABLE 2.1 – PCR PARAMETERS FOR GENOTYPING RECOMBINANT FLIES	46
TABLE 5.1 – SUMMARY OF DE REGULATED SPITZ PHENOTYPE DIFFERENCES	155

Chapter 1- Introduction

1.1 Introduction

In multicellular organisms, the control of cell number is partially mediated through the programmed cell death (PCD) pathways, most commonly apoptosis. The apoptotic programme is evolutionarily conserved and allows for the death and removal of redundant or damaged cells in response to a wide range of stimuli including cellular damage, infection, developmental signalling, and mechanosensory feedback (Fuchs and Steller, 2011; Galluzzi et al., 2012). Once a cell has undergone apoptosis, the cellular remains must be removed from the tissue, a process termed efferocytosis. The removal of these cell corpses is necessary to prevent the uncontrolled breakdown of the cell and subsequent release of pro-inflammatory cytosolic contents (Degterev and Yuan, 2008). Efferocytosis is a stepwise process requiring the responding cell to locate, phagocytose and digest the apoptotic cell, a function that is normally mediated by professional phagocytes of the immune system as well as neighbouring cells (Morioka et al., 2019). Failures in the efferocytic process have been implicated in the progression of chronic inflammatory diseases such as chronic obstructive pulmonary disease (COPD) or atherosclerosis (Li et al., 2009; Eltboli et al., 2014). The first stage of efferocytosis, referred to as the “find-me” phase is mediated by the release of chemoattract molecules from apoptotic cells which act on responding phagocytes to promote clearance.

Understanding how these find-me cues act to facilitate clearance is vital to understanding the role of dysfunctional efferocytosis in disease (Ariel and Ravichandran, 2016). Studies in vertebrates over the last few decades have identified a number of these cues *in vivo* however their existence in non-vertebrates and underlying mechanisms of phagocyte recruitment remain an active area of research. In this thesis, I sought to evaluate the existence and migratory impact of novel find-me cues and how they are prioritised *in vivo* using both the common fruit fly, *Drosophila melanogaster* and primary human cells.

1.2 Innate immunity in vertebrates and *Drosophila*

1.2.1 *Drosophila* as a model organism for the study of innate immunity

1.2.1.1 Why learn how to fly? Advantages of *Drosophila* as a model system

The common fruit fly, *Drosophila melanogaster* has been used as a model organism for well over a century and has been the source of our understanding for some of the fundamental processes in genetics and immunity (Lemaitre and Hoffmann, 2007; Tolwinski, 2017).

Drosophila has flourished as a model organism due to its many advantages over conventional vertebrate models: these include the non-protected species status afforded by the UK home office (in relation to the Animals (Scientific Procedures) Act 1986), which allows for wide scope in both experimental design and genetic intervention; Mendelian inheritance genetics and low levels of genetic redundancy, allowing for comparatively simple genetic manipulation (Nowak et al., 1997); short generation times that facilitates life-course studies and high power statistics; and an active research community with access to curated communal databases including Flybase and the Berkeley *Drosophila* genome project (BDGP) (Tomancak et al., 2002, 2007; Frise et al., 2010; Gramates et al., 2017).

1.2.1.2 *Drosophila* embryogenesis as a model of innate immunity

Drosophila melanogaster have a robust innate immune system with strong functional similarities to that of mammals. The *Drosophila* innate immune system is comprised of a humoral and cell mediated immunity (CMI), which act to respond to infection, tissue damage and the removal of apoptotic cells.

Drosophila humoral immunity is dependent on the release of anti-microbial peptides (AMPs) which act to destroy bacterial and fungal infections through interaction at the pathogen surface. The generation of these peptides occurs downstream of two key pathways: Toll and the immune deficiency (Imd) signalling cascades (Lemaitre and Hoffmann, 2007; Buchon et al., 2014). The Toll pathway is a highly conserved response that requires the recognition of activated Spätzle, a pro-peptide present within the haemolymph, which is generated by a series of proteases upon pathogen recognition (Valanne et al., 2011). The Imd pathway is a specialised bacterial response that is activated by peptidoglycan recognition via the peptidoglycan protein recognition (PGPR) family of receptors (Myllymäki et al., 2014). Both of

these pathways signal down the pro-inflammatory NF- κ b signalling pathway to produce active AMPs (Hanson and Lemaitre, 2020).

Drosophila CMI is composed of three haematopoietic cell types which are collectively referred to as hemocytes: plasmatocytes (macrophage equivalent cells), crystal cells and lamellocytes (Evans et al., 2003; Lemaitre and Hoffmann, 2007; Wood and Jacinto, 2007; Evans and Wood, 2011; Vlisidou and Wood, 2015). Plasmatocytes (hereafter referred to as *Drosophila* macrophages) are considered as the fly's equivalent of the macrophage and are professional phagocytes that make up the majority of the hemocyte population (95%). Plasmatocytes also act to remove apoptotic debris, respond to wounds and phagocytose pathogens (Wood and Jacinto, 2007). Crystal cells are part of the humoral immune response and their primary function is to initiate melanisation cascades in response to infection and tissue damage (Rizki et al., 1985; Cerenius et al., 2008). The third cell type, lamellocytes, are not typically present during normal *Drosophila* development and are derived from the macrophage population in response to parasitic invasion or stress signalling in order to carry out pathogen encapsulation (Rizki and Rizki, 1992; Stofanko et al., 2010). Post haematopoiesis, *Drosophila* macrophages undergo stereotypic dispersal to attain immune competence.

1.2.1.3 *Drosophila* embryonic haematopoiesis and immune competence

In higher vertebrates such as mice or humans, macrophages are generated either during development or through the differentiation of monocytes derived from blood haematopoiesis (Epelman et al., 2014; Perdiguero and Geissmann, 2016; Jakubzick et al., 2017). During *Drosophila* embryogenesis, haematopoiesis occurs within the procephalic mesoderm located in the anterior region of the stage 10 embryo under the control of the critical GATA-type transcription factor *Serpent* (Tepass et al., 1994). *Serpent* is required for the differentiation of the two hemocyte lineages: macrophages (plasmatocytes), and crystal cells (Rehorn et al., 1996; Crozatier and Meister, 2007). The differentiation of progenitor mesodermal cells into these distinct immune cells is driven through *serpent* via the activity of the DNA-binding factors *glial cells missing* (*Gcm*) or *lozenge* for macrophages and crystal cells, respectively (Bernardoni et al., 1997; Lebestky et al., 2000).

Once differentiation and expansion is complete at around stage 12, embryonic macrophages begin to egress from the anterior mesoderm and disperse across the embryo down stereotypical pathways (**Figure 1.1**): ventrally between the ventral nerve cord (VNC) and the epithelia/VNC-mesodermal junctions, dorsally via the amnioserosal boundary, and via infiltration of the germ-band prior to retraction at stage 12 (Tepass et al., 1994). This migration is driven by the expression of the chemotactic vascular endothelial growth factor (VEGF) ligands (specifically Pvf2) in the cells lining the dispersal path which guide pvf receptor (Pvr) expressing macrophages during dispersal (Duchek et al., 2001; Heino et al., 2001; Cho et al., 2002). Dispersal is further promoted through cell-cell repulsion between macrophages (Davis et al., 2012), and access to physical spaces created during organogenesis (Evans et al., 2010a). It should be noted that proper macrophage localisation is required for developmental tissue reorganisation including condensation of the ventral nerve cord (Olofsson and Page, 2005; Evans et al., 2010a). During this migration, macrophages encounter cells undergoing developmental apoptosis and carry out one of their core functions: the recognition and removal of apoptotic cells (Abrams et al., 1993).

In sum, *Drosophila* possess a robust innate immune response characterised by both humoral and cell mediated responses. During embryogenesis, immune cells are generated during haematopoiesis, with macrophages (plasmatocytes) accounting for most of the immune cell population. As we will discuss, these embryonic macrophages carry out several functions homologous to their vertebrate counterparts including migration, phagocytosis, wound responses, and the ability to clear dying cells.

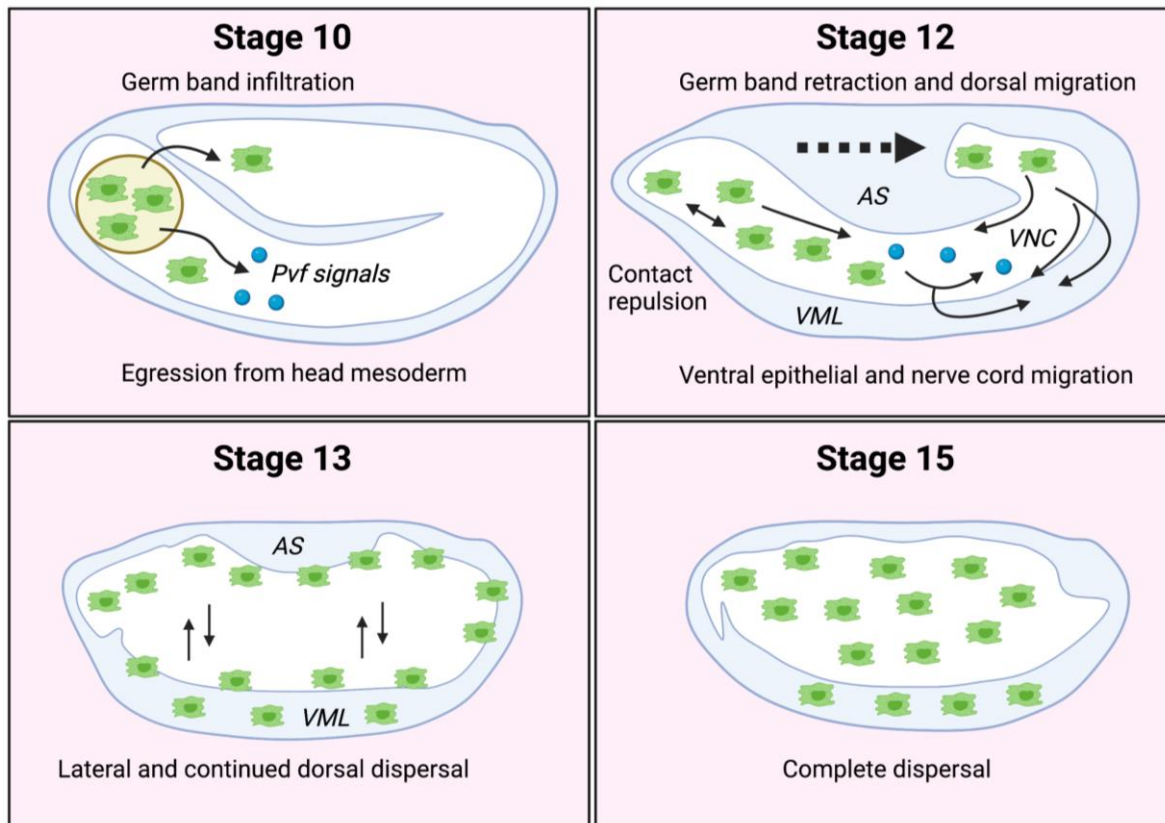


Figure 1.1 – Macrophage dispersal during *Drosophila* embryogenesis

Schematic diagram showing embryonic macrophage dispersal in *Drosophila*. After haematopoiesis is complete at stage 10, macrophages (green cells) egress from the mesoderm (orange region) and migrate ventrally and dorsally via infiltration of the germ band. By stage 12, germ band retraction localises the infiltrated macrophage population into the anterior of the embryo. At the same time, macrophages driven by contract repulsion and chemotactic Pvf ligands (blue spheres) have moved dorsally and, in concert with condensation of the ventral nerve cord (VNC) have migrated into the ventral midline region (VML) and neural tissues. Macrophages also begin to colonise the dorsal region around the amnioserosa (AS). By stage 13, macrophages have colonised the peripheral tissues and begin to disperse across the remaining lateral regions before completing their migration at stage 15. These pathways are described in (Tepass et al., 1994)

1.2.2 Macrophage functions

1.2.2.1 Macrophage polarisation and sub-types

While early work in the field divided macrophage phenotypes into the activated M1 and anti-inflammatory M2 sub-types, the plasticity of these states *in vivo* has led to the idea of a phenotype continuum based on local signalling circumstances (Liddiard and Taylor, 2015). While the M1/M2 axis is an oversimplification, it is a useful paradigm to separate the different states of macrophages and how this affects their response to pro and anti-inflammatory stimuli. M1 and M2 macrophages are distinguished by both their expression

profiles and their functions: Pro-inflammatory M1 macrophages are activated by the presence of pathogen-associated molecular patterns (PAMPs) such as bacterial lipopolysaccharide (LPS) and are characterised by upregulated of microbial killing machinery such as inducible nitric oxide synthase (iNOS) and the release of pro-inflammatory cytokines including Interleukin-6 (IL-6) and tumour necrosis factor alpha (TNF α) (Benoit et al., 2008; Xue et al., 2018). Under homeostatic conditions, macrophages are inherently anti-inflammatory and must function to suppress aberrant inflammatory induction by non-threats, e.g., regulated cell apoptosis or the presence of commensal micro-organisms (Murray and Wynn, 2011). M2 or “alternatively activated” macrophages are characterised by their expression of pro-healing and immuno-suppression chemokines such as transforming growth factor beta (TGF- β) (Gordon and Martinez, 2010).

The existence of macrophage sub-types in non-human and mouse models has recently come under greater scrutiny. Several lines of evidence have suggested the presence of sub-populations within the *Drosophila* macrophage pool: RNA sequencing data obtained from larval macrophages identified expression clusters that show differences in functional genes such as those of the Imd pathway or polarisation state metabolic markers including arginase (Neves et al., 2016; Cattenoz et al., 2020; Tattikota et al., 2020); infection experiments have shown that larval macrophages have a varied nitrogen oxide (NO) response to bacterial infection; and the presence of specialised “tissue resident” macrophages within the larval proventriculus (PV) region of the gut. In addition, recent data from our lab showed that embryonic macrophages are present in transcriptional differentiated subpopulations that have varied functionality (Coates et al., 2021).

1.2.2.2 Macrophage recognition receptors and chemotaxis mechanisms

To carry out their functions, macrophages need to be able to recognise and migrate towards many different stimuli. These chemoattractive signals can be endogenous, e.g., host-derived, or exogenous “non-self” signals. In mammals, endogenous immune cell migration is driven by the family of chemotactic cytokines known as chemokines (Griffith et al., 2014). These chemokines are critical for both the inflammatory response, e.g., CCR2 (or monocyte chemoattractant protein 1/MCP-1) produced within a tissue in response to TNF- α (Thompson

and Van Eldik, 2009) and as part of homeostatic immune trafficking e.g. CX₃CL (Fractalkine) and monocyte survival signalling (Landsman et al., 2009). Although simpler, *Drosophila* embryonic macrophages are sensitive to several developmental and inflammatory chemoattractants: as noted earlier, embryonic macrophages undergo stereotypic dispersal in response to VEGF-like Pvf2 and can respond to pro-inflammatory activators such as wound derived reactive oxygen species (ROS) (Evans and Wood, 2011, 2014).

Recognition of the non-self is mediated by the cell-surface pattern recognition receptors (PRRs) that bind to conserved molecule motifs (Gordon, 2002). Different PRRs can be activated in several ways: by binding to the target directly or through bridging molecules called opsonins e.g. FCγR binding to antibodies (Joller et al., 2011) to facilitate phagocytosis; or can simply detect and activate downstream responses, for example, activation of Toll like receptors (TLRs) will stimulate downstream activation of the pro-inflammatory NF-κB pathway (Valanne et al., 2011).

In *Drosophila*, embryonic macrophages express several PRRs that are involved in either the clearance of pathogens or the removal of apoptotic cells. Several members of the PRR repertoire allows for the recognition of pathogens including the detection of bacterial peptides via members of the peptidoglycan protein recognition (PGPR) family and scavenger type receptors such as Eater (Kurata, 2004; Kocks et al., 2005). In addition to pathogens, *Drosophila* macrophages must be able recognise and bind to apoptotic cells during development (Abrams et al., 1993). The recognition of apoptotic cells is mediated by several receptors including Croquemort, Six microns under (Simu) and Draper (Franc et al., 1996; Manaka et al., 2004; Kurant et al., 2008). These apoptotic receptors are critical for efficient efferocytosis and bind to apoptotic cells through direct interaction with the membrane ,e.g., Draper and Pretaporter (Kuraishi et al., 2009), or through the binding of intermediates, e.g., NimB4-opsonised phosphatidylserine (PS) (Petrigiani et al., 2021).

For most immune responses, the responding cell will often be required to travel to reach the source of chemoattractant. This motility requires complex cytoskeletal rearrangement and coupling of sensory input to migratory outcome.

1.2.2.3 Mechanisms of immune cell migration and chemotaxis

To migrate, a tissue resident cell must undergo changes in their cytoskeletal structure and interaction with the extracellular matrix (ECM). Cellular locomotion requires the coordinated contraction of the actomyosin network coupled to ECM adhesion and targeted degradation in response to chemoattractant (Friedl, 2004). In contrast to typically non-motile cells, leukocytes such as monocytes move in an amoeboid fashion that is less dependent on the formation of focal adhesion, allowing them to transverse through the vasculature and tissues (Moreau et al., 2018).

Migration towards gradients of chemokines is typically mediated by receptors of the G-protein coupled receptor (GPCR) family, which allow cells to detect small changes in signal concentration across the cell body (Mañes et al., 2005; Lämmermann and Kastenmüller, 2019). Upon activation, GPCRs signal through separation of the Gi protein heterotrimer to activate several secondary messenger cascades that act to polarise the cytoskeleton. Leading edge actin polymerizing, and nucleation is driven by the conversion of the membrane lipid phosphatidylinositol 3,5-bisphosphate (PIP₂) to phosphatidylinositol 3,4,5-trisphosphate (PIP₃) by phosphatidylinositol-3-kinase (PI3K). This in turn activates the Rho family small GTPases Rac and Cdc42 (Wennerberg and Der, 2004) and subsequent actin-binding proteins Arp2/3 and WAVE/SCAR (Mañes et al., 2005; Wu, 2005; Wang et al., 2011). In addition to PI3K signalling, parallel pro-migration pathways are activated including: GTPase Ras mediated activation of target of rapamycin complexes (TORC1/2), which promotes actin polymerisation through downstream regulators such as Akt, S6K and 4E-BP1 (Liu and Parent, 2011; Wang et al., 2011); patatin-like phospholipase A2 (PLA₂), which acts to polymerise actin through the conversion of PC into arachidonic acid (Chen et al., 2007; Liu and Parent, 2011); and soluble guanylyl cyclase (sGC) which is activated in response to cAMP at the leading edge and regulates myosin contractility (Veltman et al., 2005; Wang et al., 2011).

In concert with the formation of the leading edge, RhoA and Phosphatase and Tensin homolog deleted on chromosome 10 (PTEN) are active at the uropod ("cell rear") to inhibit the formation of actin structures and induce contractility of the actomyosin network to generate locomotive force (Wu, 2005). This leading edge-uropod asymmetry has been

described through the local excitation, global inhibition (LEGI), polarisation and gradient-sensing models. Together, these models propose that after initial gradient detection, intracellular feedback loops act to rapidly stabilise actin dynamics at the leading edge, while slower acting global mechanics promote the cessation of motility in the uropod (Iglesias and Devreotes, 2008). Migration dynamics of a cell are also linked to its functional state, e.g., cells performing scanning or random migratory behaviour move in a particular fashion known as intermittent searching or levy-walking which is optimal for the detection of chemoattractants in a dispersed area (Moreau et al., 2018).

In addition to PIP₃-dependent migration, mitogen activated protein kinase (MAPK) cascade, in particular p38-dependent signalling, is thought to act semi-independently to PIP₃ in response to certain high priority chemoattractants such as N-formyl-Met-Leu-Phe (fMLP) (Krump et al., 1997; Cara et al., 2001). One of the current questions in the chemotaxis field is how particular cues are integrated by the responding cell to produce the correct response in the presence of competing and often counterproductive signals. Studies in neutrophils have shown that chemoattractants can be classed as “intermediate” or “end-point” in relation to their relative chemoattractive strength and proximity to the target, e.g., the presence of a bacterial infection will result in the local generation of bacterial derived peptide such as fMLP in addition to more distal inflammation induced chemokines such as IL-8 (Lara Rodriguez and Schneider, 2013). It has been shown that neutrophils challenged with different chemoattractants that signal through either p38 (e.g., fMLP) or PI3K (e.g., IL-8), will preferentially migrate towards those that activate the p38 pathway. This prioritisation is thought to be mediated through crosstalk downstream of receptor activation (Heit et al., 2002; Kim and Haynes, 2012).

Drosophila embryonic macrophage migration occurs in an amoeboid fashion during embryogenesis. To migrate, macrophages extend a sheet like protrusion called the lamellipodia that is extended by the polymerisation of actin. As in vertebrates, initial cytoskeletal polarisation is governed by the small GTPases such as Rac1 and Rho1 which act to establish leading edge/uropod asymmetry (Stramer et al., 2005). The extension of the membrane at the leading edge is controlled by a series of actin regulating proteins that facilitate filament extension (Ena) and bundling (Fascin and SCAR/WAVE complex in

conjunction with Arp2/3), which allow the membrane to extend and retract during migration (Zanet et al., 2009; Tucker et al., 2011; Evans et al., 2013). The regulation of migration in the presence of competing stimuli in *Drosophila* is still poorly understood, however the existence of a form of signalling hierarchy is supported by observations of embryonic macrophage migration during development: macrophages undergoing Pvf2-mediated dispersal are refractile to wounds, yet will efficiently respond to apoptotic cells (Moreira et al., 2010); and macrophages of the pupal wing disc have a refractory period of at least 90 minutes after initially responding to a wound as they are unable to respond to secondary wounds in that time-period (Weavers et al., 2016b). This migratory response towards wounds is a key behaviour of macrophage-like cells.

1.2.2.4 Inflammatory wound responses

The response to a site of injury is complex and requires both pro and anti-inflammatory responses to first remove damaged or contaminated tissue and then promote healing and a return to homeostasis. In vertebrate models such as mice, the initial wound is highly pro-inflammatory due to the presence of damage-associated molecular patterns (DAMPs) and potential pathogen contamination, which act to recruit neutrophils and differentiate infiltrating monocytes into macrophages. After these initial responses, the localised macrophages must undergo a phenotypic shift from the pro-inflammatory M1-type (pro-phagocytosis, TNF- α secretion etc.) to an anti-inflammatory M2-type, characterised by TGF- β secretion and pro-resolution (Koh and DiPietro, 2011; Kotwal and Chien, 2017).

During *Drosophila* embryogenesis, wound healing has been shown to occur through contraction of actomyosin cable networks which act to stitch the wound in what has been dubbed the “purse-string model” (Redd et al., 2004). Wounding of the embryonic epithelial leads to the release of a Ca²⁺ wave emanating from the epicentre into surrounding cells. This Ca²⁺ wave induces the production of H₂O₂ via the activity of DUOX, which is required for the recruitment of local macrophages to the wound in both zebrafish and *Drosophila* (Niethammer et al., 2009; Razzell et al., 2013). During the pvf mediated stages of dispersal (pre-stage 13), macrophages are refractile to wounding stimuli (Moreira et al., 2010) but will robustly migrate towards wounds to phagocytose debris in a PI3K pathway dependent

fashion (Stramer et al., 2005; Wood et al., 2006; Razzell et al., 2011). Although the role of H₂O₂ wound signalling has been confirmed, modelling in *Drosophila* pupae has suggested that diffusion dynamics of ROS require the presence of as yet uncharacterised mediators for the observed response to occur (Weavers et al., 2016b). The release of ROS from the wound is also critical for wound healing as it activates the assembly of the actomyosin cable network in the wound-proximal cells that allow for contractile wound closure (Fernandez-Gonzalez and Zallen, 2013; Hunter et al., 2018), a process that is dependent on localised c-Jun N-terminal Kinase (JNK) and Grainyhead signalling (Razzell et al., 2011).

In non-sterile injury or during apoptotic cell clearance, macrophages not only need to migrate towards a source of chemoattractant, but also must remove any non-self-particles via phagocytosis. This requires yet another behavioural change and the rearrangement of the cytoskeleton and activation of phagocytic degradation machinery.

1.2.2.5 Mechanisms of macrophage phagocytosis

Phagocytosis is an evolutionary conserved process that allows individual cells to engulf particles greater than 0.5µm in diameter (Pacheco et al., 2013). While many cells have some degree of phagocytic capacity, large-scale engulfment is carried out by “professional phagocytes”, which express the required cell components at high levels (Rabinovitch, 1995). The ability of a cell to engulf a particular target is dependent on several factors including the recognition of the target surface (either through surface molecular patterns or through opsonised intermediates), the relative size of the object, and the geometry of the object (Cannon and Swanson, 1992; Champion and Mitragotri, 2006). Phagocytosis proceeds sequentially, requiring the recognition of the target followed by formation and maturation of the phagosome into the phagolysosome where the engulfed cargo is processed (Uribe-Querol and Rosales, 2020).

Once the target has been engaged on the cell surface, the phagocyte undergoes a series of complex cytoskeletal rearrangements to induce the formation of the phagocytic cup. This process requires the extension of lamellipodia driven by actomyosin network rearrangements: briefly, activation of PRRs leads to recruitment of Syk family kinases which

facilitate actin polymerisation and nucleation through cytoskeletal regulators such as PI3K and Vav (Uribe-Querol and Rosales, 2020). In *Drosophila*, the reorganisation of actin is dependent on concerted actions of the actin-organising proteins D-SCAR, D-WASp and Profilin (Pearson et al., 2003). These cytoskeletal changes drive the spreading of the lamellipodia across the surface of the target particle in staggered phases (Richards and Endres, 2014). Once the phagosome has been internalised, it will undergo maturation into a phagolysosome through sequential endosomal fusions. These fusions result in acidification and degradation of internalised contents through the action of proteases and the generation of reactive oxygen species (ROS) (Kinchen and Ravichandran, 2008).

In this thesis, I am focussed on one of the key functions of macrophages: the removal of apoptotic cells, known as efferocytosis. This process requires macrophages to migrate, engage and destroy dying cells while also undergoing polarisation to prevent unwarranted inflammation.

1.3 Apoptosis and efferocytosis

1.3.1 Functions and mechanisms of programmed cell death (PCD)

The number of defined PCD pathways has increased over the decades and include apoptosis, anoikis, necroptosis and NETosis amongst others (Galluzzi et al., 2012). Each of these programmes are thought to activate in response to specific cellular scenarios, including developmental cues (Fuchs and Steller, 2011), competition for growth factors (Levayer and Moreno, 2013) and as an immune defence mechanism (Remijnsen et al., 2011). Several forms of PCD, most critically apoptosis, have been described in many model organisms, including *Drosophila* (Jenkins et al., 2013).

Apoptosis is a form of PCD that occurs throughout development, homeostasis, and in disease. The choice between cell life and death is dependent upon the balance of pro- and anti-apoptotic factors within the cell, as dictated by both the environmental conditions and intracellular signalling cascades. Apoptosis is indispensable for many homeostatic processes such as gut epithelium turnover (Hall et al., 1994) and removal of excessive immune cells, e.g., the removal of dying neutrophils that have become enriched at the site of inflammation

(Summers et al., 2010). Failures in apoptosis can be catastrophic and are largely associated with abnormal growth and cellular transformation (Küppers and Hansmann, 2005; Hanahan and Weinberg, 2011).

Apoptosis is thought to occur via two interlinked but independent pathways generally referred to as the extrinsic and intrinsic apoptotic pathways (Galluzzi et al., 2012). Critical to both pathways is the activation of the caspase family proteases which act to degrade the cell via proteolysis cascades. Caspases are cysteine-dependent aspartate specific proteases that recognise a generalised flanked amino acid sequence of DXXD (Timmer and Salvesen, 2007) which are activated downstream of pro-apoptotic signalling cascades.

1.3.1.2 Extrinsic and intrinsic apoptosis in mammals

Extrinsic apoptosis is triggered through either the binding of cell surface death receptors to their ligands, e.g., Fas-FasL or tumour necrosis factor (TNF) pathway (TNFR1-TNF- α signalling), or through a sustained lack of signalling through pro-survival dependency receptors such as the deleted in colorectal cancer (DCC) receptor (Goldschneider and Mehlen, 2010; Sessler et al., 2013). After the “death signal” has been received, conformational change within the death receptors allows for the binding of specific adaptor proteins such as FAS-Associated Death Domain containing protein (FADD) and pro-peptide initiator caspases (Caspase-8 and -10) to form the death inducing signalling complex (DISC). Once assembled, the DISC can rapidly generate activated initiator caspases that will go on to perform two key functions: reinforcement of apoptosis via activation of the intrinsic apoptotic pathway and the generation of executor type caspases (Caspases-3, 6 and 7) (Sessler et al., 2013).

Intrinsic apoptosis is centred around the mitochondrion as a nexus of different pro- and anti-apoptotic signalling pathways, reviewed in Kroemer et al. (2007). During homeostasis, the mitochondrion has an electrochemical gradient (the inner mitochondrial transmembrane potential), which is critical for both oxidative phosphorylation and apoptotic regulation. During apoptosis, changes in mitochondrial permeability leads to the release of pro-apoptotic molecules, an event known as mitochondrial membrane permeabilization or mitochondrial outer membrane permeabilization (MMP/MOMP) (Kroemer et al., 2007). MOMP is regulated

by several Bcl-2 domain (BH) containing proteins, the Bcl-2 family, which act to inhibit and promote apoptosis through multiple interactions: for example, MOMP activation can occur through the Bcl-2 protein Bad undergoing relocation to the mitochondrion outer membrane and inducing the formation of pores (Czabotar et al., 2014). MOMP stimulation can occur downstream of a number of cell-stress events including DNA damage and endoplasmic reticulum stress (Tabas and Ron, 2011).

Activation of MOMP leads to changes in the mitochondrial structure and the eventual release of Cytochrome c, a key component of the apoptosome. Like the DISC, the apoptosome is a large multimeric complex that acts as a platform for initiator caspase activation, in this case caspase-9. Once Cytochrome c is released from the mitochondrion, it is free to associate with cytosolic apoptotic protease activating factor 1 (APAF-1) and pro-caspase-9 to form the apoptosome and generate active caspase-9 (Bao and Shi, 2007). Once activated, caspase-9 will go on to activate the executor class caspases. MOMP also leads to the release of Second Mitochondria-derived Activator of Caspase/Direct Inhibitor of Apoptosis-Binding protein with LOw pI (Smac/DIABLO) and Omi stress-regulated endoprotease/high temperature requirement protein A2 (Omi/HtrA2): these proteins can suppress the activity of the anti-apoptotic inhibitor of apoptosis proteins (IAPs) such as XIAP1 which normally function to suppress active caspases (Berthelet and Dubrez, 2013). It is important to remember that DISC and MOMP pathways have several layers of feedback and are strongly linked if not truly interdependent.

1.3.1.3 Regulation of apoptosis in *Drosophila*

Intriguingly, while mammalian caspase activity is locked under layers of regulation, *Drosophila* apoptosis is strongly dependent on IAP caspase suppression (Martin, 2002). In healthy cells, the apoptosome appears to be constitutively active via interaction at the mitochondrion between Drob1, Buffy and Dark (Okano and Miura, 1999; Kornbluth and White, 2005; Galindo et al., 2009). The active apoptosome will bind the zymogen initiator caspase DRONC and induce autocatalytic cleavage and activation (Pang et al., 2015). If unimpeded, DRONC would begin to activate the executor type caspases (DCP-1/2, DECAP, DrICE and DAMM) and sentence the cell to death (Kornbluth and White, 2005). This uncontrolled caspase activity is restrained by the *Drosophila* IAP proteins Diap-1 and Diap-2,

which act continuously to suppress the activity of caspases via ubiquitination and subsequent proteolytic degradation (Igaki and Miura, 2004), preventing the progression of apoptosis by maintaining a balance of caspase activation and suppression. To facilitate apoptotic progression, these IAPs must be inhibited, and caspase activation allowed to continue unsuppressed. This inhibition requires the expression of the pro-apoptotic RGH genes (*reaper*, *grim* and *hid*) which inhibit Diap-1/2 through the induction of auto-ubiquitination and attenuation of peptide translation (Holley et al., 2002; Yoo et al., 2002; Berthelet and Dubrez, 2013).

Compared to mammalian system, *Drosophila* lack the extrinsic DISC pathway for caspase activation but do register pro-apoptotic external stimuli which then act to induce RGH expression. The best studied external apoptotic pathway being through JNK signalling: the *Drosophila* JNK pathway is a member of MAPK signalling family and is composed of a kinase cascade series leading to the activation of the singular *Drosophila* JNK member, Basket (Igaki, 2009; Yue and López, 2020). One of the potent external apoptotic activators is the TNF- α homolog Eiger; Eiger can be tissue bound or secreted and induces apoptosis through binding of its receptor Wengen and subsequent JNK-mediated upregulation of RGH genes such as *hid* (Moreno et al., 2002; Kauppila et al., 2003; Igaki and Miura, 2014; Shklover et al., 2015). Once executor caspases are active, they will begin to degrade the cellular machinery and cause the phenotypic features of apoptosis, including DNA fragmentation, cell membrane blebbing and changes to the plasma membrane composition (Elmore, 2007; Julien and Wells, 2017).

The basic apoptotic pathways for both mammalian and *Drosophila* cells are summarised in **Figure 1.2**. Regardless of species, once a cell has undergone apoptosis, the remnants are retained within the tissue and must be rapidly removed, a process known as apoptotic cell clearance or efferocytosis.

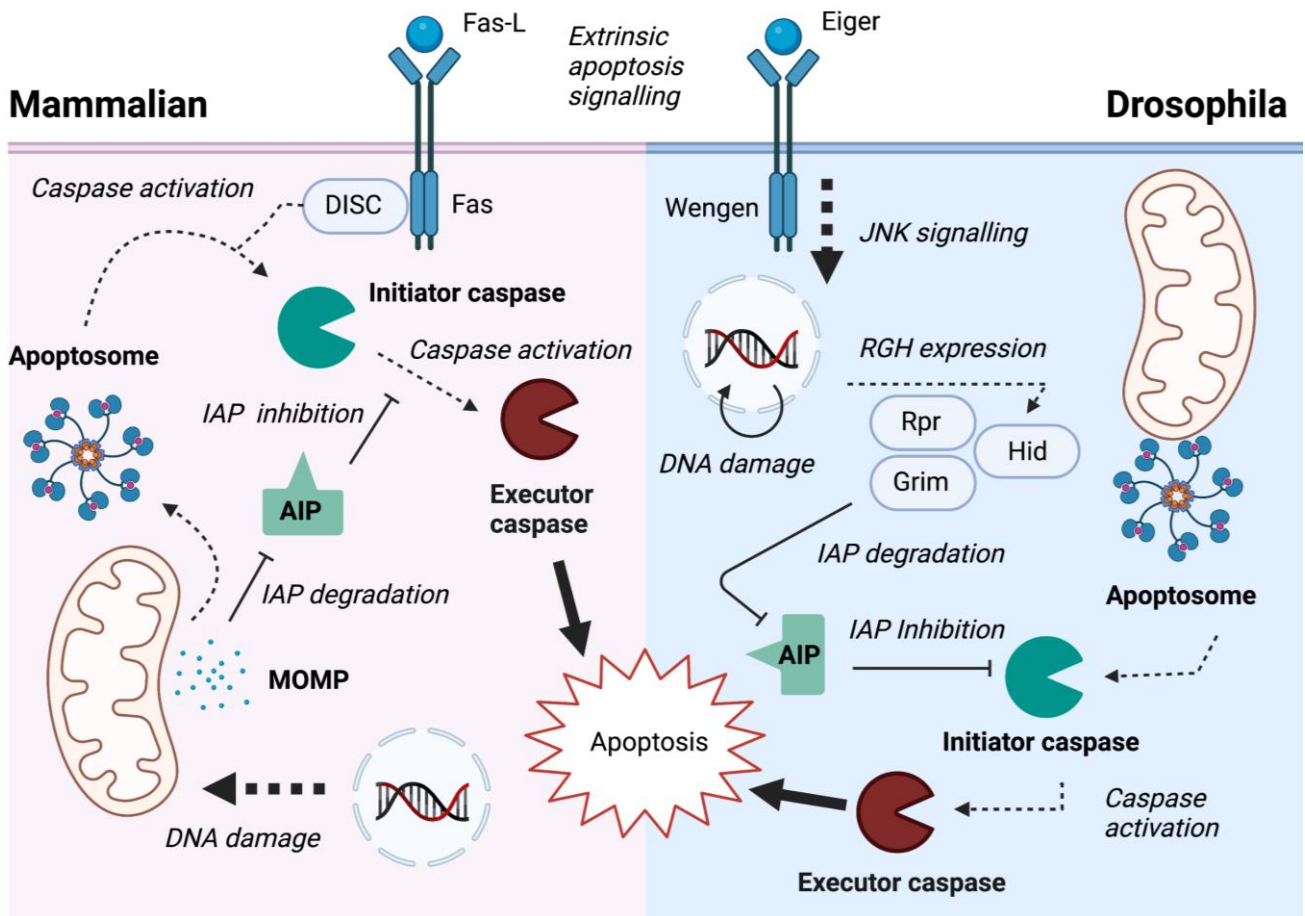


Figure 1.2 – Basic apoptotic pathways in mammals and *Drosophila*

Schematic comparing basic apoptotic pathways in mammalian and *Drosophila* cells. Both mammalian and *Drosophila* apoptosis share some form of intrinsic and extrinsic apoptotic pathway. In mammals, intrinsic apoptosis is mediated by death receptors such as Fas which, when activated, act as platforms for the assembly of the death inducing signalling complex (DISC) that can cleave initiator caspases such as Caspase-8. In the absence of a DISC homolog, *Drosophila* pro-apoptotic signalling such as Eiger-Wengen activation, leads to c-Jun N-terminal kinase (JNK) downstream signalling and up-regulation of the pro-apoptotic RGH genes (*reaper*, *grim* and *hid*). The differences between in the intrinsic pathway is more interesting; compared to the mammalian apoptosome, which is activated downstream of mitochondrial outer membrane permeabilization (MOMP), the *Drosophila* apoptosome is constitutively active and generates active initiator caspase DRONC. To prevent uncontrolled cell death, DRONC is suppressed by the inhibitor of apoptosis proteins (IAPs) Diap-1 and Diap-2. In either system, the apoptosome further activates initiators caspases. In mammals, the initiator caspases will lead to the activation of executor caspases such as Caspase-3 which will go on to degrade the cell. In *Drosophila*, DRONC mediated executor activation, of DCP-1 for example) requires the expression of the IAP inhibitory RGH genes, which when expressed under pro-apoptotic signalling will remove IAP interference and progress apoptosis. These pathways are extensively reviewed in the following: Abrams et al., 1993; Igaki and Miura, 2004; Kroemer et al., 2007; Galluzzi et al., 2012; Sessler et al., 2013; Yue and López, 2020.

1.3.2 Taking cells to the grave – efferocytosis and the role of macrophages

The efficient removal of apoptotic cells (efferocytosis) is needed to prevent dying cells from undergoing what is known as secondary necrosis, a damaging form of cell death that can lead to the release of cytotoxic substances such as DNA constituents (Degterev and Yuan, 2008). Professional phagocytes of the innate immune system, in particular macrophages, mediate this clearance process without activating an inflammatory response, i.e., it is immunologically silent (Trahtemberg and Mevorach, 2017). Efferocytosis is a stepwise process that occurs through a series of signals derived from the dying cell that act on responding cells to facilitate the seeking, engulfment, and resolution of the apoptotic target (Figure 1.3).

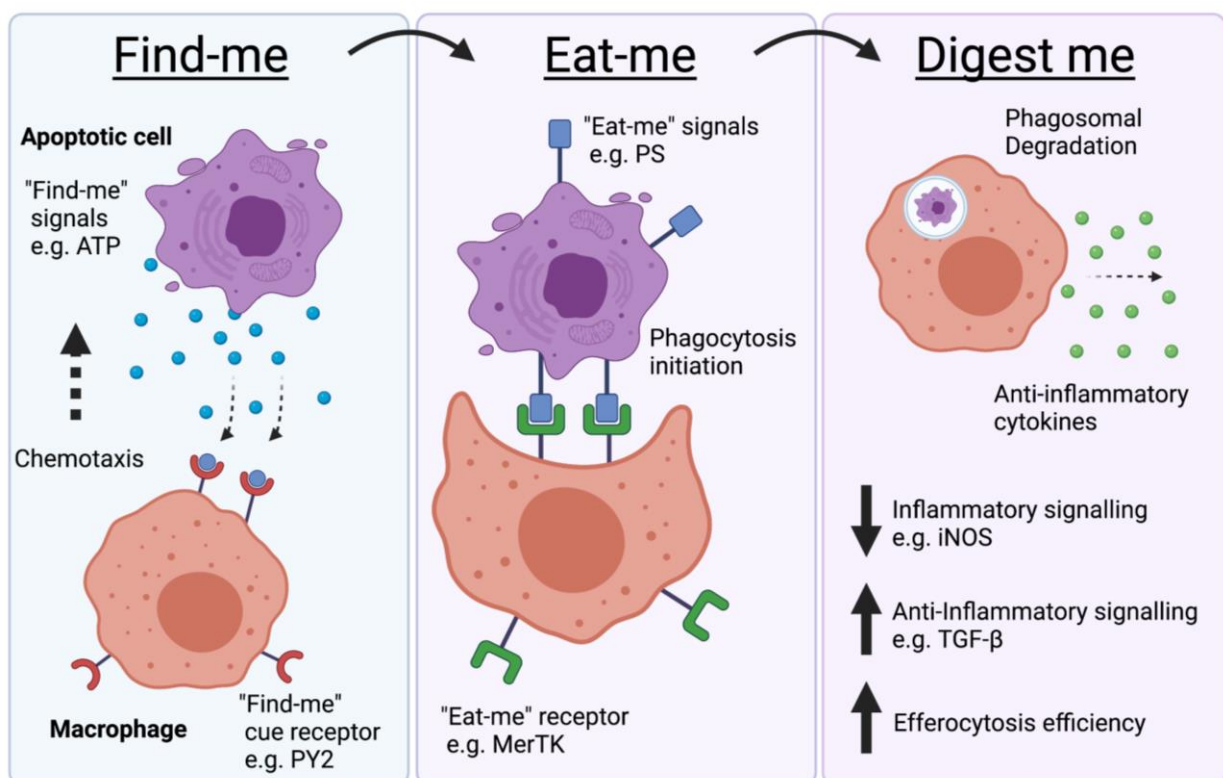


Figure 1.3 – The stages of efferocytosis

Schematic representation of vertebrate efferocytosis. The first step of efferocytosis requires the responding phagocyte (typically a macrophage) to locate the apoptotic cell through recognition and chemotaxis towards apoptotic derived recruitment signals known as “find-me cues” e.g., adenosine triphosphate (ATP). Once the macrophage has localized to the dying cell, it must bind to the cell surface to induce phagocytosis through engagement of “eat-me” signals exposed during the apoptotic program e.g., MerTK binding to phosphatidylserine (PS). Once engaged, the macrophage can phagocytose and process the dying cell, a process that is thought to alter macrophage function by promoting anti-inflammatory signaling and prime the cell for further efferocytosis.

To attract a macrophage and undergo clearance, it has been hypothesised that apoptotic cells release specific chemotactic signals, referred to as “find-me cues”. These find-me cues can be basically described as chemoattractant molecules released by apoptotic cells that recruit macrophages and enable efficient engulfment and processing (Ariel and Ravichandran, 2016; Muñoz et al., 2017). Studies in mammalian models have identified a variety of candidate molecules thought to act as find-me cues, including nucleotides, lipid mediators and proteins amongst others, which will be discussed in more detail later.

Once the macrophage has reached the apoptotic cell, membrane bound ligands (“eat-me signals”) presented on the apoptotic plasma membrane are engaged via receptors to stimulate the engulfment process. A well-studied example of this is macrophage c-Mer tyrosine kinase (MerTK) apoptotic cell receptor. MerTK is a tyrosine kinase receptor expressed on the surface of macrophages which binds to the product of *growth arrest-specific gene 6* (Gas6) (Thorp et al., 2008; Cai et al., 2017; Doran et al., 2017). Gas6 is an opsonin molecule that binds to PS exposed on the apoptotic cell surface and bridges MerTK to PS (Nagata et al., 1996; Nakano et al., 1997). This binding, in coordination with other coactivators such as T cell immunoglobulin and mucin domain 4 (TIM-4), allows macrophages to efficiently attach to the apoptotic cell and initiate phagocytosis. Conversely, “don’t eat-me” signals, such as CD47 and “keep-out” signals such as Lactoferrin may also be present to inhibit this process in certain circumstances (Bournazou et al., 2009; Kojima et al., 2016). It has been suggested that such signals also function to suppress non-desired immune responses in concert with pro-clearance, eat-me cues (Elward and Gasque, 2003).

Once apoptotic bodies have been engulfed, they must be correctly processed within the phagosome, referred to as the resolution stage. This phase is highly complex and requires the digestion of ingested apoptotic particles with a combined suppression of immune responses. The ingestion of apoptotic cells has been shown to reduce pro-inflammatory signalling via several pathways e.g. NF- κ b (Trahtemberg and Mevorach, 2017) and is thought to modulate receptor expression to promote resolution via anti-inflammatory polarisation of the macrophage towards M2-like phenotypes (Covarrubias et al., 2015). Digestion of apoptotic corpses is biochemically similar to that of pathogen phagocytosis in that the overall process is dependent on a staged acidification that is required for the activation of proteolytic enzymes

(Kinchen and Ravichandran, 2008). Intriguingly, recent evidence has suggested that the recognition of apoptotic eat-me cues such as PS may stimulate a unique form of processing known as LC3-Associated Phagocytosis (LAP) (Martinez et al., 2011). The significance of this unique processing is still under investigation, however, it has been suggested that LAP may help to suppress the pro-inflammatory response via MHC-II presentation (Romao and Münz, 2014).

1.3.3 Find-me cues: multifunctional pro-efferocytosis molecules

1.3.3.1 Sending out an S.O.S – find-me cue variation and identity

The first phase of efferocytosis requires the apoptosis-linked release of chemoattractants that can recruit local phagocytes and allow binding and phagocytosis of the dying cell. Studies primarily using mouse and cell culture approaches have uncovered several candidate find-me cues including nucleotides, lipids, and proteins.

Nucleotide triphosphates (NTPs) such as adenosine and, to a lesser extent, uridine triphosphate (ATP/UTP) are ubiquitous metabolites and are critical to several cellular processes including metabolism and signalling (Dzeja and Terzic, 2003). Several studies have linked ATP/UTP release from the apoptotic cell to efferocytosis (Elliott et al., 2010; Chekeni et al., 2011; Qu et al., 2011). Polypeptide find-me cues have been observed to be both shed from the membrane or liberated from larger complexes: Fractalkine (CX₃CL) is the only member of the CX₃C family of mammalian cytokines primarily expressed as a cell-surface ligand on resting neuronal or inflammatory induced endothelial cells, and which can be cleaved from the membrane into the extracellular space by ADAM17 (Imai et al., 1997; Gevrey et al., 2005; Truman et al., 2008; White and Greaves, 2012; Sheridan and Murphy, 2013; Sokolowski et al., 2014). In contrast to Fractalkine, several find-me cue peptides appear to be derived from apoptotic degradation of the ribosomal machinery including endothelial monocyte activating polypeptide 2 (EMAP-II), tyrosyl tRNA synthetase (TyrRS) and ribosomal protein S19 (RP-S19), which once liberated can diffuse from the cell (Knies et al., 1998; Wakasugi and Schimmel, 1999; Nishimura et al., 2001; Hou et al., 2006; Yamamoto, 2007). So far, two primary lipid-derived cues have been identified, both of which belong to the lysophospholipid class: Sphingosine-1-phosphate (S1P/S-1-P) and Lysophosphatidylcholine (LPC). S1P and LPC are plasma membrane-derived lipids that has previously been studied as a

pro-immune trafficking signal and inflammatory mediators respectively (Qin et al., 2014; Baeyens and Schwab, 2020). Both of these lipids have been shown to be released from apoptotic cells through caspase dependent enzyme activation (Lauber, 2003; Weigert et al., 2006; Gude et al., 2008).

Once released, these find-me cues are thought to recruit local phagocytes to carry out efferocytosis. It is important to note that the rapid proteolytic activities that occur during apoptosis significantly reduce the cells *de novo* translation potential (Clemens et al., 2000), which in part can explain why the find-me cues so far identified are expressed within the cell prior to apoptosis. While the structure and origin of these find-me cues is diverse, their generation has in so far been intimately linked to the activity of the apoptotic effector caspase enzymes. Caspases have been shown to induce the activation and release of find-me cue through several distinct mechanisms, ranging from the direct cleavage of precursors to the activation of intermediate enzymes or export systems.

1.3.3.2 Apoptotic generation of find-me cues

The activation of proteolytic caspase enzymes is one of the distinguishing features of apoptosis (Galluzzi et al., 2012). Active caspases have been shown to act both directly and indirectly in the generation and release of several candidate find-me cues.

Caspases act to release find-me cues through several mechanisms including direct cleavage of the pro-find-me cue and the activation of intermediate processing enzymes. The generation of S1P, LPC and Fractalkine arise from the caspase mediated activation of their processing enzymes: caspases have been shown to cleave Sphingosine kinase 2 (SphK2) into an active extracellular form that can convert Sphingosine exposed on the outer plasma membrane leaflet into S1P (Gude et al., 2008; Weigert et al., 2010); similarly, caspase mediated processing of LPC-generating Calcium-independent phospholipase A₂ (iPLA₂) leads to the conversion of phosphatidylcholine (PC) to LPC (Lauber, 2003); finally, cleavage of fractalkine from the surface of apoptotic cells has been shown to be dependent on cleavage by ADAM17, a caspase-activated matrix metalloprotease (MMP) (Chalaris et al., 2007; Truman et al., 2008; Scheller et al., 2011). As well as activating intermediate enzymes, caspases are known to induce the export of pre-existing find-me cues such as ATP/UTP: it has been shown

that caspases-3 and 7 are able to cleave and open the nucleotide-exporting Pannexin-1 hemi-channel, allowing cytosolic ATP/UTP to diffuse out of the cell rapidly (Chekeni et al., 2011; Qu et al., 2011; Yamaguchi et al., 2014).

In addition to the activation of export systems, caspases have been shown to generate mature find-me cues from precursors. An interesting example of this is the generation of the EMAP-II peptide from a component of the translational machinery (p43), which is cleaved by caspase-7 (Knies et al., 1998; Behrendorf et al., 2000), although this process remains controversial (Zhang and Schwarz, 2002). Intriguingly, preliminary research has also suggested that the apoptotic release of targeted microparticles, known to carry bioactive cargo (Norling and Dalli, 2013) may be used to deliver certain cues directly (Tsai et al., 2014), although caution should be taken here as this area is currently poorly understood compared to the previously described mechanisms. It is important to bear in mind that find-me cues may have redundant release mechanisms that could be linked to apoptotic processes independent of caspase activity. This is seen with cues derived from the translational machinery such as EMAP-II and RP-S19. EMAP-II peptide generation from TyrRS is hypothesised to be released through both MMP (Casas-Tintó et al., 2015) and/or extracellular elastase activity (Wakasugi and Schimmel, 1999), while RP-S19 dimerisation and release (Nishimura et al., 2001) is thought to be coupled to apoptotic type II transglutaminase activity (Fésüs and Szondy, 2005).

Overall, the role of caspases in the release of find-me cues is now well validated, as summarised in **Figure 1.4**. Once these cues have been released, they must diffuse throughout the tissue to reach target phagocytes.

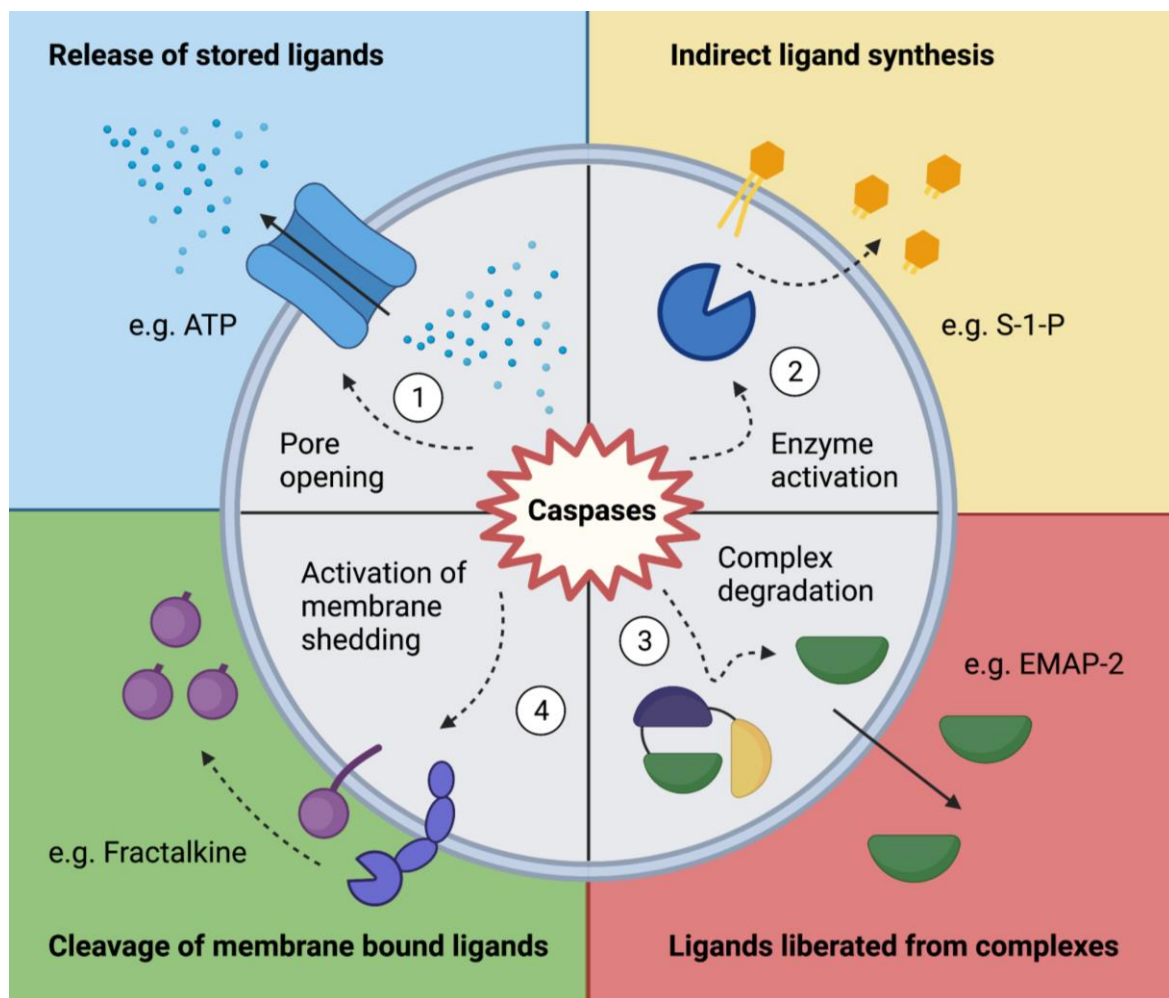


Figure 1.4 – Caspase-mediated find-me cue release

Active caspases can mediate cue release in a number of ways: the activation of pores in the membrane, such as Pannexin-1 that can allow nucleotide release (1); activation of converting enzymes e.g. Sphingosine kinase or Calcium-independent phospholipase A₂ (Sphk/iPLA₂) that can then generate cues, in this case S1P and LPC (2); Direct cleavage of precursors that are then exported e.g. the generation of EMAP-II (3); or activation of other enzymes such as MMPs that can stimulate the shedding of membrane bound cues, e.g., Fractalkine (4).

1.3.3.3 Signal propagation and gradient formation

While some find-me cues such as S1P and Fractalkine have relatively stable structures, some form of signal propagation is thought to be required for them to reach potentially distant macrophage populations. Moreover, the ability of some unstable cues such as ATP to form gradients is less straightforward due to their reactive structure and the presence of ecto-hydrolase enzymes within the tissue microenvironment (Zimmermann et al., 2012) (Yegutkin, 2008).

These issues have led a search for possible propagation molecules, with a major candidate being Ca^{2+} cations. While the role of Ca^{2+} in phagocytosis has been very well characterised (Nunes and Demaurex, 2010), recent work has begun to elucidate its role as a secondary messenger and propagation molecule for find-me cues. Indeed, the puzzle of effective nucleotide signalling has started to unravel as several lines of evidence have demonstrated an active role for Ca^{2+} : combined evidence from Dou *et al.* (2012) and Sieger *et al.* (2012) suggest that ATP-P2Y receptor binding on some cell types may stimulate Ca^{2+} influx via P2X7 pore formation, and that this event may in turn drive the mobilisation of lysosomal ATP stores to the plasma membrane. Given the homeostatic abundance of Ca^{2+} within the tissue microenvironment, this process would stimulate ATP-mediated ATP-release, thereby allowing for the propagation of the nucleotide find-me cue and potentially establishing an effective chemotactic gradient for macrophage recruitment. The inhibition of this ATP propagation process also appears to significantly reduce the effectiveness of the find-me cue in animal wound models (Davalos *et al.*, 2005). These Ca^{2+} models are further bolstered by data from Ca^{2+} channelopathy models, such as those for autosomal dominant polycystic kidney disease (ADPKD) that have identified efferocytosis defects associated with the loss of Polycystin-2 (van Goethem *et al.*, 2012).

Overall, the propagation of find-me cues signalling appears to vary, with more unstable molecules such as ATP requiring further amplification after initial apoptotic release. Once these signals reach a responsive cell, they need to be recognised to illicit both a chemotactic response but also polarise the cell to a pro-efferocytic state.

1.3.3.4 Find-me cue signalling outcomes

Macrophages express a wide range of chemotactic receptors and most known find-me cues appear to function through a receptor-ligand relationship. The major signalling pathway identified for find-me cues is through GPCRs, several of which are expressed on macrophages (Lattin *et al.*, 2008). This signalling relationship can be seen in Fractalkine binding to its lone cognate receptor CX_3CLR (Imai *et al.*, 1997), S1P to S1PRs (Weichand *et al.*, 2013), LPC to G2A (Yang *et al.*, 2005; Peter *et al.*, 2008) and the employment of purinergic nucleotide triphosphate-binding P2Y receptors (Elliott *et al.*, 2010). While EMAP-II is thought to activate PIP_3 signalling (Casas-Tintó *et al.*, 2015), the identity of its receptor is not known, with some

evidence suggesting CXCR3 as a potential candidate (Hou et al., 2006). One unusual example is that of RP-S19, which once dimerised, is thought to molecularly mimic the ligand for Complement 5a receptor (C5aR) on macrophages (Nishimura et al., 2001).

The chemotactic effects of several candidate find-me cues have been well established both *in vivo* and *in vitro*. ATP, non-hydrolysable ATP (ATP_γS), UTP and, interestingly, their diphosphate forms are chemotactic for THP-1 cells and in mouse models (Elliott et al., 2010). However, it has been suggested that different nucleotides such as ATP and UTP may well be interdependent and function in concert to stimulate migration through different pro-migratory targets (Koizumi, 2007). Similar chemotactic effects have been demonstrated for S1P (Gude et al., 2008), LPC (Lauber, 2003; Yang et al., 2005; Peter et al., 2008; Xu et al., 2016), Fractalkine (Truman et al., 2008; Zhu et al., 2009; Sokolowski et al., 2014) and EMAP-II (Kaoss et al., 1992; Wakasugi and Schimmel, 1999; Casas-Tintó et al., 2015). Several cues have also been shown to enhance eat-me signalling, e.g., through LPC surface exposure on the apoptotic cell surface (Kim et al., 2002) or Fractalkine-mediated milk fat globule-EGF factor 8 protein (MGF-E8) release (Miksa and Amin, 2007). It would also appear that many cues promote an anti-inflammatory M2 phenotype switch in incoming macrophages that promotes clearance, an activity shown by S1P-stimulated erythropoietin (Epo) signalling (Luo et al., 2016) and metabolism of ATP-derived adenosine (Bours et al., 2006). In addition to actively promoting an M2-like phenotype, other pro-inflammatory signals may be inhibited or blocked by find-me cues, e.g., RP-S19 has been shown to bind directly to macrophage migration inhibitory factor (MIF) and inhibit its function (Filip et al., 2009).

The various mechanisms of find-me cue generation, propagation and activity are summarised in **Table 1.1**.

Candidate	Precursors and generation	Export Mechanism	Variants	Receptors	Chemotaxis confirmed	References
ATP/UTP	Already abundant within the cytoplasm	Caspase dependent Pannexin-1 channel formation	Di or mono Phosphate forms, possibly adenosine	PY2 family	Mural thymocytes. Mural Bone Marrow Derived Macrophages, THP-1 cells & Zebrafish/Mural/Rat Microglia.	Chekeni <i>et al.</i> 2011; Dou <i>et al.</i> 2012; M. R. Elliott <i>et al.</i> 2009; Qu <i>et al.</i> 2011; Sieger <i>et al.</i> 2012; Yamaguchi <i>et al.</i> 2014
S1P	Sphingosine. Caspase mediated sphingosine kinase activity	Membrane release	N/A	S1PR family	THP-1, U937s Human Monocytes Human Macrophages	Gude <i>et al.</i> 2008; Weichand <i>et al.</i> 2013; Weigert <i>et al.</i> 2010
LPC	Phosphatidylcholine. Caspase mediated Calcium independent phospholipase A ₂ activity	Membrane release	N/A	G2A family	THP-1, Mural Macrophages, Zebrafish Microglia	Lauber 2003; Peter <i>et al.</i> 2008; Xu <i>et al.</i> 2016; Yang <i>et al.</i> 2005
EMAP-II	p43 or TyrRS C-terminal domain. Cleavage via caspase-7 or other proteases e.g. Elastase	Unknown	Progenitor specific sequence	Potentially CXCR3	Human Neutrophils. Human Monocytes. <i>Drosophila</i> hemocytes.	Casas-Tintó, Lolo, and Moreno 2015; Kaoss <i>et al.</i> 1992; Knies <i>et al.</i> 1998; Wakasugi and Schimmel 1999
Soluble Fractalkine	Tethered Fractalkine. Cleavage via ADAM17 during apoptosis	ADAM17 shedding	Potential micro particle form	CX ₃ CLR	ECV304, Human Monocyte-derived Macrophages, Human Bone Marrow Stromal Cells & Mural Microglia	Imai <i>et al.</i> 1997; Sokolowski <i>et al.</i> 2014; Truman <i>et al.</i> 2008; Zhu <i>et al.</i> 2009
RPS19	Monomeric form. Apoptotic dimerization via Type II transglutaminase	Unknown	N/A	C5a receptor	Human Monocytes	Fésüs and Szondy 2005; Nishimura <i>et al.</i> 2001

Table 1.1 – Summary of known find-me cues

Summarised table of known find-me cues, including name, precursor molecules, the means of their generation, export pathway, variants, and receptors. Published sources are detailed in the far-right column.

1.3.3.5 Implications of efferocytosis on health

Failure in removing dying cells has been implicated in the progression of many of chronic inflammatory diseases. These include atherosclerosis – a progressive cardiovascular disease characterised by vasculature degeneration (Weber and Noels, 2011), chronic obstructive pulmonary disease (COPD) – a group of lung diseases displaying characteristic destruction of lung architecture and persistent leukocyte infiltration (MacNee, 2005) and systemic Lupus erythematosus (SLE) – a heterogeneous autoimmune disorder (Marks and Tullus, 2012). Macrophages derived from these chronically inflamed patients often show a reduced phagocytic capacity and have an associated increase in apoptotic load within diseased tissues (Herrmann et al., 1998; Ren et al., 2003; Gaipf et al., 2007; Li et al., 2009; Dehle et al., 2013). The combined loss of phagocytic capacity in diseased macrophages and increases in apoptotic cell levels in tissues suggest that macrophages present within chronically inflamed tissues have become defective in efferocytosis, leading to the increase in local apoptotic tissue. As noted earlier, if apoptotic cells are left uncleared, they can eventually become necrotic and further drive inflammation (Trahtemberg and Mevorach, 2017). This would explain why the increase in apoptotic burden has been associated with disease progression in both COPD, where eosinophilia has been observed as a possible immune response to macrophage efferocytic failures (Eltboli et al., 2014), or in atherosclerosis, where increased apoptosis and subsequent necrosis reduce plaque stability and increase the risk of severe vessel-occlusion events (Thorp et al., 2008; Li et al., 2009; Frodermann et al., 2015; Tao et al., 2015; Kayashima et al., 2017).

While the molecular biology of these clearance defects appears multifaceted, several credible mechanisms have been put forward. One recurring factor identified is a reduction in “eat-me” signalling; several groups have reported reduced macrophage expression of apoptotic cell-binding proteins such as MerTK, hematopoietic scavenger receptor class B type I (SR-B1) and TIM-4 in atherosclerosis and CD44 in SLE (Cairns et al., 2001; Thorp et al., 2008; Tao et al., 2015; Foks et al., 2016; Cai et al., 2017). This reduced expression may hinder binding to apoptotic cells and prevent proper phagocytosis, leading to an increase in secondary necrosis and consequent tissue damage and inflammation.

Whether these effects are causal or symptomatic of such inflammatory diseases has yet to be fully elucidated. Recent investigations have linked the development of these defects with certain lifestyle factors such as smoking or diet. Tobacco smoke is a major risk factor associated with COPD and has been shown *in vitro* to reduce macrophage expression of apoptotic receptors such as CD9 or the production of pro-phagocytic opsonins like MGF-E8, also known as lactadherin (Noda et al., 2013; Wang et al., 2017). Tobacco smoking has also been implicated in increased macrophage RhoA signalling (Richens et al., 2009), which is thought to promote adhesion and may thereby reduce macrophage migration to find-me signals (Chimini and Chavrier, 2000). Diet is another major risk factor: obese mice fed on fish oil-rich diets show increased levels of apoptotic clearance compared to those on a western-style diet (Li et al., 2009), while zinc deficiency has been linked to clearance defects within COPD, possibly through failures in proper alveolar macrophage polarisation or Zn-dependent phagocytotic machinery (Hamon et al., 2014).

In most cases, failed efferocytosis has been described as arising because of ongoing inflammatory processes, however it may also act as the initiating factor in certain diseases. It has been suggested by Kuenkele *et al.* (2003) that a lack of removal of apoptotic B-cells in the lymph node could allow for the survival of auto-reactive plasma cells and the formation of anti-nuclear antigen immunoglobulin-G (ANA-IgG), a key auto-reactive antibody in SLE (Marks and Tullus, 2012).

Taken together, the continued implication of failed efferocytosis in chronic inflammation illustrates the importance of understanding the underlying molecular mechanisms as a potential source of therapeutic targets.

1.3.4 Find-me cues in *Drosophila*: evidence and potential candidates

To date, most studies on find-me cues has focussed on the use of *in vitro* and vertebrate models. As discussed earlier, one of the key functions of macrophages in *Drosophila* is the clearance of apoptotic cells, especially during development. While embryonic macrophage express a several apoptotic cell receptors such as Simu (Roddie et al., 2019), the find-me cues responsible for their recruitment remain under explored. Evidence from wounding experiments has shown that embryonic macrophages will preferentially respond to apoptotic

cells during the wound refractile period, even in the presence of pvf guidance signals (Moreira et al., 2010): this prioritisation would suggest that apoptotic cells are releasing some form of recruitment signal that redirects macrophages to perform efferocytosis. Recent work from Casas-Tintó et al. (2015) suggested that the ribosomal machinery component TyrRS derived EMAP-II like peptide acts to recruit larval macrophages, although whether this occurs in the embryo remains unknown. I sought to test other potential find-me cues active during *Drosophila* embryogenesis, which brought to my attention epidermal growth factor (EGF) as potential novel find-me cue.

1.3.4.1 *Drosophila* epidermal growth factor signalling

The EGF pathway is an evolutionarily conserved multi-functional signalling pathway that has roles in cell migration, survival, and proliferation amongst others. While mammalian EGF signalling is composed of a complex network of heterodimeric ErbB receptors and ligands (Burgess et al., 2003; Citri and Yarden, 2006), the homologous pathway in *Drosophila* is composed of a single receptor (*Drosophila* EGF receptor/DER/EGFR) that is activated by several partially redundant ligands and inhibitors (Price et al., 1989). The *Drosophila* EGFR is thought to bind five ligands: the cardinal ligand Spitz as well as Keren, Gurken, Vein and Argos. Spitz is ubiquitously expressed during embryogenesis and plays a role in tissue proliferation, apoptotic recruitment and cell differentiation (Rutledge et al., 1992; Schweitzer et al., 1995; Golembo et al., 1996; Buff et al., 1998; Liang et al., 2017). Keren has similarities to Spitz and appears to be partially redundant in some tissues, and has been largely implicated in proliferation and tissue organisation within the developing compound eye (O'Keefe et al., 1997; Reich and Shilo, 2002). Gurken has largely been studied in relation to oogenesis and has been identified as a chemoattractant for nurse cells within the developing egg (Wasserman and Freeman, 1998; Duchek et al., 2001; Ghiglione et al., 2002; Pizette et al., 2009; Revaitis et al., 2020). Vein is a Neuregulin-like ligand that has been implicated in tissue differentiation similarly to Spitz and Keren in the *Drosophila* embryo (Sturtevant et al., 1993; Schnepf et al., 1996; Wessells et al., 1999; Donaldson et al., 2004). Argos, unlike the previous ligands, is an EGFR antagonist that acts to downregulate EGFR activation through receptor antagonism and sequestering (Okabe et al., 1996; Jin et al., 2002; Klein et al., 2008).

Each of these ligands require some degree of post-translational modification before they can be secreted as an active growth factor (**Figure 1.5**). After translation, the pro-peptide form of Spitz (and likely the other ligands) is retained within the endoplasmic reticulum within a complex containing the chaperone protein Star, prior to transport to the Golgi (Kolodkin et al., 1994; Hsiung et al., 2001; Iyadurai et al., 2008).

Two critical modifications occur to the ligands within the late compartment of the Golgi complex: the addition of a palmitoyl group via the enzyme Rasp, thought to restrict extracellular diffusion, and proteolytic cleavage by Rhomboid, which removes the transmembrane region to produce an active peptide (Sturtevant et al., 1993; Urban et al., 2002; Miura et al., 2006; Yogev et al., 2008; Steinhauer et al., 2013; Shilo, 2016). It is thought that the regulation of EGF ligand secretion is dependent on the activity of the rhomboid proteases – expression of these proteases is restricted compared to that of the ligands and it has been shown that Rhomboid can cleave other processing elements such as Star to reduce processing rates (Tsruya et al., 2007; Shilo, 2016).

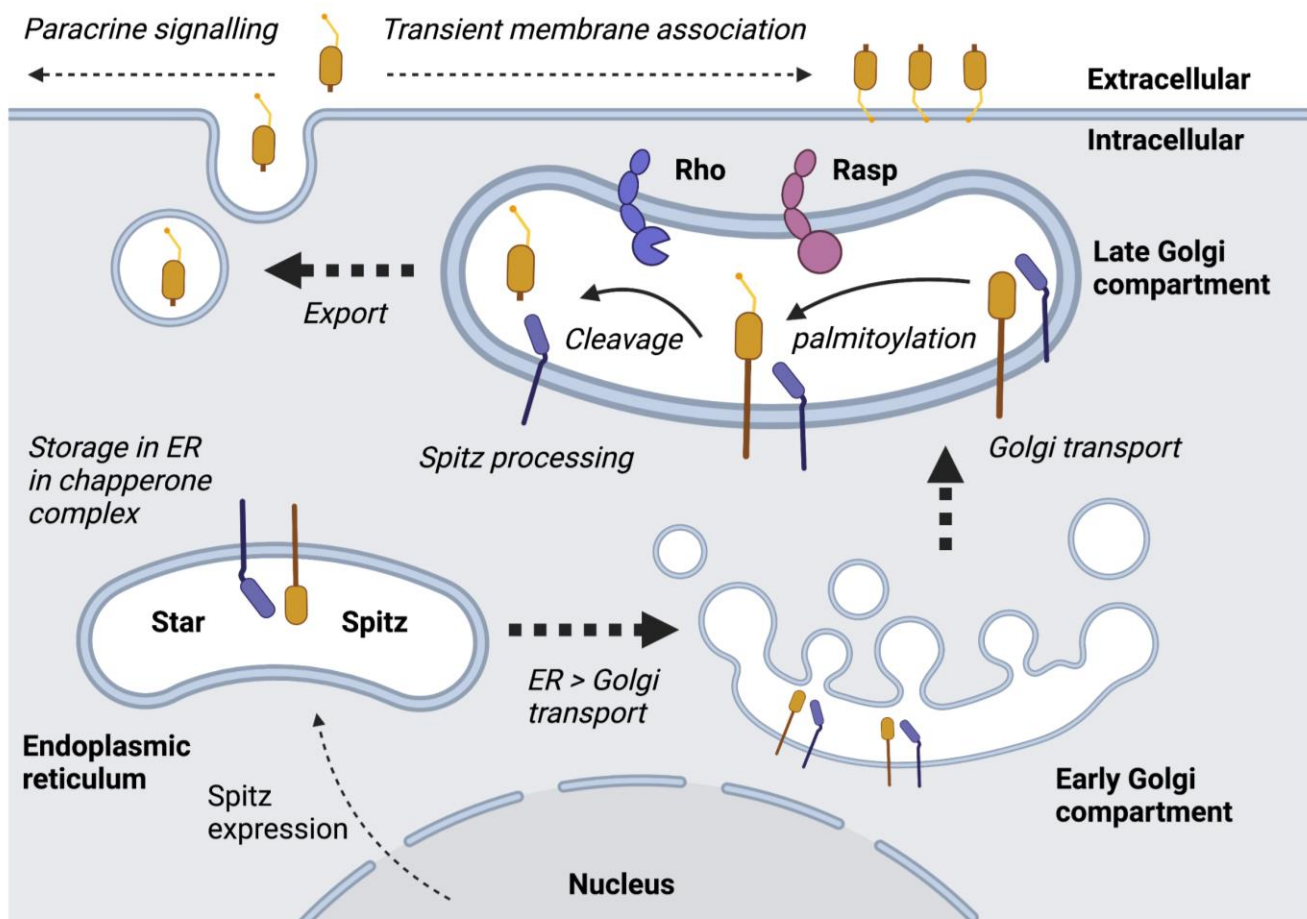


Figure 1.5 – Processing and release of Spitz in *Drosophila*

Schematic diagram of Spitz (generalised EGF processing) in *Drosophila*. After translation, Spitz is held within the endoplasmic reticulum as part of a chaperone complex with Star. This complex will be trafficked through the Golgi apparatus and undergo processing within the late compartment of the Golgi. Two key Spitz-modification events occur here: the addition of a palmitoyl group via Rasp, and the cleavage and separation of Spitz from Star via Rhomboid. After processing, the soluble and modified version of Spitz is exported from the cell. The addition of the palmitoyl group is thought to restrict diffusion through increased molecular weight and interaction with the plasma membrane, thereby concentrating spitz at the cell surface and limiting its action to paracrine and autocrine signalling. Spitz is the most widely expressed of the EGF ligands and is thought to be representative of processing for Keren and Gurken. It should be noted that Vein does not require Rhomboid-mediated processing as it is produced in a secreted form. Further information can be found in Yarden and Shilo (2007) and the references therein.

1.3.4.2 Potential role of EGF in *Drosophila* efferocytosis

Combined evidence from several papers has suggested that EGF signalling might play a role in efferocytosis, with EGF a candidate find-me cue. The chemotactic ability of EGF ligands has been demonstrated in both human monocytes and within the *Drosophila* developing oocyte (Duchek and Rørth, 2001; Lamb et al., 2004). In relation to efferocytosis, it was recently shown that the cardinal *Drosophila* EGFR ligand Spitz is released from apoptotic cells in the gut in order to recruit stem-cells, thereby maintaining gut integrity (Liang et al., 2017). Furthermore, there are several similarities between the production of EGF ligands and known find me cues such as Fractalkine. In both flies and humans, secretion of active EGF ligands is tightly regulated via activation of a proteolytic enzyme – Rhomboid (Shilo, 2016) or the matrix metalloprotease ADAM17 (Scheller et al., 2011; Rose-John, 2013), an enzyme that is known to mediate the release of Fractalkine during apoptosis (Kim et al., 2011). Intriguingly, Liang et al. (2017) suggested that the release of Spitz from mid-gut apoptotic cells was promoted by the caspase-mediated activation of Rhomboid in a similar fashion to that observed for Fractalkine (Garton et al., 2001).

In summary, members of the *Drosophila* EGF pathway represent attractive candidate find-me cues with supporting chemotactic evidence, links to apoptotic release and similarities to processing and stimulation with known find-me cues.

1.4 Experimental aims and hypothesis

While several find-me cues have been identified within mammalian systems (Ariel and Ravichandran, 2016), little is known regarding the identity of these cues within *Drosophila*, despite efferocytosis being one of the core functions of embryonic macrophages. I postulated that EGF signalling might play a role in efferocytosis during embryogenesis. In parallel to identifying potential *Drosophila* find-me cues, I sought to investigate how find-me cues are integrated into the signalling priorities of immune cells, and what this means in context of chronic inflammation, using a primary human cell model. Finally, I sought to apply novel tools for the live visualisation of apoptosis during *Drosophila* embryogenesis and what this can tell us about the dynamics of efferocytosis.

Hypotheses

1. Chemotactic find-me cues, released from apoptotic cells, exist within *Drosophila* and EGF signalling might play a role in the recruitment of macrophages to dying cells during embryogenesis.
2. Find-me cues exist within a signalling hierarchy and are prioritised over known inflammatory cues such as Complement protein fragment 5a (C5a) and will be able to induce preferential chemotaxis of macrophages.
3. Novel caspase activation reporters can be used to visualise and quantify apoptotic activation and the dynamics of efferocytosis during *Drosophila* embryogenesis.

Experimental aims

1. Use overexpression systems in *Drosophila* to test the chemotactic potential of EGF ligands towards embryonic macrophages and the impact that such signals have on efferocytosis and other cell functions including wound responses and migration.

2. Optimise monocyte-derived macrophage (MDM) chemotaxis assays and begin building a signalling hierarchy from apoptotic-derived signals and known chemoattractants to understand signal prioritisation.

3. Characterise the *Drosophila* Caspase-ON fluorophore constructs to examine the effects of apoptotic signalling on *Drosophila* embryonic macrophage dynamics *in vivo*; the overarching aim of this work is to track initiation of apoptosis and macrophage movement towards dying cells at the earliest stage possible and utilise this information to model the migratory phases of efferocytosis.

Chapter 2- Materials and methods

2.1 Fly husbandry and genetics

2.1.1 Fly stocks and transgenic constructs

Fly stocks were maintained on molasses-based media supplemented with yeast at 18°C with mating populations kept in laying cages at 22°C. Embryos were collected from apple juice/agar plates on which embryos had been laid overnight. The following *Drosophila* lines and genetic constructs were used in this study: *eyeless-GAL4* (Halder et al., 1998), *UAS-sSpitz^{CS}* (Ghiglione et al., 2002), *UAS-Spitz^{sec}* (Miura et al., 2006), *UAS-mSpitz^{CS}-GFP* (Miura et al., 2006), *UAS-LifeAct* (Hatan et al., 2011), *SrpHemo-3X-mCherry* (Gyoergy et al., 2018), *Serpent-GAL4* (Brückner et al., 2004), *Croquemort-GAL4* (Stramer et al., 2005), *TinC-GAL4* (Lo and Frasch, 2001), *Forkhead-GAL4* (Henderson and Andrew, 2000), *Srp-GMA* (James Bloor, University of Kent, UK), *Arm-GC3Ai* (in-house) *VT45229-GAL4* (Kvon et al., 2014), *UAS-GC3Ai* and *UAS-VC3Ai* (Schott et al., 2017), *daughterless-GAL4* (Rougeot et al., 2013), *Act5C-GAL4* (Ito et al., 1997), *Df(3L)H99* (Abbott and Lengyel, 1991), *CyO hs-hid* (van Doren, 1996), *EGFR-sfGFP* (Revaitis et al., 2020), *UAS-EGFR* (Lesokhin et al., 1999), *UAS-ras85D^{V12}* (Lee et al., 1996), *UAS-Ras^{N17}* (Lee et al., 1996), *UAS-Red stinger* (Barolo et al., 2004), *UAS-keren* (Brown et al., 2007), *UAS-Vein* (Schnepp et al., 1996), *UAS-Star* (Kolodkin et al., 1994), *UAS-Rasp* (Miura et al., 2006), *UAS-Apoliner* (Bardet et al., 2008), *UAS-Argos* (Buff et al., 1998), *UAS-EGFR^{DN}* (Freeman, 1996), *UAS-Vein* (Duchek et al., 2001), *UAS-Gurken* (Ghiglione et al., 2002), *UAS-Reaper* (Aplin and Kaufman, 1997), *Tub-GAL80^{ts}* (Davis, 2003). All experiments were conducted on a *w¹¹¹⁸* background.

2.1.2 Transgene recombination and Polymerase Chain Reaction (PCR) validation

Spontaneous chromosomal recombination was used to combine transgenes onto the same chromosome. Briefly, candidate recombinant heterozygous males were generated by mating heterozygote virgin females with chromosome balanced males. Recombination was confirmed through the presence of balancer chromosome markers, mini-white presence (eye-colour) and PCR. Confirmed recombinant males were mated to chromosome balanced stocks to produce genetically stable stocks.

Genotyping PCR was carried out on candidate recombinant lines with primers designed to detect the two sequences to be recombined. DNA isolation was carried out on single males euthanised by freezing at -20°C for 30 minutes. DNA extraction buffer (see appendix) was added to males and samples vigorously pulverised using a P200 pipette tip. Samples were spun at maximum speed for 2 minutes and further pulverised to release their genomic DNA. Samples were then heated at 37°C for 30 minutes in a heating block (Eppendorf) to allow proteolysis and DNA release, with the proteolysis halted by heating 95°C for 10 minutes to inactivate proteinase K (Roche). Genomic DNA samples were stored at 4°C before genotyping via PCR. PCR genotyping of extracted male genomic DNA was used to confirm recombination events. 2µl of male *Drosophila* DNA extract was added to PCR reaction mixture with primers and DNA was amplified (**Table 2.1**) using a standard thermocycler (MJ-Research)

Stage	Temperature (°C)	Time (min)	Cycle Number	Activity
1	96	1	1	Initial denaturation stage
2	96	1	28	Denaturation cycle
3	55	1	28	Primer annealing cycle
4	72	1	28	Extension cycle
5	96	1	1	Final denaturation
6	55	1	1	Final annealing
7	72	5	1	Final extension
8	4	Stay on	End	Cold Storage

Table 2.1 – PCR parameters for genotyping recombinant flies

PCR program used for the amplification of DNA from single male *Drosophila* genomic DNA. This generalised protocol was used for all PCR procedures unless otherwise stated.

The following primers were used for the validation of GC3Ai and VC3Ai recombinants:

CTGCTGGAGTTCGTGACCG (XC3Ai Forward) and GCTCCTGGACGTAGCCTTC (XC3Ai Reverse).

Amplified DNA products were separated on 1% TAE 1% agarose gels containing SYBR green Safe DNA gel stain (Invitrogen). 10µm of PCR product was mixed with 2µl of 6X loading buffer (Promega) and separated via electrophoresis using 90V for 45 minutes. A 1kb DNA ladder (Promega) was used to estimate DNA banding size. DNA gels were examined under blue light and imaged with a digital camera.

2.1.3 Transgenesis of apoptotic sensors

Transgenesis of the GC3Ai reporter under the control of the armadillo promoter (arm-GC3Ai) was conducted by the lab assistant Emma Armitage. GC3Ai cDNA was obtained from pUAST-GC3Ai obtained from Magali Suzanne of the University of Toulouse. GC3Ai was cloned via PCR using the primers GC3Ai forward (GCCGCGGCCGAGATCCCGCTTACAGGTCCT) and reverse (AGCTTGATATCGAATTGCCACCATGTACCCC) each of which contained EcoR1 sites. Partial digestion with EcoR1 followed by gel purification and extraction yielded a full-length GC3Ai cDNA fragment. Purified full length GC3Ai cDNA was ligated into a pArmP-PolyA-AttB vector that had previously been cut with EcoR1, purified, and treated with treated Antarctic phosphatase (New England BioLabs). The resulting construct was checked for orientation of GC3Ai cDNA downstream of pArm before being inserted into *Drosophila* stocks by GenetiVision services.

2.2 Microscopy and imaging

2.2.1 Imaging and wounding of *Drosophila* embryos

2.2.1.1 Preparation of embryos for live imaging and fixation

Embryos laid on apple juice/agar plates were washed off into a cell strainer (VWR) and dechorionated in 5% bleach for 1 minute, followed by five washes in distilled water. For live imaging, washed embryos were immediately mounted in 10S Voltalef oil (VWR) on glass slides as per Evans et al., 2010b. For fixation and preparation for immunostaining, live embryos were fixed as previously described (Wood et al., 2006). After being dechorionated and washed, embryos were fixed using 4% formaldehyde in phosphate-buffered saline (PBS; Oxoid), before being devitellinised by shaking in methanol. Fixed embryos were either used immediately or stored at 4°C in methanol (methanol was aspirated prior to further use).

Live embryos were imaged using a Perkin Elmer Ultraview Spinning disk system using either a 10x air objective lens (UplanSApo 10x/NA 0.4; only used to obtain lateral images of developmental dispersal of macrophages), a 20x air objective lens (UplanSApo 20x/NA 0.8; VT45229-GAL4 experiments requiring anal pad visualisation and low-magnification imaging of the dorsal vessel only), or a 40x oil immersion objective lens (UplanSApo 40x oil/NA 1.3; all remaining live imaging). Wounding was performed using a Micropoint ablation laser (Andor) attached to the Perkin Elmer Ultraview Spinning disk system to ablate the ventral epithelium on the ventral midline in the medial-most segments of the embryo as per Evans et al., 2015. For imaging of the ventral midline region or dorsal surface (macrophage wounding, random migration, macrophage dispersal assessment, apoptotic event tracking, LysoTracker red staining) of stage 13 or 15 embryos, images were taken to a depth of approximately 20 μ m with a 1 μ m spacing between z-planes. Time-lapse movies were assembled from z-stacks taken using Volocity software (Perkin Elmer).

2.2.1.2 Imaging of immunostained embryos

Images of immunostained embryos were taken using a Zeiss 880 Airyscan confocal microscopy system running ZEN software. Embryos were imaged using a 40x objective lens (Zeiss Plan-APOCHROMAT 40x oil/NA 1.4) to a depth of approximately 25 μ m with a spacing of 0.2 μ m between z-planes.

2.2.1.3 Imaging of *ex vivo* adult flies

All imaging of adult flies was conducted using a Leica MZ205 FA fluorescent dissection microscope with a 2x Plan-APOCHROMAT air objective lens. For eye-disruption assays, adult flies were culled at -20°C before being mounted laterally, such that the left eye was parallel to the lens. Single z-slice images were taken of the eye where the diameter was fully visible and in focus.

2.2.2 Imaging of Ibidi μ -slides and MDM migration

For MDM chemotaxis imaging, Ibidi μ -slides were incubated at 37°C/5% CO₂ and imaged on a Leica AF6000LX inverted microscope system. Imaging was conducted using a 10x/0.3NA Ph1 phase objective lens and images captured using LAS X software. Briefly, single points were marked per observation chamber and time-lapses imaged at a single z-plane in which the

majority of cells were in focus. All microscopy images were saved as .tiff format files for analysis.

2.3 Immunofluorescence and staining methods

2.3.1 LysoTracker Red staining of live embryos

pH-sensitive LysoTracker Red DND-99 (Life Technologies) was used to monitor acidification of phagosomes. Dechorionated embryos were transferred to glass vials containing peroxide-free heptane (Sigma) and PBS containing lysotracker red (25 μ M) in a 1:1 ratio and shaken for 30 min at 250 rpm in the dark. Post staining, embryos were transferred into Halocarbon oil 700 (Sigma). Stage 15 embryos were selected and mounted on slides and the ventral midline region imaged.

2.3.2 Acridine orange staining of live embryos

Acridine orange (Alfa Aesar) staining was used to visualise apoptosis in the live embryo (Arama and Steller, 2006). Embryos were prepared for live imaging as described before being transferred to glass vials containing a staining solution of 5 μ g mL⁻¹ solution of acridine orange diluted in PBS and heptane in a 1:1 ratio. The embryos were then shaken at 250rpm for 5 minutes and transferred into a Halocarbon oil 700 via pasture pipette. Stained embryos were then mounted on glass slides as previously described.

2.3.3 Immunostaining of *Drosophila* embryos

For immunostaining experiments, fixed embryos were washed with 0.1% Triton-X-100 (Sigma) in PBS. Subsequently, embryos were blocked in PATx (1% Bovine Serum Albumin (Sigma), 0.1% Triton-X-100 in PBS) for 1 hour. Embryos were then incubated with primary antibodies overnight at 4°C, washed in PATx and incubated with secondary antibodies for 2 hours at 4°C. After a final series of PATx washes, residual PATx was aspirated and the embryos stored at -4°C in 1,4 Diazabicyclo[2.2.2]octane (2.5%) (DABCO) mountant (Sigma) in 90% glycerol (Sigma)/1X PBS. Stained embryos were mounted in DABCO mountant on glass slides as per Evans et al., 2010b.

For staining of apoptotic cells and GFP (expressed in macrophages to enable their visualisation or to detect GC3Ai), the following primary antibodies were used: rabbit anti-

cleaved DCP-1 (cDCP-1; 1:200; 9578S, Cell Signaling) and mouse anti-GFP (1:100; ab1218, Abcam). As a read-out of EGFR activation in macrophages, embryos were stained for activated ERK (DpERK; rabbit anti-phospho-p44/42 MAPK (Erk1/2) (Thr202/Tyr204); 1:100; 197G2, Cell Signaling Technology) with GFP-labelled macrophages detected via immunostaining for GFP (1:100; ab1218, Abcam). AlexaFluor568 goat anti-rabbit IgG (1:200; A11036, Life Technologies) and AlexaFluor488 goat anti-mouse IgG (1:200; A11029, Life Technologies) were used as secondary antibodies to detect anti-GFP, anti-cDCP-1 and anti-DpERK primary antibodies. To detect EGFR-sfGFP and macrophages, respectively, Rabbit anti-GFP (1:500; ab290, Abcam) and mouse anti-Fascin (purified sn7C antibody diluted 1:1000; Developmental Studies Hybridoma Bank) were used as primary antibodies. AlexaFluor488 goat anti-rabbit IgG (1:200; A11034, Life Technologies) and AlexaFluor568 goat anti-mouse IgG (1:200; A11031, Life Technologies) were used as secondary antibodies. For the detection of Spitz^{sec} protein in macrophages, embryos were stained for anti-Spitz (1:20; rat anti-sSpitz Developmental Studies Hybridoma Bank, (Reich and Shilo, 2002) with GFP-labelled macrophages again detected via immunostaining for GFP (1:100; ab1218, Abcam). AlexaFluor568 goat anti-rat IgG (1:200; A11077, Life Technologies) and AlexaFluor488 goat anti-mouse IgG (1:200; A11029, Life Technologies) were used as secondary antibodies.

2.4 Image processing and analysis of *Drosophila* phenotypes

2.4.1 Post-capture processing of raw microscopy files

All microscopy images were converted to Tiff (.tif) format files prior to analysis in Fiji (ImageJ) (Schindelin et al., 2012) except for data obtained from the ZEISS Airyscan 880 which was analysed in native processed CZI format (.CZI_out) in Imaris (Oxford Instruments). Movies and stills obtained from the Perkin Elmer spinning disk system showing macrophage morphology, apoptotic cell clearance, caspase activation and migration were assembled as maximum projections and despeckled in Fiji to reduce background noise. All confocal images captured from the ZEISS Airyscan 880 underwent deconvolution processing according to the manufacturer's instructions and in-built software (Amos et al., 2012).

2.4.2 Quantification of macrophage morphology and migration

Macrophage clusters were counted manually from maximum projections of the ventral midline region at stage 15 in Fiji, with only definite macrophage-macrophage contact events scored. Morphological parameters, e.g., aspect ratio (AR), which is defined as the ratio of a cell's width to its height, were measured manually from maximum projections using the polygon selection tool in Fiji. Macrophage vacuolation, a read-out of apoptotic cell clearance was assessed in the z-slice corresponding to that cell's largest cross-sectional area in 5 macrophages per embryo. The Fiji manual tracking plug-in was used to track cell movements of macrophages undergoing random migration from the assembled time-lapse movies. Tracking data was then imported into the Ibidi Chemotaxis tool plugin in Fiji to calculate migratory parameters (Petrie et al., 2009), e.g., macrophage velocity.

2.4.3 Assessment of adult fly eye phenotypes

To assess the activity of EGF signalling on proliferation in the adult fly compound eye, two metrics were taken from microscopy images: "rough eye" phenotype and eye area. The presence of a "rough eye" phenotype was manually denoted from observation of blinded images and was assessed as disruption to the wild-type compound structure including consistent differences in the compartment size, shape, and structure. Eye area was calculated using the polygon selection tool in Fiji for the entire eye boundary and expressed as the area (μm^2).

2.4.4 Quantification of vital dye staining and immunostaining in embryos

Apoptotic cell clearance was also analysed using embryos containing GFP-labelled macrophages immunostained for cDCP-1 and GFP. The numbers of cDCP-1-positive punctae inside (within GFP-positive cell areas) or outside macrophages in a field of view corresponding to the medial-most ventral region of stage 15 embryos were counted in merged z-stacks of the GFP and cDCP-1 channels. These values were used to calculate the total numbers of cDCP-1 punctae and "efferocytosis efficiency" per field of view. Efferocytosis efficiency was defined as the percentage of the total numbers of cDCP-1 punctae engulfed by macrophages per embryo. Numbers of lysotracker-positive vacuoles per macrophage were counted from z-stacks of the ventral midline region; volumes of individual lysotracker-positive vacuoles were analysed using Imaris software (Oxford Instruments).

Quantification of DpERK levels within macrophages on the ventral surface of the embryo was carried out using Imaris Surpass 3D rendering software. GFP staining was used to mask macrophages and measure total DpERK intensity per cell. Total intensity per cell was then divided by the volume of each macrophage (μm^3), with 15–20 macrophages per embryo quantified. Colocalisation values for GC3Ai and DCP-1 staining was carried out using the COLOC colocalisation function in Imaris: an intensity threshold was manually applied to these images prior to analysis to remove background signal and prevent false-positive colocalisation inference and colocalisation was inferred from % channel overlap per voxel.

2.4.5 Quantification of macrophage recruitment to specific tissues

Numbers of macrophages at the dorsal vessel were counted manually from maximum projections, with the total number in this field of view counted; recruitment to the dorsal vessel was defined as those macrophages contacting the dorsal vessel in a 100 μm long region corresponding to its medial-most section. Similarly, developmental dispersal was quantified by counting numbers of macrophages on the ventral side of the embryo at stage 15, in a field of view corresponding to the most-medial region of the embryo. The distance of macrophages from the dorsal vessel was measured using the points to line distance plugin in Fiji (macro made by Olivier Burri, EPFL, Lausanne). To assess macrophage association with the anal pad, the number of macrophages present within 100 μm of the anterior pole was quantified from 50 μm thick maximum projection stacks of the anterior region. Due to microscopy constraints (e.g., lens working distances), direct imaging of the developing salivary gland was not possible: to test if the secretion of spitz from the salivary gland altered macrophage function, the stage 13 ventral midline was screened for disrupted dispersal as quantified by the number of macrophages present.

2.4.6 Apoptotic induction methods and quantification

To induce global apoptosis in embryos containing the *CyO hs-hid* construct (van Doren, 1996; Roddie et al., 2019), embryos were harvested from laying cages as stated and washed into embryo baskets. Prior to dechoriation, embryos were immersed in a 39°C water bath for 10 minutes to induce heat-shock and global *hid* expression. Post heat-shock, embryos were prepared for live imaging as described above. For tissue specific apoptotic assays involving temperature shift *UAS-reaper* expression, embryos were prepared for live imaging as

described previously and mounted on glass slides. Temperature shifting was conducted on a modified heated stage attached to the Elmer Perkin spinning disk system and slides were left to equilibrate for 20 minutes at 29°C prior to imaging. Imaging was conducted at 29°C with time-lapses taken over the course of 2 hours. For analysis of changes in macrophage dispersal after anal pad induced apoptosis experiments, images were partitioned into three 100µm-wide regions/bins starting from the anterior pole of the embryo. Macrophage numbers were counted per bin and the changes in dispersal assessed as the change in macrophage numbers present in each bin area before and after the 2h period at 29°C.

2.4.7 Tracking and quantification of caspase activation events

For experiments using GC3Ai as a marker of caspase activation in live imaging, GC3Ai activation events were determined through observation of morphology and signal intensity. An “activation event” was deemed to have occurred if there was a sustained increase in GC3Ai intensity within a feasible and defined boundary that was above threshold autofluorescence. Tracking of GC3Ai activation was conducted on maximum projection time-lapse movies with cell areas selected and quantified using the polygon tool in Fiji. Caspase intensity curves were calculated via integrated density measurements taken for each selected cell at a given time-point: integrated density was defined as the sum of the pixel intensities within the selected cellular area. Integrated density was used as the apoptotic cell underwent fluctuations in both volume and GC3Ai intensity over time and this was highly variable between individual replicates.

2.4.8 Quantification of macrophage wound responses

To quantify macrophage wound responses, wound areas were first annotated from brightfield images taken at the one-hour timepoint. The number of macrophages in contact with and/or within the perimeter of the wound at one-hour post-injury were scored as “responders”. The wound response is the number of responding macrophages divided by the wound area, normalised to the control average. As a measure of the range over which wound cues can be sensed, the shortest distance between the centre of a non-responding macrophage in the pre-wound image and the wound edge (taken from the 60-minute brightfield image) was measured manually in Fiji and averaged per embryo.

2.5 Preparation of human blood cells and derivatives

2.5.1 Ethical approval

Ethical approval for the isolation and experimentation on healthy volunteer monocyte derived macrophages (MDMs) and neutrophils was given by National Research Ethics Service (NRES) Committee Yorkshire & The Humber – Sheffield (REC reference 05/Q2305/4).

2.5.2 Isolation of whole blood peripheral blood mononuclear cells (PBMCs)

MDMs were utilised as a primary cell model. All cell work was conducted in sterile conditions in a Class II Microbiology safety cabinet. MDMs were differentiated from monocytes isolated from the whole blood of healthy volunteers by plasma/Percoll density centrifugation (Rahman et al., 2019). Blood was taken from a volunteer by a certified phlebotomist and gently added to 3.8% w/v sodium citrate (Ethypharm) at a ratio of 9:1. Sodium citrate was used to inhibit coagulation of the blood during processing. Blood samples were taken into sterile cell culture conditions and gently mixed before being centrifuged at 1200rpm for 20 minutes at 20°C. This results in an upper platelet-rich plasma (PRP) phase, which was removed from the lower blood cell phase and centrifuged at 2000rpm for 20 minutes at 20°C to generate platelet-poor plasma (PPP). Following PRP phase removal, 6µL of 6% dextran (w/v in 0.9% NaCl solution) was added to the lower cell phase, topped to 50mL with 0.9% NaCl solution (Baxter), mixed, and left to sediment at room temperature with the lid loose for 20-30 minutes. Following this, the upper white cell phase was removed and centrifuged at 1000rpm for 6 minutes at 20°C. The pellet was gently resuspended in 2mL PPP and cell populations were separated by plasma/Percoll gradient density centrifugation as described below. Percoll solution (GE healthcare) was diluted 9:10 with saline to make a 90% working solution. Plasma/Percoll gradients of 42% (840µl Percoll/1.16mL PPP) and 51% (1.02mL Percoll/980µl PPP) were made and the 42% gradient carefully layered onto the 51% gradient in a 15mL Falcon tube. White blood cells were slowly layered on to the top and centrifuged at 1100rpm for 11 minutes at 20°C (no brake). This centrifugation yields three distinct cell layers: an upper PBMC layer, a lower granulocyte layer and a dense red blood cell pellet. The PBMC layer was gently removed from the solution and transferred to a tube containing 10mL PPP and 20mL Hanks Balanced Salt Solution (HBBS, Gibco/Invitrogen) without Mg²⁺ and Ca²⁺. Cell number was counted via haemocytometer (Neubauer Improved LO - Laboroptik Ltd) and

washed in HBSS without Mg^{2+} and Ca^{2+} followed by centrifugation at 1500rpm for 6 minutes at 20°C. Cells were resuspended at a density of 4×10^6 cell mL^{-1} .

2.5.2.1 Purification and culture of monocyte-derived macrophages (MDMs)

Isolated PMBCs pellets were resuspended immediately in media without serum, plated at a density of 4×10^6 cell mL^{-1} in 6-well plates (Costar/Corning) and allowed to adhere for 1 hour at 37°C/5% CO_2 . Media and non-adherent cells were then removed and replaced with 4mL RPMI 1640 (Gibco/Invitrogen) media containing 10% Foetal Bovine Serum (FBS; Gibco). To differentiate purified monocytes into MDMs, culture cells were incubated at 37°C/5% CO_2 and the growth media changed within every 2 days for 6-9 days.

2.5.3 Generation of cell supernatants

To challenge MDMs with find-me cues, cell supernatants were generated from primary neutrophil cultures. Neutrophils were generated and purified using the percoll gradient method described above. Isolated neutrophils were plated at 5 million cells mL^{-1} and aged overnight (approximately 22 hours) to generate “apoptotic derived supernatant” (ASN) (Renshaw et al., 2003). Prior to aging, neutrophils were treated with 20 μ M Q-VD-OPh (Merck) to produce “apoptotic null supernatant” (ANN). “Necrotic supernatant” (NSN) was produced by flash-freezing suspended neutrophils at -80°C to induce cell lysis. Cell debris was removed from supernatant samples via centrifugation (10000rpm for 2 minutes).

2.6 Cell migration assay methods

2.6.1 Principles of the Ibidi® μ -slide chemotaxis chamber

The Ibidi μ -slide chemotaxis assay is designed to measure and define chemotaxis for cell types within a micro-fluidic chamber (Zengel et al., 2011). The slide is composed of a triplicate set of observation chambers linked to two media reservoirs that serve to deliver a stable chemokine gradient to cells (**Figure 2.1**). Migration of cells within the observation area can be used to assess chemotaxis, which each slide containing three conditions: an experimental chemoattractant chamber (1) wherein a directional chemoattractant gradient is applied in one direction; a chemoattract negative control chamber (2) that has opposing gradients of vehicle control, typically the solvent used in preparation of the chemoattractant

e.g., phosphate buffered saline (PBS); and a chemoattract positive control chamber (3) that has opposing gradients of the chemoattractant in question applied so that the cells are exposed to opposing gradients in the observation area. If a chemoattract is effective, it would be expected that chamber 1 would see no net migration, chamber 2 would see either no net migration or migration in both directions to a similar degree and chamber 3 would see a directional migration towards the chemoattractant side of the chamber.

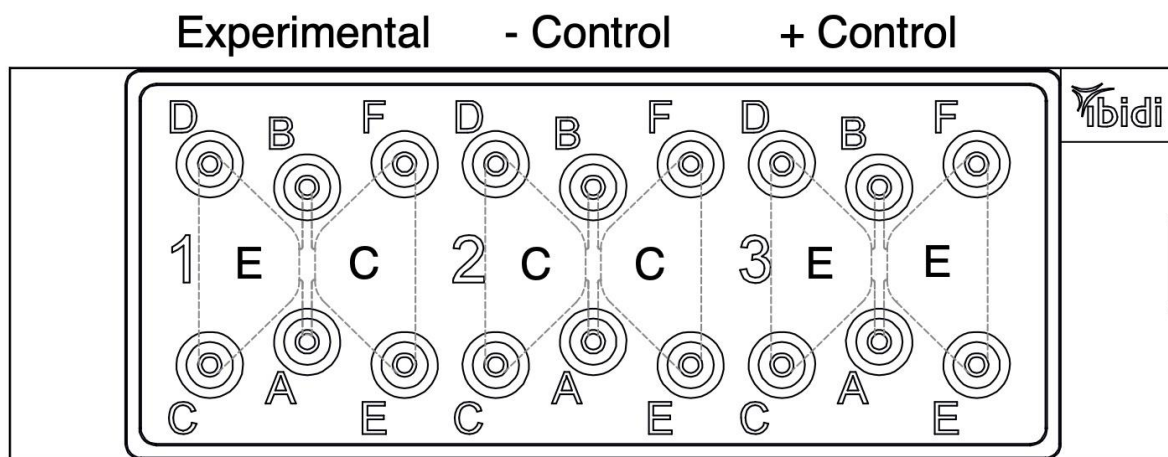


Figure 2.1 – Schematic and dimensions of the ibidi® μ-slide chamber

The ibidi μ-slide is composed of three identical chambers allowing for an experimental, double-negative, and double-positive wells. The experimental well contains a reservoir with a chemotactic (E) and vehicle control (C) solution. The negative control and positive control sections have either vehicle or chemotactic media, respectively. For each chamber, cells were loaded into port A, with media drawn from port B to aspirate cells into the observation area. Media and chemokine solution was injected into ports C and E, with media removed via ports D and F. All ports were sealed with plastic plugs after filling. Dimensions of the chamber were as follows: Chemotaxis chambers on slide = 3, volume per chamber = 120μL, observation area = 2x1mm², coating area per chamber = 3.50cm² and 0.27cm² (Full chamber and observation area respectively), distance between chambers = 18.5mm, total height with plugs = 12mm, volume chemoattractant= 30μL. Imaged reproduced from <https://ibidi.com/channel-slides/9--slide-chemotaxis-ibitreat.html> (Ibidi specifications page).

2.6.2 MDM culture methods and preparation for chemotaxis assays

At day 6-9, cells had typically reached an appropriate state of differentiation for chemotaxis experiments to be conducted (Daigneault et al., 2010). Cell cultures were gently washed in media and the media aspirated. Cells were detached from wells by addition of either 0.2% EDTA-PBS or Accutase solution (Sigma-Aldrich). For EDTA-PBS detachment, 0.5mL of 0.2%

EDTA-PBS was added to each well and the cells incubated at 4°C for 30 minutes. For Accutase-based detachment, cells were removed from culture and washed as above, before 1.2mL room temperature Accutase was added, and cells incubated at 37°C/5% CO₂ for 10 minutes. Detached cells were transferred to a tube and topped to approximately 3-5mL with either RPMI 1640 (Gibco/Invitrogen) supplemented with 10% Fetal Bovine Serum (FBS) media (EDTA-PBS method) or RPMI 1640 (no FBS added) (Accutase method). Cells were counted using a haemocytometer and centrifuged at 1500rpm for 6 minutes at 20°C before being reconstituted to a concentration of 4x10⁶ cells mL⁻¹. For experiments that used automated nuclei tracking, cultured cells were treated with 1mL NucBlue (Invitrogen) prior to detachment to stain nuclei.

2.6.3 Chemotaxis slide workflow and experimental set-up

Degassed slides and media were removed from incubation at 37°C/5% CO₂ immediately prior to loading with cells. MDM cultures between days 6-9 were detached and pelleted before being resuspended at a density of 4x10⁶ cell mL⁻¹ in RPMI 1640 without FBS. 6µl of cell suspension was loaded into each of the three observation chambers and the µ-slide sealed with a lid and placed in an incubator at 37°C with 5% CO₂ for 45 minutes to allow adhesion of MDMs. Adherent cells were washed twice with 10µl RPMI 1640 supplemented with 1% FBS in the experimental and double-negative chambers. For double-positive chambers, cells were instead twice washed in a solution containing RPMI 1640 + 1% FBS + a 50% concentration of experimental chemokine or vehicle (50% of the experimental dose); this step was required to prevent rapid unidirectional chemotaxis towards to first side to be loaded with chemokine for double-positive chamber. After washing, reservoirs were filled in a stepwise manner with 65µl of RPMI 1640 supplemented with 1% FBS and filled with 2x 15µl of appropriate chemokine or vehicle, with equal media aspirated from the other side. After loading with chemokine, chambers were sealed with plugs and taken for microscopy. The following chemoattracts were used: 1ngmL⁻¹, 500ngmL⁻¹ and 1µgmL⁻¹ N-formyl-Met-Leu-Phe (fMLP in DMSO; Sigma-Aldrich) – a bacterial antigenic peptide (Schiffmann et al., 1975), 1ngmL⁻¹, 10ngmL⁻¹ and 200ngmL⁻¹ Monocyte Chemoattractant Factor 1 (MCP-1 in DMSO) – an established immune chemokine (Audran et al., 1996) and 40nM Complement protein 5a (C5a in PBS) – a pro-inflammatory fragment of the complement immune cascade system

(Snyderman et al., 1972). For chemotaxis experiments, solvent vehicles were used as negative controls.

2.6.4 Processing and analysis of MDM chemotaxis in μ -slides

To accurately track migrating MDMs, both manual and automated tracking were used. For MDMs that did not have their nuclei stained, movies were blinded, and 40 cells tracked (10 per FOV quadrant) using the Fiji manual tracking plug-in. For cells with a nuclear stain, automated tracking was performed using the Fiji Trackmate plug-in. A Laplacian of Gaussian (LoG) algorithm (Xu et al., 2017) was used to track nuclei movements over the course of movies using the following parameters: minimal nuclei size = 5 μ m diameter, estimated nuclei diameter = 15 μ m, assumed maximum travel distance per frame = 50 μ m. Migration data was extracted from raw tracking values using the Fiji Ibidi chemotaxis tool plug-in with tracks filtered between 2-100 μ m travel distance to remove non-migratory dead cells and “loose cells” passively moving via flow in the chamber. Migration of MDMs challenged with chemoattractant was assessed by comparing the forward migration index (FMI) parallel to the gradient (FMI $_{||}$) against that perpendicular to the gradient (FMI $_{\perp}$). These values were calculated according to the following equation:

$$FMI_{\perp} = \frac{1}{n} \sum_{i=1}^n \frac{X_{i, end}}{d_{i, accum}} ; FMI_{||} = \frac{1}{n} \sum_{i=1}^n \frac{Y_{i, end}}{d_{i, accum}}$$

Where n= number of cells, $X_{i, end}$ and $Y_{i, end}$ denote the average end points of each cell track on the x and y-axis, $d_{i, accum}$ is equal to the average total accumulated distance moved by each cell (Zengel et al., 2011).

The Rayleigh test (Wilkie, 1983) was also used to test for non-randomised movement of cells. This assesses if the migration measured is significantly different to the theoretical pattern that would occur if the cells moved randomly from their starting points (Wilkie, 1983). Responses were considered chemotactic if they met the following conditions: (1) the experimental chamber FMI $_{||}$ value was significantly greater than from the experimental FMI $_{\perp}$ with Rayleigh test p values ≤ 0.05 ; (2) control FMI $_{||}$ values were not significantly different to FMI $_{\perp}$ values with Rayleigh test p-values >0.05 .

2.7 Data tabulation and statistical analyses

All manual analysis was conducted on blinded data to prevent observer bias. This includes data regarding the assessment of macrophage morphology, macrophage counts, macrophage tissue recruitment and cell tracking using the manual tracking plug-in.

Numerical data was collated in Microsoft Excel and statistical analyses performed in GraphPad Prism 9. Numerical data was statistically analysed using unpaired, two-tailed Student's t-tests or Mann-Whitney tests to compare means for parametric and non-parametric data, respectively. Where greater than two means were compared, a one-way ANOVA with a Dunnett's post-test was used. P-values were reported as significant at a threshold of $p < 0.05$. For statistics related to experiments using *Drosophila*, quoted n-numbers in legends refer to the number of *Drosophila* embryos analysed, with individual macrophage values used to calculate averages per macrophage, per embryo.

All Ibbidi chemotaxis data was statistically analysed using either a 2-tailed Student's t-test or a one-way ANOVA with Tukey's test depending on the number of conditions being compared. Comparisons between automated and manual tracking methods were analysed using Wilcoxon t-tests for paired non-parametric data. Comparisons between FMI values, migration distance or FMI difference were made using the 2-tailed Student's t-test or 1-way ANOVA with Tukey's test depending on the number of conditions. For all MDM cell migration experiments, quoted n numbers refer to the population average for a single migration experiment where the average is calculated from tracking data of a minimum of 20 individual cells.

Chapter 3: Investigating the dynamics of efferocytosis during *Drosophila* embryogenesis

3.1 Introduction

3.1.1 Apoptosis in mammals and *Drosophila*

Apoptosis is the most common form of programmed cell death (PCD) and is critical to the life course of multicellular organisms (Fuchs and Steller, 2011). The activation of apoptosis can be induced through a variety of extrinsic or intrinsic stimuli, e.g., through recognition of pro-apoptotic ligands or DNA damage (Galluzzi et al., 2012; Green and Llamby, 2015). After the apoptotic pathway has been stimulated, it is the activity of proteolytic, executor-type caspase enzymes (Caspase-3, -6 and -7) that mediates apoptotic progression through degradation of cell components and activation of downstream effectors, such as ROCK1 (Coleman et al., 2001; Pop and Salvesen, 2009). *Drosophila* share a highly-conserved apoptotic pathway with mammals, with several – but not all – forms of PCD known to occur within the adult fly (Jenkins et al., 2013). Like mammals, *Drosophila* express several pro-caspase enzymes that are inhibited during homeostasis through the activity of inhibitor of apoptosis proteins (IAPs). Apoptotic stimuli, such as ionising radiation, can activate the expression of the pro-apoptotic Reaper, Grim and Hid proteins, collectively referred to as the RHG genes (Abrams, 1999) that work to suppress the anti-apoptotic functions of the IAPs. With IAP function repressed, caspase zymogens can be activated and begin to proteolytically degrade the cell and progress apoptosis e.g., caspase-mediated DNA fragmentation (Steller, 2008). One of the key functions of these caspase cascades is the activation and release of chemoattractant molecules, collectively referred to as find-me cues, which induce the recruitment of phagocytic cells and the clearance of dying cells via phagocytosis, a process known as efferocytosis (Ariel and Ravichandran, 2016). While the existence of *Drosophila* find-me cues has not been conclusively shown, it is known that *Drosophila* embryos possess an efficient efferocytosis pathway (Evans and Wood, 2014; Roddie et al., 2019) and a robust immune system comprising macrophage-like phagocytes referred to as plasmatocytes or macrophages (Evans et al., 2003; Evans and Wood, 2011; Wang et al., 2014). By studying the activity of caspase

enzymes, and thus find-me cues in *Drosophila* embryos, it should be possible to elucidate the dynamics behind the find-me phase of efferocytosis and its relationship to caspases.

3.1.2 Assaying apoptosis via non-genetic methods

The development of accurate apoptosis reporters has been of great interest to the field for decades due to the role of apoptosis in inflammatory diseases such as atherosclerosis (Thorp et al., 2011) and its importance during development (Voss and Strasser, 2020). Apoptotic detection methods have focused on several different targets, while *ex vivo* methods typically rely on reporting the downstream effects of caspase activation through detection of apoptotic progression markers or proteolytic activity. Some of the earlier methods of apoptotic detection reported key apoptotic pathway events: these included changes to cellular pH (acridine orange) (Palmgren, 1991) damage to nuclear DNA via SYTO probes or terminal deoxynucleotidyl transferase-mediated dUTP nick end-labelling (TUNEL) (Brambilla et al., 1996; Wlodkowic et al., 2007), phosphatidylserine exposure on the outer membrane (Blankenberg et al., 1998) or direct detection of pro-caspase zymogen activation (Song et al., 1997a; Amstad et al., 2001) and subsequent protease activity (Florentin and Arama, 2012). While these methods are powerful tools to evaluate apoptosis, the key drawback regarding these reporters is that they are largely applied *ex vivo* and thus only capture apoptosis at a single time point. The lack of temporal resolution precludes their effective use in model organisms to study efferocytosis, although they are still applicable for assaying metrics such as the presence of apoptotic bodies within a given tissue or the relative ability of immune cells to remove dead cells in different conditions.

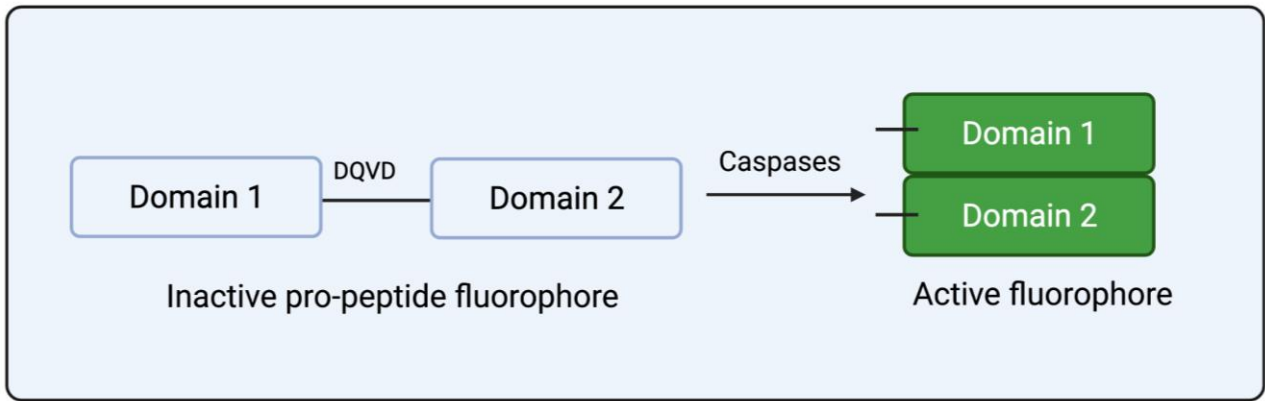
3.1.3 Genetically-encoded apoptosis reporters

While *ex vivo* methods can be highly effective, enhancements in fluorophore design and genetic manipulation has driven the development of genetically-encoded reporter systems that allow for *in vivo* visualisation (Berlin and Carroll, 2020). Several approaches have been taken to devise genetically encoded apoptosis reporters, primarily designed around the detection of caspase activity through exogenous fluorescent substrates (**Figure 3.1**).

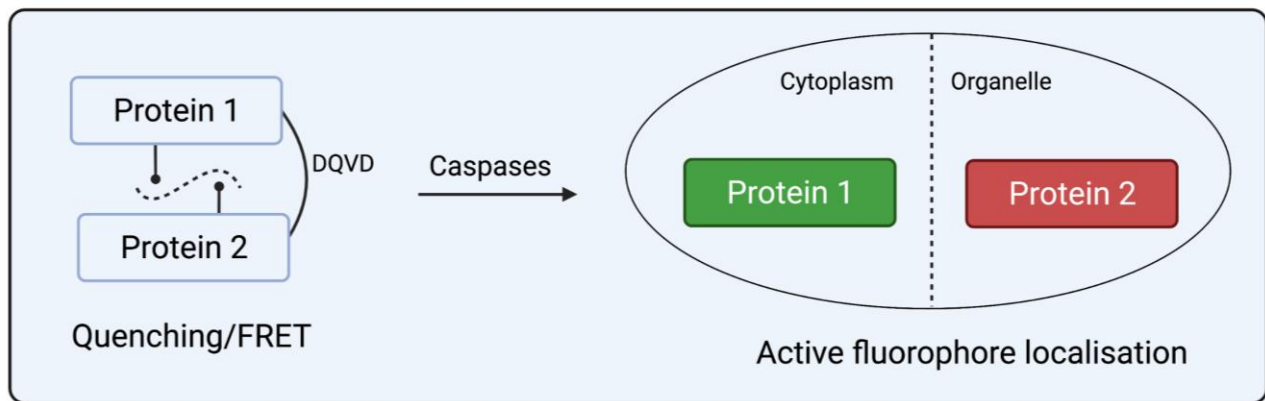
Several published tools rely on caspase-dependent Förster resonance energy transfer (FRET): In this design, the excitation of a pair of fluorophores will shift depending on their distance to each other (Piston and Kremers, 2007). By linking the FRET pair via a caspase-sensitive

sequence, the changes in fluorescence as a result of the pair separating can be used to read-out caspase activity (Takemoto et al., 2003; To et al., 2016; Zlobovskaya et al., 2016). As an alternative to FRET, several groups have used sub-cellular trafficking moieties such as the nuclear localisation sequence (NLS) (Imamoto, 2000) to induce the localisation of signal-tagged fluorophores in the presence of active caspases (Mazzalupo and Cooley, 2006; Bardet et al., 2008; Liesche et al., 2018). A more novel method is the use of split GFP, wherein the formation of active GFP is dependent on the activation of caspase harbouring a partial GFP structure that interacts with the inert freely dispersed half to produce the active fluorophore (Anson et al., 2021). One approach of note for *in vivo* models is the use of caspase-dependent transcription factors. Despite the alterations to DNA that occur during apoptosis, expression has been shown to still be active for particular genes (Bushell et al., 2006). By combining caspase-sensitive fluorophores with transcription factors such as GAL4 or the QF system, apoptotic cells can be made to produce additional fluorophores thereby boosting the signal and providing better resolution on the progression of apoptosis (Tang et al., 2015; Baena-Lopez et al., 2018).

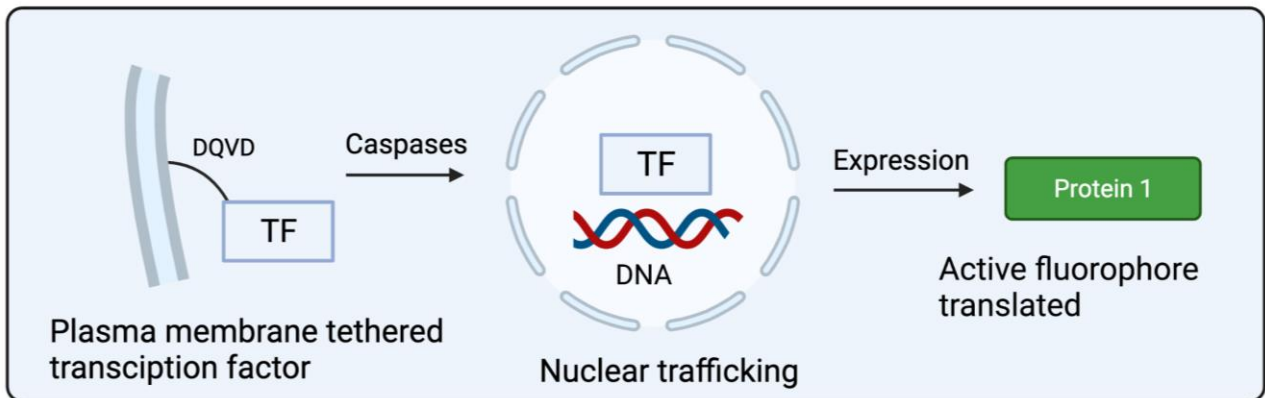
A - Direct caspase-activated fluorophores



B - Förster resonance energy transfer (FRET) and fluorophore trafficking



C - Caspase-mediated transcription of fluorophores



D - Caspase-mediated fluorophore assembly

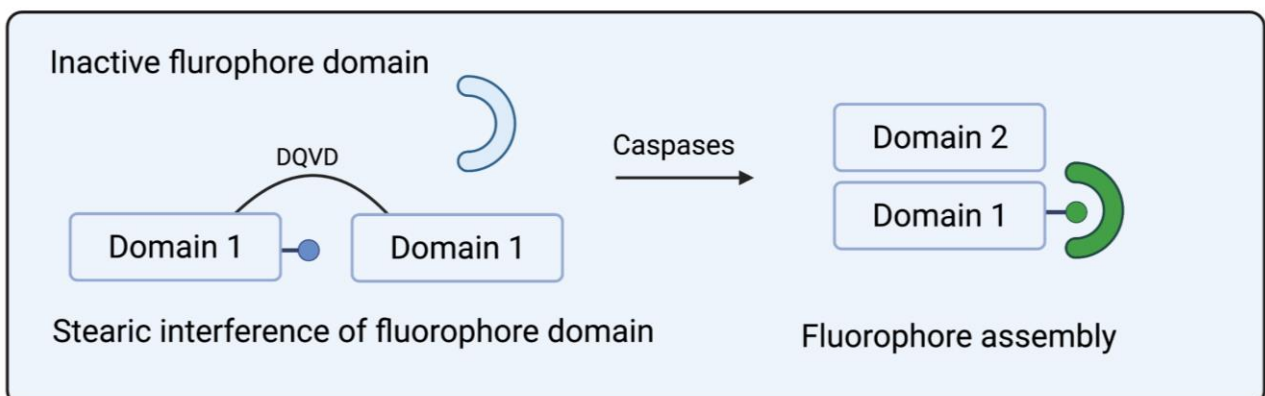


Figure 3.1 – Genetic methods for assaying apoptosis *in vivo*

(A) Schematic diagram of caspase-sensitive fluorophores; in this system, fluorophores are expressed as an inactive pro-peptide containing a caspase cleavage sequence (DQVD). Upon caspase activation, the sequence separating the domains is cleaved, allowing the protein to undergo a conformational change into the fluorescently active form e.g. GC3Ai (Schott et al., 2017). **(B)** Schematic diagram of caspase reporters based on Förster resonance energy transfer or fluorophore quenching e.g. iCasper (To et al., 2016). In this model, the presence of 2 fluorophores linked via a caspase cleavage sequence interact to either exchange electrons (FRET) or inhibit the other (quench), as indicated by the curled dashed (---) line. When caspases are active, the proteins are separated and can be trafficked to different organelles via their localisation sequences. Caspase activity can therefore be measured through the active fluorescence or through the change in FRET levels between the differently localised reporters. **(C)** Schematic diagram of transcription-based caspase reporters. This system relies on a two-step activation system wherein a transcription factor (TF) is sequestered from the nucleus, e.g., tethered to the plasma membrane via a caspase-sensitive sequence e.g. CaspaseTracker (Tang et al., 2015). Once caspases are activated, the TF can translocate to the nucleus and induce the expression of a reporter fluorophore. **(D)** Schematic diagram of split domain caspase reporters e.g. Caspase-GFP (Anson et al., 2021). This system requires the expression two reporter components: a freely available domain and a domain suppressed by steric interference on a caspase sensitive protein. When the protein is cleaved by caspase, the conformational change exposes the reporter domain, allowing it to interact with the freely localised domain and form an active fluorophore.

3.1.4 Assaying efferocytosis during *Drosophila* embryogenesis

To understand how macrophages are recruited to apoptotic cells in *Drosophila*, it is critical to use a system that allows for the live reporting of both macrophages and dying cells *in vivo* which captures the entire efferocytosis process from the stimulation of apoptosis to post-clearance. Genetically-encoded fluorescent apoptosis reporters have been extensively utilised in *Drosophila* (Bardet et al., 2008; Tang et al., 2015; Baena-Lopez et al., 2018; Roddie et al., 2019). To study efferocytosis *in vivo*, it is necessary to use reporters that:

1. specifically label tissues that are entering apoptosis at an early stage
2. label morphological features required to identify apoptotic progression

To this end, Genetically-encoded, caspase-activated variants of mCherry (CC3Ai), Venus (VC3Ai) and GFP (GC3Ai) (collectively referred to as XC3ai), recently developed by Schott *et al.* (2017), were utilised. These fluorescent proteins have been altered to contain a critical caspase cleavage DEVD motif within the β -barrel structure. This design means that these

fluorophores only become fluorescent upon cleavage by caspases within the cytoplasm, generating a distinct signal within each cell, marking the beginning of executor caspase activity.

The aim of this chapter was to validate and apply these sensors to examine the interplay between caspase activation and apoptosis *in vivo*. I sought to use the XC3Ai sensors in conjunction with macrophage reporters including *SrpHemo-3X-mCherry*, a gene fusion reporter that drives the expression of mCherry under the control of the macrophage *Serpent* promoter (Gyoergy et al., 2018) to assay the response of macrophages to “Caspase-ON” cells. Using this system, the relationship between caspase activity and the find-me phase of efferocytosis can be assayed *in vivo* to understand if find-me cues are present within the fly and if so, the timescales and distances they might act over. Additionally, the cytoplasmic nature of the reporters can allow us to study the eat-me phase of efferocytosis, especially the macrophage-apoptotic cell interface and post engulfment behaviour. Finally, by tracking the outcome of apoptotic cells it should be possible to study how caspase activation is related to the fate of the cell e.g., if it is engulfed by macrophages, undergoes necrosis or other outcomes.

3.2 Results

3.2.1 Development and validation of ubiquitous embryonic GC3Ai recombinants

To utilise XC3Ai sensors within the *Drosophila* embryo, *UAS-XC3ai* was expressed ubiquitously using *daughterless-GAL4 (da-GAL4)* (Ito et al., 1997) or *act5C-GAL4* (Wodarz et al., 1995). Recombination of the *GAL4* and *UAS* linked elements was performed using standard spontaneous *Drosophila* recombination (Hiraizumi, 1971) and successful recombinants were screened using PCR (data not shown). Stable *Drosophila* stocks were generated for *w¹¹¹⁸::daughterless-GAL4,UAS-GC3Ai* and *w¹¹¹⁸::daughterless-GAL4,UAS-VC3ai*. These constructs will herein be referred to as ubiquitous GC3Ai or VC3Ai expression systems unless otherwise stated.

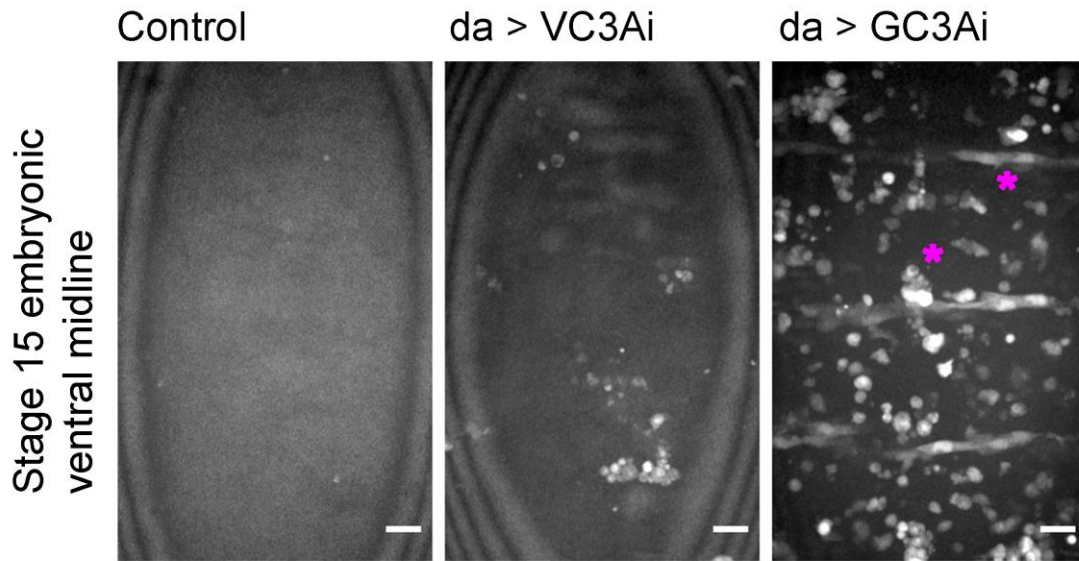
To validate expression of recombinant apoptotic sensors during development, embryos ubiquitously expressing GC3Ai and VC3Ai were imaged using confocal microscopy and

compared to *w¹¹¹⁸* controls. Both ubiquitous GC3Ai and VC3Ai reported the presence of what were presumed to be caspase-positive cell bodies compared to the apoptotic sensor-negative controls (**Figure 3.2A**). While some signal was observed in control embryos, this was much less intense and likely the result of autofluorescence within the ventral tissues (**Figure 3.2A, left**). While both GC3Ai and VC3Ai were able to resolve caspase-positive structures within the embryo, GC3Ai appeared to report a greater range of intensities and morphologies, including rounded, possibly engulfed cells and caspase-active cells still bearing an epithelial morphology (**Figure 3.2B**).

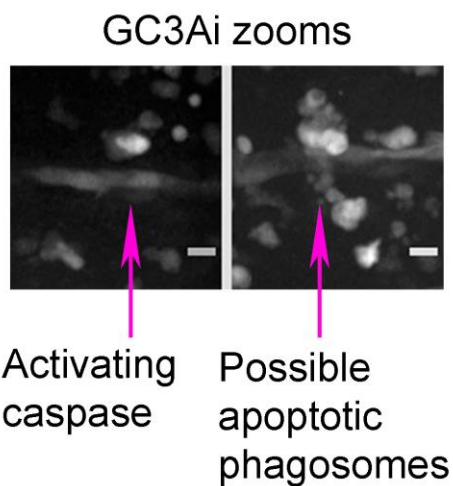
In addition to GAL4-dependent expression, GC3Ai was cloned downstream of the ubiquitous promoter from the *armadillo* gene (pArmP-PolyA-AttB vector) to produce *arm-GC3Ai*. *arm-GC3Ai* was screened in *Drosophila* embryos (**Figure 3.2C**), L3 larvae and adults (data not shown). While PCR testing and confocal microscopy confirmed the expression of *arm-GC3Ai* in the embryo, it had a detection threshold near to autofluorescence levels, even when multiple gene-copies were present (**Figure 3.2C**), rendering it sub-optimal for embryonic work. Similar detection issues were found in both L3 larvae and adult flies; these transgenics were not used further in this chapter.

These results confirm that both GAL4-dependent ubiquitous GC3Ai, VC3Ai and GAL4-independent *arm-GC3Ai* were expressed in the *Drosophila* embryo. Microscopy observations found that ubiquitous GC3Ai had a lower detection threshold, i.e., a lower light exposure requirement and greater labelling numbers than both VC3ai and *arm-GC3Ai*. While the transgenic *arm-GC3Ai* constructs were functional, the apparent low expression rate required four copies of the transgene to be present within a single embryo, making it unsuitable for practical use. Due to this, ubiquitous GAL4-mediated GC3Ai was chosen going forward for validation and efferocytosis assays.

A Confirmation of ubiquitous XC3Ai expression



B GC3Ai examples



C GAL4-independent expression

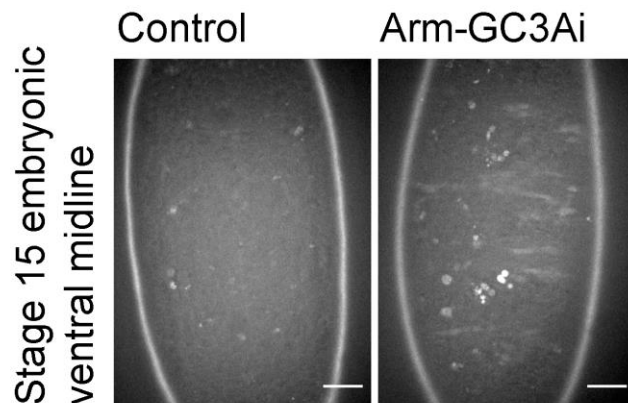


Figure 3.2 – Confocal confirmation of embryonic XC3Ai expression

(A) Cropped $\sim 21\mu\text{m}$ maximum projections of the embryonic ventral midline of w^{1118} control and embryos with ubiquitous expression of GC3Ai or VC3Ai (homozygous for GAL4 and UAS transgenes); magenta asterisk indicate corresponding regions in panel B; scale bars denote $10\mu\text{m}$. (B) Cropped, zoomed $\sim 21\mu\text{m}$ maximum projections of the embryonic ventral midline in GC3Ai-expressing embryos with magenta arrows illustrating the reporting of different cell morphologies, e.g., caspase activation in an epithelia-like cell and rounded clusters (right) presumed to be held within macrophage phagosomes; scale bar denotes $5\mu\text{m}$. (C) Single z-slice of the ventral embryonic midline for w^{1118} control and $w;arm\text{-GC3Ai}$ expressing embryos; scale bar denotes $10\mu\text{m}$. Genotypes were as follows: controls (w^{1118}), GC3Ai ($w^{1118};da\text{-GAL4,UAS-GC3Ai}$), VC3Ai ($w^{1118};da\text{-GAL4,UAS-VC3Ai}$) and $arm\text{-GC3Ai}$ ($w^{1118};arm\text{-GC3Ai};arm\text{-GC3Ai}$ – i.e., 4 copies of the transgene).

3.2.2 Embryonic GC3Ai accurately reports developmental apoptosis compared to cDCP-1

Schott et al. (2017) have previously published that the XC3Ai sensors have a better detection threshold compared to immunostaining against cleaved-caspase protein DCP-1 (cDCP-1) in the embryonic ectoderm. To validate these data and confirm that GC3Ai was specific to apoptosis, embryos expressing ubiquitous GC3Ai were stained for both GC3Ai (anti-GFP) and activated caspase (anti-cDCP-1). Several controls were used to test if GC3Ai is specific to apoptotic cells and scales with varying levels of apoptosis. To test that GC3Ai was specific to apoptosis, three controls were used: *w¹¹¹⁸* embryos not expressing GC3Ai (GC3Ai negative); embryos expressing GC3Ai ubiquitously during embryogenesis (wild-type); and *Df(3L)H99* embryos which carry a genomic deletion that removes the three core pro-apoptotic proteins encoded on chromosome 3: *reaper*, *hid* and *grim* (RHG) (Abrams, 1999) and thereby prevents the activation of apoptosis within the embryo (Zhou et al., 1995). To assess how GC3Ai performs at increased rate of apoptosis, embryos containing *CyO hs-hid* and expressing GC3Ai ubiquitously were tested: *hs-hid* is a temperature-sensitive genetic construct will express the pro-apoptotic gene *hid* under the control of the heat-shock response protein *hsp70* promoter when the embryos are incubated at 39°C (Grether et al., 1995; van Doren, 1996).

Stage 15 embryos were collected, fixed and immunostained prior to confocal imaging. Control embryos lacking GC3Ai expression showed no signal above background when compared to cDCP-1 staining, which labelled several apoptotic cells in the ventral epithelia (**Figure 3.3A-A'**). Wild-type conditions showed substantial levels of staining and a large degree of co-localisation between both GC3Ai and cDCP-1, denoted by the white colouration in the merged channel images (**Figure 3.3B**). Of note, colocalisation appeared to occur more within suspected phagosomes, possibly due to the shrinkage of the apoptotic cell body concentrating both of the reporters (**Figure 3.3B'**). At high apoptotic levels, both GC3Ai and cDCP-1 reported an increased number of apoptotic bodies compared to wild-type conditions (**Figure 3.3C**). At higher apoptotic levels, cDCP-1 staining appeared to become less specific, with non-defined staining occurring (**Figure 3.3C'***) in addition to a loss of colocalised structures (**Figure 3.3C'**). As expected, *Df(3L)H99* embryos expressing GC3Ai but lacking

apoptosis showed no discernible signal in either the GC3Ai or cDCP-1 channels (**Figure 3.3D-D'**). To compare the quantification of apoptotic levels using GC3Ai or cDCP-1, Imaris 4D rendering software was used to identify the number of positively stained punctae in each channel. Apoptotic body counts (apoptotic burden) show that at wild-type and high levels of apoptosis both GC3Ai and cDCP-1 label a comparable number of apoptotic bodies (**Figure 3.3E**).

To compare the level of GC3Ai and cDCP-1 colocalisation, the relative signal overlap between the two reporters were calculated (% voxels positive for both reporters). This measurement reports the extent to which each reporter labels the corresponding xy location in the other channel. At both wild-type ($p=0.04$) and high apoptotic conditions ($p<0.0001$), GC3Ai colocalised to a greater degree than cDCP-1, e.g., more DCP-1 positive voxels also contained GC3Ai compared to GC3Ai positive voxels containing cDCP-1 signal (**Figure 3.3F**). Taken together, these results confirm that GC3Ai accurately reports caspase activation during embryogenesis and has greater coverage compared to cDCP-1 staining in high apoptotic environments.

A Comparison GC3Ai and cDCP-1 *ex vivo*

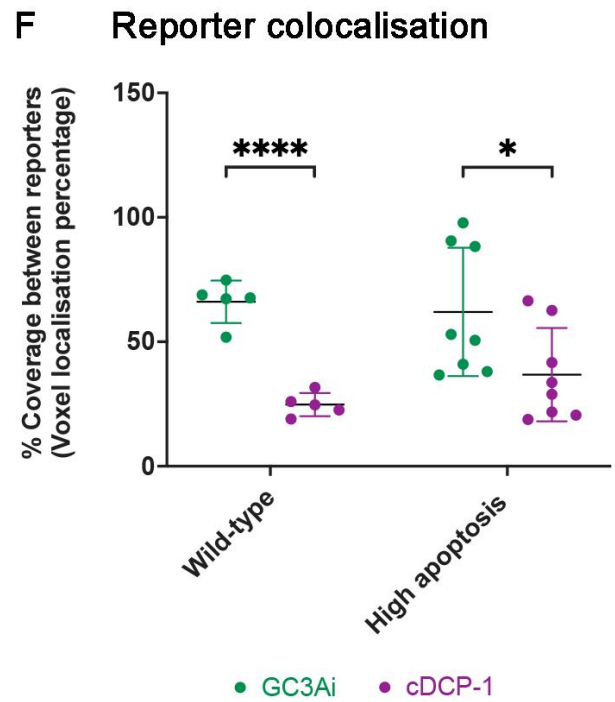
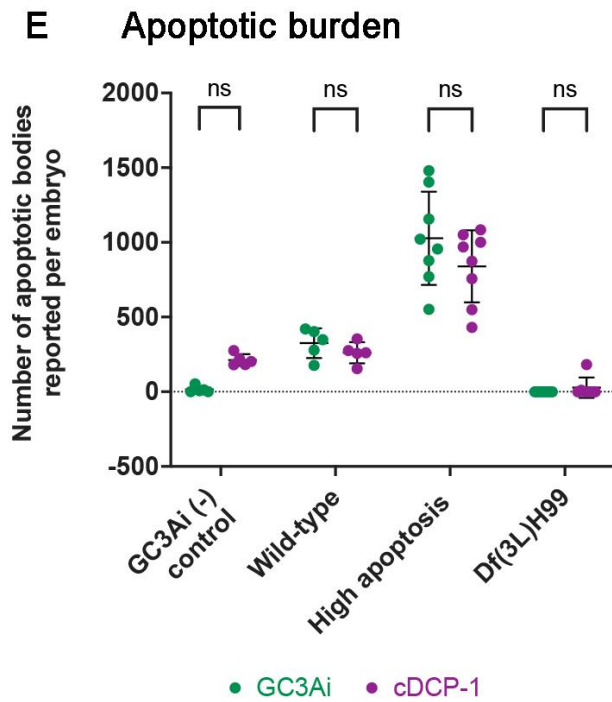
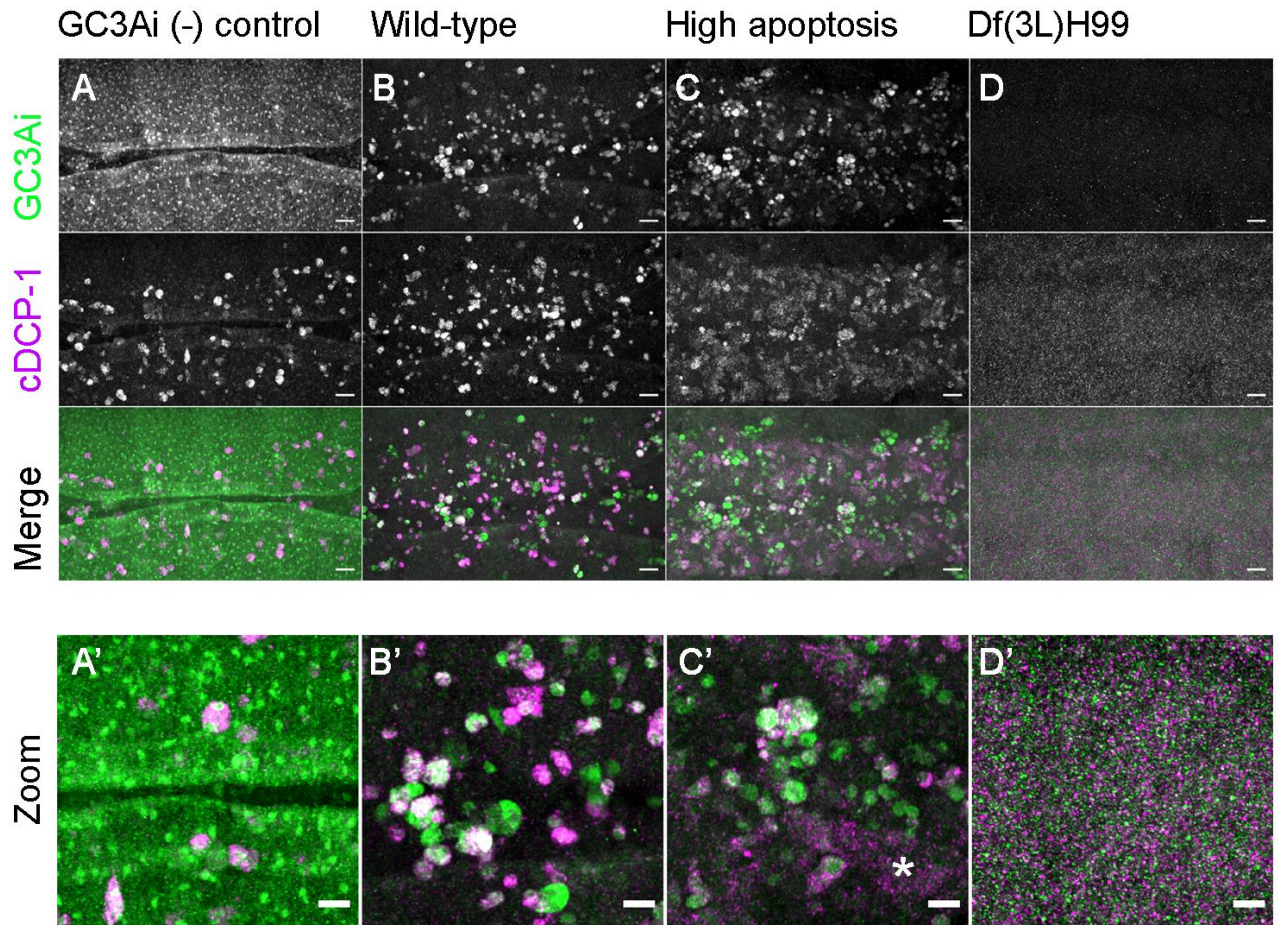


Figure 3.3 – GC3Ai accurately reports *Drosophila* embryonic apoptosis compared to cDCP-1 staining

(A-D) Maximum projection images of the ventral side of stage 15 *Drosophila* embryos immunostained for GC3Ai (anti-GFP) and cleaved DCP-1 (anti-cDCP-1); (A'-D') show zooms taken from images in (A-D). (A-A') Control w^{1118} embryo lacking GC3Ai expression showing cDCP-1 staining (A). (B-B') Embryo expressing GC3Ai ubiquitously ($w;;da-GAL4,UAS-GC3Ai$) showing both cDCP-1 and GC3Ai positive punctae with zooms highlighting individual and colocalised (white) regions (B'). (C-C') *hs-hid* containing embryos fixed 30 minutes after 10 minute 39°C heat-shock expressing GC3Ai ubiquitously ($w^{1118};+/CyO\ hs-hid;da-GAL4,UAS-GC3Ai$) showing GC3Ai and cDCP-1 staining (C) with zoomed sections highlighting dispersal of the cDCP-1 signal (*) (C'). (D-D') *Df(3L)H99* embryos lacking apoptosis expressing ubiquitous GC3Ai ($w;act5C-GAL4/UAS-GC3Ai;Df(3L)H99$) (D) with zooms showing no discernible structures in either GC3Ai and cDCP-1 channels (D'). (E) Comparison of apoptotic body numbers between GC3Ai and cDCP-1 channels per condition. (F) Comparison of percentage voxel overlap values for GC3Ai and cDCP-1 as a readout for colocalisation. Statistical significance is reported as ns= $p>0.05$, * = $p<0.05$ and *** = $p<0.0001$. Scale bars denote 10 μ m for full image panels and 5 μ m for zooms, respectively.

3.2.3 Embryonic GC3Ai outperforms other live-apoptosis tracking tools

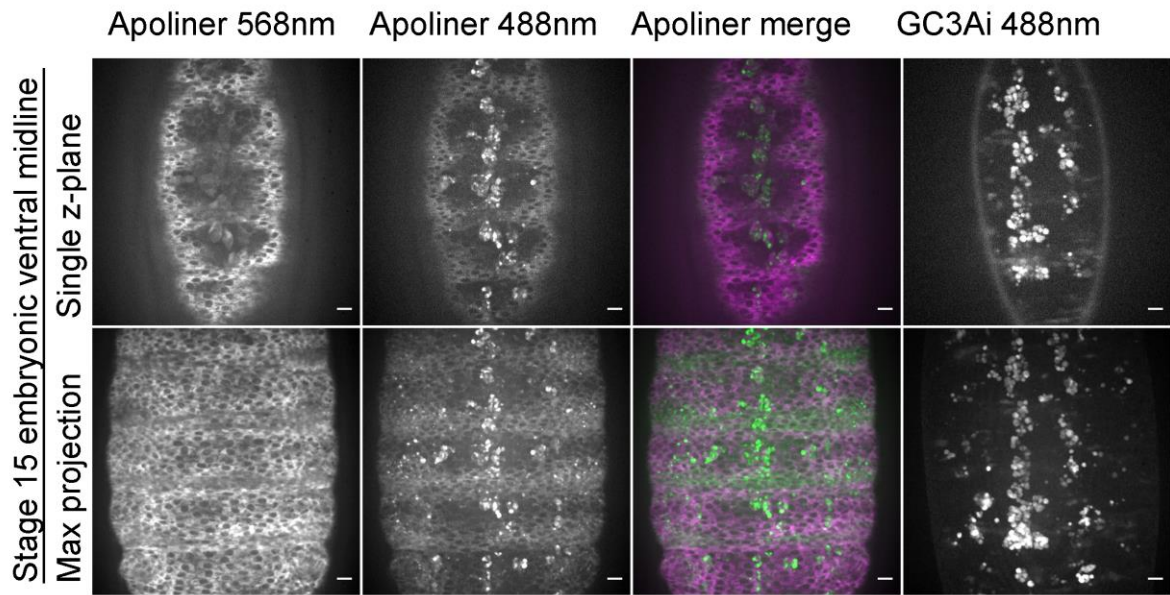
While anti-cDCP-1 is commonly used for *ex vivo* analysis of apoptosis, live staining and genetically-encoded tools have also been developed that are amenable for use in *Drosophila* embryos. Two commonly used methods are the pH-sensitive vital dye acridine orange (AO) (Palmgren, 1991) and *UAS-Apoliner* (Bardet et al., 2008). Apoliner is a caspase-sensitive reporter system that relies on caspase-induced fluorophore localisation. In the absence of caspase activity, both the RFP and GFP moieties remain at the cell membrane via a CD8 membrane tether, while caspase-mediated cleavage between the two fluorophores leads to release and delocalisation of NLS-GFP to the nucleus.

To assess the merits of GC3Ai compared to these other reagents, comparative imaging was performed on embryos expressing GC3Ai, Apoliner or stained with acridine orange. Since both GC3Ai and Apoliner rely on modified versions of GFP, direct comparison of Apoliner and GC3Ai comparison was not possible. Instead, stage 15 embryos ubiquitously expressing either Apoliner or GC3Ai were imaged at the ventral midline and compared qualitatively. Single z-slices and maximum projection comparisons highlight that Apoliner requires both 488nm and 568nm channels to distinguish apoptotic cells (Figure 3.4A-C). Merged images can be used to resolve structures such as hemocytes containing apoptotic cells visible in merged images (*,

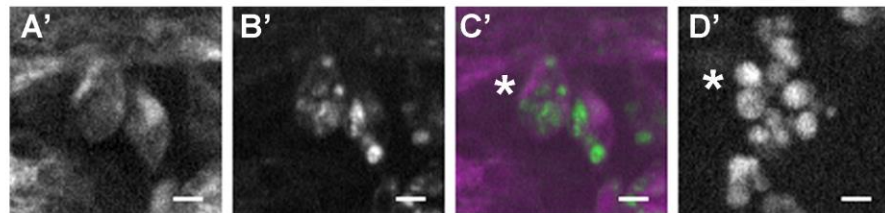
Figure 3.4C'). In contrast, embryos expressing GC3Ai report apoptosis within a single channel in a similar pattern to that observed with Apoliner (**Figure 3.4D**). As with Apoliner, GC3Ai can be used to resolve specific structures such as hemocytes that contain apoptotic cells (*****, **Figure 3.4D'**). In contrast to Apoliner and GC3Ai, acridine orange staining does not directly label a particular apoptotic process and is instead a marker of cellular acidification through a poorly defined mechanism (Palmgren, 1991; Arama and Steller, 2006). Stage 13 *w¹¹¹⁸* embryos and embryos expressing GC3Ai ubiquitously were mounted and imaged to assess apoptotic cell labelling at the ventral midline. Both GC3Ai and AO showed substantial labelling at the ventral midline, presumed to be phagosomes within hemocytes that contain multiple apoptotic cells (**Figure 3.4E-F**). The presence of phagosome-like structures in both AO and GC3Ai-labelled embryos suggests that AO can permeate phagosomes and that GC3Ai is able to survive acidification e.g., both reporters are present within presumed apoptotic cells present within the phagosome (**Figure 3.4E'-F'**).

These results show that while Apoliner and acridine orange are powerful tools to report apoptosis within the *Drosophila* embryo, they both have caveats that can be overcome using GC3Ai. Compared to GC3Ai, the 2-channel requirement of Apoliner complicates the use of other reporters while the poorly defined mechanism and rapid degradation of acridine orange makes it unsuitable for time-lapse imaging of apoptotic processing.

GC3Ai vs Apoliner during embryogenesis



Zooms



GC3Ai vs Acridine orange during embryogenesis

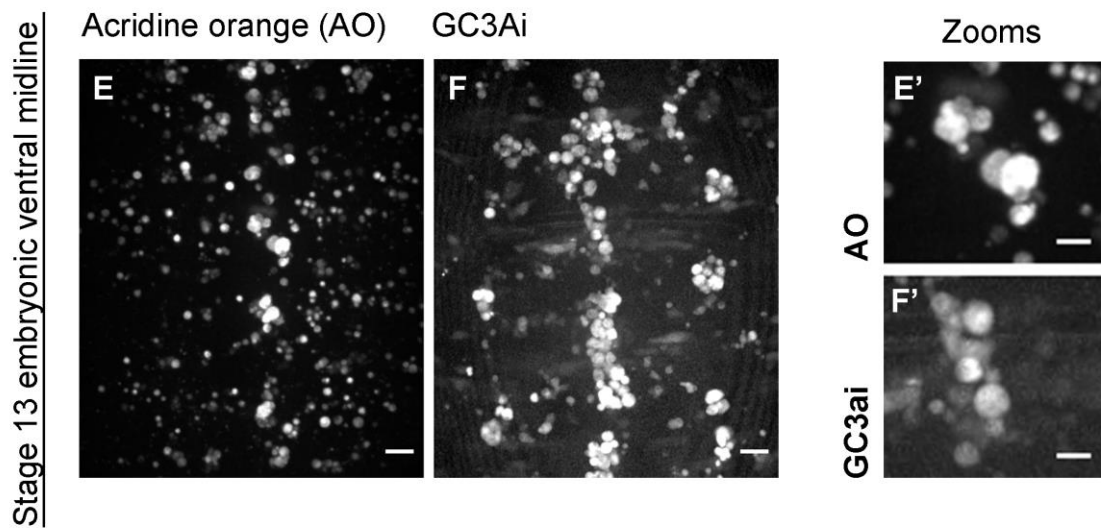


Figure 3.4 – Comparison of GC3Ai, Apoliner and AO labelling during *Drosophila* embryogenesis

(A-D) Single confocal z-slices and 21µm maximum projection of the stage 15 *Drosophila* embryonic ventral midline showing the 568nm channel (A), the 488nm channel (B) and merges of those channels (C) for embryos containing ubiquitous expression of Apoliner ($w^{1118};;da-GAL4,UAS-Apoliner$), or the 488nm channel for embryos expressing GC3Ai ubiquitously ($da-GAL4,UAS-GC3Ai$) (D). (A'-D') Zoomed images of the maximum projections for the Apoliner channels (A'-C') and GC3Ai (D') with suspected hemocytes containing phagosomes highlighted with an asterisk (*). (E-F) Maximum projections of the ventral midline at stage 15 of a w^{1118} embryo stained with AO (E) or an embryo expressing GC3Ai ($w^{1118};;da-GAL4,UAS-GC3Ai$) (F). (E'-F') Zoom of maximum projections of the ventral midline region at stage 15 of embryos stained for AO (E') or expressing ubiquitous GC3Ai (F') highlighting phagosome-like structures. Full image and zoomed image scale bars denote 10µm and 5µm, respectively.

3.2.4 Efferocytosis dynamics can be accurately studied *in vivo* using GC3Ai

Having confirmed apoptotic sensor functionality within the embryo, I sought to apply them to measure the relationship between caspase activation and efferocytosis during embryogenesis, particularly how caspase activity is related to cell fate and the timescales required for clearance. For these experiments, ubiquitous expression of GC3Ai was used in conjunction with the GAL4-independent macrophage label *SrpHemo-3X-mCherry* (Gyoergy et al., 2018). To assay the relationship between caspase activation and apoptotic cell morphology, GC3Ai activation was observed and quantified for single cells in stage 12-13 embryos on the ventral midline. Observations of GC3Ai activation appeared to show three distinct fates for cells after caspase activation: fragmentation – wherein the cell underwent blebbing and eventually separated into multiple smaller bodies (Figure 3.5); transient caspase activation – where there was a loss of caspase activation over time with cells temporarily displaying an apoptotic phenotype before losing caspase activity (Figure 3.6); and efferocytosis – characterised as engulfment of a caspase-active cell by a macrophage (Figure 3.7).

Apoptotic cells that underwent fragmentation were tracked over time with an example shown with a trace of GC3Ai fluorescence intensity (Figure 3.5). Observations of cell morphology showed that GC3Ai activity appeared to rapidly increase over the course of 30 minutes, with blebbing beginning to occur after 30-50 minutes. From this point, GC3Ai intensity continued to grow steadily as the dying cell lost volume through the release of

membrane-bound blebs. From 60-minutes onwards, this cell began to fragment with the body largely separating out into several blebs (**Figure 3.5A**). The relative change in GC3Ai activation post-detection showed that GC3Ai activity rapidly increased initially (0-20 minutes), before then reaching a plateau (20-40 minutes) and then increasing once more to a peak intensity (50 minutes). After caspase activity had peaked, the cell released several exosomes at 60 minutes (**Figure 3.5B***). While difficult to measure because of the lost cell volume, the remaining GC3Ai volumes have a relatively stable intensity up to 90 minutes post activation. The fragmentation of these cells occurs without obvious interventions from macrophages suggesting that this behaviour is intrinsic to the dying cell and not reliant on macrophage contact. While phagocytosis from adjacent cells or glia is possible, the separation and dispersal of the blebs during fragmentation does not support uptake into a phagosome.

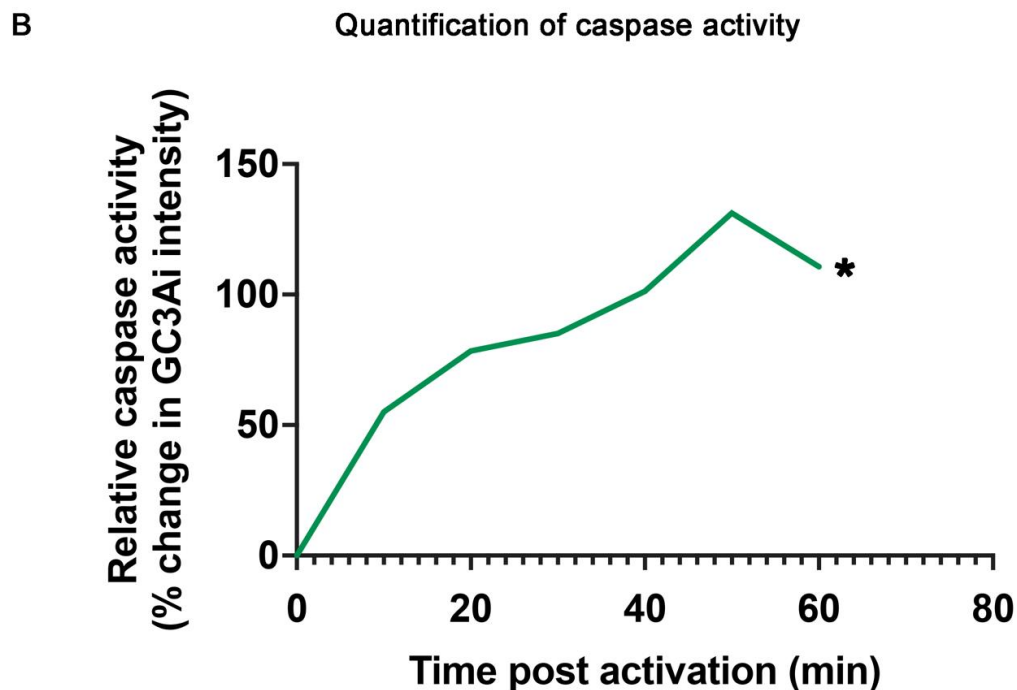
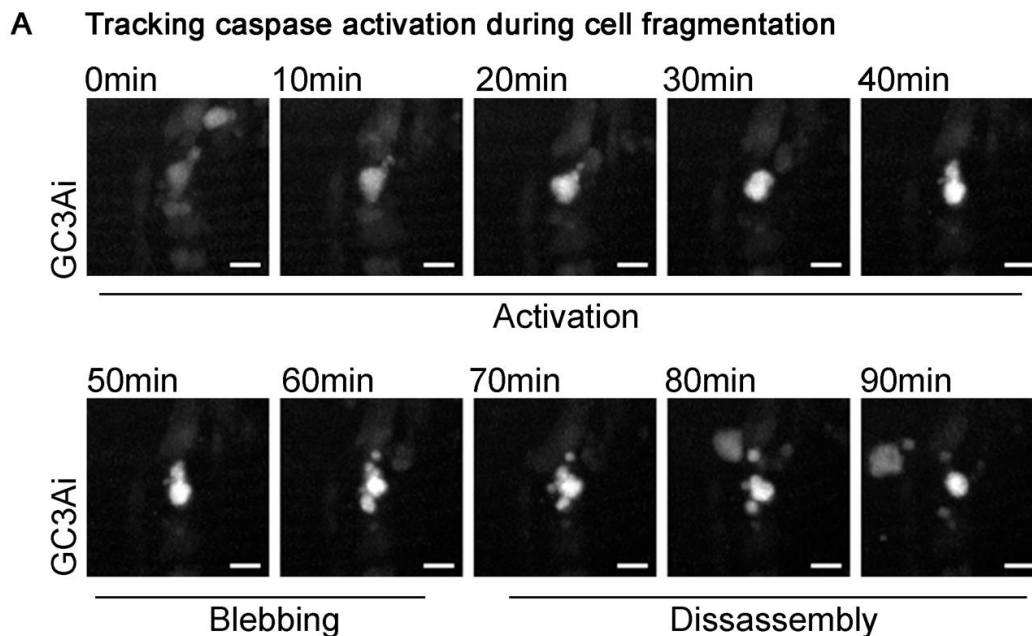


Figure 3.5 – Caspase activation leading to apoptotic cell fragmentation

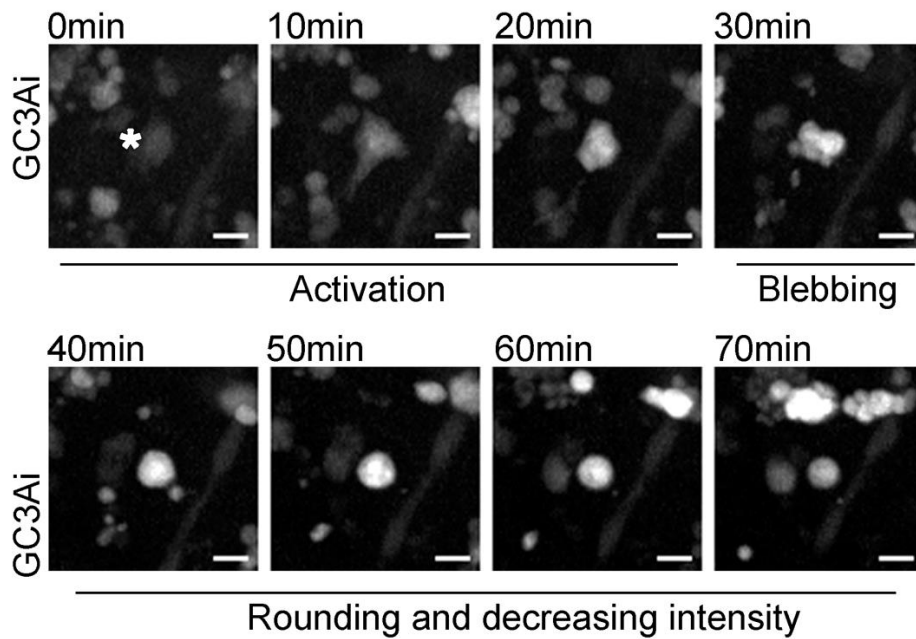
(A) Montage of stills taken from a time-lapse movie comprised of maximum projections (~21 μ m deep z-stack) showing activation of a single apoptotic cell present at the stage 13 *Drosophila* embryonic ventral midline region. Timepoints post caspase-activation and morphological notes are annotated above and below, respectively. Scale bar denotes 5 μ m.

(B) Graph showing the GC3Ai intensity values over the course of the timelapse movie as a readout of caspase activity. Caspase activity was calculated as the % change in the integrated density of the GC3Ai signal compared to the initial detection value set at 0mins. Note that the trace ends at the 60-minute timepoint (*): this is because tracking intensity values were discontinued after the cell had fragmented. Genotype was *w¹¹¹⁸; SrpHemo-3X-mCherry; da-GAL4, UAS-GC3Ai*.

In contrast to these fragmented cells, another population of GC3Ai-positive cells did not undergo large decreases in their volume through apoptotic blebbing. Instead, these cells appeared to lose caspase activity over time (**Figure 3.6**). Tracking the morphology one of these cells (**Figure 3.6***) showed that there was an initial activation phase of GC3Ai over the course of 30 minutes. This was then followed by the changes in cell shape indicative of early apoptotic blebbing, however this activity rapidly ceased by 40 minutes and the cell rounded and lost GC3Ai intensity over the next 30 minutes (**Figure 3.6A**). Quantification of the GC3Ai intensity shows that caspase activity appears to increase initially (0-10 minutes) before stalling (10-20) and then again increasing to a peak intensity value (30 minutes). After this peak, which coincides with the cell beginning to round, there is a steady decrease in caspase activity (30-50 minutes) that turns into a rapid decline from 50 to 80 minutes (**Figure 3.6B**).

This cell appears to recover from apoptosis as we see a loss of apoptotic morphology, coupled to a decrease in caspase activity. This suggests that the cell is potentially no longer in the process of apoptosis and has been prevented from dying. While it could be the case that these cells are being cleared by non-macrophages, there are indications that this is not the case: observations from macrophage engulfed apoptotic cells suggests that caspase activation does not decrease to a noticeable degree within the phagosome over these imaging timeframes; and the apoptotic cell does not move in a directed manner as would be expected if being pulled into a phagosome.

A Tracking caspase activation during apoptotic recovery



B Quantification of caspase activity

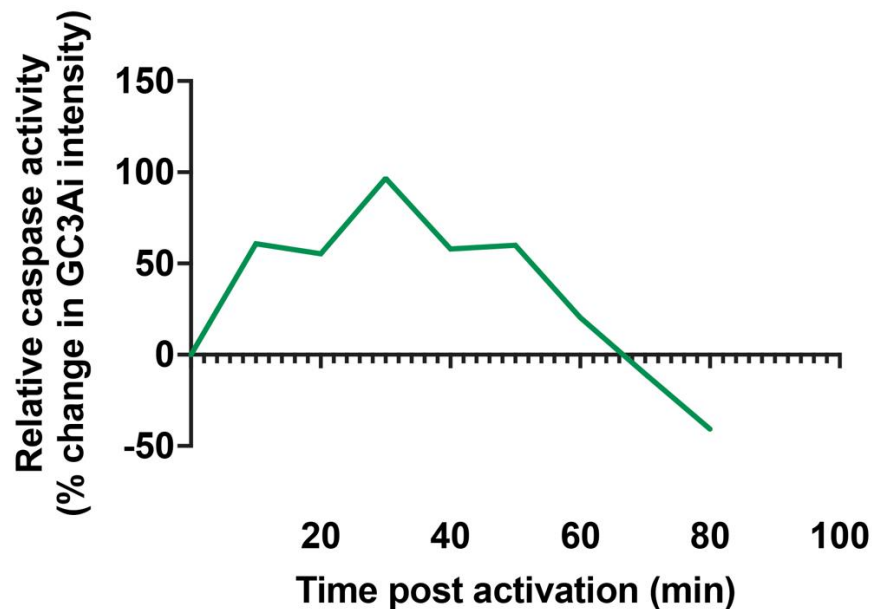
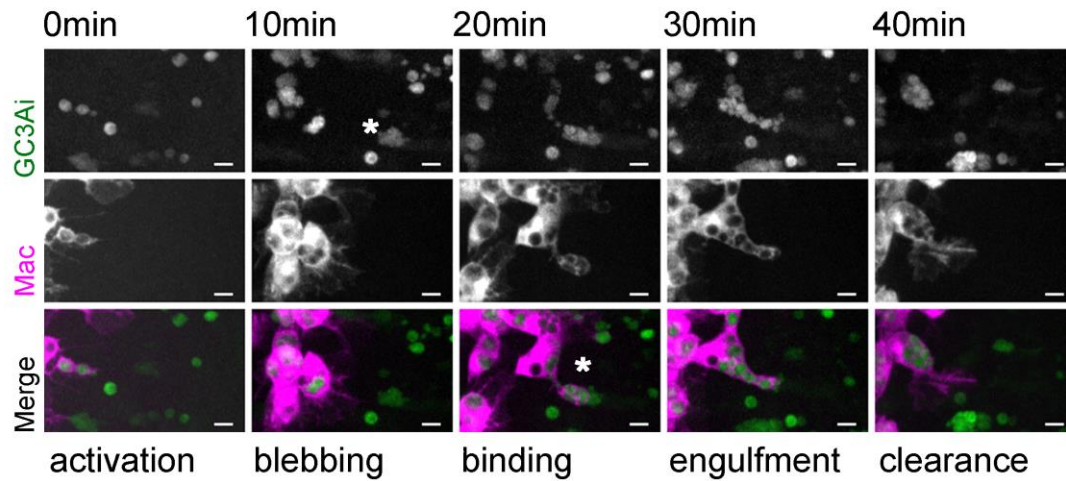


Figure 3.6 – Transient caspase activity in non-macrophage efferocytosed cells

(A) Montage of stills taken from a time-lapse movie comprised of maximum projections (~21 μ m deep z-stack) showing the activation of a single apoptotic cell present within the stage 13 *Drosophila* embryonic ventral midline region. Timepoints post caspase-activation and morphological notes are annotated above and below, respectively. Cell of interest is annotated via an asterisk (*) in the first-time frame. Scale bar denotes 5 μ m. (B) Graph showing the GC3Ai intensity trace over the course of observation as a readout of caspase activity. Caspase activity was calculated as the % change in the integrated density of the GC3Ai signal compared to the initial detection value set at 0mins. Genotype was *w¹¹¹⁸; SrpHemo-3X-mCherry; da-GAL4,UAS-GC3Ai*.

While only 15% of the observed caspase-active cells (n=2 of 13 observed caspase activation events) were subject to macrophage-mediated efferocytosis, some clearance events were observed and occurred rapidly after caspase activation. Tracking of efferocytosis at stage 12 illustrated the rapid nature of these phenomena with an example shown below (**Figure 3.7A**). After GC3Ai has become activated, caspase activity increases over the course of 10 minutes followed by the onset of changes in cell shape. At this point, a proximal macrophage at the ventral midline begins to extend towards the dying cell and binds to it (~20 minutes after activation). Phagocytosis of the apoptotic cell shows several notable differences compared to classical engulfment of a rigid target such as a bacterial or fungal cell: macrophage protrusions appear to bind several expanded sections of the membrane, resulting in a “lasso” like structure (*****, **Figure 3.7A**) and as the lasso is retracted, the target cell is separated into a series of individual phagosomes over the following 20 minutes. Post engulfment, the macrophage appears to resume its previous migration course and continues to engulf other nearby apoptotic cell fragments (data not shown). Quantification of caspase activity shows that caspase activity initially fluctuates after detection (0-10 minutes) followed by a rapid increase and plateau (10-15 minutes) before being bound by the responding hemocyte (~17 minutes) (**Figure 3.7B**). The rapid clearance of this cell suggests that if find-me cues are active, they act rapidly during the earlier stages of apoptosis.

A Observation of efferocytosis in real-time



B Quantification of caspase activity

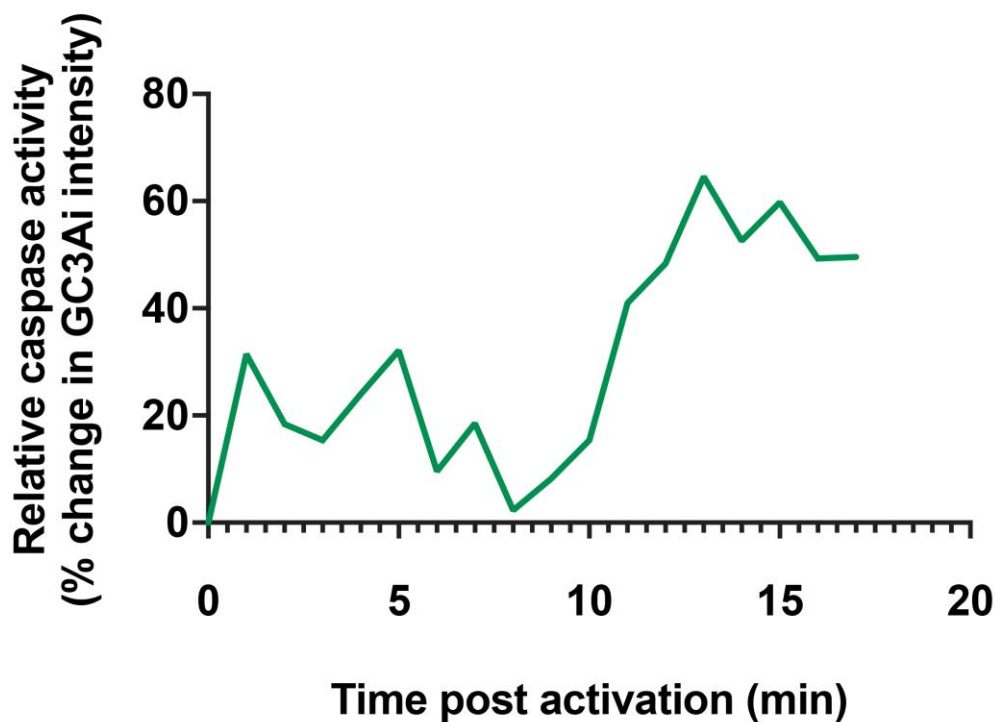


Figure 3.7 – Visualisation of efferocytic processes in real-time

(A) Montage of a $\sim 21\mu\text{m}$ maximum projection time-lapse series showing the clearance of an apoptotic cell by a migrating macrophage at stage 12 on the embryonic ventral midline. Split channels for GC3Ai, SrpHemo-3X-mCherry (macrophage/Mac) and the corresponding merge are shown. Note that the formation of the binding cup is annotated with an asterisk (*), with stage of efferocytosis noted underneath. All scale bars denote $10\mu\text{m}$. (B) Graph showing the GC3Ai intensity trace over the course of the timelapse movie as a readout of caspase activity. Caspase activity was calculated as the % change in the integrated density of the GC3Ai signal compared to the initial detection value set at 0 minutes. Genotype was $w^{1118}; \text{SrpHemo-3X-mCherry}; \text{da-GAL4}, \text{UAS-GC3Ai}$.

Quantification of the caspase dynamics of GC3Ai-positive cells at stage 13 (n= 13 caspase activation events in 3 embryos) showed a generalised intensity curve with caspase activity increasing for approximately 30 minutes before reaching a plateau and then decreasing after 60 minutes post-activation of GC3Ai (**Figure 3.8A**). Splitting the data into the three defined fates of fragmented, transient caspase activation or having undergone efferocytosis shows that these cell populations appear to have distinct caspase activation curves. Fragmented cells undergo the steepest increase in caspase activity, slowing after 20 minutes and peaking on average 50 minutes post activation prior to severe loss of cell volume (**Figure 3.8B, magenta line**). Cells that showed transient caspase activation have a slower and shallower increase in caspase activity, again plateauing out at 20 minutes, followed by a decrease in caspase activity beginning 60 minutes post activation coupled to the rounding of the cell body (**Figure 3.8B, black line**). Intriguingly, cells that undergo efferocytosis by macrophages are engulfed a short time after initial caspase activation, with no such cells lasting more than 20 minutes post caspase activation before engulfment (**Figure 3.8B, cyan line**). The activation curve gradient for fragmented cells and cells with transient caspase activation are significantly different ($p=0.0004$). These three outcomes are summarised in **Figure 3.8C**.

Overall, these results suggest that caspase activation is not a guarantor of efferocytosis, and different cells undergo different activation curves that are linked to their fate. Since the release of find-me cue is intrinsically linked to the activity of caspases (Ravichandran, 2003), failure to efferocytose these caspase-active cells would suggest that either find-me cues are not present within *Drosophila* or other factors govern which cells are targeted for clearance.

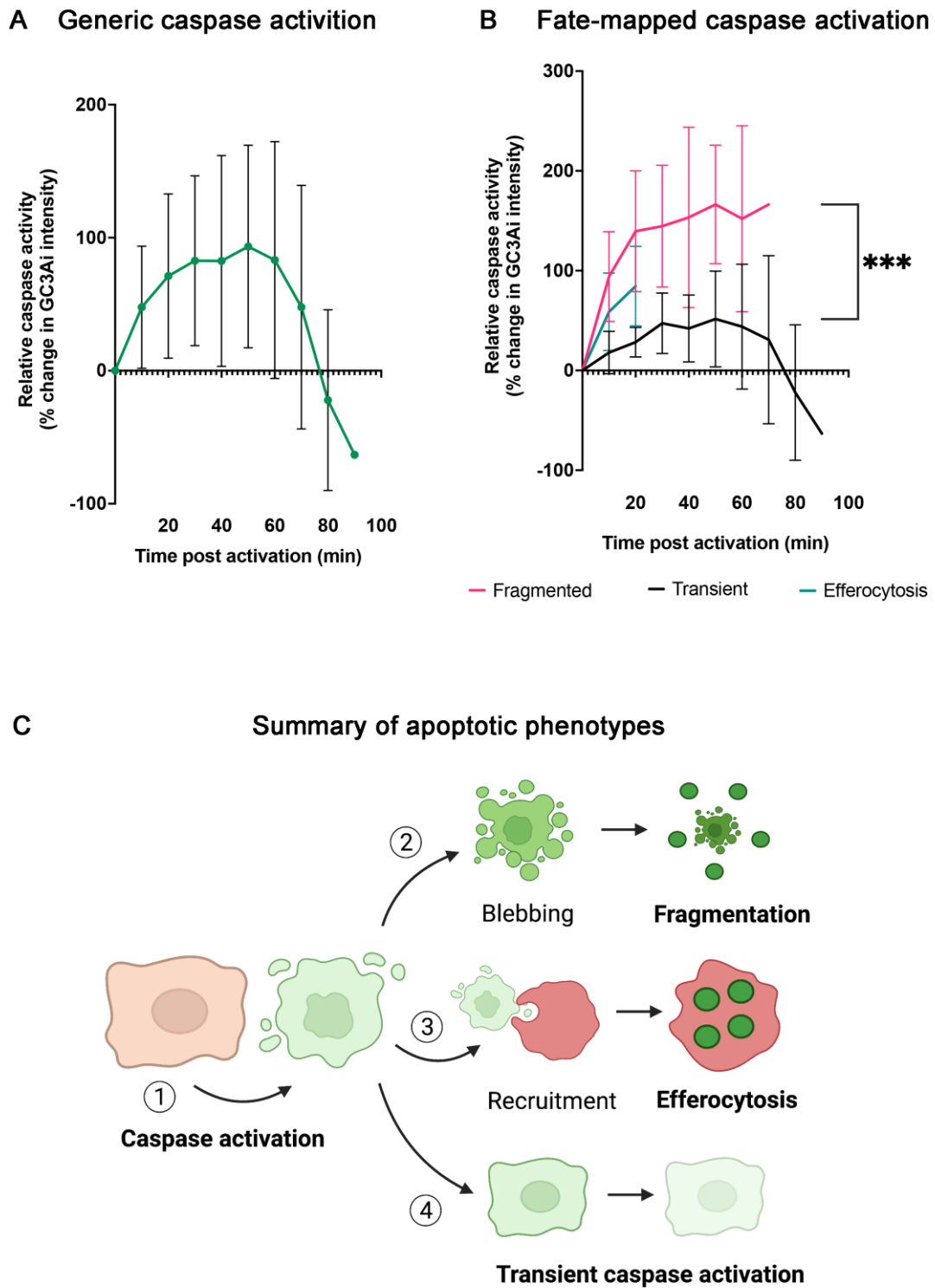


Figure 3.8 – Summary of apoptotic caspase dynamics

(A) Graph showing the change in caspase activity over time in GC3Ai-positive single cells tracked over the course of at least 60 minutes at stage 13 on the embryonic midline. Data points represent averages derived from 13 GC3Ai-positive cells tracked from activation to outcome (fragmentation, transient activation or efferocytosis) in 3 independent embryos. (B) Graph showing the change in caspase activity over time in GC3Ai-positive single cells tracked over the course of 60 minutes minimum within the stage 13 *Drosophila* embryonic midline

split according to outcome: magenta line shows average GC3Ai intensity of cells seen to undergo fragmentation (n=4 cells from 3 independent embryos); black line shows average GC3Ai intensity of cells seen to undergo recovery (n=7 cells from 3 independent embryos); cyan line shows average GC3Ai intensity of cells seen to undergo efferocytosis (n=2 cells from 3 independent embryos). All error bars represent standard deviation; statistics bars indicate the difference between the slopes for fragmented and recovered cells (p=0.0004, simple linear regression). Genotype of all embryos was *w¹¹¹⁸; SrpHemo-3X-mCherry; da-GAL4, UAS-GC3Ai*. **(C)** Schematic diagram outlining observations for the different GC3Ai activation phenotypes. After cells become caspase active (1), they appear to undergo three distinct fates: rapid increases in caspase activity and blebbing resulting in major losses of cell volume (2, fragmentation); the recruitment of migrating hemocytes (red cell) that begin to engulf the dying cell before moving on (3, efferocytosis); and a loss of caspase activity and apoptotic morphology over time (4, transient activation).

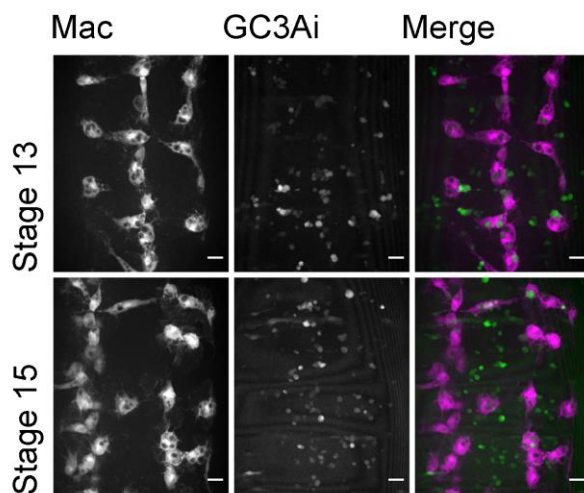
3.2.5 Optimisation of induced apoptosis models to study efferocytosis

One of the main restrictions to obtaining reproducible measurements of efferocytosis is the changing *in vivo* environment within a developing embryo. Apoptosis frequency and macrophage behaviour changes from stage 13-15 with very few apoptotic events observed from stage 15 (**Figure 3.9A**). Stage 15 is preferable for studying macrophage chemotaxis as by this point in development the ventral nerve cord (VNC) has separated from the ventral epithelium, resulting in less restriction of macrophage movement (Olofsson and Page, 2005; Page and Olofsson, 2008; Evans et al., 2010a). At the same time there is a reduction in VEGF-stimulated migration due to downregulation of chemoattractive Pvf ligands (Wood et al., 2006; Mondal et al., 2014), reducing the amount of competing signals in the tissue region. Unfortunately, after observation of confocal timelapse movies, it became apparent that by this point in embryogenesis apoptosis is more sporadic and infrequent: fewer than 5 GC3Ai-activation events were detected per hour on average alongside minimal macrophage-mediated examples of efferocytosis (**Figure 3.9B**). Due to this, I attempted to modulate levels of efferocytosis in a controlled manner using tissue-specific approaches and induction of apoptosis. Heat-shock of stage 15 embryos carrying *hs-hid* and with macrophages and apoptosis labelled via *SrpHemo-3X-mCherry* and ubiquitous expression of GC3Ai, respectively, was used to induce large amounts of apoptosis (**Figure 3.9C**). Timelapse imaging revealed a rapid increase in the number of apoptotic cells over the course of an hour.

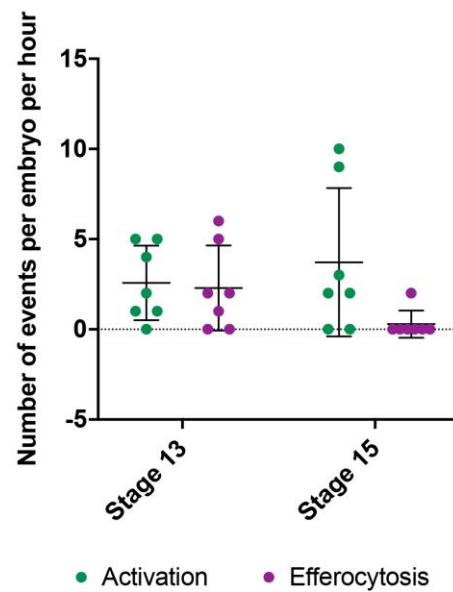
While an extreme example, these results show that timed heat-shock treatments can be used to increase apoptosis in the embryo. Unfortunately, genetic issues with the *Drosophila* stocks

and disruption due to COVID-19 halted this experiment before proper optimisation of the heat-shock conditions could be conducted. However, the increase in apoptosis and continued migration of macrophages in this system suggests it could be used to efficiently increased apoptosis to statistically comparable levels, especially as macrophages appear protected from apoptosis via this technique (Evans and Roddie, unpublished data; Roddie et al., 2019).

A Developmental efferocytosis



B Quantifying caspase events



C Global induction of embryonic apoptosis

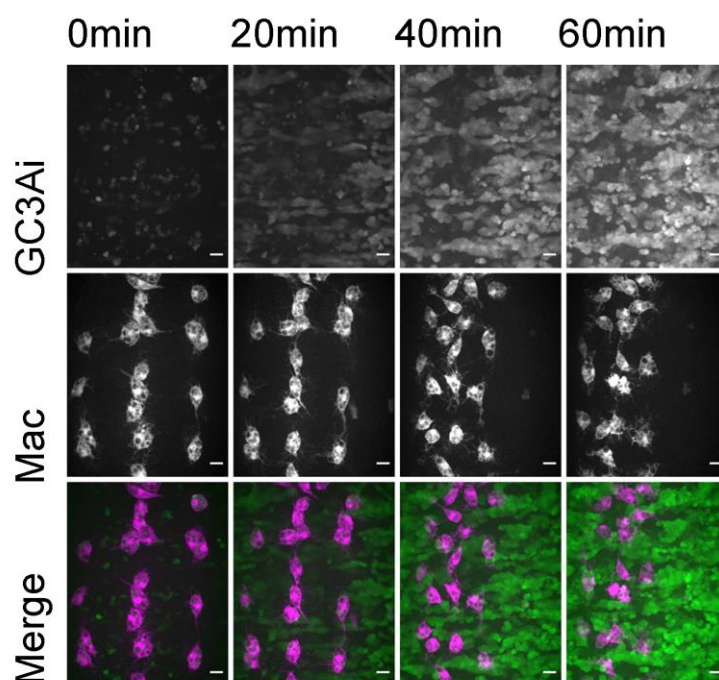


Figure 3.9 – Frequency of apoptosis during developmental and induced apoptotic systems

(A) Cropped confocal 21µm maximum projection representative images of hemocytes and apoptotic cells at the stage 13 and stage 15 *Drosophila* embryonic midline. Channels have been split between GC3Ai, *SrpHemo-3X-mCherry* (macrophage/Mac) and the corresponding merged image. **(B)** Scattergraph showing the average frequency of caspase-activation events and efferocytosis events observed per embryo over the course of one hour at stage 13 and stage 15 of embryogenesis. Data points represent single embryos (n=7, 8 for stage 13 and 15 embryos, respectively) with lines and error bars showing mean and standard deviation, respectively. The genotype of embryos was $w^{1118}; da-GAL4, UAS-GC3Ai/SrpHemo-3X-mCherry$. **(C)** Cropped confocal 21µm maximum projection images of *hs-hid* induced apoptosis over the course of 1 hour in embryos at stage 15 on the ventral midline. Channels have been split into GC3Ai, *SrpHemo-3X-mCherry* and merge images, respectively, for each time point. Heat-shocked embryos were of the genotype $w^{1118}; +/85y Ohs-hid; da>GC3Ai/SrpHemo-3X-mCherry$. All scale bars denote 10µm.

3.2.6 Tissue-specific apoptosis can be induced to study find-me cue dynamics

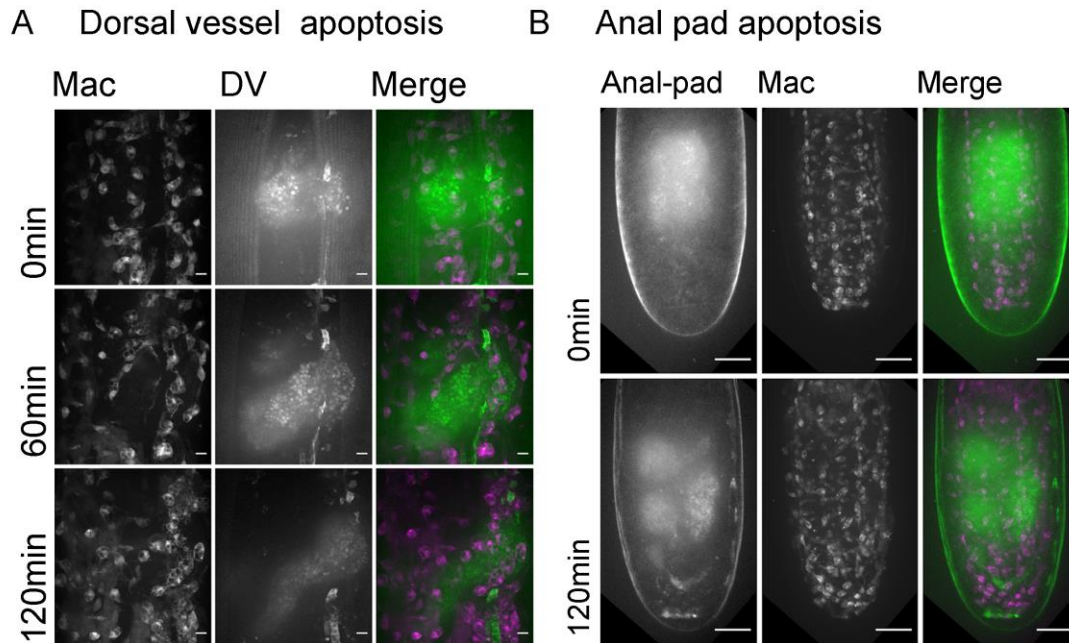
Given that caspase activation in a single cell did not guarantee macrophage-mediated efferocytosis at the embryonic ventral midline, the numbers required to reproducibly assay efferocytosis required the induction of additional apoptosis. To this end, tissue-specific apoptotic induction was used to assess the effect of large-scale apoptosis on the macrophage population to assay the ranges and timescales that find-me cues might act to recruit hemocytes to a defined site. Temperature-sensitive *GAL80^{ts}* was expressed ubiquitously under the control of the tubulin promoter (*Tub-GAL80^{ts}*; McGuire et al., 2003) and used in conjunction with the pro-apoptotic *UAS-Reaper* (Aplin and Kaufman, 1997) and *UAS-LifeAct* (Hatan et al., 2011) to create a system wherein embryos can be temperature shifted to induce apoptosis under the control of tissue specific drivers, in this instance the embryonic anal pad *VT45229-GAL4* (Kvon et al., 2014) and cardiocyte-specific *TinC-GAL4* (Bodmer, 1993; Lo and Frasch, 2001; Qian et al., 2007). In this system, GAL4 driven expression of LifeAct (Actin-GFP) and Reaper are suppressed at room temperature by the presence of temperature-sensitive *GAL80^{ts}*, produced under the control of the constitutively active *Tub* promoter. When the embryos are temperature shifted to 29°C, the temperature sensitive *GAL80* was prevented from suppressing *GAL4* expression, thereby allowing tissue-specific expression of *GAL4*, in turn leading to expression of the LifeAct and Reaper, which will label and induce apoptosis within the specific tissue respectively.

For dorsal vessel imaging, heat-shocked embryos were mounted dorsally and imaged over the course of two hours. During this time-course there was an observable increase in LifeAct levels, suggesting that the temperature shift was acting correctly. Unfortunately, induced apoptosis of the dorsal vessel appeared to compromise the structure of the embryo as evidenced by the malformation of the gut visible and eventual collapse of the embryo (**Figure 3.10A**). The damage sustained to the embryo precluded the accurate measurement of macrophage recruitment and this experiment was subsequently discontinued.

To assess macrophage recruitment to the anal pads following induction of apoptosis, temperature-shifted embryos were ventrally mounted and imaged for 2 hours. Note that a reduced magnification was required due to the depth of the tissue, requiring use of an objective lens with a greater working distance. As previously, shifting the temperature induced expression of LifeAct within the anal pads over the time-course (**Figure 3.10B**). To quantify potential macrophage recruitment, the relative change in macrophage dispersal (number of macrophages per region) was calculated in heat shocked control embryos (lacking UAS-reaper, and therefore heat induced apoptosis) and those in which apoptosis was induced. To assay overall changes in macrophage localisation after the induction of apoptosis, it was necessary to quantify the dispersal of macrophages across the embryo: this was done by dividing the embryo into 100 μ m regions (bins) that would allow for consistent comparison of macrophage localisation across the embryo. Dispersal counts showed that apoptosis of the anal pads did not significantly alter macrophage dispersal across three regions of the embryo (300-200 μ m, 200-100 μ m and <100 μ m from the embryo posterior) (**Figure 3.10C**). While this result is less accurate due to the low magnification, these results do suggest that even large clusters of apoptotic cells do not induce obvious recruitment of hemocytes. The lack of changes in dispersal might suggest that if find-me cues are being released from apoptotic cells, they are acting in an extremely localised manner.

Unfortunately, these experiments were discontinued due to the COVID-19 national lockdown. However, this pilot data in which I induced apoptosis using a temperature-shift strategy shows promise as a method to assay macrophage recruitment *in vivo*. The pilot data suggests that careful modulation of apoptosis via *hs-hid* induction can be used to increase the rate of apoptosis to levels more appropriate for gathering consistent efferocytosis data.

Similarly, tissue-specific cell death can be modulated to accurately track macrophage migration *in vivo* and is therefore suitable to assay immune cell recruitment. While these pilot results are therefore encouraging, the data also suggests that find-me cues are acting over small distances and would therefore require more sensitive approaches.



C Effect of anal pad apoptosis on macrophage dispersal

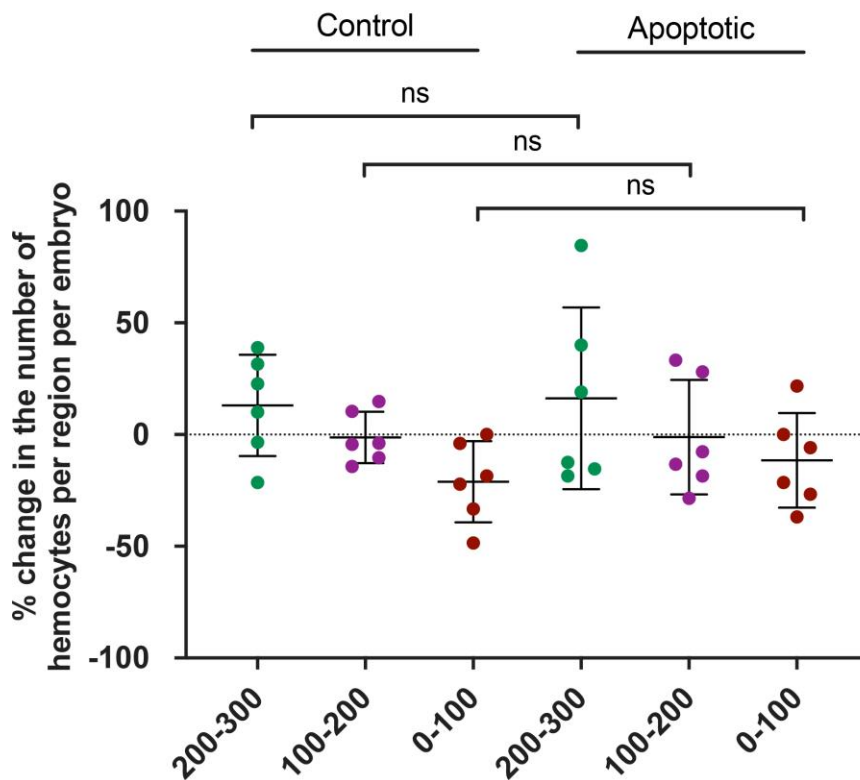


Figure 3.10 – Optimisation of induced apoptotic models in *Drosophila* embryos

(A) Cropped confocal 21µm maximum projection images of the dorsal face of a stage 15 *w; tub-GAL80^{ts}/+; UAS-reaper/TinC-GAL4, UAS-LifeAct, SrpHemo-3X-mCherry* embryo expressing heat-induced Reaper within the dorsal vessel over the course of 2 hours. Channels have been split into LifeAct, SrpHemo-3XmCherry (macrophage/Mac) and merged images, respectively, for each time point. Scale bars denote 10µm. **(B)** Cropped confocal 50µm maximum projection images of the ventral face of a stage 15 *w; tub-GAL80^{ts}/+; UAS-reaper VT45229-GAL4, UAS-LifeAct, SrpHemo-3X-mCherry* embryo expressing heat-induced Reaper within the anal pad region over the course of 2 hours. Channels have been split into LifeAct, SrpHemo-3XmCherry (macrophage/Mac) and merged images, respectively, for each time point. Scale bars denote 50µm. **(C)** Scatter graph showing the change in dispersal of hemocytes relative to the posterior end of the embryo in controls or 2-hours post-induction of anal pad apoptosis in stage 15 embryos. n=6 and 6 for control and Reaper-induced apoptosis conditions. Columns show the % change in the number of macrophages in a 100µm distance bin (where 0 = posterior end of the embryo) with comparisons between 200-300 (p=0.872), 100-200 (p=0.990) and 0-100 (p=0.419) regions. Each data point represents a single embryo with each embryo generating 1 value per distance bin. Statistical comparisons between bins of the same distance were made via a 2 tailed Student's t-test. Error bars and lines represent the mean and standard deviation. Statistical significance is noted of ns = p>0.05.

3.3 Discussion

The aims of this chapter were two-fold: to validate and apply the use of GC3Ai as a tool for the study of efferocytosis in the *Drosophila* embryo and to study the dynamics of macrophages in response to local caspase activation. The results presented herein show that GC3Ai can be used to accurately assess efferocytosis and that find-me cue dynamics are complex and perhaps context-dependent *in vivo*. I have shown that: GC3Ai reporters can be used during embryogenesis to accurately label apoptotic cells, with comparable if not improved performance compared to contemporary tools; that caspase activity can be quantified and linked to apoptotic progression and fate; and we have piloted several induced apoptotic systems that might allow us to gather further data on the dynamics of find-me cues and efferocytosis.

3.3.1 GC3Ai accurately reports embryonic apoptosis in *Drosophila* and is beneficial compared to contemporary methods

In their initial publication, Schott et al. (2017) showed that GC3Ai could be utilised in embryonic, L3 larvae and pupal tissues. Given that imaging constraints, gene expression and macrophage function differ considerably between the embryonic, larval and adult life stages of *Drosophila*, it was important to further validate the use of these apoptotic sensors within

the embryo. To do so, ubiquitously expressed GC3Ai was compared to several of the most common tools used to report apoptosis in *Drosophila*, namely anti-cleaved caspase immunostaining (Song et al., 1997a), Apoliner (Bardet et al., 2008) and acridine orange (Palmgren, 1991; Arama and Steller, 2006). Comparison of anti-GFP (GC3Ai) and anti-cDCP-1 staining showed that both reporters significantly colocalised, were absent in embryos lacking apoptosis and that GC3Ai had greater sensitivity (as measured by signal overlap) to DCP-1 at higher apoptotic levels. There are several potential explanations for this variation. Firstly, higher levels of cDCP-1 could result in a lack of available antibody, although this is unlikely due to saturating levels of antibody being used. Secondly, it was observed that cDCP-1 staining was poorly defined at higher induced apoptotic levels; this could be the result of anti-cDCP-1 epitopes being degraded at faster rates than GC3Ai, or because of higher GC3Ai concentration compared to cDCP-1 within apoptotic cells. It can also be speculated that GC3Ai is more stable than cDCP-1 and is therefore retained in late apoptotic cells after cDCP-1 has degraded. Taken together, these results confirm that GC3Ai is specific to apoptotic caspase activity in the embryo and is comparable or an improvement on anti-caspase staining.

While powerful tools, genetically-encoded apoptotic reporters present unique difficulties. The choice of expression system must be carefully made as the use of cell-specific expression systems may bias results towards certain cell phenotypes in heterogenous tissues. The use of artificial substrate reporters that are activated by proteases must also be used with caution as they could potentially interfere with the normal activities of these proteins by directly competing with the *in vivo* targets of these proteins. With the quality of apoptotic reporting validated, GC3Ai was qualitatively compared to both Apoliner and acridine orange staining as a live apoptosis reporter. Acridine orange is a pH-sensitive cell-permeable dye known to preferentially label apoptotic cells (Palmgren, 1991) and has been used as a proxy for apoptosis in *Drosophila* (Reed et al., 2004; Arama and Steller, 2006; Evans et al., 2013). Apoliner is a caspase-sensitive, dual-colour fluorescent protein developed for use in *Drosophila* and used extensively to assay embryonic apoptosis (Moreira et al., 2010; Shen et al., 2013; Roddie et al., 2019). Comparative imaging was used to illustrate the differences between these GC3Ai and these other methods. While GC3Ai is undetectable when inactive, Apoliner is clearly present within all the expressing cells regardless of status. Additionally,

while Apoliner can be used to quantify the number of apoptotic cells via nuclear counts, it is difficult to precisely resolve the apoptotic cell morphology compared to the broad cytoplasmic coverage seen with GC3Ai. Of practical note, the mechanism of Apoliner fluorescence precludes automated thresholding of the apoptotic cell and its use in conjunction with other reporters but does allow for nuclear counts to be effectively conducted. Comparative staining of acridine orange and GC3Ai-labelled embryos showed similar signal patterning, especially on the ventral midline where there is likely a concentration of dying cells within macrophage phagosomes. While both reporters functioned similarly, the primary advantage of GC3Ai compared to acridine orange is its stability under continuous exposure to fluorescent light and defined mechanism of action. Embryonic acridine orange staining must be conducted rapidly and is thus only useful for short term imaging (Arama and Steller, 2006), while GC3Ai stability has been observed for up to 2 hours under confocal laser microscopy.

Overall, the results show that GC3Ai can be used to accurately report apoptosis in the *Drosophila* embryo and is a viable and beneficial alternative to other contemporary *in vivo* methods. It should be noted that the use of caspase-sensitive substrates may impact progression of apoptosis through competition with endogenous targets, although this is unlikely given that no differences were observed between cDCP-1 and GC3Ai in wild-type embryos.

3.3.2 GC3Ai can be used to study the efferocytosis process in real-time

To our knowledge, the use of GC3Ai and macrophage labelling is the first example of imaging of live macrophage-mediated efferocytosis within the *Drosophila* embryo (Roddie et al., 2019). Previous studies have made great progress in understanding this critical process using other live tools, however the ability of GC3Ai to report apoptosis in a single channel with cytoplasmic coverage opens several avenues of research, notably the role of immune cells in the response to find-me cues and the fragmentation of apoptotic cells. All the currently identified mammalian find-me cues are known to be released downstream of caspase activation, typically through the cleavage of processing enzymes or secretion pathways, e.g., Sphingosine-1-phosphate (S1P) generation via caspase activation of Sphingosine kinases (Sphk1/2) (Gude et al., 2008; Weigert et al., 2010). Intriguingly, observations of GC3Ai

activation showed that caspase activity alone did not guarantee clearance even when proximal to macrophages, suggesting that the find-me phase of efferocytosis has additional prerequisites.

Tracking of GC3Ai activation in stage 13 embryos found that cells with caspase activity underwent three distinct fates: blebbing and fragmentation, rounding and reduced caspase activity or efferocytosis via hemocytes. For all three of these fates, the GC3Ai-positive cells underwent an initial phase of caspase activation followed by morphology changes and release of membrane blebs, a well-defined apoptotic event triggered by caspase 3-mediated activation of ROCK1 (Caruso and Poon, 2018). After the onset on blebbing, apoptotic cell behaviour appeared to diverge, leading to different outcomes. The fragmentation of apoptotic cells has been observed in a number of cell types *in vivo* and is thought to be a result of controlled changes of the cytoskeletal structure in the dying cell that allow for the production of smaller bodies more amenable to engulfment (Atkin-Smith and Poon, 2017; Smith et al., 2017). The appearance of transient caspase active cells is likely due to the activation of a program leading to the abortion of apoptosis – a process recently coined as “anastasis” (Tang et al., 2012). Anastasis is thought to be a mechanism for cells to recover from transient apoptotic stimuli through the upregulation of pro-survival genes such as those encoding cell cycle components (Sun et al., 2017). Compared to cells that underwent fragmentation or recovery, cells cleared by migrating macrophages (efferocytosis) were short lived: macrophage-apoptotic cell binding occurred no later than 20 minutes post-caspase activation and was followed by engulfment and sorting of individual apoptotic bodies into phagosomes.

The prevalence of these caspase-active cells that macrophages failed to clear has implications for our understanding of how find-me cues function *in vivo*. Given the different activation curves (GC3Ai intensity) observed for fragmenting and recovered apoptotic cells, it could be postulated that the decision to recover is based on the amplitude of pro-apoptotic stimuli upstream of caspase activation. While the data presented here did not assay the presence of pro-apoptotic factors, the steeper caspase activation curve observed in fragmenting cells could be the result of sustained pro-apoptotic signalling that was significantly higher than

cells that underwent recovery. This hypothesis is supported by *in vitro* studies showing enhanced recovery of cells exposed to transient apoptotic stimuli (Sun et al., 2017).

Intriguingly, cells that were cleared by macrophages or had transient caspase activity showed similar early caspase activation curves, morphology, and broad accessibility to macrophages dispersed across the ventral epithelia, suggesting that there are other factors at play that dictate outcome. While there appeared to be no obvious spatial preferences related to outcome, it is known that the circulating macrophage population is functionally heterogeneous (Coates et al., 2021) and it could be the case that the chance of being engulfed relies on proximity to a pro-clearance macrophage. Since the identity of the dying cells was not known, it may be the case that only specific cell-types release find-me cues and are designated for clearance by macrophages: studies using specific find-me cue knockdowns have suggested that the find-me response could be contextual, depending on the identity of the dying and responding cells: for example, inhibition of LPC release completely abrogated chemotactic effects of apoptotic MCF7 cells upon THP-1 cells (Lauber, 2003), yet it would appear that nucleotides are largely required for the THP-1 migration towards apoptotic Jurkat cells (Elliott et al., 2009). This might also suggest that find-me cues act in concert to induce efferocytosis. Finally, the activity of caspase-independent processes could drive variation in these responses. This could include the processing of cues via other proteases such as Calpains (Wang, 2000), or through the upregulation of anastasis-related genes that suppress release of find-me cues.

Imaging of macrophage-apoptotic cell interactions found that the protrusions of responding macrophages become intertwined on the apoptotic cell surface and uptake appeared to be on a piecemeal basis: macrophages were observed binding to several membrane regions and not necessarily engulfing the entirety of the cell during a single phagocytic event. Apoptotic blebs have been viewed as a pro-phagocytosis morphology (Fransen et al., 2009) and the observed interactions fit with data showing that macrophages prefer smaller attachment targets (0.5 μ m) (Pacheco et al., 2013). Several lines of evidence have found that uptake of apoptotic cells follows a specialised phagocytic mechanism akin to autophagic degradation, dubbed LC3-associated phagocytosis (LAP) (Romao and Münz, 2014). This type of live *in vivo*

imaging could be applied to study the particulars of LAP mediated phagocytosis and the link between processing and immune sub-types (Coates et al., 2021).

Overall, the data presented here suggests that clearance of apoptotic cells during *Drosophila* may not simply be mediated by caspase activation and that macrophages conduct the find-me and eat-me phases of efferocytosis in a similar fashion to the phagocytes found in mammals.

3.3.3 Apoptosis can be artificially induced to study efferocytosis

From observations of GC3Ai activity during *Drosophila* embryogenesis, it became apparent that the rapid clearance of developmental apoptosis presented a restriction on the possibility of obtaining statistically relevant measurements. To remedy this, exogenous means of inducing apoptosis were optimised to design a reproducible method of assaying efferocytosis and ascertain the timescales and distances potential find-me cues might act over. To this end, *Tub-GAL80^{ts}* in combination with *UAS-Reaper* was used to induce apoptosis in a tissue specific manner (Ryoo et al., 2004; Santabárbara-Ruiz et al., 2015) and heat-shock induced *hid* expression (Fan et al., 2014; Roddie et al., 2019) was used to induce global apoptosis.

Global induction of apoptosis via *hs-hid* (van Doren, 1996) was used to generate increased levels of apoptosis during development. The results showed that induced global *hid* expression can be used to increase the frequency of apoptosis without causing severe structural issues in the embryo during imaging. Unfortunately, these experiments had to be discontinued due methodological issues related to the genetics and the COVID-19 pandemic. Despite this, pilot data suggests that apoptotic frequency can be increased to increase replicate number this system could be of use in modelling the immune response to high local levels of apoptosis, such as that found in atherosclerotic plaques (Thorp, 2010) or chronic obstructive pulmonary disorder (COPD) (Mukaro et al., 2015). To assay the dynamics of apoptosis-induced macrophage migration, models of tissue-specific, induced apoptosis were optimised using the dorsal vessel and anal pad, both of which are known to be colonised by macrophages during their developmental dispersal. While both assays worked in principle, high levels of cardiocyte apoptosis appeared to cause severe structural damage to the embryo, suggesting it is not appropriate for time-lapse study. Anal pad cell death was

reproducible: however, the results showed no significant shifts in the dispersal of hemocytes because of apoptosis. There could be number of reasons behind these results: macrophage density is partially regulated by contact inhibition (Stramer et al., 2010; Davis et al., 2012) and thus an initial attraction of macrophages towards an apoptotic region might act to prevent further recruitment via contact inhibition, leading to no gross change in in dispersal; chemoattraction of macrophages is highly localised and thus beyond the detection of this assay; or the anal pad tissue does not produce find-me cues or is otherwise inaccessible to increased numbers of macrophages. While continued data collection for these experiments was cut short, the use of induced-apoptotic systems to study find-me cue dynamics can be practically applied.

3.3.4 Future work and COVID-19 impact

Due to time-constraints and COVID-19 related disruption, it was not possible to obtain data on several efferocytosis metrics, however this work could now be carried further because of optimisation and observational presented here. One of the most pressing questions related to efferocytosis is the mechanisms and dynamics of immune cell recruitment towards apoptotic cells. In a biological context, the recruitment of immune cells must strike a fine balance between several factors including the prioritisation of signals, the physical range at which find-me cues can effectively signal and desired specificity of the responding cell.

As shown here, GC3Ai can be used to elucidate a number of outstanding questions regarding apoptosis such as the fragmentation of apoptotic cells (Atkin-Smith and Poon, 2017; Smith et al., 2017) and the biophysical impacts of cell death (Hayes and Solon, 2017). While the GAL4-dependent GC3Ai system used here was adequate for observing efferocytosis, the expression of ubiquitous GAL4 independent GC3Ai, through either transgenesis or use of an alternative expression system, e.g., QUAS system (Potter et al., 2010) would allow for GC3Ai and macrophage labelling in the background of GAL4-dependent manipulation of the find-me signal machinery.

The question of the physical range of find-me cue can be more adequately addressed using induced-apoptotic models such as the *hs-hid* or temperature sensitive pro-apoptotic expression outlined previously. By activating apoptosis in a spatiotemporally controlled

manner, the behaviour of responding cells can be quantified, including the dispersal, morphology, or migration speeds. Using tissue-specific induction of apoptosis, it is possible to assay the distances over which macrophages will respond in a migratory fashion to a dying tissue. By comparing the pre- and post-apoptosis immune cell infiltration and impact on known migratory events, such as the stereotypical developmental macrophage dispersal pattern, the chemoattractive potential of apoptotic cells can be assessed indirectly. In contrast, global induction of apoptosis achieved using *hs-hid* is of greater value in understanding the role of immune cells in the context of a high apoptotic burden and can be used to evaluate the limits of effective efferocytosis and the ability of immune cells to perform non-efferocytic processing such as secretion of extracellular matrix (Nelson et al., 1994). To maximise the impact of efferocytosis data, it would be beneficial to use in silico modelling systems, such as the Biological Dynamic Modeller (BioDynaMo) (Bauer et al., 2016; Breitwieser et al., 2016). Using these platforms, it should be possible to derive the mathematical underpinnings of find-me cue mediated recruitment and thus shed light on the broader areas of cell motility and signal integration.

3.3.5 Concluding remarks

Over the course of this chapter, GC3Ai has been shown to function efficiently as a live reporter for apoptosis during *Drosophila* embryogenesis. The results show that ubiquitously expressed GC3Ai has similar accuracy to contemporary methods such as cleaved caspase immunostaining, acridine orange and Apoliner. Confocal imaging shows that when used in combination with macrophage reporters, GC3Ai can be used to visualise efferocytosis in exquisite spatiotemporal detail, with new light shed on the complex nature of apoptotic recruitment. Pilot induced apoptosis models also build on previous systems to allow for more accurate study of immune recruitment and disease pathologies associated with increased cell death.

Chapter 4: Assessing chemotactic competition using a 2D *ex vivo* cell model

4.1 Introduction

Understanding how motile cells integrate and prioritise the array of signals they face in the complex *in vivo* environment is a fundamental question in biology. For multifunctional cells such as macrophages this is a particularly important process, since it determines their subsequent behavior, be it migration to sites of damage, or clearance of pathogens and dying cells. The integration of a specific cue is highly contextual and depends on a number of parameters including crosstalk between signal transduction pathways (Heit et al., 2008), calcium levels within cells (Dou et al., 2012; Sieger et al., 2012), and the diffusion properties of a given ligand (Foxman et al., 1997). The exact mechanisms governing chemotaxis vary depending on the nature of the provocation, although the G-protein coupled receptor (GPCR) family of signaling proteins have long been known as key regulators of cell motility in response to chemokine gradients (Lämmermann and Kastenmüller, 2019). However, even before we can understand how cells prioritise and migrate towards different cues *in vivo*, it is necessary to identify a more complete range of cues to which macrophages can respond.

The removal of apoptotic cells, known as efferocytosis, is a rapid and efficient process requiring responding phagocytes to find and engulf the dying cell (Arandjelovic and Ravichandran, 2015). Apoptotic tissue must be removed quickly cleared to prevent secondary necrosis, which would otherwise create substantial pro-inflammatory trauma (Ariel and Ravichandran, 2016). During development, apoptotic cells can be readily detected and are critical for proper tissue remodelling and organ function (Fuchs and Steller, 2011), yet they are rapidly cleared within mature tissues. To facilitate this rapid response, dying cells are thought to release a set of chemotactic pro-efferocytic signals (“find me”) that are able to recruit local phagocytes and override other responses such as wounding stimuli (Moreira et al., 2010). Several groups have previously performed chemotactic experiments using apoptotic cell signals *in vitro* (Gude et al., 2008; Peter et al., 2008; Elliott et al., 2009; Sokolowski et al., 2014; Casas-Tintó et al., 2015), or have shown a strong chemotactic

response to cell-free, apoptotic cell-derived supernatant (Lauber, 2003). Although these studies are robust, they do not fully take account of the natural system in which find-me cues are active – i.e., within active tissues that are likely saturated with other migration, survival and growth factors that must be overcome if immune cells are to successfully find their target.

For this study, monocyte-derived macrophages (MDMs) were utilised as an *ex vivo* primary cell model. This cell type has been used in disease modelling (Hsiao et al., 2013; Eltboli et al., 2014) and cell chemotaxis studies (Audran et al., 1996). Compared to immortalised cell lines, MDMs can be generated *ex vivo* from whole blood monocytes (Bianchi et al., 2008) to produce a heterogeneous macrophage population (Vogel et al., 2014; Tedesco et al., 2015; Eligini et al., 2019) similar in phenotype to tissue resident macrophages (Yona et al., 2013). To assess competitive chemotaxis, the Ibidi μ -slide chemotaxis chamber was chosen as the method to challenge MDMs with competing chemokine. This approach was chosen as it can be used to observe the migration of slow cells under tissue culture conditions with the potential to challenge cells using multiple, linear gradients of chemokines at the same time (Zengel et al., 2011).

The aims of this chapter were threefold: firstly, to establish a protocol for the culturing and transfer of MDMs into the μ -slide chamber. Secondly, to perform single chemoattractant and competitive chemotaxis assays to begin assessing the place of different chemoattractants within a proposed signalling hierarchy. Finally, to assess how known chemoattractants compete with apoptotic derived ‘find-me’ cues when presented to *ex vivo* macrophages.

4.2 Results

4.2.1 MDMs undergo chemotaxis towards C5a using the Ibidi μ -slide chemotaxis

4.2.1.1 Optimisation of MDM transfer conditions for migration assays

Human MDMs were differentiated from peripheral blood monocytes for 6-9 days in standard tissue culture conditions. Post differentiation, MDMs are strongly adherent cells and thus transfer from culture vessels to the chemotaxis chambers required efficient detachment and re-adherence procedures to ensure cell viability. The initial transfer methods used a combination of cold-shock and chelation at 4°C using EDTA-PBS solution (Hui et al., 2009; Leidi et al., 2009) to dissociate MDMS from culture dishes, followed by scraping and transfer to chemotaxis chambers. Although this method facilitated detachment of MDMs, recovered cells failed to re-adhere to the chemotaxis chamber medium (**Figure 4.1**).

To overcome this, EDTA-PBS was substituted with Accutase (an alternative dissociation reagent). Accutase is a commercially available proteolytic dissociation solution that has been shown to increase viability of harvested MDMs compared to EDTA-PBS + cold shock methods (Chen et al., 2015). Use of Accutase resulted in a substantial increase in cell re-adherence to the chemotaxis chamber substrate in comparison to use of EDTA-PBS (**Figure 4.1**). It should be noted that there was significant donor-donor and cell preparation variation between MDMs in terms of viability post transfer.

EDTA-PBS

Accutase

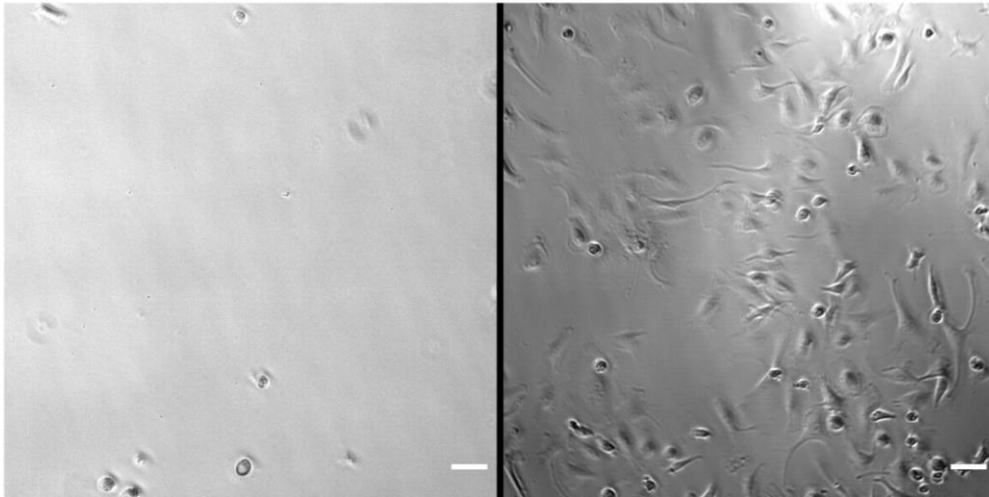


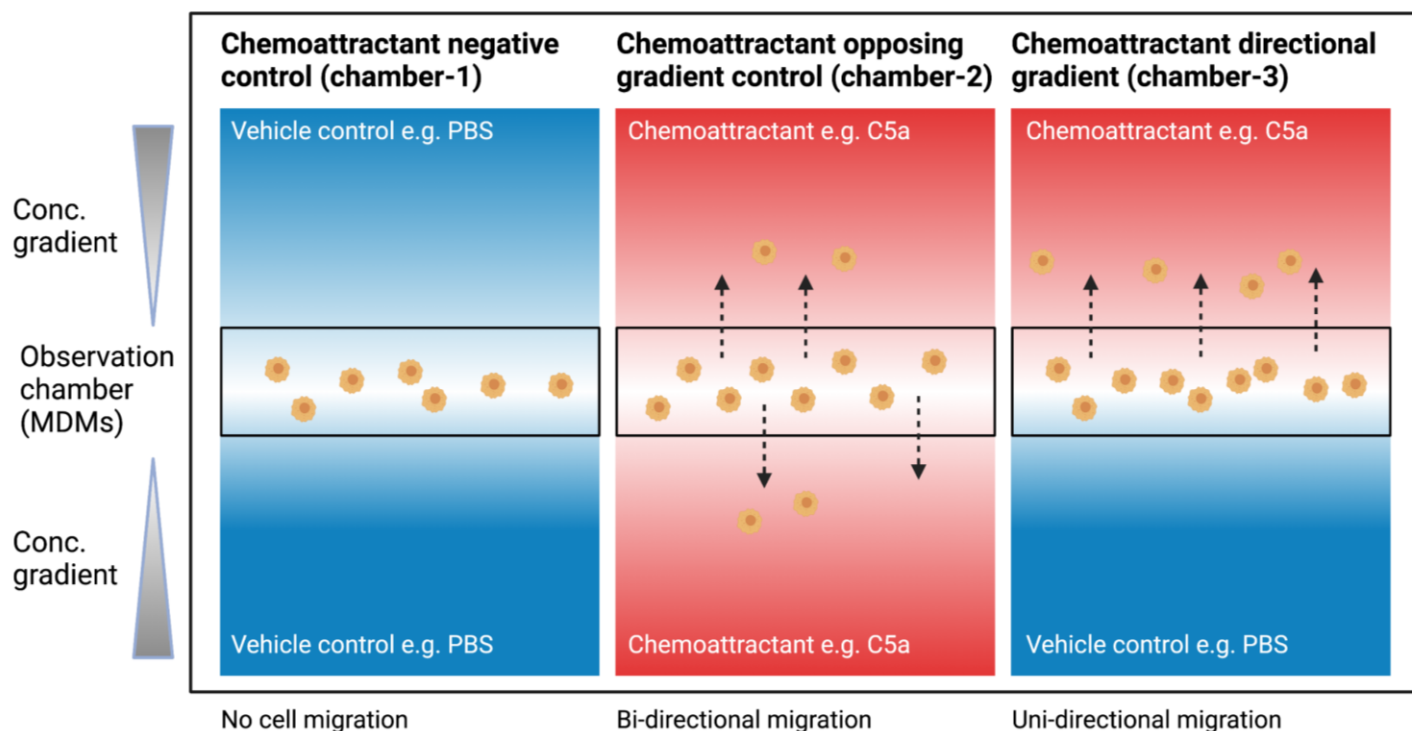
Figure 4.1 – Optimisation of cell culture transfer conditions

Phase contrast images of Ibidi μ -slide cell cultures from MDM cultures transferred via two different methods: Addition of EDTA-PBS and cold shock (left) and incubation with Accutase. After dissociation, cells were scraped and resuspended to a concentration of 6 million cell mL^{-1} before being added to the of Ibidi μ -slide cell observation chamber. Scale bar denotes 10 μm .

4.2.1.2 MDMs undergo chemotaxis towards C5a using the Ibidi μ -slide chemotaxis

With transfer methods optimised, I sought to begin establishing a signalling hierarchy. To do so, MDMs were first challenged with several established chemokines to investigate which could induce chemotaxis in this experimental set-up. Three established macrophage chemoattractants were chosen for initial experiments: N-formyl-Met-Leu-Phe (fMLP), monocyte chemoattractant protein-1 (MCP-1) and Complement protein fragment 5a (C5a) (Snyderman et al., 1972; Schiffmann et al., 1975; Audran et al., 1996). The μ -slide is composed of three migration chambers: a positive control chamber with chemoattractant on both sides, a negative control chamber with solvent vehicle control on both sides, and an experimental chamber with opposing gradients of chemoattractant and vehicle control (Figure 4.2).

The Ibidi μ -slide chemotaxis assay - experimental set up



Predicted outcomes if chemoattractant is effective

Figure 4.2 – Ibidi μ -slide experimental set up for single chemoattractants

Schematic diagram of the Ibidi μ -slide experimental design. The slide is composed of three independent chambers, each of which has different chemoattractant conditions. Each chamber contains a central observation chamber wherein cells (in this case MDMs) are seeded and allowed to adhere. Once cells have adhered in the observation area, chemoattractant gradients are applied on either side. There are three conditions used when testing a single chemoattractant: a chemoattractant negative control chamber (1) that has opposing gradients of vehicle control, typically the solvent used in preparation of the chemoattractant e.g., phosphate buffered saline (PBS); a chemoattractant positive control chamber (2) that has opposing gradients of the chemoattractant in question applied so that the cells are exposed to opposing gradients in the observation area; and an experimental chemoattractant chamber (3) wherein a directional chemoattractant gradient is applied in one direction. If a chemoattractant is effective, it would be expected that in chamber 1 would see no net migration, chamber 2 would see either no net migration or migration in both directions to a similar degree and chamber 3 would see a directional migration towards the chemoattractant side of the chamber.

Differentiated MDMs were transferred to the observation chamber and allowed to adhere prior to the application of chemoattractant gradients. After chemoattractant addition, MDM migration was recorded for 3 hours; this timescale was chosen based on advice from the manufacturer and comparable chemotaxis experiments (Gendelman et al., 2009). MDM chemotaxis movies were processed in Fiji (ImageJ) and blinded before manual tracking. Cells were tracked and the data analysed via the Ibidi chemotaxis toolkit in ImageJ. Track data was

processed, and the forward migration index (FMI) calculated for parallel (FMI_{||}) to and perpendicular (FMI_⊥) to the gradient. If a chemoattractant is effective, the following would be predicted: a significant difference between the two FMI values; visible and consistent migration of cells; significant changes in the velocity/directionality/distance travelled; and movement that is not random. It would also be predicted that the control chambers with opposing chemoattractant or vehicle should show no significant differences in these metrics.

MDMs challenged with 20nM recombinant human C5a underwent a reproducible chemotactic response over a 3-hour time-course. MDMs were challenged with either PBS vehicle (**Figure 4.3A left**), C5a on both sides (**Figure 4.3A centre**) or a gradient of C5a (**Figure 4.3A right**). FMI analysis showed that MDMs migrated towards the directional C5a gradient (FMI_{||} > FMI_⊥; p=0.0256) compared to either PBS vehicle (p=0.603) and opposing C5a gradients (p=0.649) where there was no preference parallel to the gradient (FMI_{||} = FMI_⊥) (**Figure 4.3B**). Comparing the cell migration pattern to the hypothetical random distribution, expressed as a Rayleigh value shows that the MDM migration in response to a directional gradient of C5a was directed (p<0.05) and not a result of random migration (chemokinesis; Sarris and Sixt, 2015) unrelated to the presence of chemoattractants (**Figure 4.3C**). These results confirm that MDMs can efficiently migrate towards a gradient of C5a in the μ -slide system. Due to this robust response, we opted to use 20nM C5a as a positive chemotaxis control for proceeding experiments.

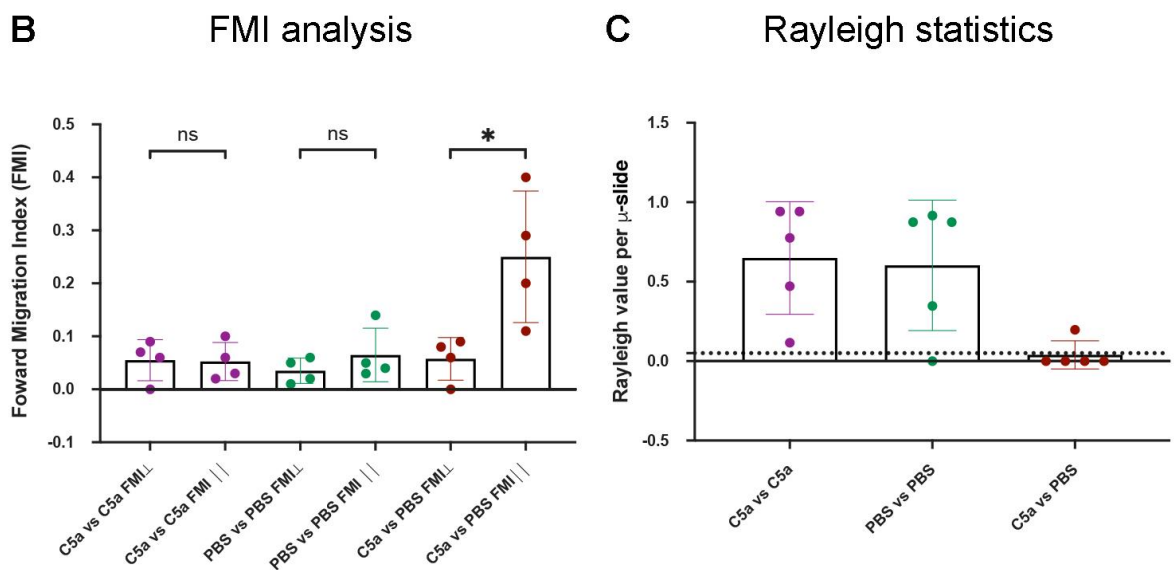
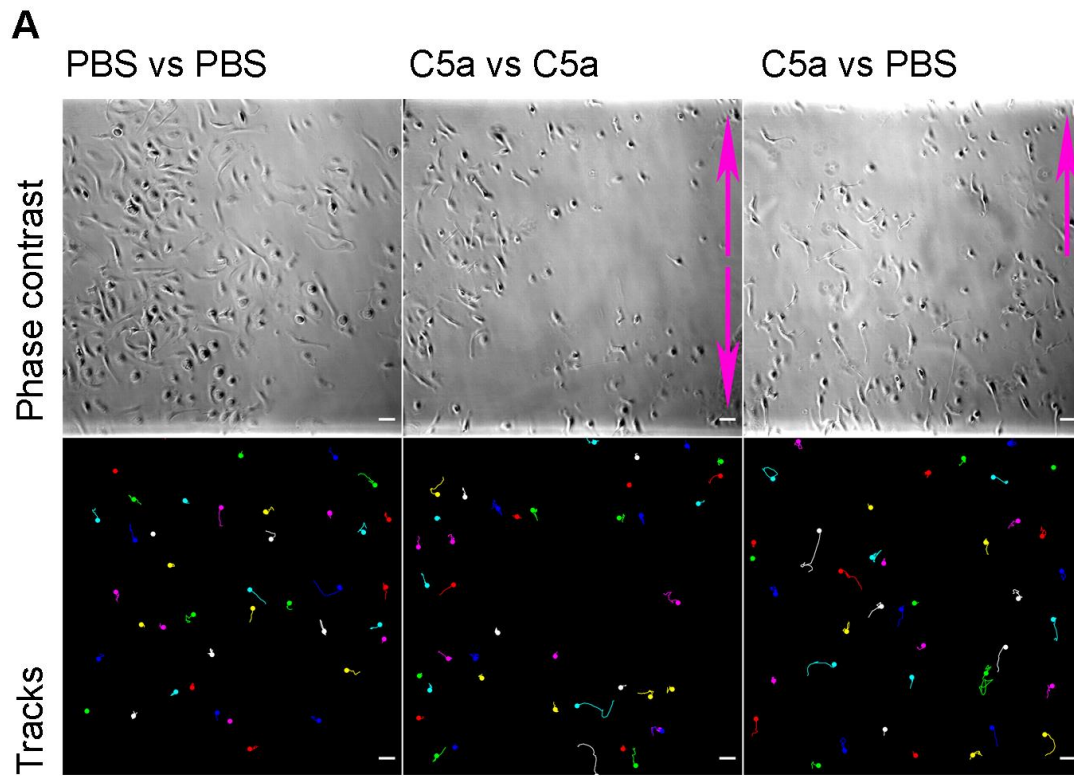


Figure 4.3 – C5a stimulates MDM chemotaxis using the Ibidi μ -slide

(A) Phase contrast images of migrating MDMs 3-hours post-chemokine addition in absence of C5a (chemokine null, left), when C5a is applied on both sides (20nM C5a opposing gradients, centre) and in the presence of a C5a gradient (directional 20nM C5a gradient, right) with associated MDM tracks (lower panels); Scale bars denote 100 μ m and magenta arrows indicate ascending chemoattractant gradient. 40 cells were tracked from a sample of each quadrant using the Fiji manual tracking and chemotaxis plugins. (B) Scatter graph of forward migration indices (FMI) with comparisons made between the FMI \perp (gradient perpendicular) and FMI \parallel (gradient parallel) for MDMs challenged with opposing C5a gradients (n=4, p=0.928), PBS control (n=4, p=0.325) and directional C5a gradient (n=4, p=0.0256). (C) Scatter graph showing the average Rayleigh value for MDMs challenged with uniform C5a

($n=4$, $p=0.649$), uniform PBS ($n=4$, $p=0.603$) and directional C5a ($n=4$, $p=0.039$). Dotted line corresponds to $p<0.05$, indicating that the migration pattern observed in directed and not the result of random movement. All data points denote the average value per μ -slide. Error bars denote the dataset mean and standard deviation per condition. FMI data was compared using Student's t-test between the average FMI $_{||}$ and FMI $_{\perp}$ values per condition. ns and * denote $p>0.05$ and $p<0.05$ respectively.

4.2.1.3 Optimisation of MDM chemotaxis tracking and quantification

Once culture conditions were optimised, chemotaxis assays could be conducted and manually quantified, however manual analysis of cell tracking was inefficient and open to sample bias. To reduce analysis time and increase throughput, culture conditions were further altered to facilitate automated tracking of cells. Pilot experiments were quantified via manual tracking of MDMs from phase-contrast time-lapse movies. While this was appropriate, it required long processing times and was subject to human and sampling error. To overcome this, MDMs were treated with the live-nuclei marker NucBlue (Invitrogen) prior to their resuspension and transfer to chemotaxis chambers (**Figure 4.4A**). This allowed for the use of automated tracking software using the Fiji (ImageJ) Trackmate plug-in.

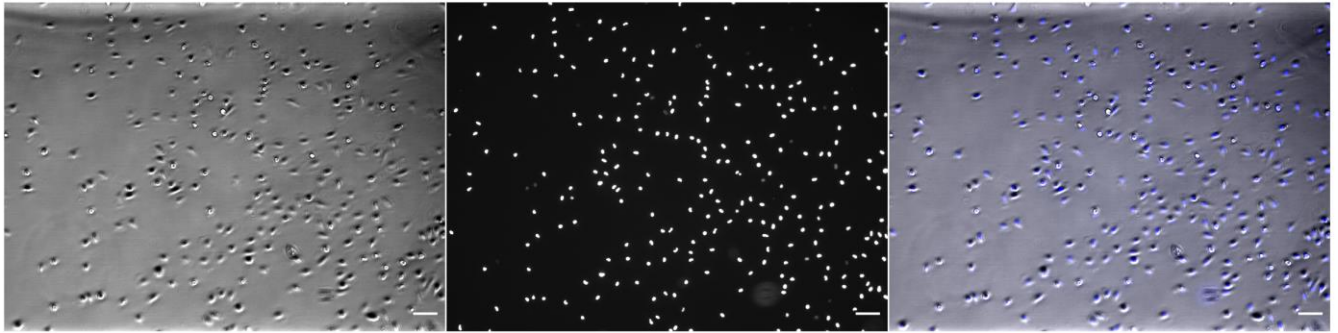
To confirm that automated and manual tracking produced similar results, a representative dataset was analysed via both approaches and the results compared. These datasets contained FMI values from the additional 20nM directional gradient C5a chemotaxis experiments. Per data-point pairwise analysis shows that there is no significant difference between the values obtained by manual or automated tracking ($p=0.382$; **Figure 4.4B**). When comparing full datasets, there are differences in results generated, likely due to increased sample size per replicate using the automated method (**Figure 4.4C**). These results show that automated tracking of stained nuclei allows for efficient analysis of MDM migration with minimal variation compared to manual methods. In addition, the larger sample size may reduce the effect of localised concentration differences and heterogenous cell-seeding which might otherwise produce sampling bias.

A

Phase contrast

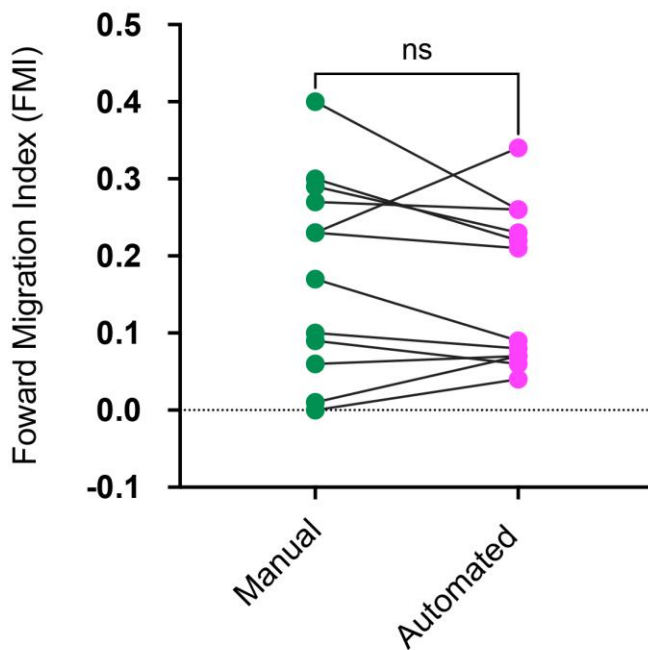
NucBlue

Merge



B

Pairwise comparison



C

Example dataset

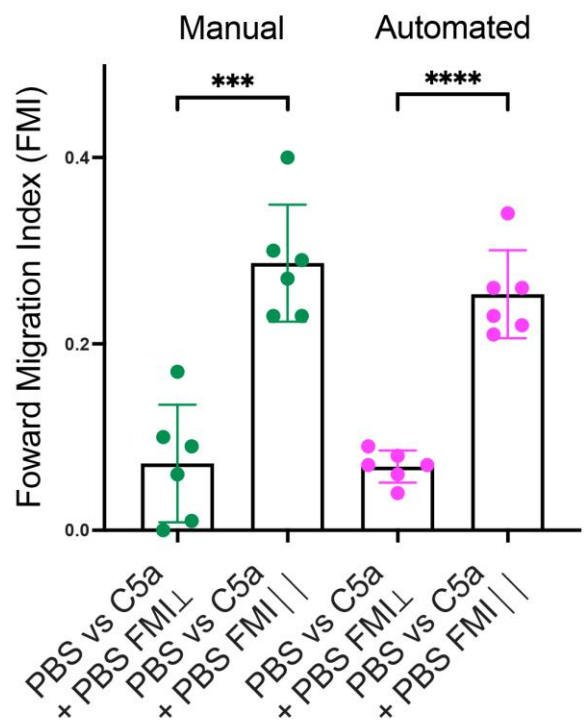


Figure 4.4 – Optimisation of cell culture transfer conditions

(A) Confocal images of Ibidi μ -slide adhered MDMs with NucBlue stained nuclei showing split channels for the phase contrast (left), 460nm blue channel (centre) and merged images (right) (B) Graph showing pairwise comparison of forward migration indices (FMI) for MDMs challenged with 40nM C5a as per Figure 4.3. Cells migration was tracked via manual and automated tracking approaches (Fiji manual tracking and Trackmate plug-in respectively). n=12 paired values; paired values are not significantly different with pairing significantly effective ($p < 0.0004$) between individual values. Lines and error bars denote the mean and standard deviation respectively Comparisons between FMI \perp and FMI \parallel values for each condition were compared via the students 2-tailed t-test. Statistical analysis via a Wilcoxon test for paired, non-parametric values. Note that a non-parametric test was used due to the non-normal distribution of data for the automated tracking approach. ns, *** and **** denote $p > 0.05$, $p < 0.001$ and $p < 0.0001$ respectively.

4.2.1.4 MDMs did not chemotax towards fMLP or MCP-1 using the Ibidi μ -slide

While 20nM C5a proved effective as an MDM chemoattract in this system, initial attempts to challenge MDMs with fMLP and MCP-1 failed to illicit chemotactic responses (data not shown). Once assay conditions had been optimised, a range of previously established concentrations were tested for both chemoattractants: fMLP was tested at 1ngmL^{-1} , 500ngmL^{-1} and $1\mu\text{gmL}^{-1}$; MCP-1 was tested a 1ngmL^{-1} , 10ngmL^{-1} and 200ngmL^{-1} (Palmer and Salmon, 1983; Grimshaw and Balkwill, 2001; Vancraeynest et al., 2003). Neither MCP-1 or fMLP were able to induce notable migration of MDMs (**Figure 4.5A; Figure 4.6A**). None of the tested MCP-1 concentrations tested produced visible migration, with small differences in FMI values noted (**Figure 4.5B**). fMLP showed a similar lack of effect (**Figure 4.6B**), with further controlled attempts with opposing 1ngmL^{-1} fMLP gradients, DMSO control and directional 1ngmL^{-1} fMLP having similar FMI differences (**Figure 4.6C**). Given that these chemoattractants have been previously validated at these concentrations, I would suggest that either poor reagent quality or changes in MDM sensitivity/viability because of processing are potentially responsible for the lack of MDM chemotaxis. Further experiments would be required to elucidate the reason behind these results.

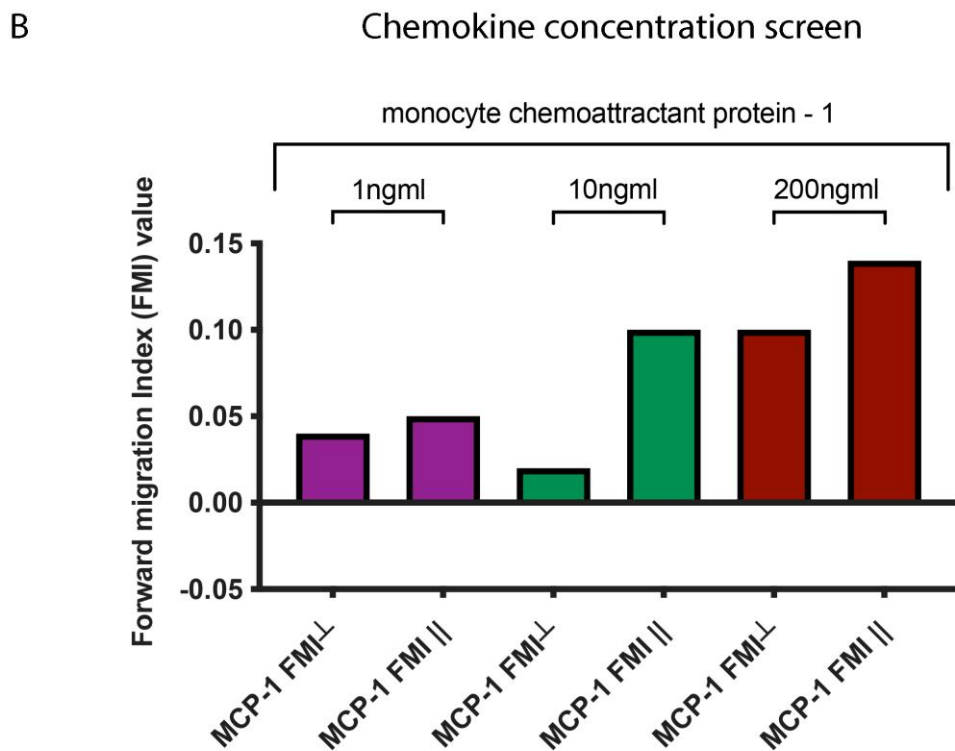
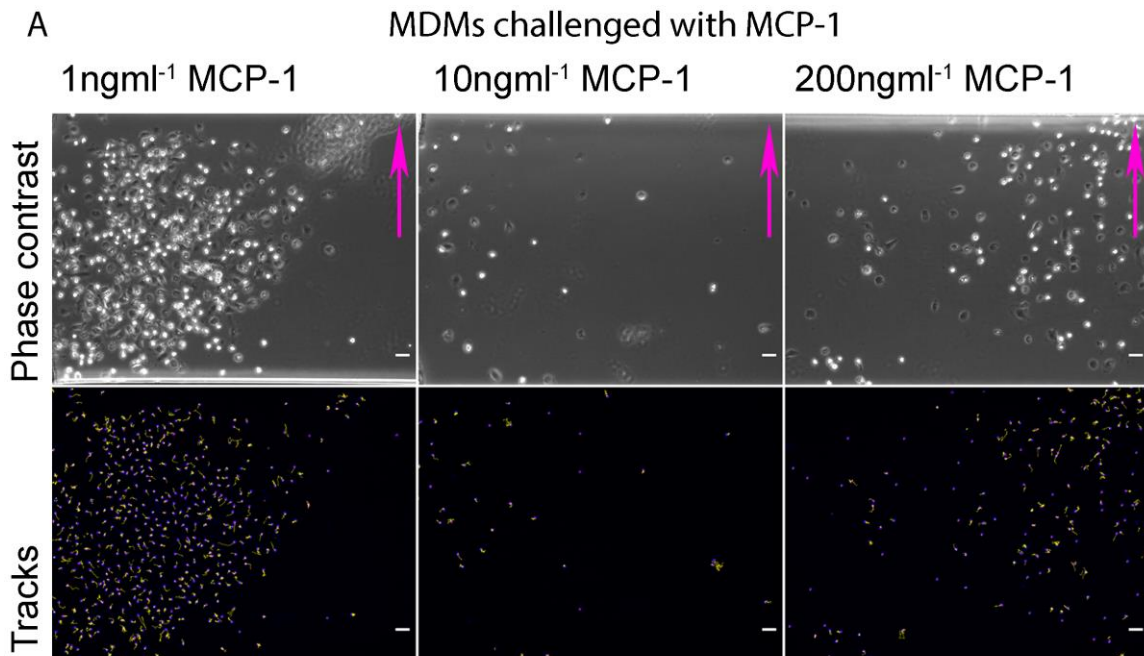
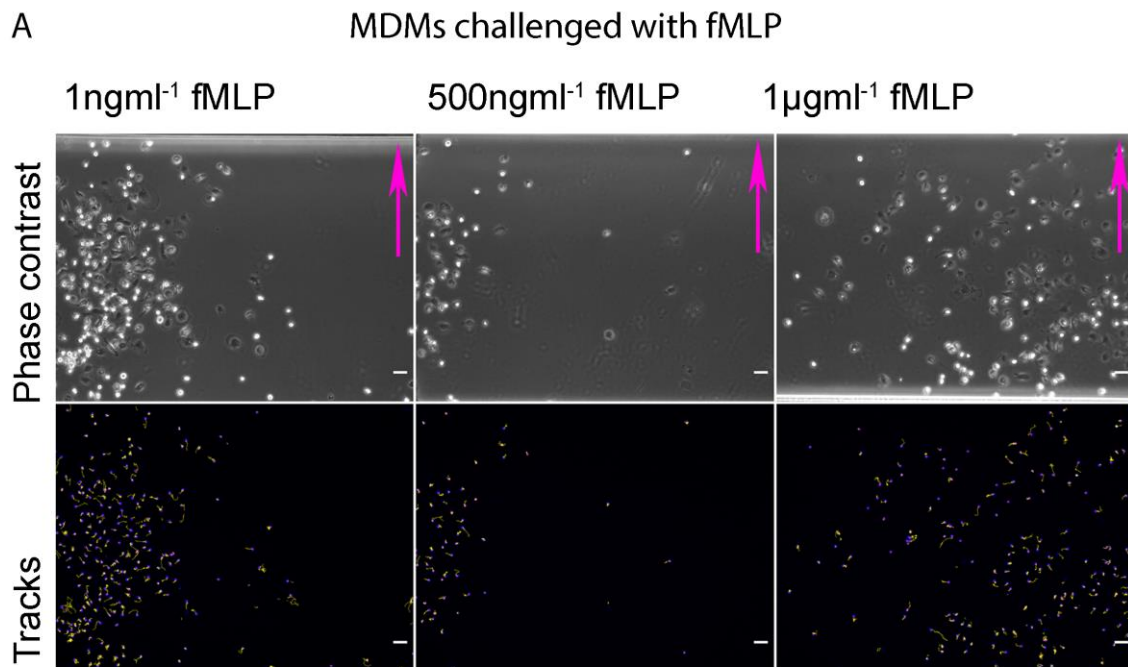
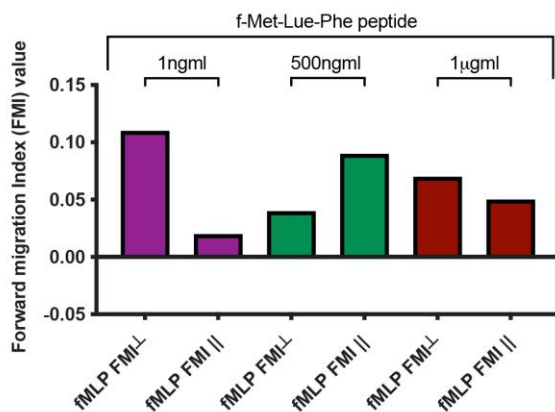


Figure 4.5 –MCP-1 did not induce migration of MDMs in the Ibidi μ -slide system

(A) Phase contrast images of migrating MDMs 3-hours post-chemokine addition for a range of concentrations of MCP-1 (1ngmL⁻¹/10ngmL⁻¹/200ngmL⁻¹ with associated MDM tracks (lower panels); Scale bars denote 50 μ m and magenta arrows indicate ascending chemoattractant gradient. (B) Comparisons of forward migration indices (FMI) for the FMI \perp (gradient perpendicular) and FMI \parallel (gradient parallel) as a measure of directed chemotaxis. n=1 μ -slide per condition. Data points represent the mean FMI value for the tracked population of cells (minimum 40 individual MDM tracks). n=1 μ -slide per condition, statistics non-applicable.



B Chemokine concentration screen



C fMLP FMI analysis

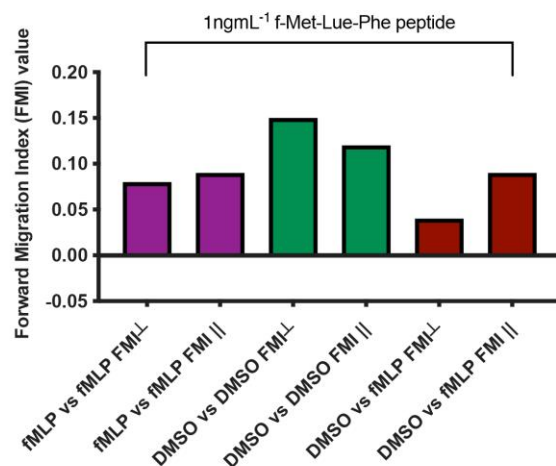


Figure 5.6 – fMLP did not induce migration of MDMs in the Ibidi μ-slide system

(A-B) Phase contrast images of migrating MDMs 3-hours post-chemokine addition for a range of concentrations of fMLP (1ngml⁻¹/500ngml⁻¹/1μgml⁻¹) (A) with associated MDM tracks (lower panels); Scale bars denote 50μm and magenta arrows indicate ascending chemoattractant gradient. (C) Comparisons of forward migration indices (FMI) for the FMI⊥ (gradient perpendicular) and FMI|| (gradient parallel) as a measure of directed chemotaxis. n=1 μ-slide per condition. Data points represent the mean FMI value for the tracked population of cells (minimum 40 individual MDM tracks). (D) FMI analysis of MDMs challenged with 2nM (~1ngml⁻¹) fMLP gradient compared to chemokine null (DMSO only) and gradient null (fMLP loaded on both sides of the chamber). n=1 μ-slide per condition. Data points represent the mean FMI value for the tracked population of cells (minimum 40 individual MDM tracks). Statistics non-applicable.

4.2.2 MDMs do not respond to long-range apoptotic signal gradients in 2D chemotaxis experiments

It has been shown that in *Drosophila*, apoptotic cells can distract macrophages from their normal migratory behaviours *in vivo* (Moreira et al., 2010; Roddie et al., 2019). This behaviour suggests that chemoattractants released by dying cells, known as find-me cues, are prioritised over other signals. To understand how find-me cues act efficiently in the presence of biological noise in a system relevant to vertebrates, we planned to compare apoptotic find-me cues against other chemotactic factors in a competition assay. With C5a induced MDM chemotaxis established, I sought to test if MDMs will migrate towards find-me cues and if so, how they prioritise find-me cues in the presence of a competing chemoattractant. To generate find-me cues, neutrophils derived from healthy volunteer blood were cultured and aged for 22 hours in order to induce apoptosis: this protocol has been previously shown to reliably produce apoptotic cultures with minimal necrosis (Renshaw et al., 2003). Apoptotic neutrophils were removed via centrifugation to produce cell-free, apoptotic-derived supernatant (ASN) media. To control for the presence of apoptosis independent chemoattractants in the ASN, apoptotic null supernatant (ANN) was generated from aged neutrophils treated with the pan-caspase inhibitor Q-VD-OPh (Merck) i.e., media extracted from aged neutrophils cultures in which apoptosis was prevented.

As per previous experiments, MDMs within the observation chamber were challenged with either opposing gradients of ANN, opposing gradients of ASN or a directional gradient of ASN and cell movements tracked from the resultant time-lapse movies (**Figure 4.7A**). FMI analysis shows that MDMs did not migrate ($FMI_{||} = FMI_{\perp}$) in response as control ANN and ASN opposing gradients ($p=0.282$; $p=0.387$) nor directional ASN ($p=0.8567$) (**Figure 4.7B**). To confirm that the ageing protocol was indeed producing apoptotic neutrophils, cytospin histology was conducted on culture samples. Aging for 22 hours generated significantly greater levels of apoptosis (78%) compared to incubation with the anti-apoptotic pan-caspase inhibitor Q-VD-OPh (31%; $p<0.001$) (**Figure 4.7C**). These results suggest that apoptotic supernatant generated from primary neutrophil cultures cannot induce the recruitment of MDMs when supplied to MDMs as a directional gradient in this assay.

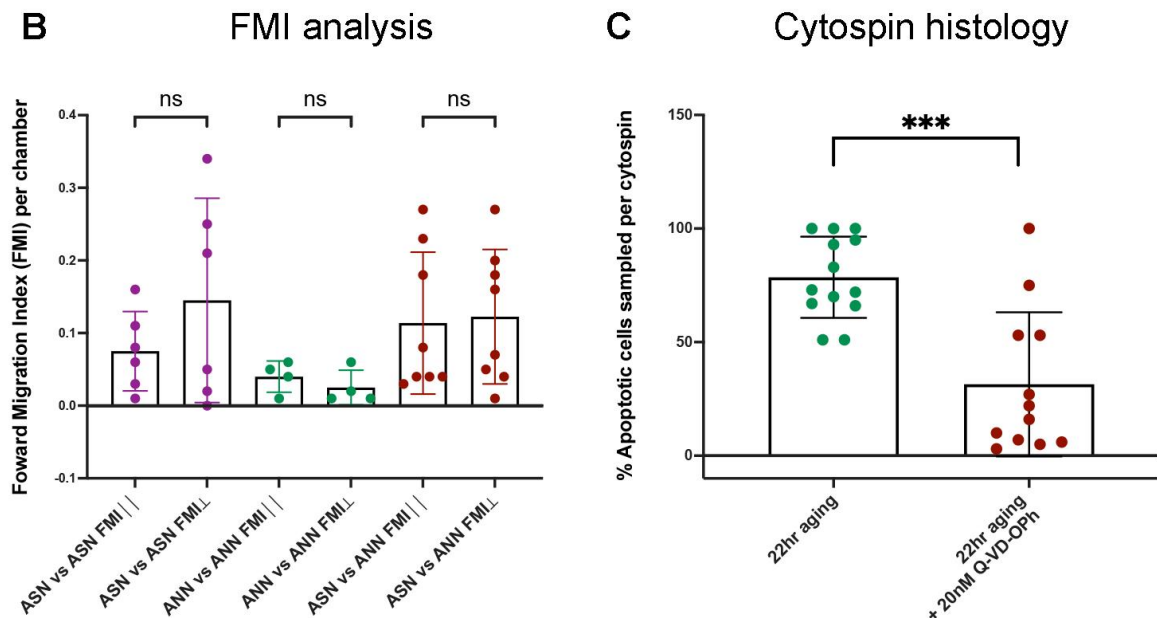
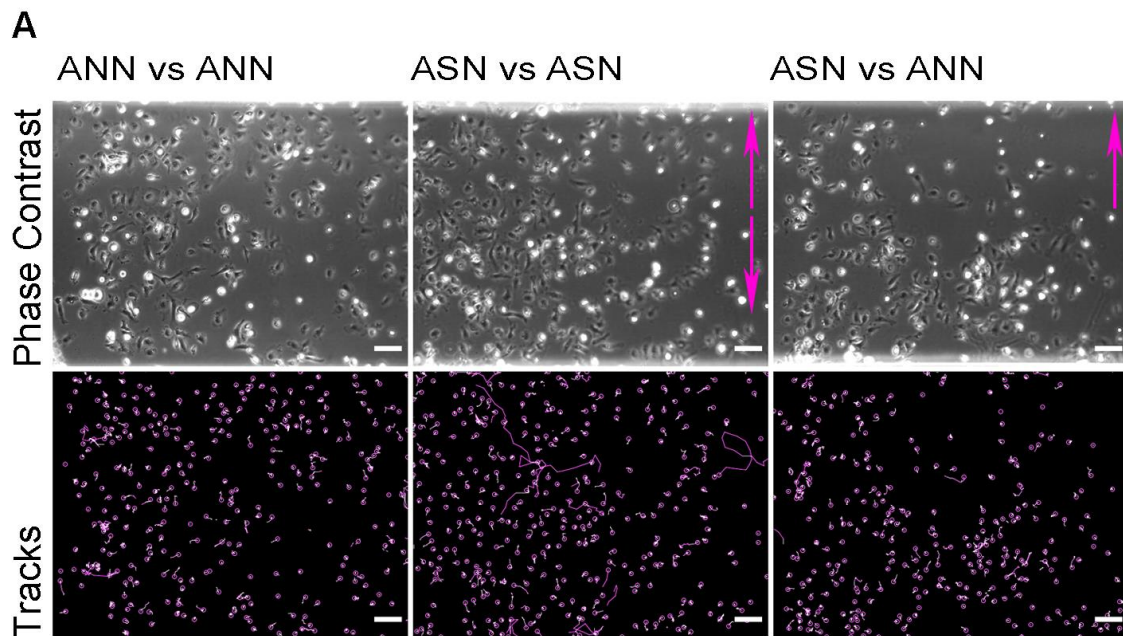


Figure 4.7 – Apoptotic supernatant does not induce MDM migration at long range

(A) Phase contrast images of migrating MDMs 3-hours post-chemokine addition showing chemokine null (left), gradient null (centre) and directional ASN gradient (right). Fiji track-mate plugin automated tracking of stained cell nuclei (lower panels); scale bars denote 100 μ m and magenta arrows indicate ascending chemoattractant gradient. (B) Comparisons of forward migration indices (FMI) as a measure of directed chemotaxis. N=8, 4, and 6 for the following conditions: ASN vs ASN (p=0.387), ANN vs ANN (p=0.282) and ASN vs ANN (p=0.857). All data points denote the average value per μ -slide. Line and error bars denote the dataset mean and standard deviation per condition. FMI data was compared using a two tailed Student's t-test between the average FMI_{||} and FMI_⊥ values per condition. (C) Percentage of aged neutrophils that had undergone aging stimulated apoptosis after 22 hours to produce ASN and apoptotic inhibited Q-VD-Oph culture (calculated from cytospin histology). Percentage apoptosis was analysed using the 2-tailed Student's t-test. Note that the y-axis is plotted into negative values due to the standard deviation of the dataset.

4.2.3 Local apoptotic supernatant partially inhibits the migration of MDMs towards a defined source of C5a

Given that the current literature supports the chemotactic ability of ASN in several cell types, including THP-1, Mono Mac 6 and MDMs (Lauber, 2003), we theorised that the lack of an MDM response to ASN derived from aged neutrophils (**Figure 4.7**) may be the result of a lack of find-me cue diffusion towards the MDMs or batch-batch variation in the generation of ASN. To test if the diffusion distance was responsive for the lack of response to ASN, the experimental design was altered so that MDMs were saturated with a local concentration of ASN followed by a gradient of C5a: once MDMs were adhered to the chamber, the media was aspirated and replaced with ASN, ANN or control media (**Figure 4.8**).

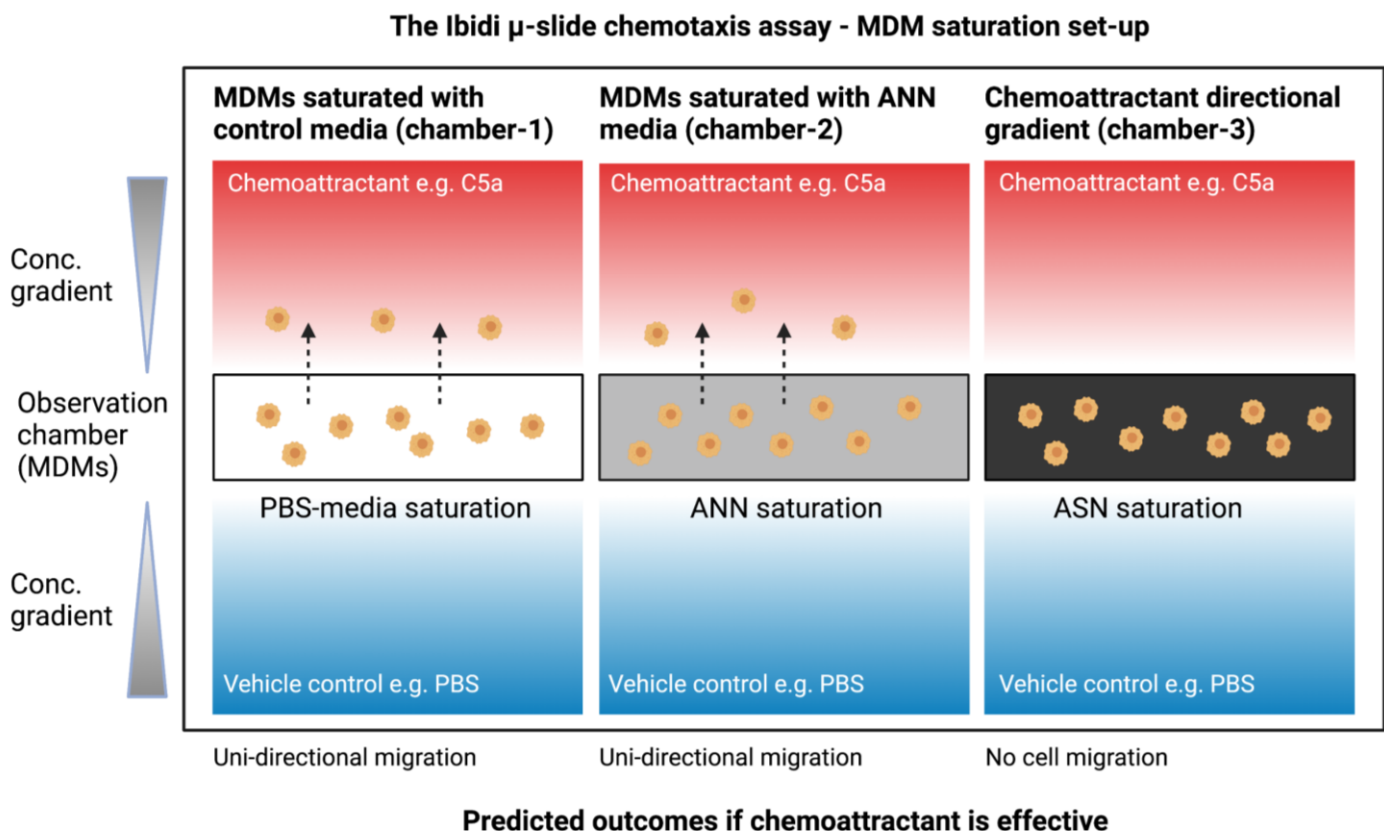


Figure 4.8 – Ibidi μ -slide experimental set up for MDM saturation with ASN

Schematic diagram of the Ibidi μ -slide experimental design modified to test the effect of MDM saturation with apoptotic derived supernatant (ASN). The slide is composed of three independent chambers, each of which has different chemoattractant conditions. Each chamber contains a central observation chamber wherein cells (in this case MDMs) are seeded and allowed to adhere. Once cell have adhered in the observation area, chemoattractant gradients are applied on either side. In contrast to the normal single

chemoattractant set-up (Figure 4.2), all the chambers have a unidirectional gradient of chemoattractant applied, in this case 40nM C5a. There are three conditions used when testing the effect of cell saturation with ASN: a saturation negative control chamber (1) wherein MDMs saturated with media containing only the vehicle control for the directional chemoattract; a apoptotic null control chamber (2) wherein MDMs are saturated with media derived from Q-VD-OPh treated neutrophils to produce an apoptotic null supernatant (ANN); and an experimental chemoattractant chamber (3) herein MDMs are saturated with ASN. Directional C5a gradients were only applied once cells had been saturated in the appropriate condition. If ASN is effective in inhibiting MDMs from migrating towards C5a, it would be expected that chambers 1 and 2 would see migration towards C5a while chamber 3 would see either no net migration or reduced migration.

MDMs were exposed to a 20nM directional gradient of C5a after saturation with either ASN, ANN or PBS control media (**Figure 4.9A**). FMI analysis showed that MDMs saturated with ASN did not migrate towards the C5a gradient ($FMI_{||} = FMI_{\perp}$; $p=0.484$) compared to the cells exposed to ANN ($p=0.0019$) or PBS control media ($p<0.0001$), which both showed significant migration towards the directional C5a gradient ($FMI_{||} > FMI_{\perp}$) (**Figure 4.9B**). Comparison of difference between the FMI values per chamber showed a trending but non-significant difference between the conditions ($p=0.115$), likely due to high inter-replicate variation (**Figure 4.9C**).

Since MDM saturation with ASN prevented proper migration towards C5a, correlation analysis was performed between the chemotactic response (i.e., the differences between $FMI_{||}$ and FMI_{\perp}) and the proportion of neutrophils undergoing apoptosis in the individual cultures used to generate batches of ASN (Cytospin histology); a positive correlation between levels of apoptosis and inhibition of chemotaxis supports the idea that find-me cues can impact MDM migration towards C5a and could also explain batch-batch variation in the assay (**Figure 4.9D**). Correlation of FMI difference ($FMI_{||} - FMI_{\perp}$) to cytospin % apoptotic cell counts showed that the reduced MDM response to C5a was linked to the relative concentration of ASN (as an indirect readout of find-me cue concentration) added to the cell chamber ($p=0.0064$). These results suggest that ASN can disrupt the migration of MDMs towards C5a, however, due to variation in the apoptotic levels in aged neutrophil cultures, it is important to test whether the preparation of ASN influenced its ability to alter MDM responses to C5a.

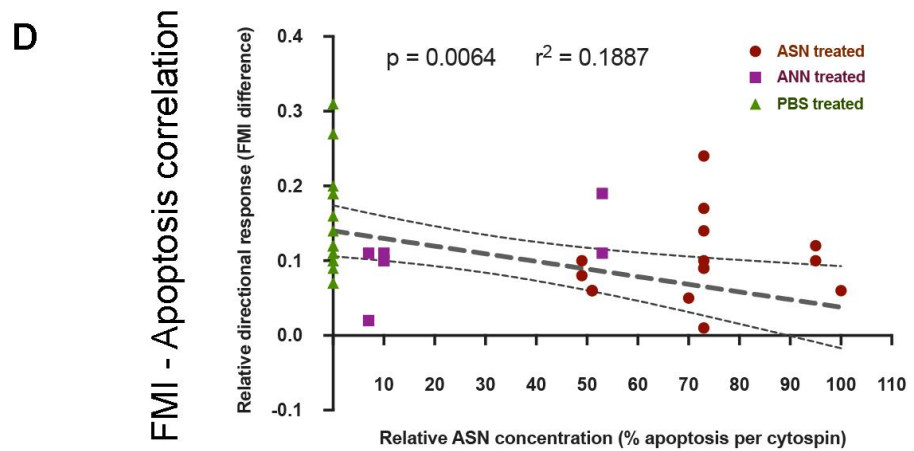
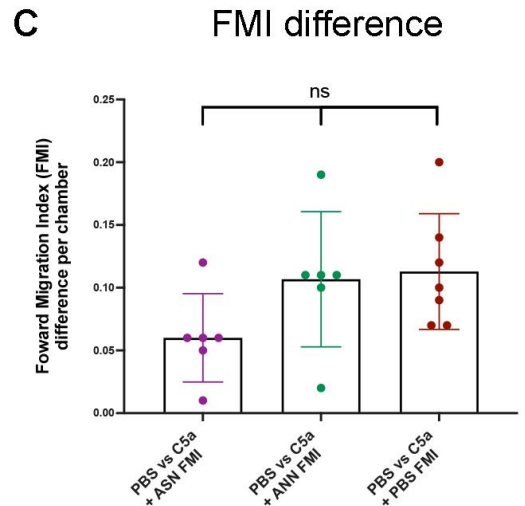
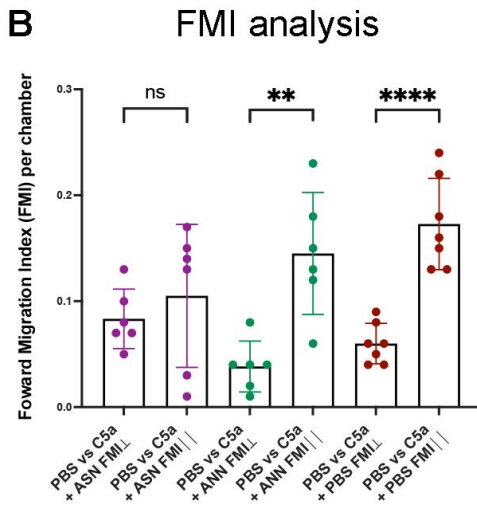
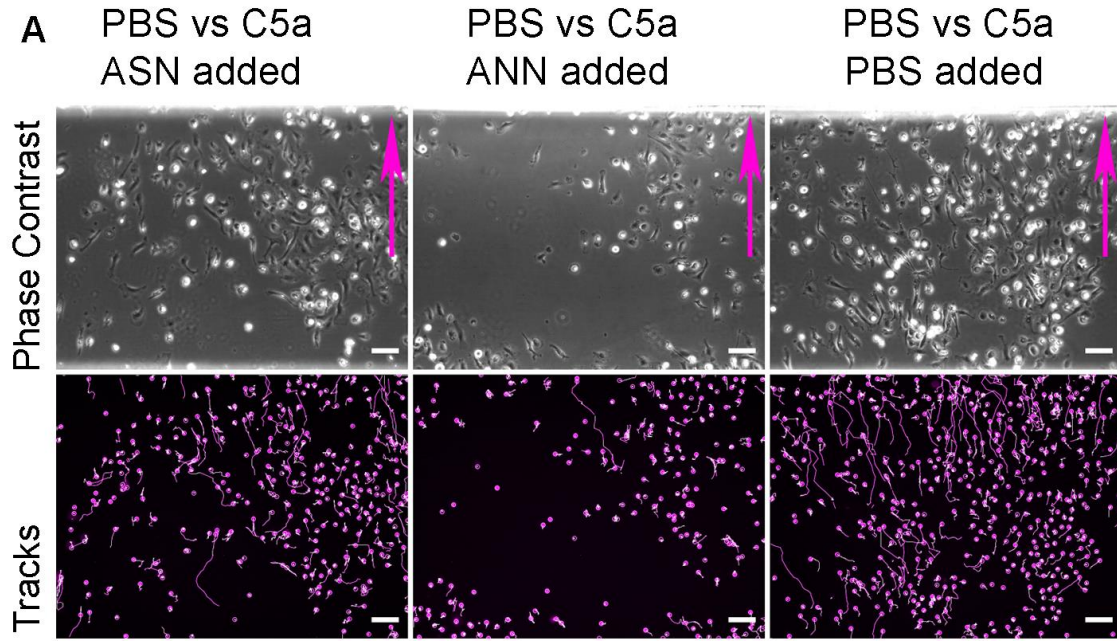


Figure 4.9 – Exposure to ASN inhibits MDM migration towards C5a

(A) Phase contrast images of migrating MDMs 3-hours post-chemokine addition (upper panel) with their corresponding tracks for this period (lower panel). MDMs were challenged with C5a after saturation with either ASN (left), ANN (centre) or PBS (right). Scale bars denote 100 μ m and magenta arrows indicate ascending chemoattractant gradient. **(B)** Scattergraphs showing the comparisons of forward migration indices (FMI) as a measure of directed chemotaxis for MDMs treated with ASN (n=6, p=0.482, ANN (n=6, p=0.0019) and PBS (n=7, p<0.0001). **(C)** Scattergraph showing the comparison of the FMI differences per chamber between ASN, ANN and PBS treated MDMs. All data points denote the average value per μ -slide. Line and error bars denote the dataset mean and standard deviation per condition, respectively. FMI data was compared using a two tailed Student's t-test between the average FMI $_{||}$ and FMI $_{\perp}$ values per condition. **(D)** Correlation analysis (linear regression) between the relative concentration of local ASN and the corresponding MDM response to C5a after treatment with ASN (n=13) ANN (n=6) and PBS (n=10). Data is labelled per condition with a line of best fit (black --) and 95% confidence limits (-- black curves) with p and r² values shown on graph. Correlation was calculated via simple linear regression. Statistical significance is reported as NS = p>0.05, ** = p<0.01 and **** = p<0.0001, respectively.

To confirm that the reduced MDM response to directional C5a gradients in the presence ASN was not due to the presence of necrotic factors, purified human neutrophils in media suspension were flash-frozen at -80°C to induce lysis and spun down to produce necrotic cell supernatant (NSN). As per the previous experiment, MDMs were saturated with either NSN or PBS media prior to challenge with C5a (**Figure 4.10A**) and allowed to migrate for 3 hours. FMI analysis showed that saturation of MDMs with NSN migrated towards a directional gradient of C5a (p= 0.0461) to a similar degree as those saturation with PBS media (p= 0.0053) (**Figure 4.10B-B'**).

For experiments requiring generation of ASN, supernatants were either used immediately after harvesting or stored at -80°C for later use. Given the relatively high variation seen with ASN treatment of MDMs challenged with C5a, I sought to exclude any freeze-thaw effects on the chemotactic potency of ASN. To test this, data obtained using “fresh” and “frozen” ASN samples were compared from experiments wherein MDMs saturated with ASN were challenged with C5a. FMI analysis showed that MDMs treated with fresh ASN had no preference for C5a (0.6779) compared to frozen ASN treated MDMs that showed a small but significant migration response (p=0.0072) (**Figure 4.10C**). Comparison of FMI differences showed that the per chamber response was not significantly different (p=0.754) (**Figure 4.10-C'**).

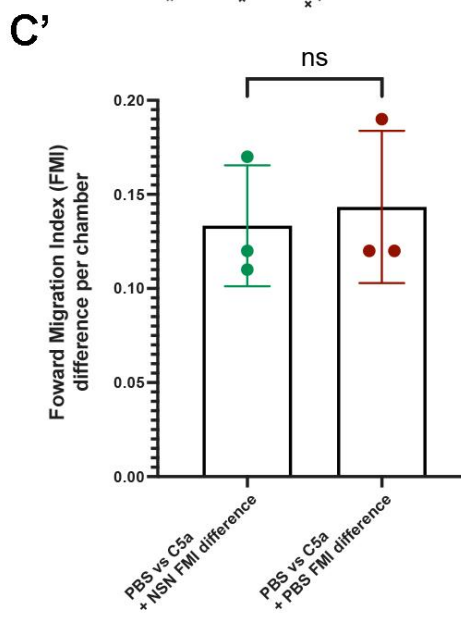
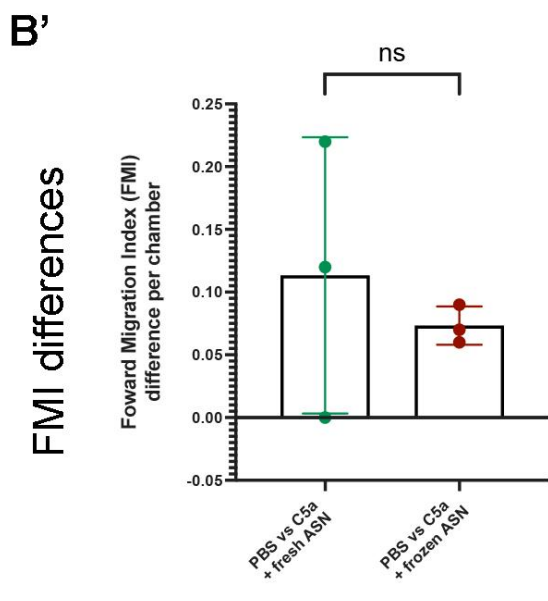
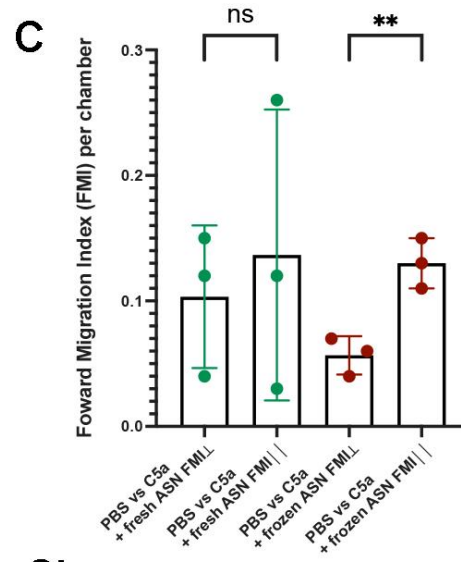
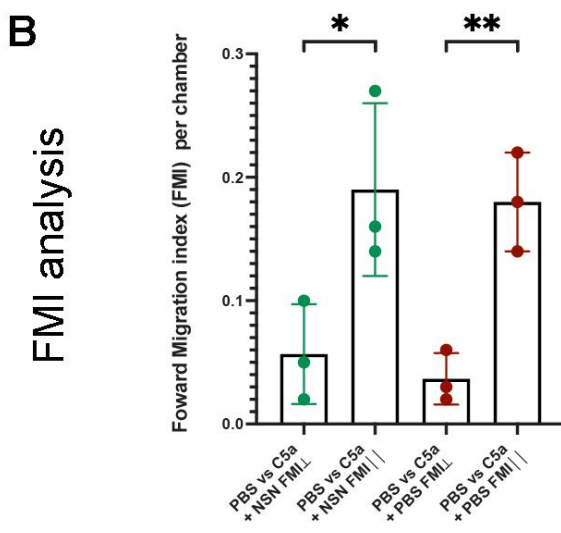
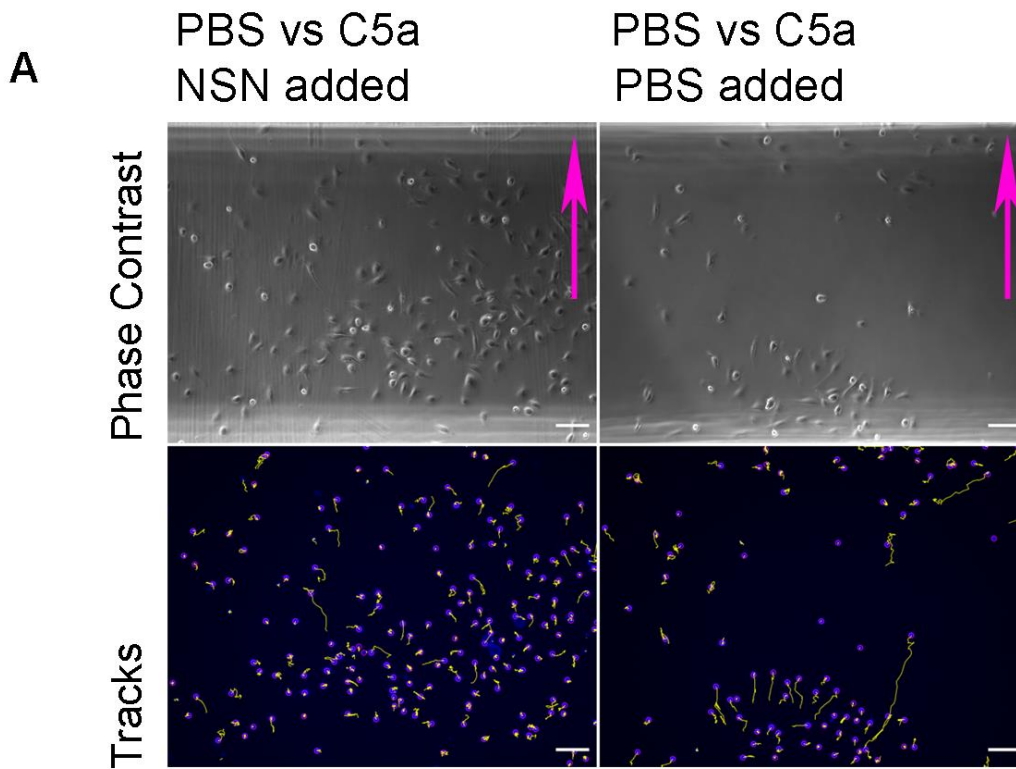


Figure 4.10 – Necrotic supernatant does not alter MDM migration towards C5a

(A) Phase contrast images of migrating MDMs 3-hours post-chemokine addition (upper panels) with corresponding tracks (lower panels) for MDMs challenged with C5a with and without NSN treatment (left and right panels, respectively; scale bars denote 100 μ m, magenta arrow indicates the direction of the C5a gradient (low-high concentration)). **(B)** Scattergraphs showing the comparisons of forward migration indices (FMI) as a measure of directed chemotaxis; n=3 and 3 for NSN (p= 0.0461) and PBS-treated MDMs (p=0.0053). **(B')** Scattergraph showing comparison of the FMI differences per chamber between NSN and PBS-treated MDMs (p=0.754). **(C)** Scattergraphs showing the comparisons of forward migration indices (FMI) for MDMs challenged with fresh or frozen ASN; n=3 and 3 for fresh ASN (0.0072) and frozen ASN-treated MDMs (p=0.6779). **(C')** Scatter graph showing the comparison of the FMI differences per chamber between NSN and PBS-treated MDMs (p=0.754). All data points denote the average value per μ -slide. Lines and error bars denote the dataset mean and standard deviation per condition, respectively. FMI data was compared using a two-tailed Student's t-test between the average FMI_{||} and FMI_⊥ values or the calculated difference between the two values (FMI difference) per condition. Statistical significance is reported as * = p<0.05 ** = p<0.01, respectively.

Overall, these results confirm that saturation of MDMs with ASN can inhibit their chemotaxis towards a directional gradient. NSN and ANN controls confirm that this inhibition is at least in part due to apoptosis and not the release of independent neutrophil factors or the presence of necrotic cell debris. While there does appear to be variation between ASN batches, the response of MDMs saturated with ASN is nonetheless robust and its ability to inhibit responses to C5a correlates with the proportion of apoptotic cell death within the cultures used to generate it – which presumably correlates with the relative concentration of find-me signals or other modulatory cues within this conditioned media.

4.2.4 The pan-caspase inhibitor Q-VD-OPh reduces MDM migration towards C5a

To produce the ANN treatment control used in previous experiments, we used the pan-caspase inhibitor Q-VD-OPh to inhibit apoptosis. MDMs saturated with ANN did not fail to respond to C5a to the same degree as ASN. However, when compared to controls, the migration was reduced when compared to PBS-media saturated controls, suggesting that the presence Q-VD-OPh may reduce the migratory capacity of MDMs (**Figure 4.9**). While this may have been due to lower (but still significant) levels of apoptosis in ANN cultures, it is also known that several members of the caspase protein family regulate non-apoptotic processes,

including cell migration (Nakajima and Kuranaga, 2017). For these reasons, we investigated whether Q-VD-OPh treatment itself impacts migration of MDMs towards C5a.

To understand if Q-VD-OPh was interfering with the migratory capacity of MDMs, these cells were saturated with media containing 20nM Q-VD-OPh at the same concentration used to inhibit apoptosis of aging neutrophil cultures prior to challenge with C5a. MDMs were saturated in media containing 20nM Q-VD-OPh, ASN or PBS-media and challenged with a directional gradient of 40nM C5a (**Figure 4.11A**). FMI analysis shows that Q-VD-OPh treatment inhibited MDM migration towards C5a ($p=0.843$) similarly to ASN treatment ($p=0.0718$) and in contrast to PBS-treated cells ($p=0.0023$) (**Figure 4.11B**). Comparison of FMI value differences shows that MDMs saturated with ASN ($p=0.0166$) or Q-VD-OPh media ($p=0.0029$) had a significant reduction in their response to C5a, compared to controls (**Figure 4.11B'**). In addition, ASN ($p=0.0085$) or Q-VD-OPh ($p=0.005$) saturation significantly reduced MDM motility, as measured by the average travel distance (**Figure 4.11C**). These data suggests that the inhibition of caspase enzymes can affect the non-apoptotic functions of these enzymes and prevent proper MDM migration, at least in response to C5a.

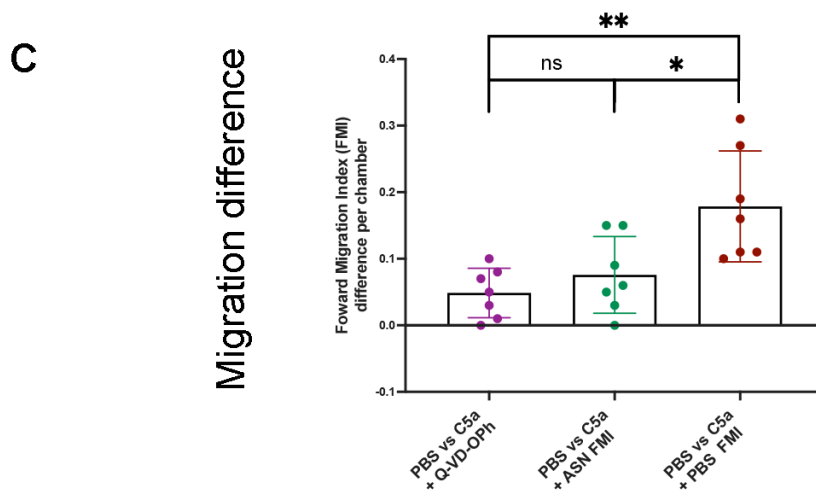
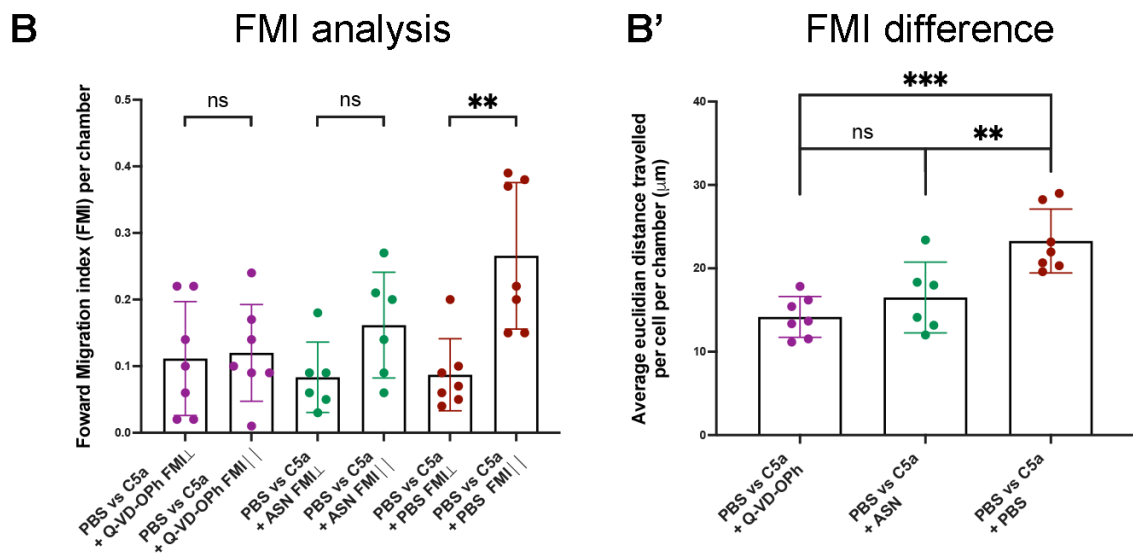
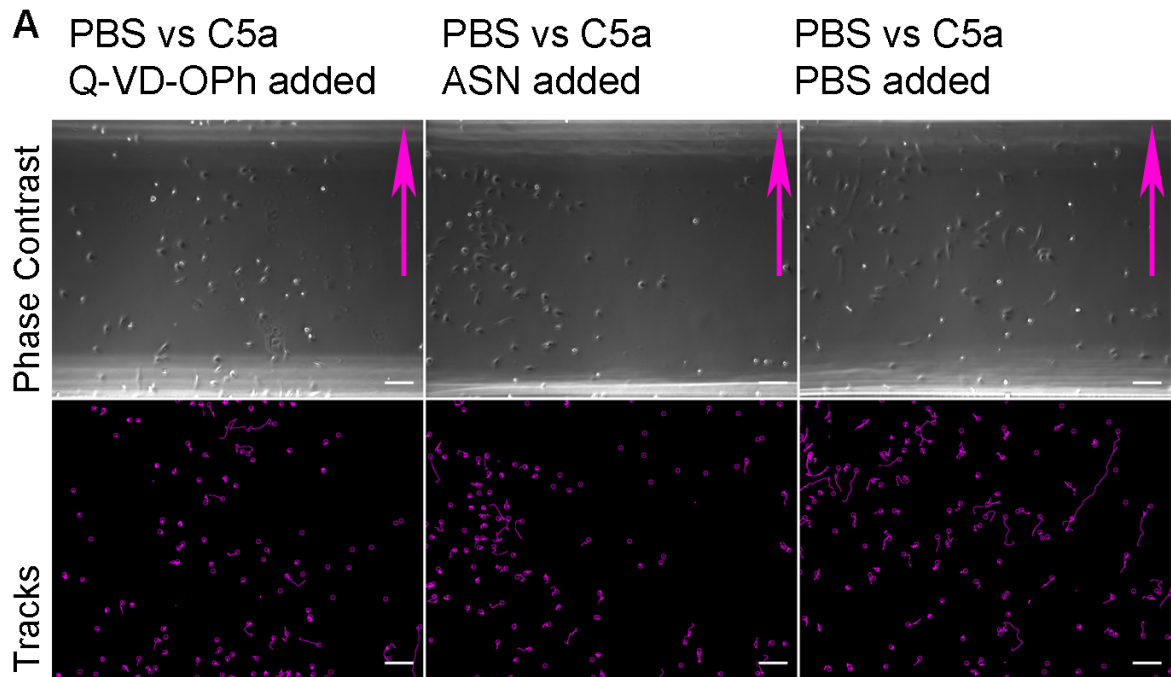


Figure 4.11 – Treatment with Q-VD-OPh reduces the chemotactic response of MDMs to C5a

(A) Phase contrast images of migrating MDMs (upper panels) 3-hours post-chemokine addition after treatment with either Q-VD-OPh (left), ASN (centre) or PBS (right) with corresponding tracks (lower panels). Direction of the chemokine gradient (low – high concentration) is annotated as magenta triangles to the side. Scale bars denote 100 μ m. **(B)** Scattergraph of forward migration indices (FMI) with comparisons made between the FMI $^{\perp}$ (gradient perpendicular) and FMI $||$ (gradient parallel) for MDMs treated with Q-VD-OPh (n=7, p=0.843), ASN (n=6, p=0.0718) and PBS (n=7, p=0.0023) prior to challenge with C5a. **(B')** Scattergraph showing the average FMI difference per chamber value for MDMs treated with Q-VD-OPh (n=7, p=0.0029 compared to PBS, p=0.699 compared to ASN), ASN (n=6, p=0.0166 compared to PBS) or PBS (n=7). **(C)** Scattergraph showing the average distance that each MDM migrated over the course of 3 hours (μ m) after treatment with Q-VD-OPh (n=7, p=0.005 compared to PBS, p=0.479 compared to ASN), ASN (n=6, p=0.0085 compared to PBS) and PBS (n=7). All data points denote the average value per μ -slide. Lines and error bars denote the dataset mean and standard deviation per condition, respectively. FMI data was compared using two-tailed Student's t-test between the average FMI $||$ and FMI $^{\perp}$ values per condition. FMI difference data and Euclidian distance comparisons were analysed using a one-way ANOVA with Tukey's test. Statistical significance is reported as * = p<0.05, ** = p<0.01, *** = p<0.001, respectively.

4.3 Discussion

Over the course of this chapter, I have shown how we have optimised the Ibidi μ -slide micro-fluidic chamber for use with primary differentiated macrophages. Initial results show that viable MDMs could be transferred into the μ -slide system and undergo chemotactic behaviour in response to at least one validated chemokine (C5a). It was also shown that the presence of apoptotic-derived supernatant was able to override macrophage chemotactic responses towards C5a. Of a practical note for the field, these data also suggest that the commonly used apoptotic inhibitor Q-VD-OPh may also exert inhibitory effects on macrophage migration.

4.3.1 MDMs can undergo chemotaxis in response to 2D chemokine gradients

The use of *in vitro* chambers for assaying cell migration has become more assessable due to ongoing system development in recent decades (Irimia and Ellett, 2016). Since the inception of the early Boyden type chamber (Boyden, 1962), migration chambers have expanded to assay several motile cell functions, including wound healing (Barbero et al., 2008), ECM interactions (Wolf et al., 2013) and chemotaxis (Muinonen-Martin et al., 2010). Herein, I have

used Ibidi μ -slides, as the design of this system enables direct challenging of cells with different signals, facilitating competition assays.

The initial protocol underwent several rounds of optimisation as there was no known examples of *ex vivo* MDM migration using this system. This optimisation was largely concerned with conserving the viability of MDMs after transfer from differentiation conditions to the migration chamber and streamlining analysis through automated tracking. Initial attempts to maintain MDM viability post transfer failed due to a lack of MDM attachment to the collagen substrate. Standard scraping procedures or cold-shock resulted in MDMs failing to re-adhere post treatment – successful transfer was ultimately achieved using Accutase dissociation solution (Chen et al., 2015). Having successfully optimised MDM transfer conditions, I validated chemotaxis towards established macrophage chemokines. Experiments using a range of fMLP, or MCP-1 concentrations failed to illicit chemotactic responses, however the addition of 20nM C5a did induce robust MDM movement towards this cue. This macrophage response towards C5a is consistent with previous reports using the Ibidi μ -slide system with peritoneal mural macrophages (Kronlage et al., 2010). Querying recent RNA sequencing data of MDMs generated from whole blood monocytes, suggests that MDMs that are differentiated according to similar protocols to those used in this study (6-9 days in culture with RPMI 1640 containing 10% FCS and 1% penicillin/streptomycin), express the fMLP, but not MCP-1 receptor (Baidžajevs et al., 2020). While this may explain why MDMs failed to migrate to MCP-1, the lack of a response to fMLP may be due to changes in the MDM expression profile because of transferring culture conditions for migration assays.

4.3.2 Apoptotic-derived signals are short range and can inhibit chemotaxis towards C5a

As stated previously, we used an *ex vivo* migration chamber approach to test a variety of chemotactic ligands. For those that elicited a chemotactic response I then analysed the ability of apoptotic cell supernatant to impair that response. This is a proxy to address whether find-me cues can override other chemokines and characterise whether the hierarchies/signal prioritisation that have been identified in simpler model organisms (Moreira et al., 2010; Roddie et al., 2019) are paralleled in vertebrates. We chose to generate apoptotic supernatant (ASN) via ageing of primary neutrophils (Renshaw et al., 2003), with apoptotic-

null media (ANN) derived from neutrophils aged in the presence of a caspase inhibitor (Q-VD-OPh); necrotic supernatant (NSN) was generated by lysing neutrophils via freeze-thaw cycles.

To test the chemotactic potential of apoptotic find me cues, I initially challenged MDMs with a directional gradient of ASN. Interestingly, MDMs did not respond to these signals and did not significantly migrate down the gradient. There are several explanations for this: given that *in vivo* apoptosis does not result in inflammation or the mass infiltration of immune cells, it has been theorised that find-me cues act in a relatively local manner (Morioka et al., 2019), and thus it could be the case that any find-me cues present in ASN are not able to diffuse the ~1mm distance towards the MDM observation chamber to a detectable level; It is also known that certain cues such ATP/UTP nucleotides are relatively unstable and require propagation within a tissue e.g., Ca²⁺ secondary messengers and ATP-mediated ATP release through the activation of pannexin channels (Zimmermann, 2000; Dou et al., 2012; Sieger et al., 2012), meaning that the find-me cues might not be at a high enough concentration if extracted from apoptotic cells alone; finally, various groups have shown that inhibition of single cues can significantly abolish the chemotactic potential of ASN (Lauber, 2003; Elliott et al., 2010), suggesting that a cocktail of structurally-divergent, non-redundant cues may act in concert to exert their effects most efficiently. To rule out these factors, there are a several potential experiments that could be conducted: direct addition of apoptotic cells into the chemoattract chamber could allow for find-me cues to be released over time and form gradients more akin to those that might occur within a tissue; or challenging MDMs with singular purified find me cues could be done to confirm they can diffuse and form gradients within this assay, however since the composition of ASN remains unknown this would be of limited relevance.

Since ASN did not appear to be chemotactic when applied as a direct gradient, I decided to saturate MDMs with ASN prior to challenge with C5a to test if MDMs within an apoptotic environment are still able to respond effectively to other chemoattractive signals. The results show that MDMs saturated in ASN had a blunted response to C5a which was due to apoptosis and not necrosis or other factors released during neutrophil aging. One potential explanation is that the find me cues present within ASN signal via pathways that take precedence over C5aR signalling; this form of signalling hierarchy has been explored in

neutrophils, with studies showing that p38 signal transduction is prioritised over signals requiring the PI3K pathway e.g. neutrophil chemotaxis towards a gradient of fMLP is prioritised via p38 over IL-8 mediated PI3K signalling (Heit et al., 2002; Kim and Haynes, 2012). Interestingly, it has been suggested that one of the known find-me cues could be act through C5aR, namely the ribosomal derived peptide RP-S19: RP-S19 is a small ribosomal subunit that has previously been established as one of the causative mutations in Diamond-blackfin congenital erythroblastopenia (Choesmel et al., 2007), a disease characterised by dysfunctional erythrocyte haematopoiesis. Dimeric RP-S19 is known to interact with the C5a receptor expressed on macrophages (Nishimura et al., 2001; Yamamoto, 2007). It has been suggested that this peptide acts as an apoptotic find-me cue, in particular during the resolution of inflammation, wherein neutrophils undergoing apoptosis might release it to both induce efferocytosis and reprogram macrophages that arrive at such sites to an anti-inflammatory state (Yamamoto, 2007). While further experimentation would be required, this could provide a mechanism for the observed loss of MDM saturated in ASN migration towards C5a (direct competition for binding to the C5a receptor). This mechanism could be explored in this assay by challenging MDMs with opposing gradients of C5a and purified dimeric RP-S19 or protein-interaction assay e.g., Glutathione S-transferases (GST)-pull-down with dimeric RP-S19 and C5aR.

4.3.3 Pan-caspase inhibition can perturb macrophage motility

To control for the apoptosis-independent changes to aged neutrophil media, the pan-caspase inhibitor Q-VD-OPh was used. During our initial ASN experiments, it was observed that cells treated with ANN containing Q-VD-OPh had a reduction in their overall movement. MDMs treated with Q-VD-OPh alone also showed a loss of motility, suggesting the C5a chemotactic response was partly caspase-dependent. It has been shown that certain members of the caspase family such as Caspase-11 and 8, are linked to actin-dependent migration processes and that these functions do not strictly depend on their proteolytic activity (Gdynia et al., 2007; Li et al., 2007; Barbero et al., 2008). Q-VD-OPh is known to bind irreversibly to the catalytic domain of caspase enzymes and thus could result in conformational changes to the proteins structure that alter the function of the other domains. This result is of technical value to the field as the use of anti-apoptotic drugs is commonplace in the inhibition of apoptosis in culture and as control conditions. Our data suggests that the application of

caspase inhibitors of this type may not be appropriate in circumstances where cell migration is being assayed.

4.3.4 COVID-19 impact statement and future work

At the time of writing, there has been major disruption to university access and public life due to the ongoing COVID-19 pandemic (March 2020 – present). This has unfortunately affected cell-culture work in several ways including a fall in the availability of blood donors and phlebotomists, in addition to access to cell culture and microscopy facilities. As a result of this disruption, there are several further experiments that would have been conducted which shall be discussed here as to highlight the direction of ongoing work and as a foundation for possible resumption of research in the future.

Although we challenged MDMs with several different chemoattractants, only C5a produced a robust chemotactic response. Unfortunately, the lack of broad chemoattractant sensitivity precluded the establishment of a signalling hierarchy using this cell model. Due to this, it is recommended that further attempts to achieve this aim should attempt to utilise other cell model systems such as mouse bone marrow-derived macrophages (BMDMs) (Ocana-Morgner et al., 2011) . Given the highly variable viability of human MDMs after transfer into the μ -slide, it would be recommended to use a migration assay that does not require detachment of cells from the culture substrate, such as Insall migration chambers (Muinonen-Martin et al., 2010). Alternatively, other read-outs could be utilised to measure the effect of chemoattractants on MDMs, such as western-blotting to assess the expression of migration-associated genes or immunostaining for receptor activation (Bagher et al., 2018). Such experiments might reveal the relative strength of chemoattractants through comparison of their downstream target expression and receptor activation levels.

As previously discussed, the results showed that MDMs treated with ASN had a reduced response to C5a, possibly because of the presence of RP-S19. To further evaluate this finding, it would be recommended to first test for the presence of RP-S19 in neutrophil generated ASN through standard western blotting procedure and if present, confirm MDM chemotaxis towards purified recombinant RP-S19 and towards RP-S19 depleted ASN. These data would

confirm if the reduced MDM response to C5a in the presence of ASN is wholly the result of RP-S19 – C5a receptor binding or if other ASN constituents are acting in a similar manner.

4.3.5 Concluding remarks

In summary, the data presented here shows that *ex vivo* cells such as MDMs can be effectively used in the Ibidi μ -slide for chemotactic and signal prioritisation experiments. Our experiments using apoptotic supernatant have produced results consistent with the hypothesised role of find-me cue signal superiority (Moreira et al., 2010; Roddie et al., 2019) and the interaction between find-me cues and C5a agree with data from previous studies (Nishimura et al., 2001; Yamamoto, 2007). In addition, our finding that pan-caspase inhibitors can interfere with such experiments are of useful technical note to the field as such drugs are commonly used as controls in experiments involving apoptotic cells.

Chapter 5: The epidermal growth factor ligand Spitz modulates macrophage efferocytosis, wound responses and migration dynamics during *Drosophila* embryogenesis

5.1 Introduction

5.1.1 *Drosophila* immunity, apoptosis and efferocytosis

Drosophila melanogaster fruit flies have a robust cellular immune response, composed principally of motile and highly-phagocytic plasmatocytes (Evans and Wood, 2011), which perform many analogous functions to vertebrate macrophages, e.g., phagocytosis of apoptotic cells and pathogens, migration to wounds and secretion of extracellular matrix (Buchon et al., 2014; Weavers et al., 2016a). These cells (referred to hereafter as embryonic macrophages) have been extensively used to investigate cell polarisation and migration *in vivo*, although we are yet to understand the full complement of cues that regulate their behaviours. Post hematopoiesis, embryonic *Drosophila* macrophages undertake stereotypical patterns of dispersal across the embryo. This dispersal is governed by PDGF/Vegf-related ligands (Pvfs) that act both as chemoattractants and pro-survival signals (Cho et al., 2002; Brückner et al., 2004; Wood et al., 2006), cell-cell repulsion between macrophages (Davis et al., 2012), and access to physical spaces created during organogenesis (Evans et al., 2010a). Once dispersed over the embryo (stage 15 onwards), macrophages become competent to respond to wounding stimuli (Moreira et al., 2010) and undergo “random migration”, a process driven in part by cell-cell repulsion (Stramer et al., 2010). Two further migration-dependent functions of these macrophages that require their polarisation and migration towards a specific target are clearance of apoptotic cells (efferocytosis) and responses to acute wound stimuli.

Apoptosis is the major form of programmed cell death in multicellular organisms (Fuchs and Steller, 2011; Galluzzi et al., 2012) and rapid efferocytosis is required to prevent secondary necrosis, a highly pro-inflammatory event that can lead to subsequent tissue damage (Degterev and Yuan, 2008; Ariel and Ravichandran, 2016). Failures in efferocytosis are linked to a range of disease pathologies in humans, particularly those associated with chronic inflammation, including atherosclerosis and chronic obstructive pulmonary disease (Eltboli et al., 2014; Morioka et al., 2019). The recruitment of macrophages to apoptotic cells is mediated by a family of chemoattractants released as part of the apoptotic cell death program and collectively referred to as “find-me” cues (Ravichandran, 2003). While find-me cues have been extensively studied in mammals, e.g., ATP or sphingosine-1-phosphate (Lauber, 2003; Elliott et al., 2009), the identity of such signals remains unknown in *Drosophila*. *Drosophila* embryonic macrophages also undertake polarised migration when responding to tissue damage (Stramer et al., 2005). This process requires the generation of reactive oxygen species (Razzell et al., 2013; Evans et al., 2015), resembling inflammatory responses in other model organisms, including zebrafish (Niethammer et al., 2009; Yoo et al., 2011). Again, the precise nature of wound cues remains to be determined in flies.

5.1.2 Epidermal growth factor signalling in *Drosophila*

Recent evidence in *Drosophila* suggested that an epidermal growth factor (EGF) ligand homolog, Spitz, is secreted from midgut cells undergoing apoptosis. This facilitates recruitment of stem cells to replenish the cells in those apoptotic regions, thereby maintaining gut integrity (Liang et al., 2017). A chemoattractive role for EGF ligands is conserved across evolution with, amongst others, both human whole blood monocytes and border cells in the developing *Drosophila* oocyte shown to chemotax towards EGF ligands (Duchek and Rørth, 2001; Lamb et al., 2004). In contrast to mammalian EGF receptor signalling, which is composed of multiple heterodimeric ErbB receptors and ligands (Burgess et al., 2003; Citri and Yarden, 2006), *Drosophila* possess only a single EGF receptor (Torpedo). Torpedo is activated by several partially redundant ligands (Spitz, Vein, Keren and Gurken) that are expressed in a tissue-specific manner (Price et al., 1989). In both flies and humans, secretion of active EGF ligands is tightly regulated via activation of the proteolytic enzymes Rhomboid (Shilo, 2016) and ADAM17 (Scheller et al., 2011; Rose-John, 2013). During *Drosophila* development, Spitz is ubiquitously expressed. However, the key processing

enzyme Rhomboid is expressed in a tissue-specific pattern, including by the cells of the ventral midline (Tomancak et al., 2007; Frise et al., 2010). This post-translational control enables spatial specificity of action, for instance the role of Spitz in development of the midline glia (Raz and Shilo, 1992). The combined evolutionary and developmental evidence suggested to us that Spitz might have a role as a chemoattractant regulating *Drosophila* macrophage behaviour.

I hypothesised that EGF signalling, and most likely Spitz, can act as a macrophage chemoattractant during *Drosophila* embryogenesis and may play a role in efferocytosis, either as an apoptotic find-me cue or as a modulator of macrophage behaviour. In this chapter, I have used tissue-specific expression of two active variants of the EGF ligand Spitz to investigate how high levels of EGF signalling can alter the migration and function of *Drosophila* macrophages *in vivo*.

5.2 Results

5.2.1 Screening for EGF activity using disruption of eye development

Of the four cardinal EGFR activating ligands, all except Vein are produced as inactive pro-peptides (Price et al., 1989; Reich and Shilo, 2002). To understand if active EGF signalling does alter macrophage function, it was necessary to first identify which ligands/transgenic constructs were biologically active. To do so, *eyeless-GAL4* (Hazelett et al., 1998) was used to drive the misexpression of several EGF pathway components in the developing *Drosophila* compound eye, with changes in eye-shape and size taken as a marker of proliferative activity (Freeman, 1996; Lyko et al., 1999). Several proteins were tested via misexpression: these included signalling apparatus, such as the EGFR receptor and a dominant negative variant (EGFR and EGFR^{DN}), and constitutively active (Ras^{V12}) and dominant negative (Ras^{N17}) variants of Ras85D (Buff et al., 1998; Frise et al., 2010; Pérez et al., 2017), ligand processing components, such as Star and Rasp (Kolodkin et al., 1994; Miura et al., 2006) and the ligands themselves: Spitz (mSpitz^{CS}, sSpitz^{CS} and Spitz^{sec}), Keren, Vein and Gurken (Ghiglione et al., 2002; Donaldson et al., 2004; Brown et al., 2007; Steinhauer et al., 2013; Adrain and Freeman, 2014; Kim et al., 2017).

Significant eye tissue overgrowth (“rough eye”) was observable in adults expressing *Ras85D^{N17}* or *sSpitz^{CS}* (**Figure 5.1A-C**), with a reduction in eye-area also noted (**Figure 5.1D**). Unexpectedly, several of experimental genotypes appeared to be partially or completely lethal with a severe reduction or complete lack of hatched adults: this included both protease-independent variants of Spitz (*sSpitz^{CS}* and *Spitz^{sec}*) as well as signalling components *EGFR* and *Ras85D^{V12}* (**Figure 5.1D**). There also appeared to be a degree of sex-specificity as *Ras85D^{N17}* and *sSpitz^{CS}* were only male lethal.

These results suggested that the non-regulated variants of Spitz (*sSpitz^{CS}* and *Spitz^{sec}*) were biologically active (**Figure 5.1**). Since Spitz is the most widely tissue expressed ligand in *Drosophila*, it was chosen going forward as the best candidate for testing embryonic macrophage responses to EGF. Lethal phenotypes are indicative of overexpression activity as the *eyeless* enhancer element is known to have a role in neuronal development, a process that is highly sensitive to EGF signalling (Hazelett et al., 1998). The variation between phenotypes in males and females was unexpected, suggesting some degree of sex-specificity in the activity of these ligands, although at what stage in the life cycle this occurs would require additional experimentation.

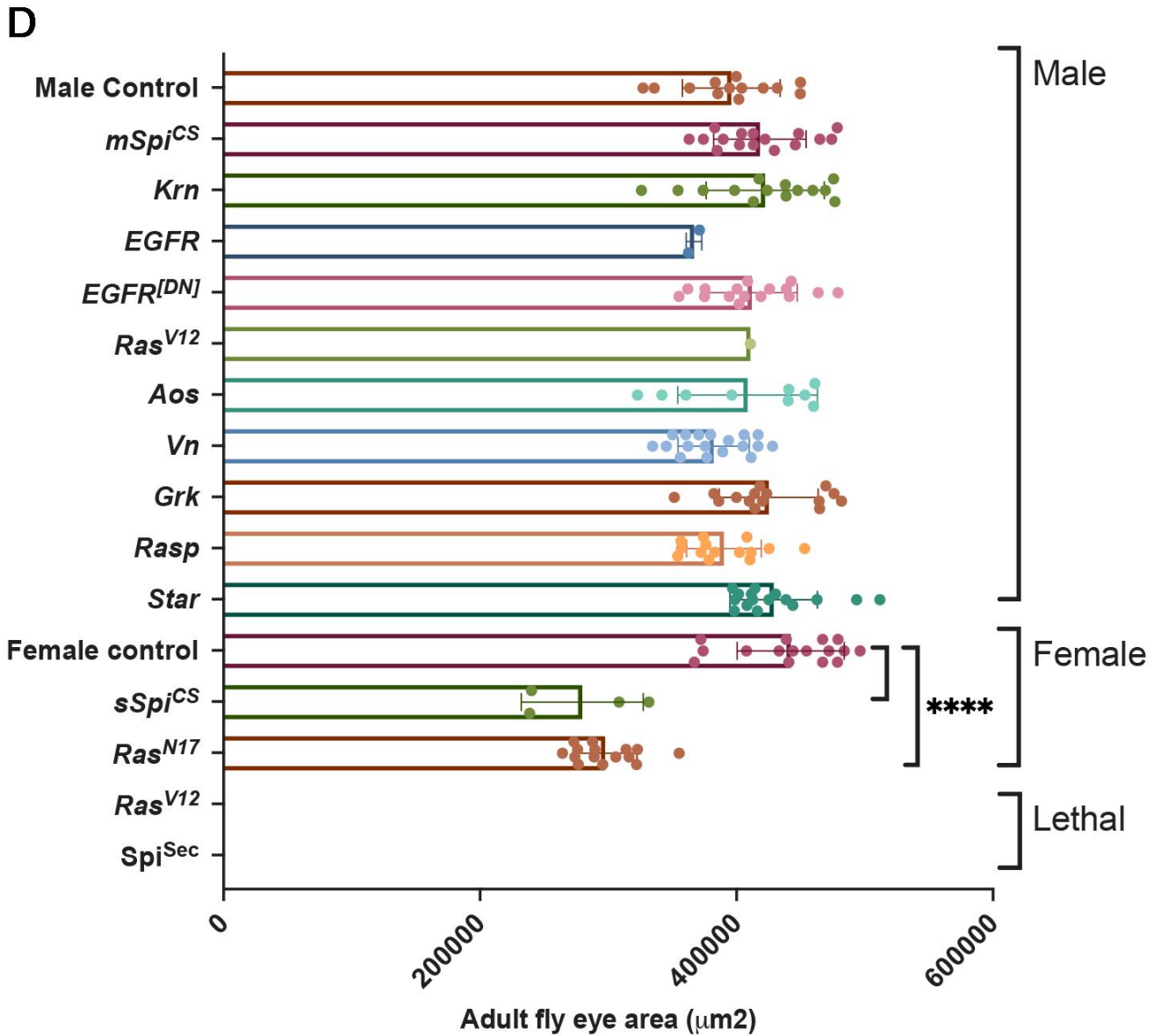
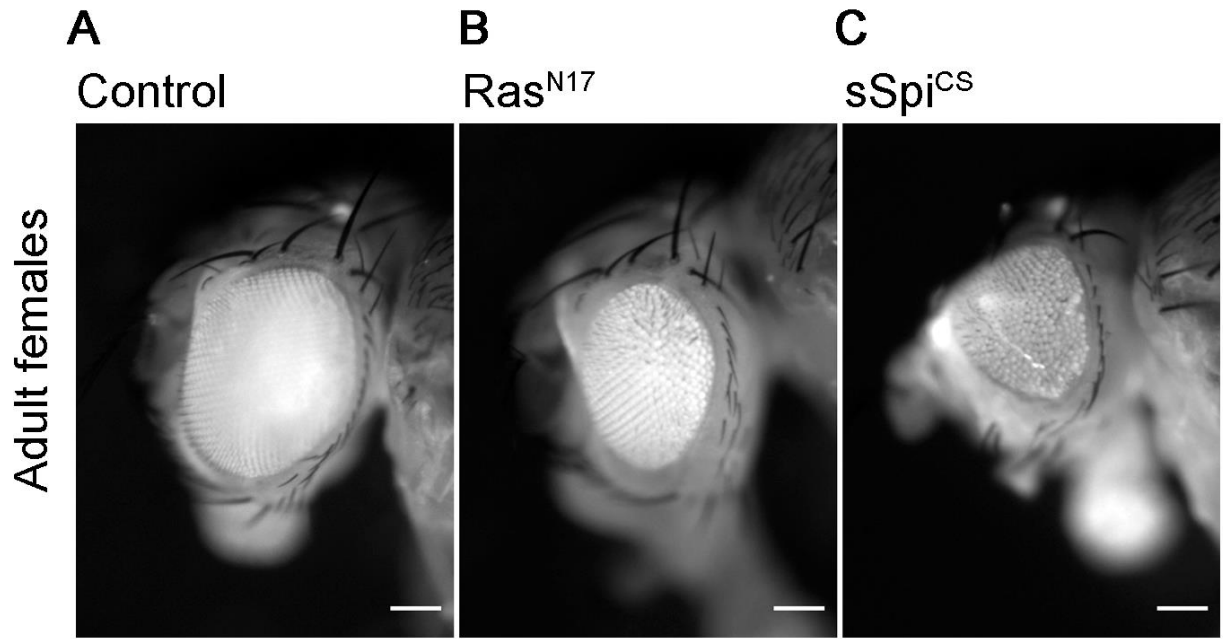


Figure 5.1 – Identification of active UAS lines through eye-specific proliferation assay

(A-C) Representative brightfield still images of female adult *Drosophila* expressing EGF signalling components under the control of the *eyeless-GAL4* enhancer element. Example “rough eye” phenotypes are shown for control flies (A) and flies expressing the dominant negative variant Ras^{N17} (B) and the unregulated, non-palmitoylated variant of Spitz (sSpi^{CS}) (C). Scale bar denotes 0.2mm. (D) Scattergraphs showing the quantification of eye phenotypes as a measure of total eye area. Statistics were performed using a 1-way ANOVA between sex-matched controls. Note that several genotypes appeared partially lethal with minimal progeny hatching (male flies expressing Ras^{v12} or *EGFR*) and no adults hatched expressing Spitz^{sec}. Significant loss in area was observed in adult female flies expressing Ras^{N17} and sSpi^{CS} ($p < 0.0001$ for both genotypes). Statistical significance is reported as **** = $p < 0.0001$; absence of a bar denotes lack of a significant difference compared to control ($p > 0.05$). Genotypes and n numbers were as followed: *w;ey-GAL4/+* (female and male control, n=13, 16 for males and females respectively), *w;ey-GAL4/UAS-ras^{v12}* (Ras^{v12} , n=1 male, 0 female), *w;ey-GAL4/UAS-mSpi^{CS}* (mSpi^{CS}, n=16 males), *w;ey-GAL4/+;UAS-Spitz^{sec}* (Spi^{sec}, n=0 due to lethality), *w;ey-GAL4/UAS-EGFR* (EGFR, n=2), *w;ey-GAL4/UAS-Keren* (Krn, n=14 males), *w;ey-GAL4/UAS-Rasp* (Rasp, n=14 males), *w;ey-GAL4/UAS-Star* (Star, n=16 males), *w,UAS-Ras^{N17};ey-GAL4/+* (Ras^{N17} n=14 female), *w;ey-GAL4/UAS-Vn* (Vn, n=18 males), *w;ey-GAL4/UAS-Grk* (Grk, n=16 males), *w;ey-GAL4/UAS-argos;UAS-argos/+* (Aos, n=9 males), *w;ey-GAL4/UAS-EGFR^{DN};UAS-EGFR^{DN}/+* (EGFR^{DN}, n=16 males).

5.2.2 Spitz alters the morphology and migration dynamics of *Drosophila* embryonic macrophages

Given the role of *Drosophila* EGFs in regulation of border cell migration in the oocyte and stem cell migration in the midgut (Duchek and Rørth, 2001; Liang et al., 2017), I hypothesised that Spitz may also regulate macrophage behaviour in the developing *Drosophila* embryo. Since Spitz requires proteolytic cleavage for activation, two constitutively-active variants of Spitz were used: Spitz^{sec} and sSpi^{CS} (Ghiglione et al., 2002; Miura et al., 2006). In contrast to wild-type Spitz, these variants do not require cleavage via Rhomboid for their activation and secretion. Additionally, sSpi^{CS} lacks a post-translational palmitoylation modification that normally restricts diffusion of wild-type ligand via interactions with plasma membranes (Miura et al., 2006). Comparison of these variants also enables investigation of how the diffusion properties of Spitz contribute to alterations in macrophage behaviour. Consequently, we expressed these Spitz variants specifically in macrophages to provide a local source of this growth factor, imaging fluorescently-labeled macrophages within developing embryos.

Given that Spitz is a pro-proliferative factor in *Drosophila* (Kim et al., 2017), total macrophage counts were performed to test if Spitz overexpression altered haematopoiesis rates and gross macrophage dispersal. Embryos with macrophages expressing the nuclear marker Red Stinger and either sSpitz^{CS} or Spitz^{sec} were imaged laterally at stage 13 and 15 with ventral images also taken to assess ventral midline (VML) dispersal (**Figure 5.2A-F**). Quantification of the number of macrophages on the ventral midline at stage 15 showed no differences in the ability of macrophages to disperse over the embryo in the presence of either Spitz variant (**Figure 5.2G-G'**) nor any difference in total macrophage numbers (**Figure 5.2H**). Observations at stage 13 also confirmed that there was not a delay in macrophage dispersal due to Spitz release pre-dispersal (data not shown).

The initial findings showed that developmental dispersal of macrophages was grossly normal on expression of either sSpitz^{CS} or Spitz^{sec}, compared to controls at both stage 13 and stage 15/16 (**Figure 5.2**). However, while macrophages were able to reach the ventral midline, the expression of Spitz appeared to alter their distribution, polarisation, and morphology in this region when these cells were imaged at higher resolution (**Figure 5.3A**).

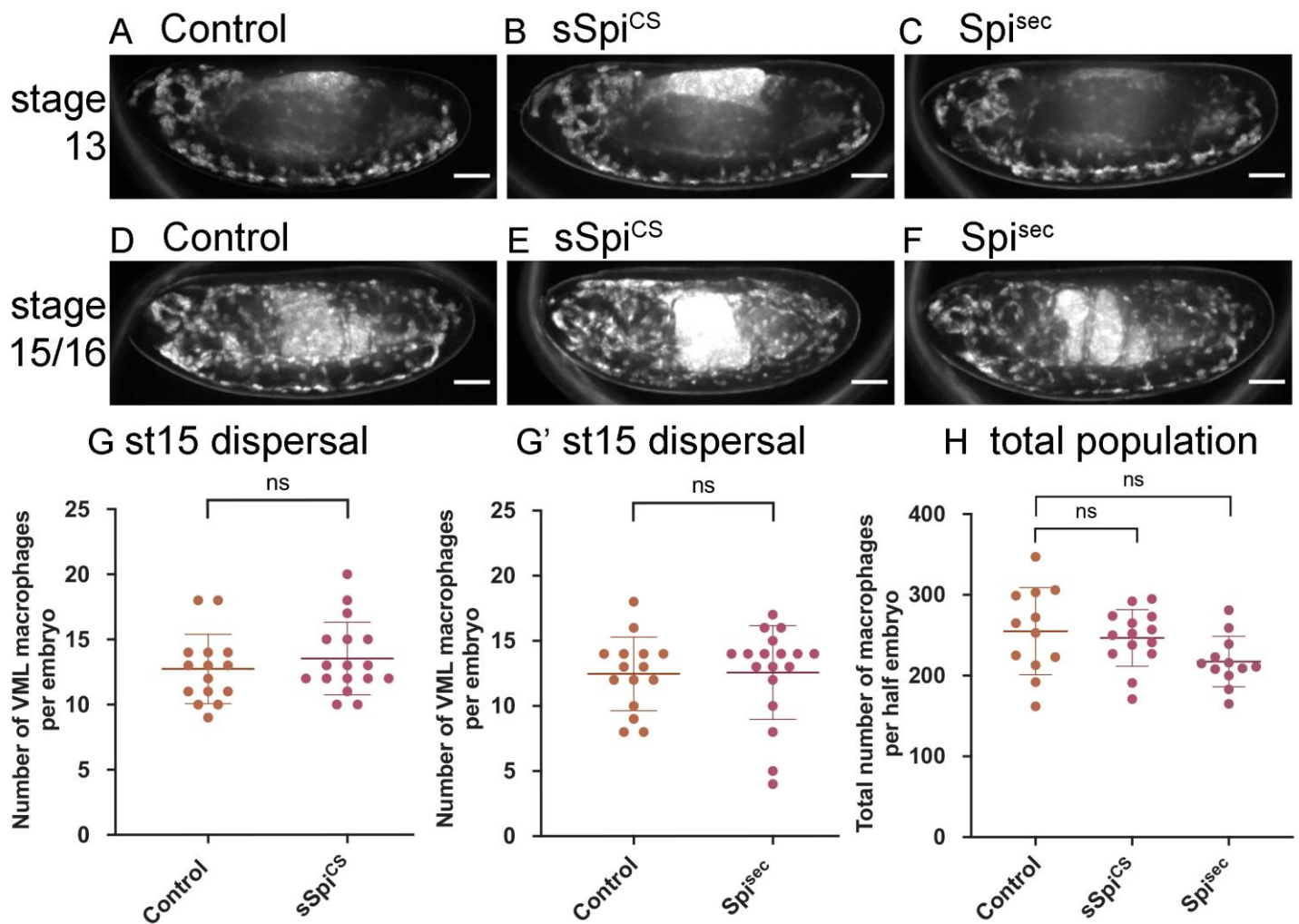
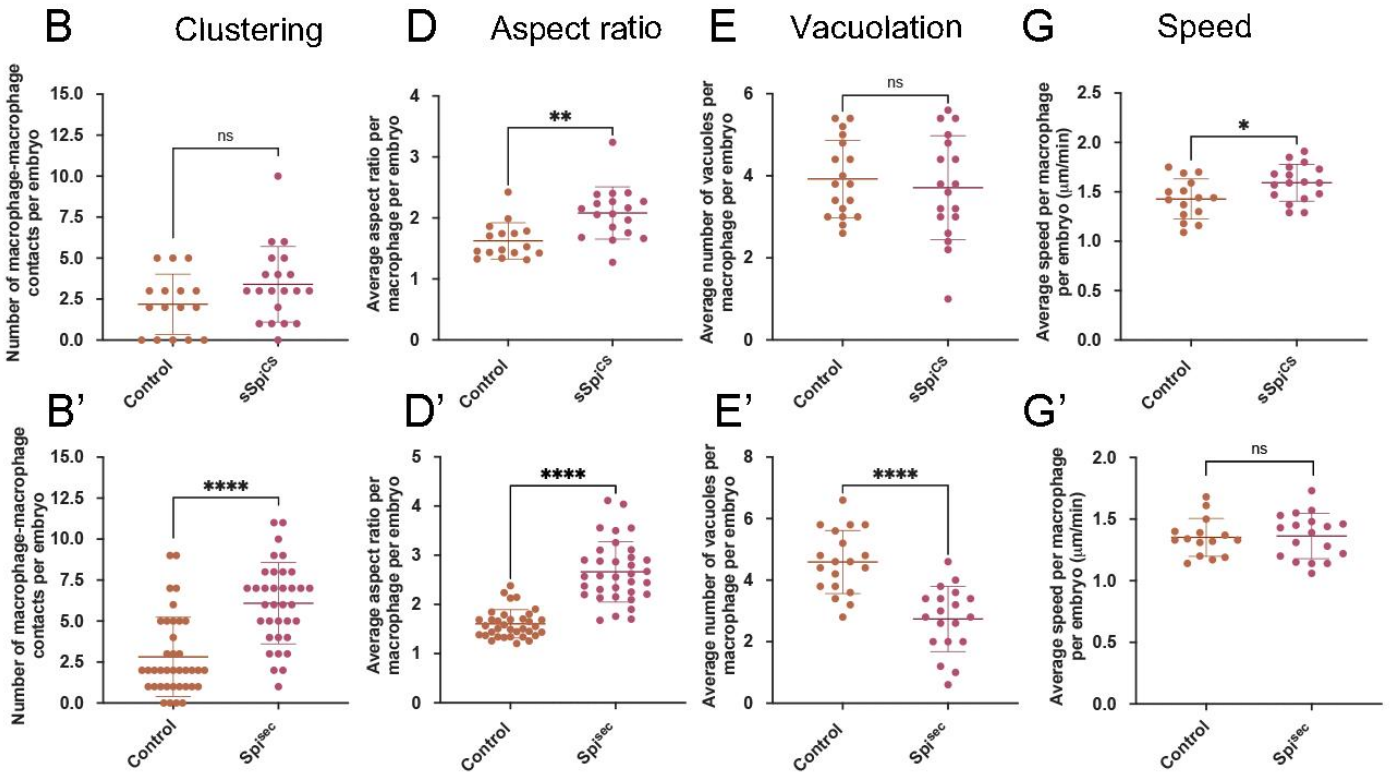
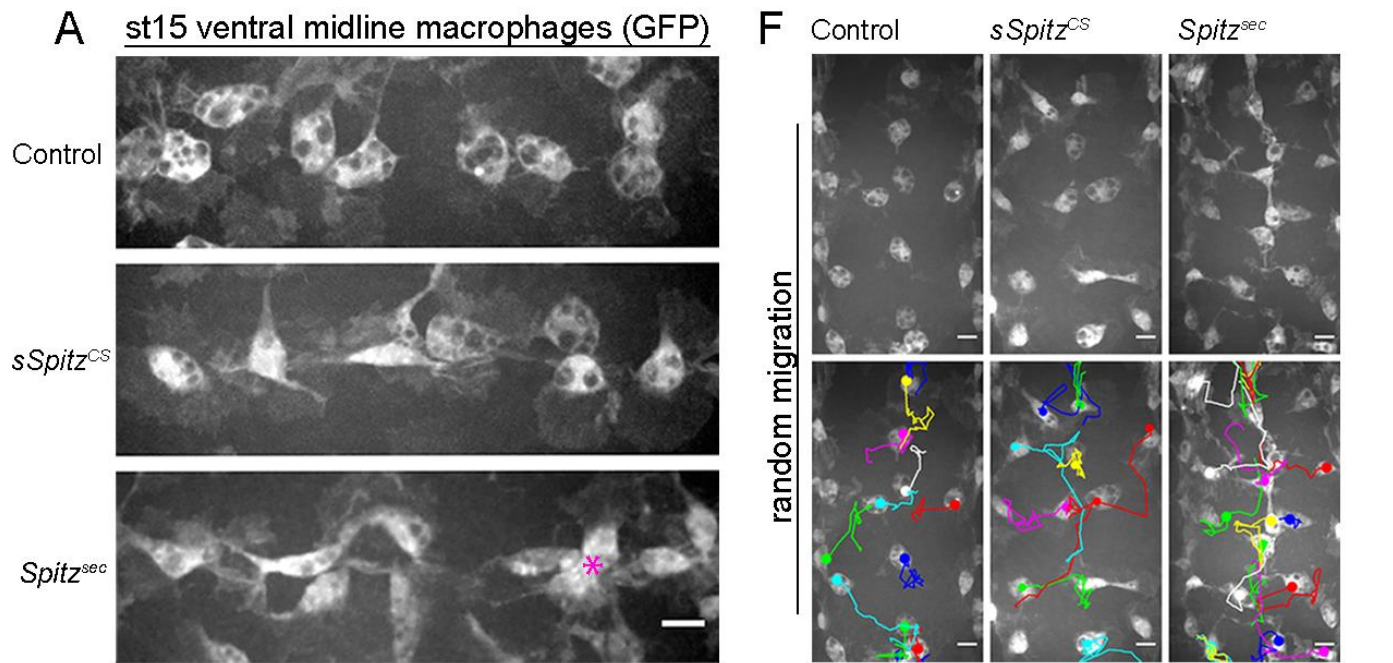


Figure 5.2 – Macrophage-specific expression of Spitz does not alter developmental dispersal or total numbers of macrophages in the embryo

(A-F) Lateral images showing developmental dispersal of macrophages at stage 13 (A-C) and stage 15/16 (D-F) in controls (A, D) and in the presence of macrophage-specific expression of sSpi^{CS} (B, D) or Spi^{sec} (C, E). (G-G') Scattergraphs showing number of macrophages per embryo on the ventral midline at stage 15 in controls and in the presence of macrophage-specific expression of sSpi^{CS} (n= 15, 17 embryos; $p = 0.417$ via an unpaired, two-tailed Student's t-test) (G) or Spi^{sec} (n= 15, 18 embryos; $p = 0.939$ via an unpaired, two-tailed Student's t-test) (G'). (H) Scattergraph showing number of macrophages per embryo at stage 15 in the indicated genotypes. Number of Red Stinger (nuclear RFP) labelled macrophages scored per half of an embryo – imaged laterally from most superficial side to midline (n = 12 control, 14 sSpi^{CS} and 12 Spi^{sec} embryos; one-way ANOVA with a Dunnett's post-test used to compare control group with Spitz embryos; control vs. sSpi^{CS} $p = 0.82$, control vs. Spi^{sec} $p = 0.056$). Scale bars denote 50 μ m (A-F); ns denotes not significant; lines and error bars represent mean and standard deviation, respectively. Embryo genotypes are as follows: *w;Srp-GAL4,UAS-GFP/+;Crq-GAL4,UAS-GFP/+* (control; A, D, G-G'), *w;Srp-GAL4,UAS-GFP/UAS-sSpitz^{CS};Crq-GAL4,UAS-GFP/+* (sSpi^{CS}; B, E, G-G'), *w;Srp-GAL4,UAS-GFP/+;Crq-GAL4,UAS-GFP/UAS-Spitz^{sec}* (Spi^{sec}; C, F-G'), *w;Srp-GAL4,UAS-red stinger/+;Crq-GAL4,UAS-red stinger/+* (control; H), *w;Srp-GAL4,UAS-red stinger/UAS-sSpitz^{CS};Crq-GAL4,UAS-red stinger/+* (sSpi^{CS}; H) and *w;Srp-GAL4,UAS-red stinger/+;Crq-GAL4,UAS-red stinger/UAS-Spitz^{sec}* (Spi^{sec}; H).

Analysing the number of touching macrophages on the ventral midline showed that, while sSpitz^{CS}-expressing macrophages displayed a “wild-type-like” distribution, Spitz^{sec} significantly increased the number of macrophages contacting other macrophages, leading to the formation of cell clusters (**Figure 5.3A-B'**). It has previously been shown that overexpression of EGFR in larval blood cells drives their overproliferation, presumably via autoactivation of this receptor tyrosine kinase (Zettervall et al., 2004). Similarly, removal of a negative regulator of EGFR signalling (Graf) also leads to expansion of larval blood cells (Kim et al., 2017). However, an increase in cell numbers cannot explain the clustering phenotype in the embryo (**Figure 5.3A-B'**), as we could not detect an increase in cell numbers on the ventral side of the embryo at stage 15 (**Figure 5.3C-C'**), nor was there an increase in overall numbers of macrophages in the embryo (**Figure 5.2**). This also suggests that, in contrast to the situation in larvae, EGFR signalling does not have the potential to drive macrophage proliferation in the embryo. To analyse changes in macrophage morphology in more detail, macrophage elongation was assessed by measuring the aspect ratio (AR) of the cell body: in the presence of either sSpitz^{CS} or Spitz^{sec}, macrophages were more elongated compared to control ls lacking expression of either variant (**Figure 5.3A, D-D'**). Additionally, macrophages also appeared to contain fewer vacuoles in the presence of Spitz, structures previously established to contain engulfed apoptotic cells that can be used as an indirect read-out of macrophage efferocytosis (Evans et al., 2013). Quantification of the numbers of vacuoles per cell showed that in the presence of Spitz^{sec}, but not sSpitz^{CS}, macrophages contained fewer vacuoles and likely fewer apoptotic cells (**Figure 5.3E-E'**). To assess if Spitz perturbed macrophage migration, macrophage movements (“random migration”) on the ventral midline of the embryo were tracked for 1 hour at stage 15 (**Figure 5.3F**). Expression of sSpitz^{CS} increased macrophage random migration speeds, but no difference was seen on expression of Spitz^{sec} (**Figure 5.3G-G'**).



Numbers on ventral side

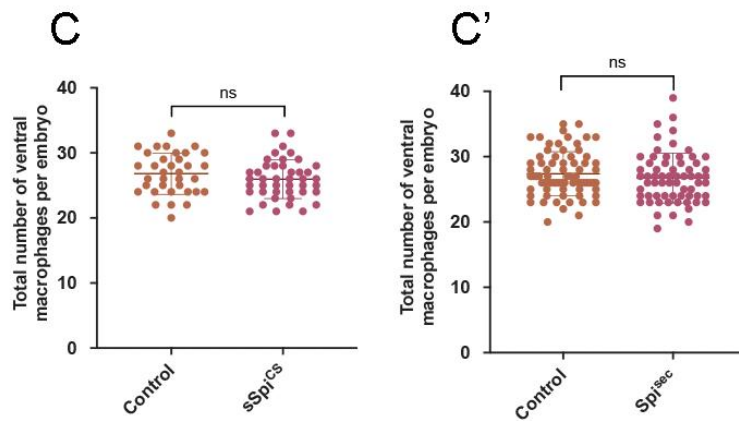


Figure 5.3 – Spitz stimulates macrophage elongation, impairs efferocytosis and alters migration dynamics

(A) Maximum projections of GFP-tagged macrophages on the ventral midline at stage 15 in control embryos and in embryos with macrophage-specific expression of sSpitz^{CS} or Spitz^{sec}; asterisk (*) shows cluster of macrophages on midline; anterior is left. **(B,B')** Scattergraphs showing degree of macrophage clustering via number of macrophage-macrophage contacts per embryo in the presence of sSpitz^{CS} **(B)** (n = 16, 20; p = 0.0977) or Spitz^{sec} **(B')** (n = 38, 35; p < 0.0001). **(C,C')** Scattergraphs showing number of macrophages in the ventral midline region (VML) per embryo at stage 15 in the presence of sSpitz^{CS} **(C)** (n = 35, 43; p = 0.229) or Spitz^{sec} **(C',D)** (n = 73, 65; p = 0.247). **(D,D')** Scattergraphs showing aspect ratio per macrophage per embryo in the presence of sSpitz^{CS} **(D)** (n = 16, 18; p = 0.0018) or Spitz^{sec} **(D')** (n = 35, 34; p < 0.0001). **(E,E')** Scattergraphs showing average numbers of vacuoles per macrophage per embryo in controls in the presence of sSpitz^{CS} **(E)** (n = 18, 18; p = 0.574) or Spitz^{sec} **(E')** (n = 19, 19; p < 0.0001). **(F)** Maximum projections and macrophage tracking data of GFP-labelled macrophages on the ventral midline at stage 15 in control embryos and in embryos with macrophage-specific expression of sSpitz^{CS} or Spitz^{sec}; anterior is up. **(G,G')** Scattergraphs of speed per macrophage per embryo over a 1-h period of random migration in controls and in the presence of sSpitz^{CS} **(G)** (n = 15, 17; p = 0.0229) or Spitz^{sec} **(G')** (n = 15, 18; p = 0.858). Scale bars denote 10µm **(A,F)**; lines and error bars represent mean and standard deviation on scattergraphs, respectively; significance bars denote ns p > 0.05, *p < 0.05, **p < 0.01, and ****p < 0.0001, respectively; statistical comparisons made via unpaired, two-tailed Student's t-test **(C,E,E',G,G')** or Mann–Whitney test **(B,B',C',D,D')**. Embryo genotypes are as follows: w; Srp-GAL4,UAS-GFP/+; Crq-GAL4,UAS-GFP/+ **(Control)**, w; Srp-GAL4,UAS-GFP/UAS-sSpitz^{CS}; Crq-GAL4,UAS-GFP/+ **(sSpi^{CS})**, w;Srp-GAL4,UAS-GFP/+;Crq-GAL4,UAS-GFP/UAS-Spitz^{sec} **(Spi^{sec})**.

Taken together, these results show that macrophage-specific expression of active Spitz alters macrophage elongation, induces clustering, and affects macrophage migration and phagocytosis in a variant-specific manner. The stimulation of macrophage elongation, clustering and increase in speed potentially indicates a role for Spitz as a macrophage chemoattractant, such as previously observed for border cells and gut stem cells in this organism (Duchek and Rørth, 2001; Liang et al., 2017). Alternatively, Spitz could operate as a chemokinetic molecule with a specific role in increasing migration speeds, though it is not clear how this might drive cluster formation.

5.2.3 Cleavage is necessary for Spitz-mediated regulation of macrophage behaviour

To investigate whether release from the processing via Rhomboid is required for Spitz-induced changes in macrophage behaviour, a membrane-bound variant was expressed in macrophages (mSpitz^{CS}; Miura et al., 2006). Expression of mSpitz^{CS} did not alter macrophage clustering, numbers of cells in the ventral region, their morphology, vacuolation or migration speeds on the ventral midline (**Figure 5.4**). Interestingly, expression of the Spitz-like ligand Keren, which is functionally redundant to Spitz in certain tissues (Brown et al., 2007) did show an increase in macrophage clustering (**Figure 5.5**), suggesting that some EGF effects are independent of cleavage.

These results suggest that cleavage and release of Spitz from the plasma membrane are needed for induction of macrophage phenotypes and that these phenotypes are not a non-specific consequence of overexpression of Spitz. However, the increase in clustering seen in Keren-expressing embryos suggests this regulation may not completely prevent EGF ligand activity.

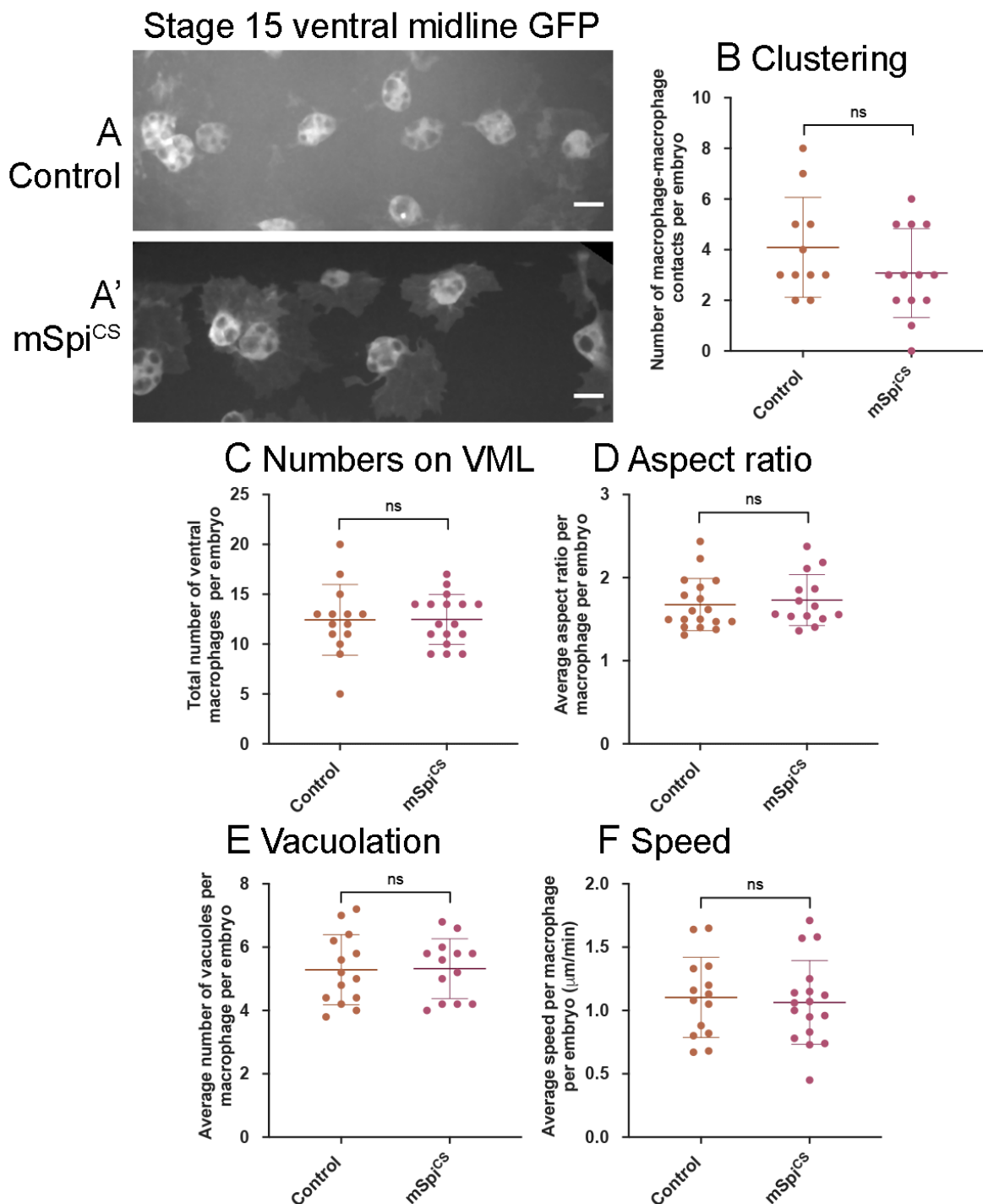


Figure 5.4 – Expression of a membrane-bound form of Spitz fails to induce changes in embryonic macrophage behaviour

(A,A') Representative images of GFP-labeled macrophages in control embryos **(A)** and embryos containing macrophages expressing mSpi^{CS}-GFP **(A')** on the ventral midline at stage 15; mSpi^{CS}-GFP macrophages appear more defined due to additional GFP expression due to the GFP tag that is part of the mSpi^{CS}-GFP transgene; scale bars represent 10 μ m. **(B–F)** Scattergraphs showing average number of macrophage-macrophage contacts per embryo to assay macrophage clustering **(B)** ($n = 11, 13$; $p = 0.690$), numbers of macrophages on the ventral midline **(C)** ($n = 14, 17$; $p = 0.188$), cell body aspect ratio per macrophage, per embryo **(D)** ($n = 18, 14$; $p = 0.464$), vacuoles per macrophage, per embryo **(E)** ($n = 14, 13$; $p = 0.926$) and

random migration speed in μm per minute (F) ($n = 14, 17$; $p = 0.743$) at stage 15 in controls and embryos with macrophage-specific expression of mSpi^{CS} . Lines and error bars represent mean and standard deviations on Scattergraphs respectively; significance bars denote $p > 0.05$ (ns); statistical comparisons made via Mann–Whitney test (D) or unpaired, two-tailed Student’s t-test (B,C,E,F). Embryo genotypes are as follows: w; $\text{Srp-GAL4,UAS-GFP/+}$; $\text{Crq-GAL4,UAS-GFP/+}$ (Control), w; $\text{Srp-GAL4,UAS-GFP/+}$; $\text{Crq-GAL4,UAS-GFP/UAS-mSpi}^{\text{CS-GFP}}$ (mSpi^{CS}).

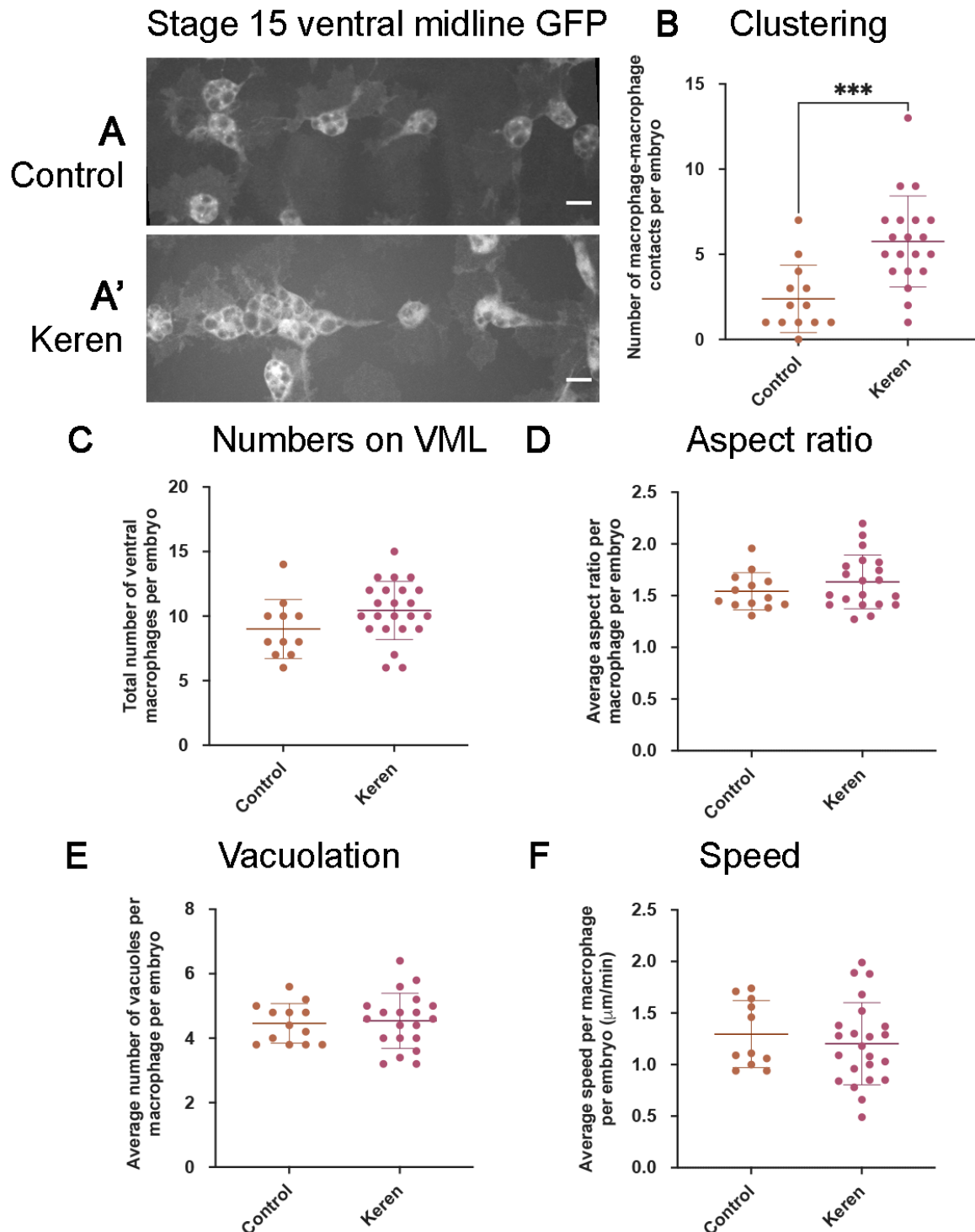


Figure 5.5 – Expression of a regulated EGF ligand Keren increases macrophage clustering but does not alter other behaviour during embryogenesis

(A,A') Representative images of GFP-labeled macrophages in control embryos (A) and embryos containing macrophages expressing Keren (A') on the ventral midline at stage 15; scale bars represent 10µm. (B–F) Scattergraphs showing number of macrophage-macrophage contacts per embryo to assay macrophage clustering (B) (n = 13, 20; p = 0.0005), numbers of macrophages on the ventral midline (C) (n = 11, 23; p = 0.0931), cell body aspect ratio per macrophage, per embryo (D) (n = 13, 20; p = 0.2790), vacuoles per macrophage, per embryo (E) (n = 13, 20; p = 0.7771) and random migration speed in µm per minute (F) (n = 11, 23; p = 0.5063) at stage 15 in controls and embryos with macrophage-specific expression of Keren. Lines and error bars represent mean and standard deviations on Scattergraphs respectively; significance bars denote p > 0.05 (ns); statistical comparisons made via unpaired, two-tailed Student's t-test (B,C,D,E,F). Embryo genotypes are as follows: *w; Srp-GAL4,UAS-GFP/+; Crq-GAL4,UAS-GFP/+* (Control), *w; Srp-GAL4,UAS-GFP/UAS-Keren; Crq-GAL4,UAS-GFP/+* (Keren).

5.2.4 Macrophages express EGFR and show increased ERK activity in the presence of Spitz

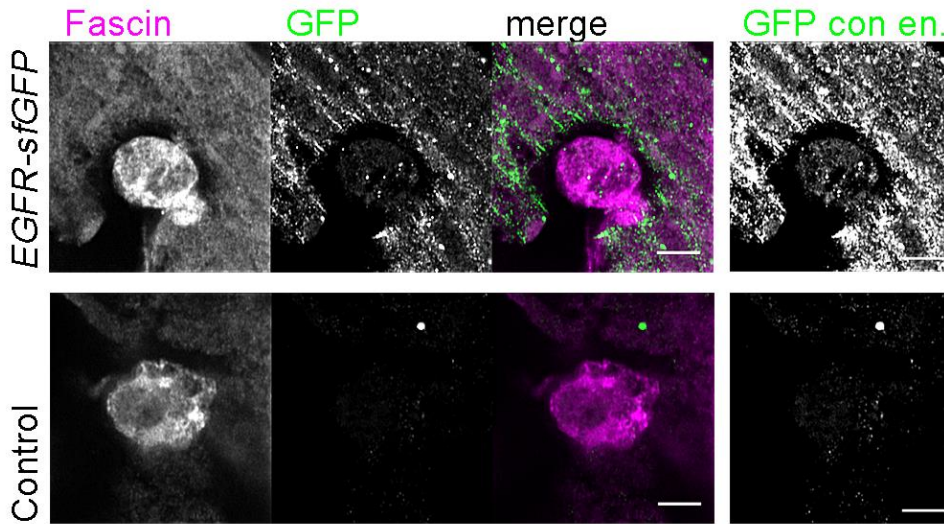
While Spitz signalling through the EGFR (*Torpedo*) has been observed in larval macrophages (Kim et al., 2017), it has not been confirmed whether embryonic macrophages express this receptor. To test this, embryos expressing a GFP-tagged version of the EGFR protein (knocked into the endogenous EGFR locus; Revaitis et al., 2020) were fixed and stained for macrophages (anti-Fascin) and the EGFR-GFP (anti-GFP). The results found that embryos expressing EGFR-GFP did have visibly detectable levels of the receptor within macrophages at the stage 15 ventral midline compared to controls, and that this expression is consistent with the expected surrounding epithelial tissue expression (Figure 5.6A). While we were unable to confirm the presence of EGFR on live macrophages due to time-constraints, these data suggests that embryonic macrophages do indeed express EGFR.

With macrophage expression of the EGFR confirmed, it was critical to show if the Spitz-induced phenotypes observed in macrophages were the result of macrophage-specific EGFR activation. Canonical Spitz signalling occurs via the MAPK pathway following EGFR activation (Shilo, 2003, 2014). To assess if the phenotypes observed in macrophages expressing Spitz were the result of MAPK activity, embryos with macrophages expressing spitz were fixed and immunostained for the activated form of ERK: di-phospho-ERK (dpERK), a critical component

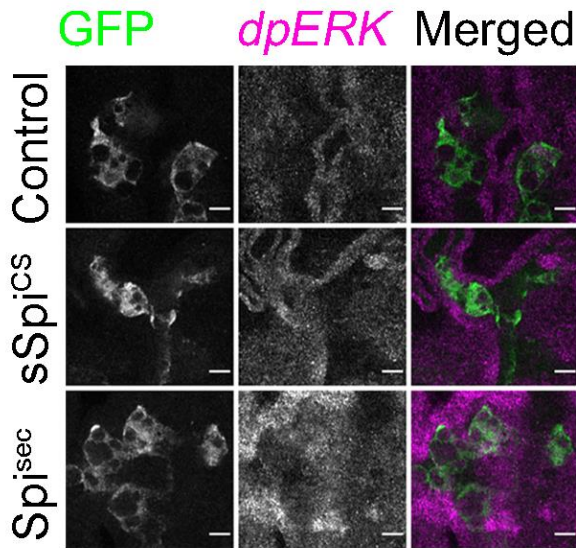
in the *Drosophila* embryonic MAPK pathway (Lim et al., 2015). The data shows that while there are high levels of dpERK even within macrophages in control embryos (**Figure 5.6B**), the presence of either sSpitz^{CS} or Spitz^{sec} enhances this read-out of EGFR activity within macrophages (**Figure 5.6B'**). These results suggest that the exogenous expression of Spitz does lead to the release of active Spitz into the local tissue area and the activation of MAPK signalling in surrounding cells. To control for any non-specific genetic effects of the exogenous Spitz constructs or proteolytic stress in the macrophage, it was important to show that macrophages expressing exogenous Spitz were producing an intact peptide. To confirm that active Spitz was being produced, embryos with GFP-tagged macrophages expressing Spitz^{sec} were fixed and immunostained for GFP (anti-GFP) and Spitz (anti-Spitz) (**Figure 5.6C**). The results show that macrophages expressing exogenous Spitz had significantly higher levels of Spitz immunostaining, suggesting that the exogenous protein was indeed being expressed within macrophages (**Figure 5.6C'**). It should be noted that only embryos expressing Spitz^{sec} were tested as the only available antibody was raised against an epitope containing the palmitoylation region, rendering it inappropriate for the detection of sSpitz^{CS}, which contains mutations in this region.

Taken together, these results show that embryonic macrophages express EGFR and that the exogenous expression of Spitz does result in the generation of Spitz peptide, with increased MAPK activity occurring as a result within the macrophages. While this does not exclude the possibility of EGFR independent MAPK signalling, it confirms that the canonical pathway appears to be active in the observed phenotypes.

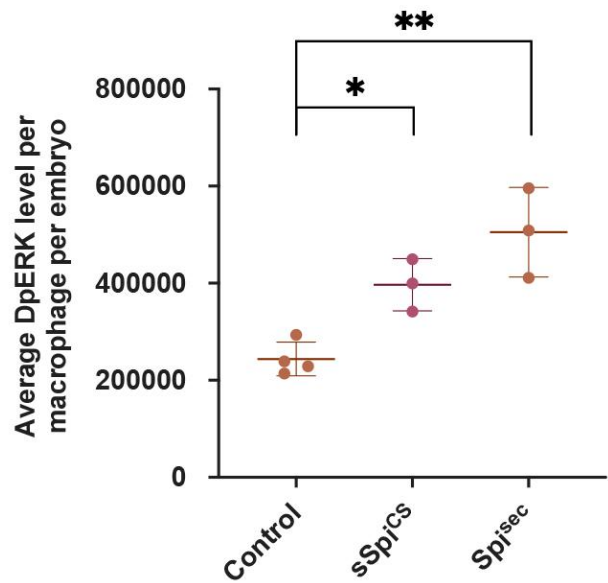
A EGFR expression in hemocytes



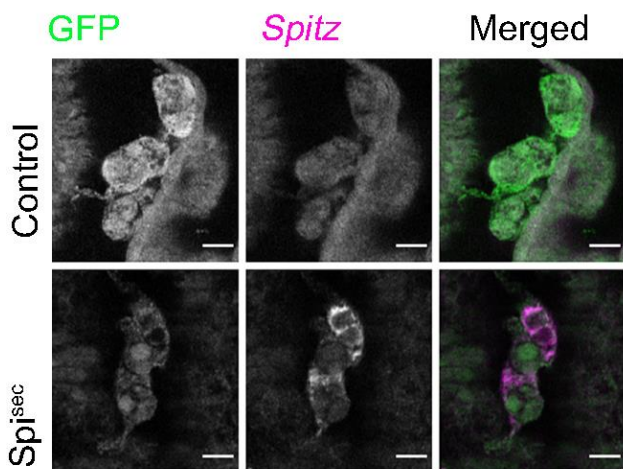
B dpERK activity



B' Quantification



C Spitz expression



C' Quantification

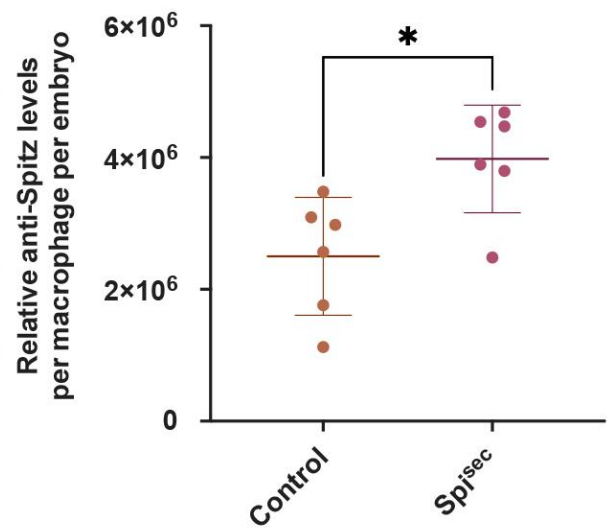


Figure 5.6 – Embryonic Macrophages express EGFR and exogenous Spitz activates ERK signalling

(A) Images of macrophages on the ventral midline at stage 15 in embryos containing GFP-tagged EGFR (EGFR-sfGFP) under the control of its endogenous promoter and a control embryo lacking a modified EGFR locus. Embryos were immunostained for GFP (green in merge) and Fascin (magenta in merge) to reveal EGFR-sfGFP expression and identify macrophages, respectively; panels to the right of the merged images show contrast enhanced GFP channel. Scale bar denotes 5 μ m. **(B)** Images of single 0.1 μ m thick optical sections of GFP-labelled macrophages on the ventral midline at stage 15. Optical sections taken of embryos immunostained for GFP (green in merge) and activated ERK (DpERK; magenta in merge) to show macrophage localisation and as a read-out of EGFR activation, respectively. Top row shows control embryo; middle row shows overexpression of sSpi^{CS}; bottom row shows overexpression of Spi^{sec}. Scale bars denote 5 μ m; dotted magenta lines show edge of macrophages in DpERK channels. **(B')** Scattergraph showing quantification of dpERK staining (total intensity per macrophage, per μ m³, per embryo) in indicated genotypes (n = 3 embryos). Lines and error bars represent mean and standard deviation, respectively. Statistical analysis via one-way ANOVA with a Dunnett's post-test used to compare control group with Spitz embryos; control vs. sSpi^{CS} $p = 0.0253$, control vs. Spi^{sec} $p = 0.0016$. **(C)** Images of single 0.1 μ m thick optical sections of GFP-labelled macrophages on the ventral midline at stage 15. Optical sections taken of embryos immunostained for GFP (green in merge) and cleaved spitz (Spitz^{sec}; magenta in merge) to show macrophage expression of UAS-Spitz^{sec}. **(C')** Scattergraph showing quantification of anti-Spitz staining (total intensity per macrophage, per mm³, per embryo) in indicated genotypes (n = 6 embryos). Lines and error bars represent mean and standard deviation, respectively. Statistical analysis via a 2-tailed Student's t-test to compare control group with Spitz embryos; control vs. Spi^{sec} $p = 0.0135$. Significance values are denoted as * $p < 0.05$ and ** $p < 0.01$ respectively. Genotypes were as followed: *w*; *EGFR-sfGFP* and *w*¹¹¹⁸ **(A)** and *w*; *Srp-GAL4, UAS-GFP/+* ; *Crq-GAL4, UAS-GFP/UAS-Spitz^{sec}* **(B-C)**.

5.2.5 Tissue-specific release of Spitz alters macrophage localisation and vacuolation

Under normal developmental conditions, macrophages may not be the source of activated Spitz within the embryo. To test if the effect of Spitz on macrophages was not due to macrophage specific expression, Spitz was expressed in an alternative tissue that macrophages encounter during their dispersal. Thus, sSpitz^{CS} or Spi^{sec} were expressed in several regions in a tissue-specific manner: the developing heart, a structure called the dorsal vessel, using *TinC-GAL4*, a driver derived from the enhancer region of *Tinman* (Lo and Frasch, 2001), the embryonic salivary gland, using *Fkh-GAL4*, a driver derived from the *fork head* enhancer region (Henderson and Andrew, 2000), and the embryonic anal-pads, using *VT45229-GAL4*, an Vienna tiling array reporter identified to be active in the anal pad tissue (Kvon et al., 2014). We hypothesised that misexpression of Spitz in these tissues would alter

macrophage morphology and behaviour, enabling us to determine whether cell-autonomous expression was necessary for the effects of Spitz expression and confirm our previous results using macrophage-specific expression.

Tinman encodes a transcription factor expressed across the early embryonic mesoderm before becoming restricted to the progenitor heart and lateral visceral muscles by stage 15 (Bodmer, 1993). During development, clusters of cardiocytes begin to form the dorsal vessel, which is then colonised by migrating macrophages (**Figure 5.7A**). Embryos with LifeAct-labelled cardiocytes expressing either sSpitz^{CS} or Spitz^{sec} were mounted dorsally and imaged at the most-medial point of the developing dorsal vessel and compared to controls lacking Spitz expression (**Figure 5.7B-B'**); macrophages were labelled using the *SrpHemo-3X-mCherry* reporter construct (Gyoergy et al., 2018). The presence of either sSpitz^{CS} or Spitz^{sec} appeared to inhibit phagocytic uptake of apoptotic cells, since dorsal vessel-associated macrophages contained significantly fewer vacuoles compared to controls (**Figure 5.7C-C'**), consistent with phenotypes achieved using macrophage-specific expression of Spitz. Quantification of macrophage dispersal showed that the presence of Spitz^{sec}, but not sSpitz^{CS} altered the total numbers of macrophages recruited to this dorsal region (**Figure 5.7D-D'**). To assess local macrophage recruitment, numbers of dorsal vessel-associated macrophages were quantified: expression of Spitz^{sec} but not sSpitz^{CS} decreased the number of dorsal vessel-associated macrophages (**Figure 5.7E-E'**). The reduction in macrophages at the dorsal vessel in the presence of Spitz^{sec} would appear counterintuitive to the hypothesis that Spitz may operate as a macrophage chemoattractant, however *TinC-GAL4* also drives expression in regions lateral to the dorsal vessel (Azpiazu and Frasch, 1993) (asterisk in **Figure 5.7A**) and this may be responsible for recruitment of macrophages away from the dorsal vessel. Interestingly, the observed phenotypes corroborate the loss of apoptotic clearance by macrophages in the presence of Spitz at the ventral midline but are more obvious with sSpitz^{CS} driving this phenotype.

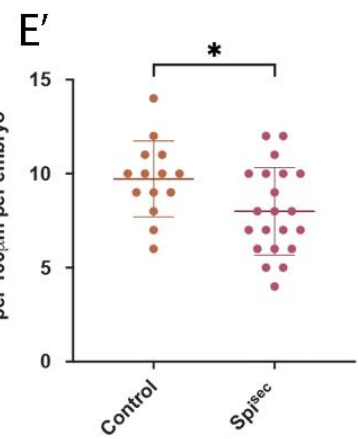
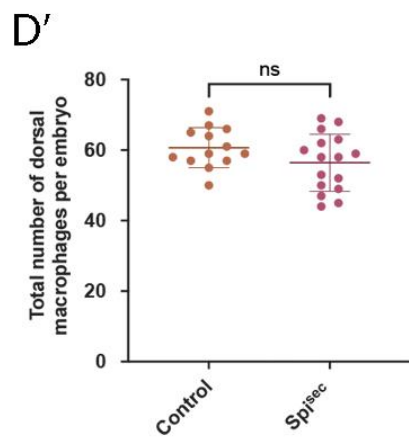
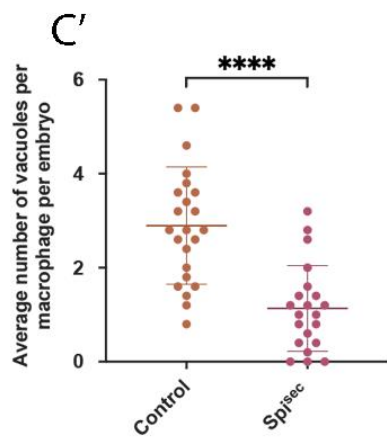
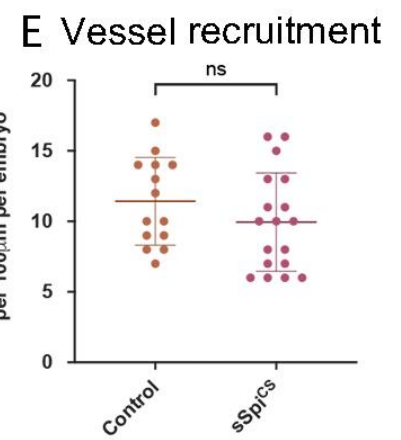
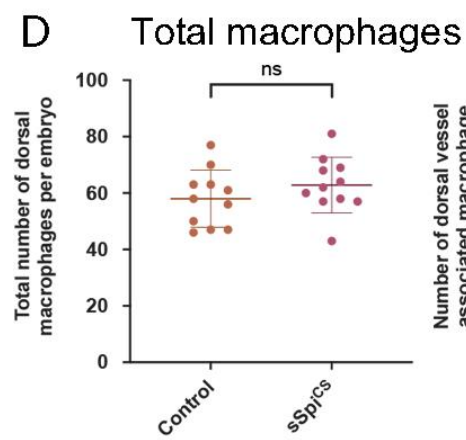
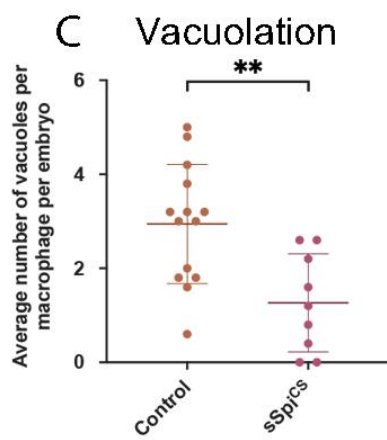
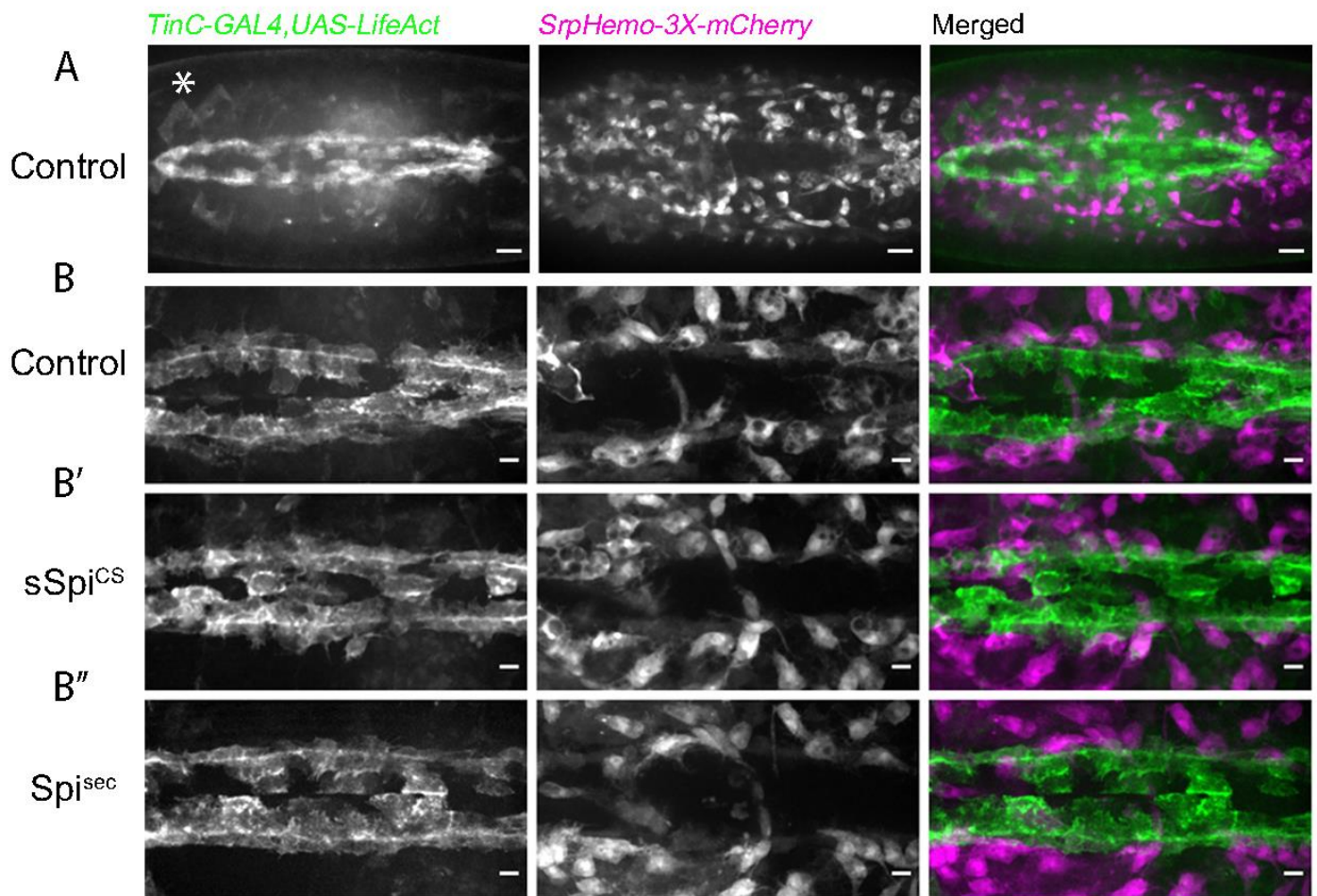


Figure 5.7 – Expression of Spitz in the developing fly heart alters macrophage localisation and vacuolation

(A–B'') Maximum projections of dorsal side of stage 15 embryos showing the dorsal vessel (labeled using TinC-GAL4,UAS-LifeAct; green in merge) and associated macrophages (labeled via *SrpHemo-3X-mCherry*) in controls (A,B) and embryos with TinC-GAL4 mediated expression of sSpitz^{CS} (B') or Spitz^{sec} (B''). Anterior is right; asterisk (*) denotes TinC-GAL4 driven expression in lateral regions away from the dorsal vessel. (C,C') Scattergraphs of vacuole counts per macrophage in controls and in the presence of dorsal vessel-expressed sSpitz^{CS} (C) (n = 24, 22; p < 0.0001) or Spitz^{sec} (C') (n = 27, 18; p = 0.0020). (D,D') Scattergraphs of the total number of macrophages present in the field of view at the dorsal face in controls and in the presence of dorsal vessel-expressed sSpitz^{CS} (D) (n = 14, 19; p = 0.497) or Spitz^{sec} (D') (n = 15, 14; p = 0.0170). (E,E') Scattergraphs of the number of macrophages contacting the dorsal vessel in controls and in the presence of dorsal vessel-expressed sSpitz^{CS} (E) (n = 14, 18; p = 0.221) or Spitz^{sec} (E') (n = 14, 21; p = 0.0312). Scale bars denote 20µm (A) and 10µm (B–B''); lines and error bars represent mean and standard deviation on scattergraphs, respectively; significance bars denote ns p > 0.05, *p < 0.05, **p < 0.01, ****p < 0.0001, respectively; statistical comparisons made via a Mann–Whitney test (C,D) or unpaired, two-tailed Student's t-test (C',D',E,E'). Embryo genotypes are as follows: *w;; TinC-GAL4,UAS-LifeAct, SrpHemo-3X-mCherry/+* (Control), *w;+/UAS-sSpitz^{CS}; TinC-GAL4,UAS-LifeAct, SrpHemo-3X-mCherry/+* (sSpi^{CS}) and *w;;TinC-GAL4,UAS-LifeAct, SrpHemo-3X-mCherry/UAS-Spitz^{sec}* (Spi^{sec}).

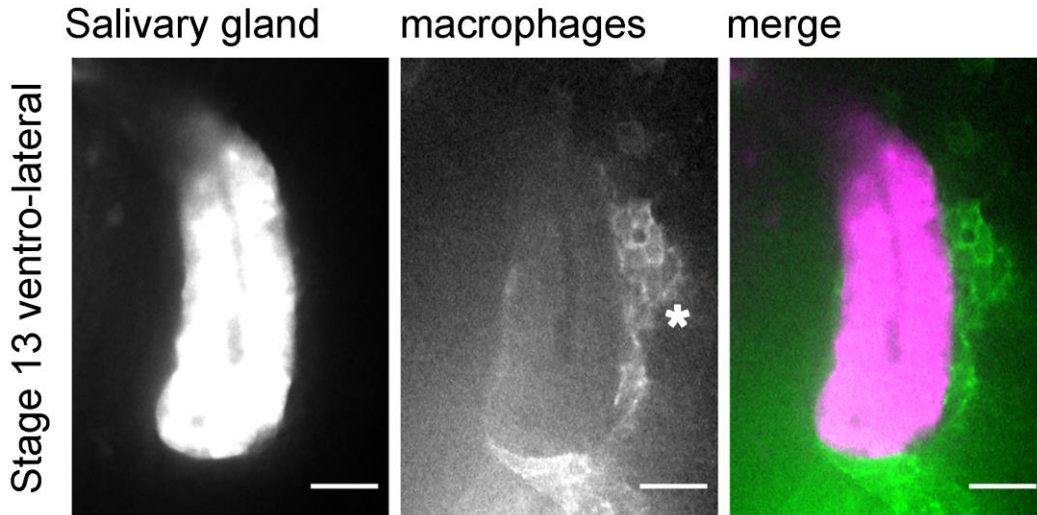
Forkhead is a developmental transcription factor that is expressed during embryogenesis in the *Drosophila* salivary gland from stage 10 onwards within the secretory cell population (Andrew et al., 2000; Chandrasekaran and Beckendorf, 2003). During the developmental dispersal, macrophages colonise the surrounding tissue and can be observed in contact to the gland lobes (Figure 5.8A). Since *forkhead-GAL4* was used to express Tdtomato and Spitz in the salivary gland, macrophages were labelled using the globular actin-binding domain of Moesin fused to GFP (GMA) (Dutta et al., 2002) under the control of *Serpent* (SrpGMA). Due to technical limitations in assessing macrophage numbers associated with the gland (tissue depth and low SrpGMA fluorescence makes microscopy of the region difficult), it was not possible to accurately assess macrophage-salivary gland association. Since macrophages migrate proximal to the salivary gland during their dispersal, the stage 13 ventral midline was used as a proxy to screen for reductions in macrophage numbers that might be indicative of Spitz mediated chemoattraction towards the salivary gland. Imaging of the stage 13 VML showed no obvious differences in macrophage dispersal (Figure 5.8B) and quantification of the number of macrophages in the ventral region showed no differences between control embryos and embryos expressing spitz in the salivary gland (Figure 5.8B').

The embryonic rectum and anal pads are formed during the development of the wider hind-gut organ (Lengyel and Iwaki, 2002) and are located at the posterior of the developing embryo. *VT45229* is an enhancer fragment that was identified as part of the Vienna Tiling array (VT) screen (Kvon et al., 2014), with expression occurring from stage 13 onwards in the anal pads. This tissue was chosen as a source of Spitz as it has a small, defined structure (i.e., may act as a point source) and local macrophages with the potential to be recruited. To assess macrophage recruitment to the anal pads, cell counts were performed in control embryos and embryos expressing Spitz^{sec} from the anal pads (**Figure 5.8C**). To assess macrophage recruitment to the anal pads, the number of macrophages present within 100µm of the posterior embryo were counted. Cell counts showed no significant difference in the number of macrophages associated with the anal pad (**Figure 5.8C'**).

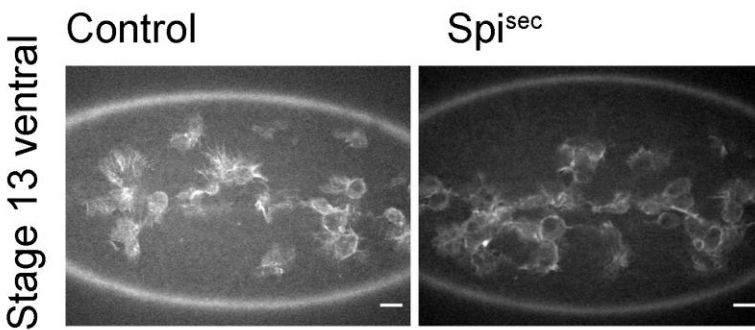
Taken together these results suggest that the phenotypes seen with Spitz-secreting macrophages is not intrinsic and is likely due the activity of Spitz, independent of the source of Spitz. While expression of Spitz from the dorsal vessel disrupted dispersal and efferocytosis, salivary gland and anal pad assays did not show increased macrophage recruitment. The reason for the differences in recruitment may be related to what extent macrophages are able to infiltrate the tissue and at which point in development the assay was conducted e.g., whether developmental dispersal signals are still active.

While evidence of chemotactic effects of Spitz from other tissues was mixed, the consistent reduction of efferocytosis in macrophages exposed to Spitz^{sec} at the ventral midline and dorsal vessel drove us to examine how Spitz affects apoptotic cell-macrophage interactions in more detail.

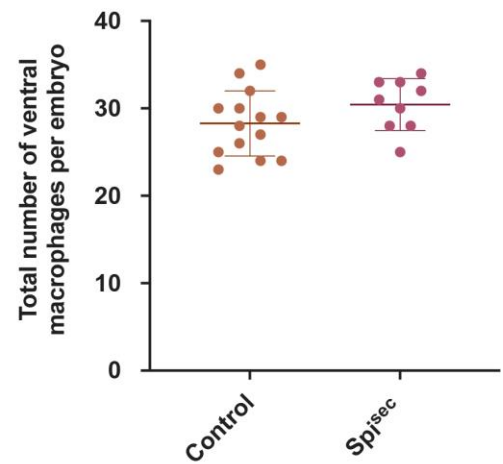
A Embryonic salivary gland development



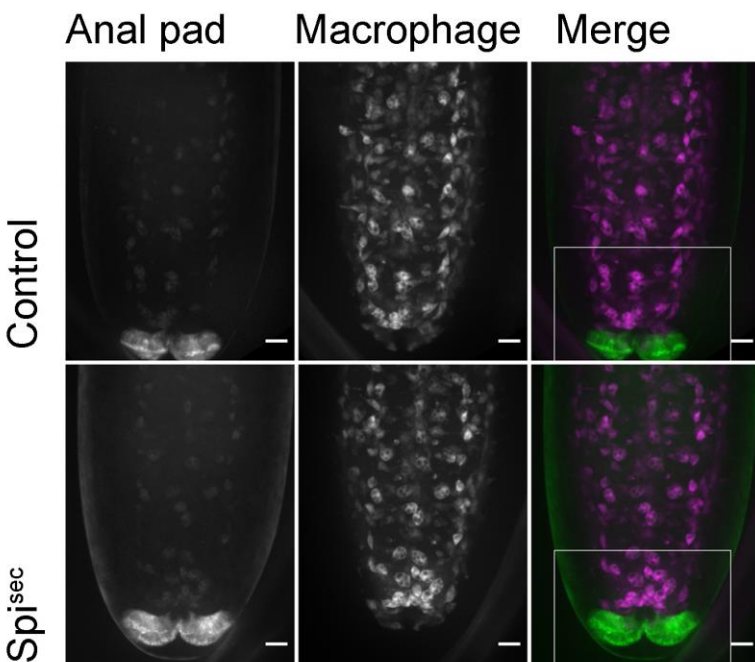
B VML macrophage dispersal



B' Macrophage counts



C Anal pad macrophage recruitment



C' Macrophage counts

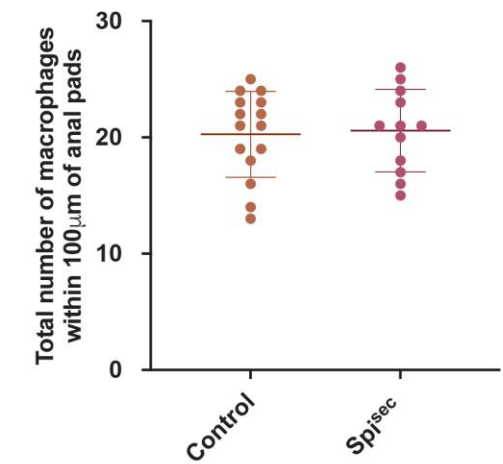


Figure 5.8 – Spitz secretion from the Salivary gland and anal pad does not affect macrophage dispersal

(A) 1µm thick single z-slice of the stage 13 embryonic ventro-lateral anterior showing the development of the salivary gland (labeled via tdTomato) and colonisation of the tissue by macrophages (labeled via SrpGMA, *) with the corresponding merged image. Anterior is up, scale bar denotes 20µm. (B) 1µm thick single z-slice of the embryonic ventral midline of stage 15 embryos showing macrophages (labelled via SrpGMA) in controls and embryos with *Fkh-GAL4* mediated expression of Spitz^{sec}. Anterior is right, scale bars denote 10µm. (B') Scattergraph of total number of ventral macrophage counts per embryo in controls and in the presence of salivary gland derived Spitz^{sec} (n = 14, 9; p = 0.159). (C) Maximum projections of ventral side of stage 15 embryos showing the anal pads (labeled using *VT45229-GAL4,UAS-LifeAct*; green in merge) and associated macrophages (labeled via *SrpHemo-3X-mCherry*; magenta in merge) in controls and embryos with *VT45229-GAL4* mediated expression of Spitz^{sec}. Anterior is up, scale bars denote 10µm, region of interest is annotated on the merged image (white box). (C') Scattergraphs of the total number of macrophages present within 100µm of the embryonic posterior = in controls and in the presence of anal pad-expressed Spitz^{sec} (n = 15, 12; p = 0.824). Lines and error bars represent mean and standard deviation on scattergraphs, respectively; lack of significance bars denote not significant, p>0.05. Statistical comparisons made via unpaired, two-tailed Student's t-test. Embryo genotypes are as follows: *w;SrpGMA;Fkh-GAL4,UAS-t-d-Tomato/+* (Control), *w;SrpGMA;Fkh-GAL4,UAS-t-d-Tomato/UAS-Spitz^{sec}* (Spi^{sec}), *w;;VT45229-GAL4,UAS-LifeAct,SrpHemo-3X-mCherry/+* (Control), *w;;VT45229-GAL4,UAS-LifeAct,SrpHemo-3X-mCherry/UAS-Spitz^{sec}* (Spi^{sec}).

5.2.6 Spitz exposure reduces efferocytic capacity of macrophages

Expression of Spitz in macrophages or the dorsal vessel induced a loss of vacuoles assumed to contain apoptotic cells within macrophages on the ventral midline or dorsal surface, respectively, suggesting that Spitz can interfere with efferocytosis. It is also possible that expression of this growth factor alters overall levels of apoptosis in the developing embryo, such that there are fewer corpses for macrophages to clear. Therefore, to address the effects of Spitz on apoptotic cell clearance, embryos with or without macrophage-specific expression of either sSpitz^{CS} or Spitz^{sec} were immunostained for the cleaved form of the *Drosophila* caspase DCP-1 (cDCP-1), used as a proxy for apoptotic cells (Song et al., 1997b) (Figure 5.9A-A''). To quantify the efficiency of efferocytosis, we manually counted the total number of cDCP-1 punctae on the ventral side of the embryo at stage 15 and calculated the proportion of these engulfed by macrophages. Macrophage-specific expression of either Spitz variant did not alter the total numbers of apoptotic cells in these regions compared to control embryos (Figure 5.9A-B). This suggests that Spitz does not inhibit apoptosis of surrounding cells, nor

does it cause a dramatic build-up of apoptotic corpses due to the reduction in engulfment by macrophages. As per the analysis of macrophage vacuolation (**Figure 5.3E-E'**), there was a decrease in the relative efficiency of apoptotic cell clearance specific to the expression of Spitz^{sec}, with a lower proportion of cDCP-1 punctae present within macrophages in this genotype (**Figure 5.9C**). The reduction of efferocytosis in macrophages in the presence of Spitz^{sec} was associated with an expected increase in the number of non-engulfed (uncleared) apoptotic cells (**Figure 5.9D**).

To check that the decrease in vacuoles and cDCP-1 punctae was not a consequence of more rapid phagosome maturation, acidification of phagosomes was investigated using lysotracker staining (**Figure 5.10A**). As per cDCP-1 staining, there was a significant decrease in the number of acidified phagosomes in the presence of Spitz^{sec} but not sSpitz^{CS}, compared to controls (**Figure 5.10B**). Importantly, there was no difference in the sizes of lysotracker-positive phagosomes between experimental conditions (**Figure 5.10C**), suggesting it is not the case that phagosomes mature and fuse at a faster rate in the presence of Spitz.

These data therefore support the idea that less apoptotic cell clearance is being carried out by macrophages in the presence of Spitz, but without the consequence of large changes in the number of cells undergoing cell death or remaining uncleared by phagocytes. That these phenotypes were again specific to Spitz^{sec} reinforces the idea that differences between these two Spitz variants is due to the loss of the palmitoyl modification on sSpitz^{CS}, which may prevent this variant from signalling in some contexts. Having established that Spitz^{sec} alters the efficiency of macrophage-mediated efferocytosis in addition to morphology, I sought to establish if Spitz was able to disrupt macrophage chemotaxis to non-developmental stimuli.

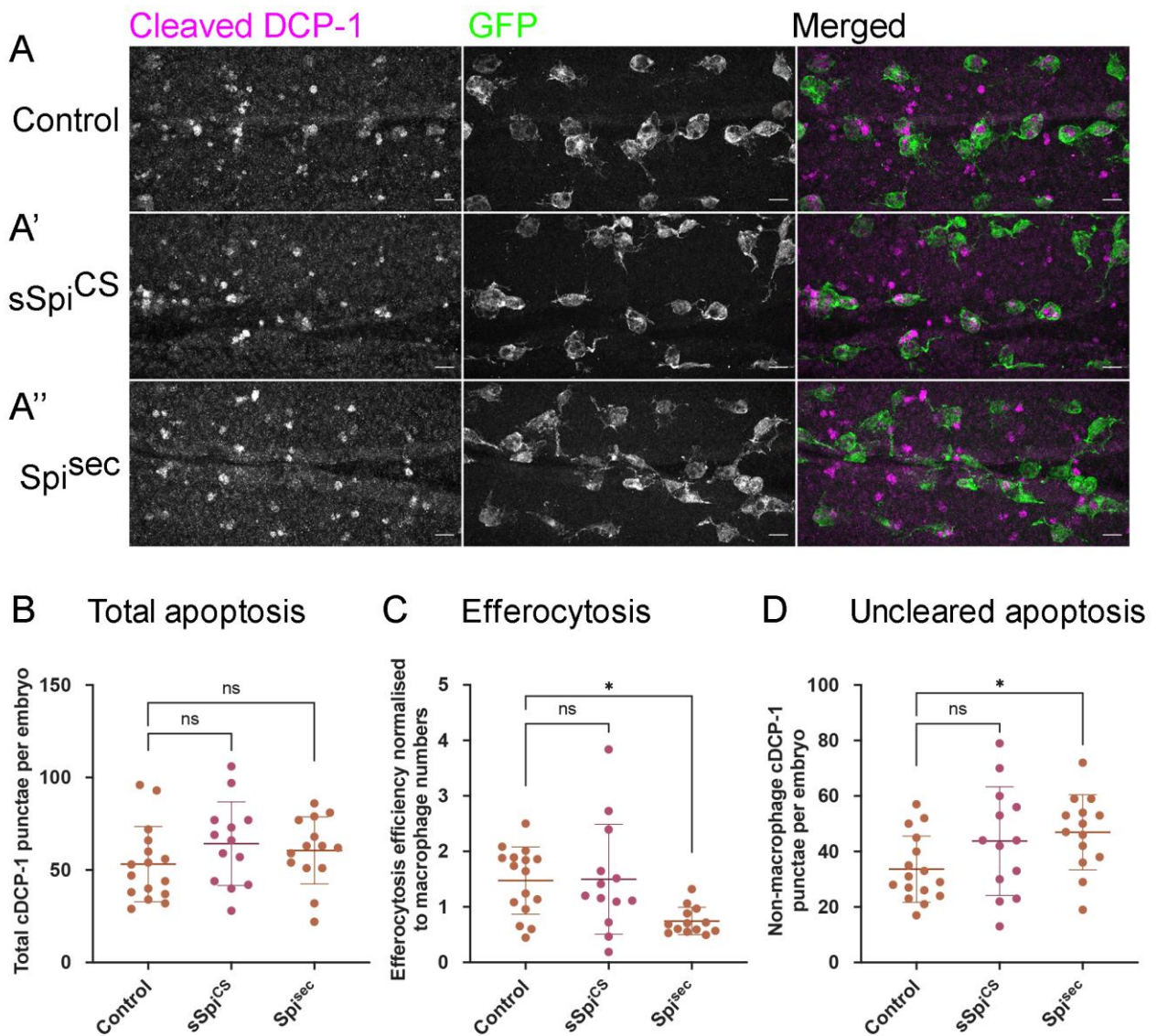


Figure 5.9 – Spitz impairs macrophage-mediated apoptotic cell clearance

(A) Maximum projections of the ventral region of stage 15 embryos immunostained for cleaved DCP-1 (cDCP-1; magenta in merge) and GFP (green in merge). Control embryos (A) were compared with embryos in which sSpitz^{CS} (A') or Spitz^{sec} (A'') were specifically expressed in macrophages. (B) Scattergraph showing the total numbers of cDCP-1 positive punctae present within the ventral field of view per embryo (B) (n = 16, 13, 14; p = 0.265 and p = 0.519 for comparison of control vs. sSpi^{CS} and control vs. Spi^{sec}, respectively). (C) Scattergraph showing efficiency of apoptotic cell clearance/efferocytosis (percentage of cDCP-1 punctae engulfed by macrophages per field of view, per embryo, normalized according to numbers of macrophages in the field of view; n = 16, 13, 13; p = 0.994 and p = 0.0125 for comparison of control vs. sSpi^{CS} and control vs. Spi^{sec}, respectively). (D) Scattergraph showing average number of cDCP-1 punctae not engulfed by macrophages per field of view, per embryo (n = 16, 13, 14; p = 0.142 and p = 0.0386 for comparison of control vs. sSpi^{CS} and control vs. Spi^{sec}, respectively). Scale bars denote 10µm; lines and error bars represent mean and standard deviation on scattergraphs, respectively; significance bars denote not significant (ns) p > 0.05, and * p < 0.05, respectively; all statistical comparisons made via one-way ANOVA with a Dunnett's post-test. Embryo genotypes are as follows: *w; Srp-GAL4,UAS-GFP/+;Crq-GAL4,UAS-GFP/+* (Control), *w;Srp-GAL4,UAS-GFP/UAS-sSpitzCS;Crq-GAL4,UAS-GFP/+* (sSpi^{CS}) and *w;Srp-GAL4,UAS-GFP/+;Crq-GAL4,UAS-GFP/UAS-Spitz^{sec}* (Spi^{sec}).

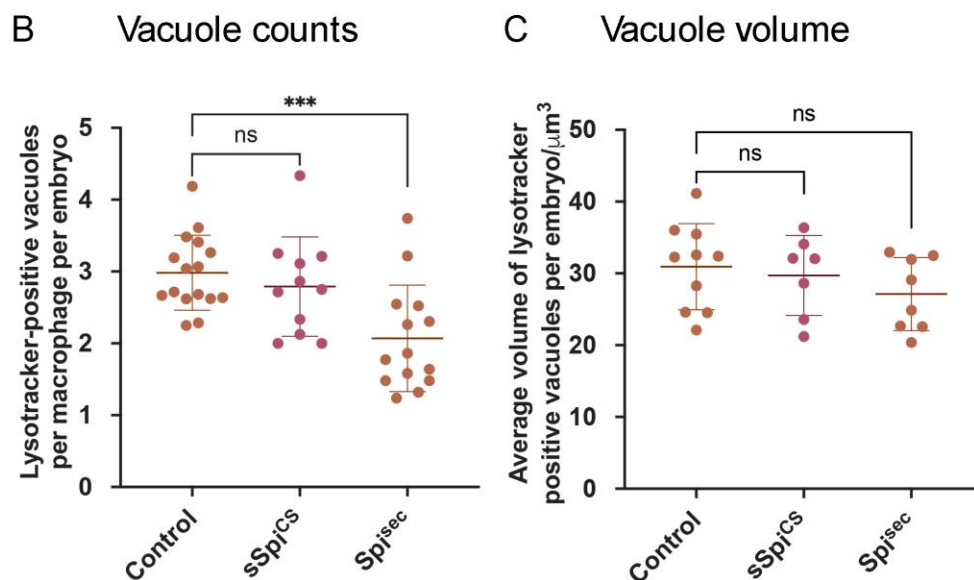
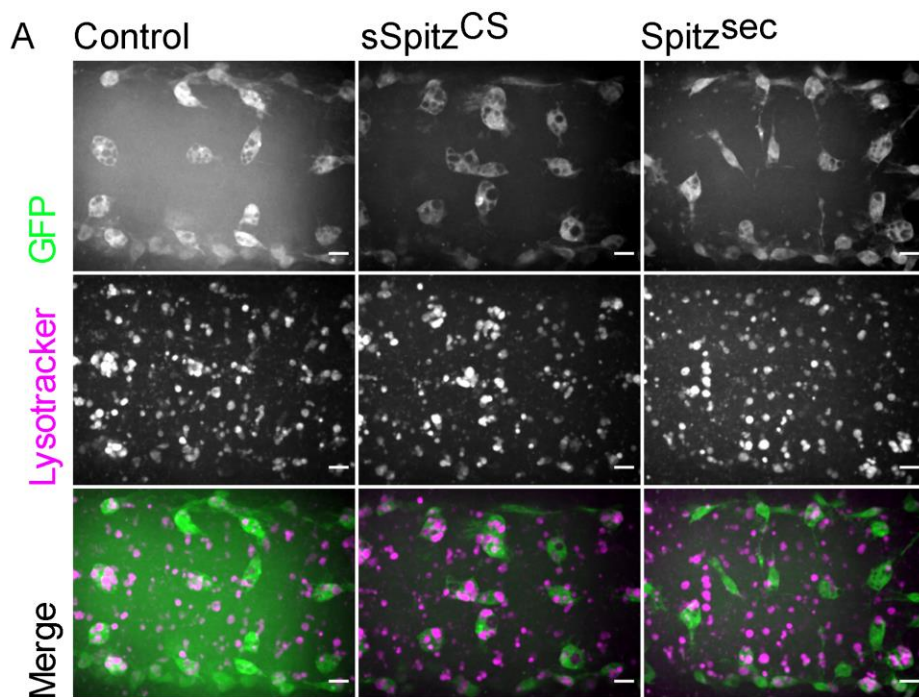


Figure 5.10 – *Spitz* does not alter phagosome volume in macrophages

(A) Images of macrophages (green in merge) with acidified phagosomes labeled using lysotracker red (magenta in merge) at stage 15 on the ventral midline in genotypes indicated. (B) Scattergraph showing numbers of lysotracker-positive punctae per macrophage, per embryo in the presence and absence of *Spitz* expression ($n = 16, 11, 14$; $p = 0.678$ and $p = 0.0009$ for comparison of control vs. $sSpi^{CS}$ and control vs. Spi^{sec} , respectively). (C) Scattergraph showing average volume of lysotracker-positive phagosomes per macrophage, per embryo in the presence and absence of *Spitz* expression ($n = 10, 7, 8$; $p = 0.873$ and $p = 0.284$ for comparison of control vs. $sSpi^{CS}$ and control vs. Spi^{sec} , respectively). Scale bars denote $10\mu m$; lines and error bars represent mean and standard deviation on scattergraphs, respectively; significance bars denote $nsp > 0.05$, and $***p < 0.001$, respectively; all statistical comparisons made via one-way ANOVA with a Dunnett's post-test. Embryo genotypes are as follows: $w;Srp-GAL4,UAS-GFP/+;Crq-GAL4,UAS-GFP/+$ (Control), $w;Srp-GAL4,UAS-GFP/UAS-sSpitz^{CS};Crq-GAL4,UAS-GFP/+$ ($sSpi^{CS}$) and $w;Srp-GAL4,UAS-GFP/+;Crq-GAL4,UAS-GFP/UAS-Spitz^{sec}$ (Spi^{sec}).

5.2.7 Spitz exposure dampens wound responses in macrophages in a distance-dependant manner

Drosophila embryonic macrophages exhibit robust wound responses by polarising towards and then migrating to sites of tissue damage (Stramer et al., 2005). These cells are refractile to wounding stimuli prior to late stage 14 due to persisting developmental signals, although they are still able to chemotax towards and engulf cells undergoing apoptotic cell death at this point in development (Moreira et al., 2010). This suggests that a hierarchy between different signals and that the integration of those signals can impact wound responses. Therefore, to address the effects of Spitz on inflammatory responses to injury, controls and embryos containing macrophage-specific expression of sSpitz^{CS} or Spitz^{sec} were laser wounded on the ventral surface of the embryo at stage 15 and the subsequent responses of GFP-labelled macrophages imaged (**Figure 5.11A**). One-hour post wounding, there was a significant reduction in the macrophage wound response (number of macrophages at the wound divided by wound area, normalised to the control average) in the presence of either Spitz^{sec} or sSpitz^{CS} compared to controls (**Figure 5.11A-B'**). As previously, cleavage of Spitz appears necessary to induce changes in macrophage behaviour, since expression of a membrane-bound form of Spitz (mSpitz^{CS}) failed to impact macrophage recruitment to wounds (**Figure 5.11B''**). The decrease in wound responses was paralleled by a decrease in the percentage of cells present in the field of view prior to wounding that are able to respond to injury for Spitz^{sec} but not sSpitz^{CS} (**Figure 5.11C-C'**), again highlighting the stronger effect of this variant.

Given the lack of a dramatic change in the numbers of apoptotic cells in the embryonic environment on expression of Spitz (**Figure 5.9**), it seems unlikely that distraction of macrophages by apoptotic cells (e.g., as observed in Roddie et al., 2019) accounts for this phenotype. Instead, a loss of sensitivity to wound signals at more distal sites, where wound cues may be weaker, could explain why a smaller proportion of macrophages respond. Therefore, to assess whether the loss of responses from regions further away from the wound site explained the reduction in numbers of macrophages reaching wounds, the distances of non-responsive macrophages from wound edges was measured. There were no differences in these measurements when sSpitz^{CS} and control embryos were compared

(Figure 5.11C). However, the average distances of non-responding macrophages from the wound were significantly lower in the presence of Spitz^{sec} compared to controls (Figure 5.11D') – i.e., more macrophages further away from the wound fail to respond in the presence of Spitz^{sec} compared to those within controls. Therefore, a loss recruitment of more distal macrophages to wound sites in the presence of Spitz^{sec} contributes to impaired wound responses. The variation between the reduction in macrophages at the wound but not a corresponding reduction in percentage recruitment in sSpitz^{CS} embryos may be due to a failure in the recruitment of distal macrophages to the wound.

In conclusion, the impairment of macrophage inflammatory responses in the presence of either Spitz^{sec} or sSpitz^{CS} highlights the capacity of this molecule to regulate a range of innate immune behaviours that depend on efficient polarisation and migration in the developing *Drosophila* embryo. The fact that Spitz specifically impacts the recruitment of more distal macrophages to wound sites would indicate it modulates or overrides the ability of these important cells to sense or respond to those signals produced at wound sites or by apoptotic cells.

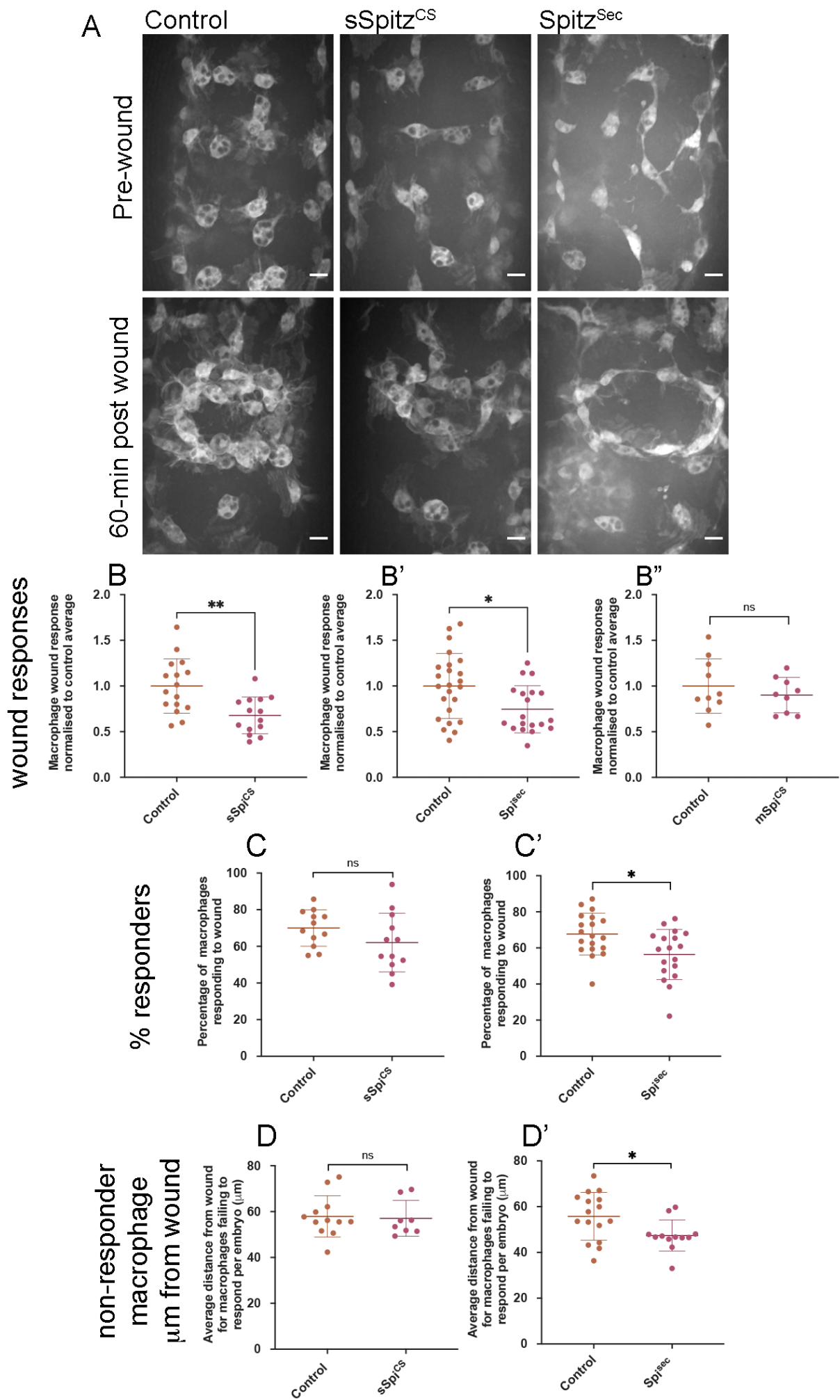


Figure 5.11 – Spitz impairs macrophage wound responses

(A) Maximum projections showing images of GFP-labeled macrophages on the ventral midline region in controls and in embryos containing macrophages expressing sSpitz^{CS} or Spitz^{sec}; upper panels show stage 15 embryos immediately prior to wounding; lower panels show corresponding embryo 1-h post wounding. (B–B'') Scattergraphs showing macrophage wound responses (number of macrophages responding to the wound normalized to wound area and to control responses) in controls and embryos with macrophage-specific expression of sSpitz^{CS} (B) (n = 16, 14; p = 0.0020), Spitz^{sec} (B') (n = 24, 19; p = 0.0160), or mSpitzCS (n = 9, 10; p = 0.406). (C,C') Scattergraphs showing percentage of macrophages responding to wound per embryo (% of those in the field of view that reach the wound) per embryo for control embryos compared to embryos with macrophage specific-expression of sSpitz^{CS} (C) (n = 12, 12; p = 0.159) or Spitz^{sec} (C') (n = 19, 18; p = 0.0105). (D,D') Scattergraphs showing average distance from the wound edge (immediately prior to wounding) of those macrophages that fail to respond, per embryo, for control embryos compared to embryos with macrophage specific-expression of sSpitz^{CS} (D) (n = 12, 8; p = 0.678) or Spitz^{sec} (D') (n = 16, 12; p = 0.0421). Scale bars denote 10µm; lines and error bars represent mean and standard deviation on scattergraphs, respectively; significance bars denote not significant (ns) p > 0.05, * p < 0.05, and ** p < 0.01, respectively; statistical comparisons made via a Mann–Whitney test (B',B'',D,D') or an unpaired, two-tailed Student's t-test (B,C,C'). Embryo genotypes are as follows: *w;Srp-GAL4,UAS-GFP/+;Crq-GAL4,UAS-GFP/+* (Control), *w;Srp-GAL4,UAS-GFP/UAS-sSpitz^{CS};Crq-GAL4,UAS-GFP/+* (sSpi^{CS}), *w;Srp-GAL4,UAS-GFP/+;Crq-GAL4,UAS-GFP/UAS-Spitz^{sec}* (Spi^{sec}) and *w;Srp-GAL4,UAS-GFP/+;Crq-GAL4,UAS-GFP/UAS-mSpitz^{CS}-GFP* (mSpi^{CS}).

5.3 Discussion

Here we show for the first time that the *Drosophila* epidermal growth factor pathway modifies immune cell function in the developing embryo, representing a new cue regulating the behaviour of this organism's macrophages *in vivo*. De-regulated release of Spitz disrupts macrophage migration, induces elongation, and perturbs the ability of macrophages to respond to wounds and clear apoptotic cells. The experiments presented herein have undergone peer review and been published in Tardy et al. (2021). In this study, two variants of protease-independent Spitz with different diffusion properties were used to assess the role of Spitz as a macrophage chemoattractant in the *Drosophila* embryo. Surprisingly, macrophage phenotypes varied according to the Spitz isoform used, suggesting different physical properties of this cue can influence macrophage behaviour in subtle ways. These phenotypic differences are summarised below in **Figure 5.12**

		sSpitz^{CS}	Spitz^{sec}
Phenotype:	Region:	Active, lacks palmitoylation – diffuses further, shallower gradients?	Active, has palmitoylation – steeper, local gradients?
Clustering	VML	No change	↑
Aspect ratio	VML	↑	↑
Vacuolation	VML	No change	↓
cDCP-1/Lysotracker	VML	No change	↓
Vacuolation	DV	↓	↓
Speed	VML	↑	No change
DV recruitment	DV	No change	↓
Wound response	VML	↓	↓
Non-responder distance	VML	No change	↓

VML, ventral midline; DV, dorsal vessel.

mSpi^{CS} does not induce any macrophage phenotypes.

Table 5.1 – Summary of de regulated spitz phenotype differences

5.3.1 Spitz as a chemoattractant and its possible mechanisms of action

Two non-mutually exclusive scenarios may explain how Spitz alters macrophage morphology and speed: regulation of macrophage chemotaxis by Spitz, which causes an override of endogenous signals, and/or reprogramming of macrophages to different activation states with different migratory and morphological characteristics. EGF ligands can function as chemoattractants in a number of situations: human EGF and the *Drosophila* EGF ligand Gurken regulate monocyte chemotaxis and *Drosophila* border cell migration, respectively (Duchek and Rørth, 2001; Lamb et al., 2004), while Spitz was itself identified as a stem cell attractant released by *Drosophila* midgut cells undergoing apoptosis (Liang et al., 2017). We found that, in the presence of Spitz, macrophages on the ventral midline became more highly polarised and migrated at greater speeds (sSpitz^{CS} specifically). The changes in cell shape could be indicative of a chemotactic response towards a gradient (Sarris and Sixt, 2015), through enhanced formation or stabilisation of a cell's leading edge, or may be the result of

macrophage reprogramming events that have previously been linked to morphological distinctions between pro-inflammatory and anti-inflammatory macrophages (McWhorter et al., 2013). Single-cell RNA-sequencing studies have shown that blood cell populations may be more complicated in *Drosophila* than previously anticipated (Cattenoz et al., 2020; Cho et al., 2020; Tattikota et al., 2020). At present these approaches are limited to larval stages, although recent work suggests that subpopulations of functionally-distinct macrophages may also exist in the developing fly embryo (Coates et al., 2021). The expression of Spitz under the control of *TinC-GAL4* corroborated midline efferocytosis defects and revealed that macrophage-specific expression was not necessary for an impact on this behaviour. The reduction in the numbers of macrophages at the dorsal vessel on expression of Spitz^{sec} is possibly the result of distal *TinC-GAL4* activity within the lateral visceral muscles (Bodmer, 1993) attracting macrophages away from this tissue. Again, the fact that Spitz^{sec}, but not sSpitz^{CS} altered macrophage recruitment potentially reflects the stronger phenotypes obtained with Spitz^{sec}, which may in turn relate to the differences in diffusion of these two variants (see below).

5.3.2 Spitz as a potential apoptotic-derived find-me cue

EGF signalling can block apoptosis through its action as pro-survival signal (Henson and Gibson, 2006) and can also stimulate compensatory proliferation (Fogarty and Bergmann, 2017). However, Spitz expression did not dramatically alter the total number of apoptotic cells in vivo but did impair clearance by macrophages. This may reflect reprogramming to an activation state that is less efficient at engulfing dying cells, since the capacity to clear apoptotic cells can vary across macrophage subpopulations in some organisms (Zizzo et al., 2012).

Alternatively, chemotaxis towards Spitz or signal integration mechanisms may impair detection of apoptotic corpses – if Spitz represents a chemoattractant it may distract macrophages from their clearance duties (e.g., towards each other leading to clustering or increased migration speeds). Intriguingly, Spitz and human EGF share similar processing and secretion mechanisms to a known find-me cue for apoptotic cells, Fractalkine (Sokolowski et al., 2014). Both Fractalkine and EGFs require activation via caspase-regulated proteases – Rhomboid and ADAM-17, respectively (Rose-John, 2013; Liang et al., 2017). The changes in

macrophage shape and their responses to stimuli that are induced by Spitz, and the similarities in how Spitz and other find-me cues are secreted, raises the potential role of Spitz as a chemoattractant used in the “find-me” phase of efferocytosis (Ravichandran, 2003). High levels of this cue may therefore interfere with detection of apoptotic cells (i.e., signals from apoptotic cells are “drowned out” by misexpressed Spitz), though considerably more work would be required to establish Spitz as a find-me cue. Furthermore, these experiments are not straightforward given the role of EGF signalling in midline development (Golembo et al., 1996) and the fact that disruption of that process blocks macrophage dispersal (Paladi and Tepass, 2004; Evans et al., 2010a).

Similarly, we have shown that the presence of Spitz^{sec} or sSpitz^{CS}, inhibits the ability of macrophages to respond to wounding stimuli. Uncleared apoptotic cells can impair wound responses in the developing embryo (Roddie et al., 2019). However, since no substantial changes in overall levels of apoptosis were detected in the presence of either Spitz variant, nor did Spitz^{CS} expression impact efferocytosis on the ventral midline, we do not favour the explanation that uncleared apoptotic cells undermine macrophage inflammatory responses to injury in this context. Instead impairment of wound responses may result from competition between Spitz and the damage-associated molecular signals released at wound sites (Koh and DiPietro, 2011), or macrophage reprogramming as discussed above. Indeed, our results showed that Spitz prevented more distal macrophages from responding to the wound, supporting the idea of competing chemotactic gradients as opposed to a general reprogramming of macrophages that results in desensitisation to wound signals. This disruption of macrophage responses may be specific to regions of the embryo more distal to wound sites, as wound signals may be present at lower concentrations in those environments.

5.3.4 Effect of post-translational modification on Spitz function

The phenotypic differences observed between Spitz^{sec} and sSpitz^{CS} likely reflect the absence of a palmitoyl group in the latter (Miura et al., 2006). Palmitoylation is known to increase tethering of ligands at the plasma membrane post-secretion (Salaun et al., 2010). Additionally, mutation in the palmitoylation site of signalling proteins is known to alter cell-cell signalling, e.g., Fas-mediated cell death (Guardiola-Serrano et al., 2010), and significantly

reduce diffusion speed of ligands (Sowa et al., 1999). This may allow sSpitz^{CS} to diffuse further from its source, forming shallower gradients over longer distances. In contrast, Spitz^{sec} would remain more highly concentrated at its source leading to steeper gradients over a shorter range. This potentially explains why Spitz^{sec} can drive macrophage clustering between neighbouring macrophages and effect larger changes in macrophage AR and vacuolation and why sSpitz^{CS} may impair inflammatory migration further away from wound sites. Shallower, more long-range gradients may enable increased migration speeds with sSpitz^{CS}, whereas Spitz^{sec} promotes clustering more locally. While our initial screen in using ey-GAL4 confirmed the effects of Spitz, there is no current reason to restrict these effects to this ligand alone without further experimentation with Rhomboid processing ligands e.g., secreted Gurken.

5.3.5 Future work and COVID-19 impact

Due to disruption resulting from the COVID-19 pandemic, there were several experiments that had to be discontinued. Chief among these were genetic complementation experiments using the dominant negative variant of EGFR to confirm that the phenotype seen in macrophages in the presence of Spitz were in fact the result of EGFR activation and not working through an indirect mechanism. Initial experiments were conducted to rescue the macrophage secreted spitz phenotypes using *UAS-EGFR^{DN}* (Buff et al., 1998), however despite PCR validation of construct it was not possible to confirm dominant negative activity in the *ey-GAL4* proliferation screen discussed earlier. In addition, it would be useful to confirm downstream effects of EGFR signalling such as the release of the Spitz sequestering protein Argos (Jin et al., 2002). Further experimentation would be required to study the role of Spitz as an apoptotic derived find me cue. The use of EGF component loss of function mutants such as Spitz¹ (Rutledge et al., 1992) or Rhomboid^{VE-1} (Sturtevant et al., 1993) would allow for the role of Spitz in efferocytosis to be further examined by assaying apoptotic clearance of cells unable to secrete active Spitz. To confirm if Spitz is acting to polarise macrophages into specific sub-types, it would be useful to test the effect of Spitz secretion on macrophage labelled using the VT array e.g., to see if macrophages exposed to Spitz undergo changes in enhancer element expression and if so, what affect this might have on their behaviour.

5.3.6 Conclusions

Taken together, these results show that Spitz can alter macrophage migration and functional responses to wounds and apoptotic cells during *Drosophila* development. These processes are important immune cell behaviours that can become dysregulated in a diverse array of human conditions including cancer, atherosclerosis, and chronic inflammatory conditions. These results therefore have clear implications for our understanding of the role that EGF ligands play during development and in the progression of chronic inflammation.

Furthermore, these findings have implications and relevance to therapeutic strategies that seek to interfere with EGF signalling – indeed, targeting the EGF pathway shows promise as a therapeutic strategy in models of chronic inflammation (Qu et al., 2012; Omachi et al., 2017; Rahman et al., 2019). Future work will establish the exact mechanisms of actions via which *Drosophila* EGFs regulate macrophage function and whether these functions are conserved through evolution.

Chapter 6- Final discussion

6.1 Project summary and discussion

The aims of this thesis were to examine the regulation and dynamics of apoptotic cell clearance using *Drosophila* as an *in vivo* model and to optimise the use of *ex vivo* primary cell culture to understand signalling prioritisation. This project took the form of three distinct experimental strands: using novel fluorescence tools in *Drosophila* to study the dynamics of apoptotic progression and efferocytosis in real time (chapter 4); challenging MDMs with apoptotic derived signals to understand how signals are prioritised (chapter 5); and using *Drosophila* to evaluate the chemotactic potential of EGF signalling during development (chapter 6).

Each line of inquiry has yielded interesting and novel data related to the conserved function of efferocytosis. Live imaging of efferocytosis using GC3Ai caspase reporters confirmed the value of these tools compared to contemporary methods and has shown that embryonic efferocytosis by macrophages is not guaranteed, with dying cells seen to undergo a variety of different outcomes. While initial optimisation proved arduous, I was able to optimise the use of Ibidi μ -slide chemotaxis chambers for use with monocyte derived macrophage (MDMs) and showed that the presence of apoptotic find me cues did indeed dull the migration of MDMs towards pro-inflammatory stimuli (C5a). Screening for novel find-me cues in *Drosophila* led us to EGF signalling, with Spitz now shown to be able to modulate *Drosophila* embryonic macrophage function and migration *in vivo*.

6.1.1 Live imaging of caspase dynamics underlines the complexity of efferocytosis in *Drosophila*

To understand the relationship between caspase activation and the recruitment of macrophages in the *Drosophila* embryo, the genetically encoded caspase reporter GC3Ai was used (Schott et al., 2017). All of the known find-me cues are either directly or indirectly dependent on the activation of caspases to initiate their release (Ravichandran, 2010):

by measuring caspase dynamics during apoptosis and the subsequent behaviour of local macrophages, I sought to assess the timescales and ranges required for efferocytosis and thereby elucidate the potential properties of the active find-me cues (chapter 4)

Validation experiments confirmed that GC3Ai was suitable for assaying apoptotic death and had comparable sensitivity to other contemporary methods both *ex-vivo* (cDCP-1 comparison) and *in vivo* (AO and Apoliner). These experiments showed that the ubiquitous expression of GC3Ai had a higher sensitivity for apoptotic cells compared to anti cleaved caspase staining (cDCP-1) and had the key advantage of single-channel imaging over AO and Apoliner live methods.

Imaging of efferocytosis during embryogenesis found that apoptotic cells within the ventral midline region appeared to undergo three distinct outcomes which were associated with caspase activation patterns. These outcomes were described as: efferocytosis, wherein a short caspase activation period was rapidly followed by engulfment of the apoptotic cell by migratory macrophages; transient caspase activation, observed as a brief increase in caspase activity and the development of apoptotic morphology followed by a loss of cell blebbing and decrease of caspase activity; and disassembly, characterised by a rapid increase in caspase activity followed by the collapse of the cell and release of suspected membrane exosomes.

The speed at which macrophages responded to apoptotic cells that were engulfed (>20 minutes) is informative to what find-me cues may be active at this point in embryogenesis. The time-frame largely negates the possibility of apoptosis induced *de novo* translation (Bushell et al., 2006), suggesting that any released cues are already present within the dying cell in an inactive or controlled form. This could point to either the activation of find-me cue processing enzymes such as Shpk2 or ADAM17 (Gude et al., 2008; Rose-John, 2013) or the “venting” of molecules present at high concentrations within the dying cell e.g. Pannexin-1 cleavage and cytoplasmic ATP/UTP externalisation (Chekeni et al., 2011; Qu et al., 2011; Penuela et al., 2013). The identity of any release cues could be further examined in several ways. To assay the activation of cues via caspase activated enzymes, fluorescent artificial substates could be expressed in conjunction with GC3Ai. The expression of probes against nucleotides e.g. ATP-reporters (Tsuyama et al., 2013) would allow for the relative level of

nucleotides to be assessed during apoptosis, giving an indication of any substantial caspase linked release.

Tracking of apoptotic outcomes found that, despite the relative abundance of local macrophages within the ventral epithelia, several apoptotic cells did not undergo efferocytosis via macrophages. The structural disassembly of dying cells has been recognised as a distinct apoptotic process (Atkin-Smith and Poon, 2017; Caruso and Poon, 2018). While it would appear that the release of membrane vesicles into the extracellular space is independent of efferocytosis, it is known that such exosomes can contain a variety of bioactive molecules (Norling and Dalli, 2013) and may interact with immune cells to facilitate sub-type modulation or enhance the efferocytic response.

The presence of cells that appear to undergo transient caspase activation could be indicative of two processes: transient caspase activation (anastasis) or efferocytosis via adjacent non-professional phagocytes. Anastasis has been identified as a “abort program” for apoptosis, with cells showing the initial stages of death (detachment, blebbing, caspase activity etc.) before recovering through the upregulation of pro-survival genes (Tang et al., 2012; Sun et al., 2017). This process has been observed to occur during *Drosophila* embryogenesis and could explain the presence of these transient caspase active cells (Sun et al., 2017). The clearance of dying cells in *Drosophila* by non-professional phagocytes has been observed to occur in both the ovary and CNS (Han et al., 2014; Serizier and McCall, 2017): while it could therefore be the case that these cells are indeed being eaten by their neighbours e.g. adjacent epithelial or glial cells present in the VNC, there is provisional evidence that such non-professional phagocytosis occurs on a longer timescale (hours) to what has been observed here (Parnaik et al., 2000).

Several assays could be conducted to further elucidate the relationship between caspase activity and efferocytosis. While the data presented here has largely focussed on the stage 13-15 embryonic ventral midline as a region of interest, it would be important to assay the progression of apoptosis in other contexts, such as within the ventral nerve cord where glia process apoptotic cells (Armitage et al., 2020). In addition, while this thesis has tested the effectiveness of GC3Ai in the *Drosophila* embryo, these reporters have been validated by tool

developers for use in other *Drosophila* life-stages: it would be of interest to see if the observations made in the embryo translate into larval or adult *Drosophila* which have distinct haematopoiesis and immune processes such as sessile macrophages (Lanot et al., 2001).

The results of this chapter have several implications for our understanding of *in vivo* efferocytosis. In healthy tissues, efferocytosis has been viewed as a rapid process that requires the removal of apoptotic cells prior to the onset of secondary necrosis (Ravichandran, 2003); the data presented here suggests that during *Drosophila* embryogenesis at least, apoptotic clearance by macrophages makes up only a part of the efferocytic response, although the rapid nature of macrophage-apoptotic cell engulfment does support the idea of find-me cues being highly prioritised. The combined use of macrophage markers with cytosolic caspase reporters has allowed for the direct visualisation of efferocytosis within the developing embryo, a process which appears to occur in a distinct mechanical fashion dissimilar to the phagocytic cup formation typically observed when macrophages engulf other targets such as bacteria.

6.1.2 *Ex vivo* migration chambers can be used to investigate how macrophages prioritise apoptotic cell signals

The rapid removal of dying cells *in vivo* had led to the idea that find me cues are highly prioritised signals that are able to override other migratory cues to ensure efferocytosis and prevent secondary necrosis. To study the existence and structure of this proposed signalling hierarchy, *ex-vivo* monocyte derived macrophages (MDMs) were challenged with chemoattractants using the Ibidi μ -slide micro-fluidic migration chamber (chapter 5).

After initial issues surrounding the viability of MDMs, the transfer methods were eventually optimised and MDMs were successfully generated in culture and adhered within the migration chamber. Initial attempts to induce migration to established chemokines fMLP and MCP-1 failed to illicit a response, however the use of human recombinant C5a at 20nM produced a robust chemotactic effect on MDMs. Given that fMLP and MCP-1 have been extensively shown to induce chemotaxis at the tested concentrations (Schiffmann et al., 1975; Audran et al., 1996), it is possible that the transfer procedure altered the receptor expression pattern of the MDMs. There are changes that could be made to the transfer

technique that might mitigate against short-term alterations in receptor expression. For example, the time between seeding and the migration assay was kept relatively short (~45 minutes) in line with manufacturers instruction and increasing this may allow the cells to better equilibrate. Although given the small volume of culture medium in the chamber (6µl), media may be lost due to evaporation, making this challenging. Alternatively, monocytes could be directly seeded into the Ibidi chamber and differentiated *in situ*, although this has not been established by others and would require considerable optimisation.

To assess the chemotactic potential of find me cues, apoptotic neutrophils were aged to produce apoptotic supernatant (ASN) for use in chemotaxis experiments (Renshaw et al., 2003). Interestingly, our results found that ASN alone was not able to induce the migration of MDMs. There are several explanations for this lack of response: the concentration of aged neutrophils used (5 million cells mL⁻¹) produced a relatively dilute concentration of find-me cues that were not within the detection threshold of MDMs; MDMs are not responsive to the find-me cues released by neutrophils; the time-scales of apoptosis via neutrophil aging (22 hours at 37°C/5% CO₂) leads to the degradation of the majority of the find-me cues present within the ASN (especially potentially unstable nucleotide tri-phosphates). The first option can be easily tested by increasing the ratio of aging neutrophils to media to produce a higher concentration ASN. To address the relationship between cell type and ASN, it would be useful to use other cell types that have been used for the generation of ASN e.g. cells lines including AsPC-1 or W3 (Nishimura et al., 2001; Yamaguchi et al., 2014) or another primary cell model such as germinal centre B-cells (Segundo et al., 1999). While the aging procedure has been shown to produce consistent apoptotic cultures, the use of more rapid apoptotic induction techniques could be used to produce ASN in a short period e.g., the addition of pro-apoptosis drugs such as staurosporine or via exposure to ultraviolet radiation (Schlatter et al., 2009; To et al., 2016).

The results showed that while ASN in of itself did not produce a chemoattractive response, the saturation of MDMs with ASN prior to challenge did blunt their migratory response towards a directional gradient of 20nM C5a. This suggested that ASN was able to alter the migratory behaviour of MDMs, although this may be the result of either find-me cue competition with C5a or the modulation of the MDM sub-type via ASN to a C5a insensitive

phenotype. One potential reason for this response is the presence of RP-S19 within the ASN, a find-me cue peptide derived from the ribosomal machinery that is known to bind the C5a receptor (Revollo et al., 2005; Choemmel et al., 2007; Yamamoto, 2007; Filip et al., 2009). To test if this were the case, RPS-19 presence would need to be confirmed via western blotting of ASN combined with MDM treatment with ASN depleted of RPS-19. While this effect could be the result of direct chemotactic competition between ASN constituents and C5a, it is known that find-me cues are able to reprogram immune cells towards an anti-inflammatory phenotype (Bours et al., 2006; Kolb and Martinez, 2016). This modulation could reduce the relative expression of the C5aR on MDMs, thereby preventing them from responding to the C5a gradient proper. RNAseq analysis of MDMs treated with ASN could be used to assess changes in gene expression and better define any phenotypic shift.

To control for the non-apoptotic effects of ASN addition to MDMs, the pan-caspase inhibitor Q-VD-OPh was added to aging neutrophils. The results showed that while ASN + Q-VD-OPh (ANN) treatment did not inhibit the MDM response to C5a, but nor did it rescue migration to control levels. Given that non-apoptosis caspase activity has been implicated in cell migration (Gdynia et al., 2007; Li et al., 2007; Barbero et al., 2008), it was postulated that the presence of Q-VD-OPh within ASN may be acting to inhibit MDM migration independently of find-me cues. Treatment of MDMs with Q-VD-OPh confirmed that the drug was indeed inhibiting the migration of MDMs, although this is likely not specific to C5a and instead a general loss of motility through disruption of caspase activity.

In summary, while there were initial optimisation issues relating to culture conditions and the validation of chemoattracts, the results show that MDMs can be used in the Ibidi μ -slide microfluidic chamber, and this assay can be used to understand how find-me cues released from apoptotic cells are prioritised in multi-signal environments.

6.1.3 Epidermal growth factor as an immuno-chemoattractant in *Drosophila*

One of the aims of this project was to examine the role of epidermal growth factor signalling on the *Drosophila* immune system during embryogenesis. This was driven by previous reports that showed EGF ligands were chemoattractive in *Drosophila* and humans in certain tissues (Duchek and Rørth, 2001; Lamb et al., 2004; Liang et al., 2017). Since EGFs are critical for the

proper development of the *Drosophila* embryo, we sought to understand if and how it interacts with the developing immune system (Schweitzer et al., 1995; Golembo et al., 1996; Buff et al., 1998; Spencer et al., 1998; Yogev et al., 2008).

Overexpression of EGF signalling during *Drosophila* embryogenesis showed that the cardinal *Drosophila* EGF ligand, Spitz, did have some impact on the migration and function of embryonic macrophages *in vivo*. While we were unable to firmly conclude a chemotactic effect of Spitz, the phenotypes exhibited by macrophages in the presence of Spitz (increased clustering, changes in migration speeds, cell body elongation) are all indicative of changes in migration dynamics. In addition, our results showed that in the presence of Spitz, macrophages had a reduced capacity to clear apoptotic cells and respond to wounds, suggesting either a modulation in macrophage sub-type or the presence of a competing chemoattractant, i.e., Spitz.

The loss of effective efferocytosis was of particular interest as Spitz is known to be released from apoptotic cells as part of the compensatory proliferative response that is activated in response to apoptosis (Ryoo et al., 2004; Fan et al., 2014; Fogarty and Bergmann, 2017; Liang et al., 2017) and shares similar processing mechanism to certain members of the “find me cue” group of apoptotic derived chemoattractants. The release of find-me to facilitates efferocytosis has been well studied in mammalian systems (Ariel and Ravichandran, 2016). These cues are structurally diverse, with lipoprotein, small peptides and nucleotides all implicated in the recruitment of phagocytes to apoptotic cells (Lauber, 2003; Truman et al., 2008; Chekeni et al., 2011). Of note, the mammalian find-me cue Fractalkine shares similar secretory mechanism to Spitz: The generation of active Fractalkine or Spitz require proteolytic cleavage by metalloprotease enzymes (ADAM17 and Rhomboid respectably), proteases that are tightly regulated and appear to become active during apoptosis as a result of caspase activity (Chalaris et al., 2007; Liang et al., 2017).

Since find-me cues are thought to be highly prioritised, the loss of efferocytosis in spitz-secreting macrophages suggests that Spitz is either preventing macrophages from registering find me cues, altering macrophages phenotypes resulting in a reduced efferocytotic capacity or Spitz is acting as a pro-survival signal and is directly suppressing local apoptosis through.

cDCP-1 and lysotracker red staining showed that apoptotic levels and macrophage phagosome processing remains intact, largely ruling out decreased apoptosis as a causative factor in these phenotypes. Given that the release of Spitz has been shown to occur in dying gut cells, it would seem unlikely that it would act to reduce the efferocytic capacity of macrophages since it is probably acting in concert with pro-recruitment find-me cues released by the same cell. This leaves competition between Spitz and other find-me cues as the most viable explanation for the observed macrophage phenotypes, although there are several experiments that would be required to confirm this.

To confirm that Spitz is acting as a find-me cue during *Drosophila* embryogenesis, several conclusions would first need to be drawn from other experiments. Firstly, we would need to establish that Spitz is being released by apoptotic cells during embryogenesis. One way to detect this would be the detection of active rhomboid within apoptotic cells; this assay could be conducted via co-immunostaining for apoptotic cells (cDCP-1/GC3Ai) and activated spitz (anti-Spitz) or rhomboid (antibodies not currently available). Alternatively, the induction of apoptosis in cultured S2 cells could be used to show if dying cells lead to enriched Spitz in the culture media. If Spitz is confirmed to be released during apoptosis, it would be important to show that there is a loss of efficient efferocytosis in embryos lacking proper spitz secretion. Due to the developmental functions of Spitz, the use of ubiquitous knockouts via RNAi or genomic deficiency would likely be unsuitable. Using GAL4 driven siRNA or dominant negative variant of Spitz processing e.g., siRNA against Rhomboid, it would be possible to remove proper Spitz processing in a tissue specific manner and compare efferocytosis rates. In addition, using GC3Ai in concert with these methods, it would be possible to track the role of Spitz in efferocytosis in real time and screen for defects in recruitment, binding or processing of apoptotic cells within macrophages.

6.1.4 Perspectives for future work

While the work presented within each chapter of this thesis stand as they are, there is great potential for the combination of these techniques, some of which was planned prior to the COVID-19 pandemic.

Since GC3Ai can be used to during live imaging, I planned to use the reporter in conjunction with Spitz mis expression to better assess the defective efferocytosis phenotypes that were observed (DCP-1; **Figure 5.9**): this approach might have allowed us to assess if the presence of Spitz altered macrophage recruitment or the engulfment of apoptotic cells, which in turn would have shed light on potential mechanisms e.g., if Spitz was acting in a chemoattractive manner or somehow reducing the macrophages ability to bind apoptotic cells. While the work presented here suggests a role for Spitz as a macrophage chemoattractant, this evolutionary conservation of this activity could be confirmed by translating these experiments into human models using the Ibidi μ -slide chemotaxis assay optimised for use with MDMs. Previous experiments have been shown to human EGF can attract macrophages *ex vivo* (Lamb et al., 2004). Using the C5a challenge system described previously (chapter 4), MDMs challenged with C5a could be treated with ASN with or without the addition of ErBB inhibitors such as Gefitinib (Rahman et al., 2019). If apoptotic derived EGF was present and playing a chemoattractive role, the loss of EGFR activity in MDMs may result in the loss in the potential of ASN to reduce migration towards C5a.

6.1.5 Limitations and caveats of this study

In this study we have utilised *Drosophila melanogaster* as a model organism, and specifically the mid-stages of embryogenesis (stages 12-15). While this stage is ideal for the study of embryonic macrophage function, it should be noted that the later life-stages of *Drosophila* (Larvae, Imago/adult) have distinct hematopoietic processes and macrophage mobility (Lanot et al., 2001). The motility of macrophages could have implications on how efferocytosis is conducted and thus is it important to be aware of these differences. For several assays including macrophage random migration, wounding and tracking of apoptosis, the ventral epithelial midline has been used as a region of interest. The main reason for this is that structure and macrophage dispersal in this region is stereotypical and thus easily screened for phenotypic change. While this region is useful for understanding macrophage migration dynamics, there are alternative models including the pupal notum that could be used to assay apoptosis in a monolayered tissue (Valon et al., 2021).

For *ex vivo* migration experiments, MDMs were used as a cell model for tissue resident macrophages that typically perform efferocytosis *in vivo*. Due to the requirement for initial

optimisation of MDMs for use in the Ibidi u-slide, a 2D model was used. While this was sufficient to assay the prioritisation of different chemoattractants, it should be noted that *in vivo*, tissue resident macrophages will be present in an extracellular matrix which will feedback into mobility by presenting different adhesion factors as well as mechanical properties such as stiffness and porosity (Wolf et al., 2013).

6.1.6 Conclusion

In this thesis, I have investigated the process of efferocytosis and the role of find me cues using a combined model organism and primary cell culture approach. The results of this thesis have added to our understanding of efferocytosis as a conserved biological process and how it plays a role in the function of the immune system. Using novel apoptosis reporters, I have found a relationship between the caspase levels within cells and their behaviour *in vivo*. In addition, by using these reporters in conjunction with macrophage labels it has been possible to image and dissect the efferocytosis process in real time. Building on previous observations on EGF, the results of the effect of Spitz on macrophages has provided evidence that Spitz is chemoattractive and a possible member of the find me cue family. Finally, I have optimised the use of the microfluidic Ibidi μ -slide chamber for use with MDMs and developed a novel assay for competing chemoattraction.

Appendix

Standard *Drosophila* medium is prepared by according to the following recipe:

1 litre cold tap water, 80g medium cornmeal, 18g dried yeast, 10g soya flour, 80g malt extract, 40g molasses, 8g agar, 25ml nipagin in absolute ethanol, 4ml propionic acid.

DABCO recipe: 1g DABCO (sigma) + 4ml 10x PBS + 36ml glycerol.

DNA digestion buffer: 4890µl MQ H₂O + 50µl 1M Tris-cl pH 8.2 + 10µl 0.5M EDTA + 25µl 5M NaCl + 25µl 20mg/ml Proteinase K.

References

- Abbott, M. K., and Lengyel, J. A. (1991). Embryonic head involution and rotation of male terminalia require the drosophila locus head involution defective. *Genetics* 129, 783–789. doi:10.1093/genetics/129.3.783.
- Abrams, J. M. (1999). An emerging blueprint for apoptosis in Drosophila. *Trends Cell Biol.* 9, 435–440. doi:10.1016/S0962-8924(99)01646-3.
- Abrams, J. M., White, K., Fessler, L. I., and Steller, H. (1993). Programmed cell death during Drosophila embryogenesis. *Development* 117, 29–43. doi:10.1242/dev.117.1.29.
- Adrain, C., and Freeman, M. (2014). Regulation of receptor tyrosine kinase ligand processing. *Cold Spring Harb. Perspect. Biol.* 6, 1–18. doi:10.1101/cshperspect.a008995.
- Amos, B., McConnell, G., and Wilson, T. (2012). “2.2 Confocal Microscopy,” in *Comprehensive Biophysics* (Elsevier), 3–23. doi:10.1016/B978-0-12-374920-8.00203-4.
- Amstad, P. A., Yu, G., Johnson, G. L., Lee, B. W., Dhawan, S., and Phelps, D. J. (2001). Detection of caspase activation in situ by fluorochrome-labeled caspase inhibitors. *Biotechniques* 31, 608–616. doi:10.2144/01313pf01.
- Andrew, D. J., Henderson, K. D., and Seshiah, P. (2000). Salivary gland development in Drosophila melanogaster. *Mech. Dev.* 92, 5–17. doi:10.1016/S0925-4773(99)00321-4.
- Anson, F., Kanjilal, P., Thayumanavan, S., and Hardy, J. A. (2021). Tracking exogenous intracellular casp-3 using split GFP. *Protein Sci.* 30, 366–380. doi:10.1002/pro.3992.
- Aplin, A. C., and Kaufman, T. C. (1997). Homeotic transformation of legs to mouthparts by proboscipedia expression in Drosophila imaginal discs. *Mech. Dev.* 62, 51–60. doi:10.1016/S0925-4773(96)00649-1.
- Arama, E., and Steller, H. (2006). Detection of apoptosis by terminal deoxynucleotidyl transferase-mediated dUTP nick-end labeling and acridine orange in Drosophila embryos and adult male gonads. *Nat. Protoc.* 1, 1725–1731. doi:10.1038/nprot.2006.235.
- Arandjelovic, S., and Ravichandran, K. S. (2015). Phagocytosis of apoptotic cells in homeostasis. *Nat. Immunol.* 16, 907–917. doi:10.1038/ni.3253.
- Ariel, A., and Ravichandran, K. S. (2016). “This way please”: Apoptotic cells regulate phagocyte migration before and after engulfment. *Eur. J. Immunol.* 46, 1583–1586. doi:10.1002/eji.201646505.
- Armitage, E. L., Roddie, H. G., and Evans, I. R. (2020). Overexposure to apoptosis via disrupted

- glial specification perturbs *Drosophila* macrophage function and reveals roles of the CNS during injury. *Cell Death Dis.* 11. doi:10.1038/s41419-020-02875-2.
- Atkin-Smith, G. K., and Poon, I. K. H. (2017). Disassembly of the Dying: Mechanisms and Functions. *Trends Cell Biol.* 27, 151–162. doi:10.1016/j.tcb.2016.08.011.
- Audran, R., Lesimple, T., Delamaire, M., Picot, C., Van Damme, J., and Toujas, L. (1996). Adhesion molecule expression and response to chemotactic agents of human monocyte-derived macrophages. *Clin. Exp. Immunol.* 103, 155–160. doi:10.1046/j.1365-2249.1996.d01-4.x.
- Azpiazu, N., and Frasch, M. (1993). Tinman and bagpipe: Two homeo box genes that determine cell fates in the dorsal mesoderm of *Drosophila*. *Genes Dev.* 7, 1325–1340. doi:10.1101/gad.7.7b.1325.
- Baena-Lopez, L. A., Arthurton, L., Bischoff, M., Vincent, J. P., Alexandre, C., and McGregor, R. (2018). Novel initiator caspase reporters uncover previously unknown features of caspase-activating cells. *Dev.* 145. doi:10.1242/dev.170811.
- Baeyens, A. A. L., and Schwab, S. R. (2020). Finding a Way Out: S1P Signaling and Immune Cell Migration. *Annu. Rev. Immunol.* 38, 759–784. doi:10.1146/annurev-immunol-081519-083952.
- Bagher, A. M., Laprairie, R. B., Kelly, M. E. M., and Denovan-Wright, E. M. (2018). *Methods to Quantify Cell Signaling and GPCR Receptor Ligand Bias: Characterization of Drugs that Target the Endocannabinoid Receptors in Huntington's Disease.* , eds. S. V. Precious, A. E. Rosser, and S. B. Dunnett New York, NY: Springer New York doi:10.1007/978-1-4939-7825-0.
- Baidžajevs, K., Hadadi, É., Lee, B., Lum, J., Shihui, F., Sudbery, I., et al. (2020). Macrophage polarisation associated with atherosclerosis differentially affects their capacity to handle lipids. *Atherosclerosis* 305, 10–18. doi:10.1016/j.atherosclerosis.2020.05.003.
- Bao, Q., and Shi, Y. (2007). Apoptosome: A platform for the activation of initiator caspases. *Cell Death Differ.* 14, 56–65. doi:10.1038/sj.cdd.4402028.
- Barbero, S., Barilà, D., Mielgo, A., Stagni, V., Clair, K., and Stupack, D. (2008). Identification of a critical tyrosine residue in caspase 8 that promotes cell migration. *J. Biol. Chem.* 283, 13031–13034. doi:10.1074/jbc.M800549200.
- Bardet, P.-L., Kolahgar, G., Mynett, A., Miguel-Aliaga, I., Briscoe, J., Meier, P., et al. (2008). A fluorescent reporter of caspase activity for live imaging. *Proc. Natl. Acad. Sci.* 105,

- 13901–13905. doi:10.1073/pnas.0806983105.
- Barolo, S., Castro, B., and Posakony, J. W. (2004). New Drosophila transgenic reporters: Insulated P-element vectors expressing fast-maturing RFP. *Biotechniques* 36, 436–442. doi:10.2144/04363st03.
- Bauer, R., Breitwieser, L., Di Meglio, A., Johard, L., Kaiser, M., Manca, M., et al. (2016). The BioDynaMo Project. Available at: <http://arxiv.org/abs/1607.02717>.
- Behrendorf, H. A., Van De Craen, M., Knies, U. E., Vandenabeele, P., and Clauss, M. (2000). The endothelial monocyte-activating polypeptide II (EMAP II) is a substrate for caspase-7. *FEBS Lett.* 466, 143–147. doi:10.1016/S0014-5793(99)01777-9.
- Benoit, M., Desnues, B., and Mege, J.-L. (2008). Macrophage Polarization in Bacterial Infections. *J. Immunol.* 181, 3733–3739. doi:10.4049/jimmunol.181.6.3733.
- Berlin, S., and Carroll, E. C. (2020). Editorial: Next-Generation Genetically-Encoded Fluorescent Sensors. *Front. Cell. Neurosci.* 14, 1–2. doi:10.3389/fncel.2020.627792.
- Bernardoni, R., Vivancos, V., and Giangrande, A. (1997). Glide/Gcm Is Expressed and Required in the Scavenger Cell Lineage. *Dev. Biol.* 191, 118–130. doi:10.1006/dbio.1997.8702.
- Berthelet, J., and Dubrez, L. (2013). Regulation of Apoptosis by Inhibitors of Apoptosis (IAPs). *Cells* 2, 163–187. doi:10.3390/cells2010163.
- Bianchi, S. M., Prince, L. R., McPhillips, K., Allen, L., Marriott, H. M., Taylor, G. W., et al. (2008). Impairment of apoptotic cell engulfment by pyocyanin, a toxic metabolite of *Pseudomonas aeruginosa*. *Am. J. Respir. Crit. Care Med.* 177, 35–43. doi:10.1164/rccm.200612-1804OC.
- Blankenberg, F. G., Katsikis, P. D., Tait, J. F., Davis, R. E., Naumovski, L., Ohtsuki, K., et al. (1998). In vivo detection and imaging of phosphatidylserine expression during programmed cell death. *Proc. Natl. Acad. Sci. U. S. A.* 95, 6349–6354. doi:10.1073/pnas.95.11.6349.
- Bodmer, R. (1993). The gene tinman is required for specification of the heart and visceral muscles in Drosophila. *Development* 118, 719–729.
- Bournazou, I., Pound, J. D., Duffin, R., Bournazos, S., Melville, L. A., Brown, S. B., et al. (2009). Apoptotic human cells inhibit migration of granulocytes via release of lactoferrin. *J. Clin. Invest.* 119, 20–32. doi:10.1172/JCI36226.
- Bours, M. J. L., Swennen, E. L. R., Di Virgilio, F., Cronstein, B. N., and Dagnelie, P. C. (2006). Adenosine 5'-triphosphate and adenosine as endogenous signaling molecules in

- immunity and inflammation. *Pharmacol. Ther.* 112, 358–404.
doi:10.1016/j.pharmthera.2005.04.013.
- Boyden, S. (1962). THE CHEMOTACTIC EFFECT OF MIXTURES OF ANTIBODY AND ANTIGEN ON POLYMORPHONUCLEAR LEUCOCYTES. *J. Exp. Med.* 115, 453–466.
doi:10.1084/jem.115.3.453.
- Brambilla, E., Robert, C., Lorimier, P., Negoescu, A., Guillermet, C., Drouet, C., et al. (1996). In situ apoptotic cell labeling by the TUNEL method: improvement and evaluation on cell preparations. *J. Histochem. Cytochem.* 44, 959–968. doi:10.1177/44.9.8773561.
- Breitwieser, L., Bauer, R., Di Meglio, A., Johard, L., Kaiser, M., Manca, M., et al. (2016). The BioDynaMo project: Creating a platform for large-scale reproducible biological simulations. *CEUR Workshop Proc.* 1686.
- Brown, K. E., Kerr, M., and Freeman, M. (2007). The EGFR ligands Spitz and Keren act cooperatively in the Drosophila eye. *Dev. Biol.* 307, 105–113.
doi:10.1016/j.ydbio.2007.04.025.
- Brückner, K., Kockel, L., Duchek, P., Luque, C. M., Rørth, P., and Perrimon, N. (2004). The PDGF/VEGF receptor controls blood cell survival in Drosophila. *Dev. Cell* 7, 73–84.
doi:10.1016/j.devcel.2004.06.007.
- Buchon, N., Silverman, N., and Cherry, S. (2014). Immunity in Drosophila melanogaster - from microbial recognition to whole-organism physiology. *Nat. Rev. Immunol.* 14, 796–810.
doi:10.1038/nri3763.
- Buff, E., Carmena, A., Gisselbrecht, S., Jiménez, F., and Michelson, A. M. (1998). Signalling by the Drosophila epidermal growth factor receptor is required for the specification and diversification of embryonic muscle progenitors. *Development* 125, 2075–2086.
- Burgess, A. W., Cho, H.-S., Eigenbrot, C., Ferguson, K. M., Garrett, T. P. J., Leahy, D. J., et al. (2003). An open-and-shut case? Recent insights into the activation of EGF/ErbB receptors. *Mol. Cell* 12, 541–52. Available at:
<http://www.ncbi.nlm.nih.gov/pubmed/14527402>.
- Bushell, M., Stoneley, M., Kong, Y. W., Hamilton, T. L., Spriggs, K. A., Dobbyn, H. C., et al. (2006). Polypyrimidine Tract Binding Protein Regulates IRES-Mediated Gene Expression during Apoptosis. *Mol. Cell* 23, 401–412. doi:10.1016/j.molcel.2006.06.012.
- Cai, B., Thorp, E. B., Doran, A. C., Sansbury, B. E., Daemen, M. J. A. P., Dorweiler, B., et al. (2017). MerTK receptor cleavage promotes plaque necrosis and defective resolution in

- atherosclerosis. *J. Clin. Invest.* 127, 564–568. doi:10.1172/JCI90520.
- Cairns, A. P., Crockard, A. D., McConnell, J. R., Courtney, P. A., and Bell, A. L. (2001). Reduced expression of CD44 on monocytes and neutrophils in systemic lupus erythematosus: relations with apoptotic neutrophils and disease activity. *Ann. Rheum. Dis.* 60, 950–5. doi:10.1136/ard.60.10.950.
- Cannon, G. J., and Swanson, J. A. (1992). The macrophage capacity for phagocytosis. *J. Cell Sci.* 101, 907–913. doi:10.1242/jcs.101.4.907.
- Cara, D. C., Kaur, J., Forster, M., McCafferty, D.-M., and Kubes, P. (2001). Role of p38 Mitogen-Activated Protein Kinase in Chemokine-Induced Emigration and Chemotaxis In Vivo. *J. Immunol.* 167, 6552–6558. doi:10.4049/jimmunol.167.11.6552.
- Caruso, S., and Poon, I. K. H. (2018). Apoptotic cell-derived extracellular vesicles: More than just debris. *Front. Immunol.* 9. doi:10.3389/fimmu.2018.01486.
- Casas-Tintó, S., Lolo, F. N., and Moreno, E. (2015). Active JNK-dependent secretion of Drosophila Tyrosyl-tRNA synthetase by loser cells recruits haemocytes during cell competition. *Nat. Commun.* 6, 1–12. doi:10.1038/ncomms10022.
- Cattenoz, P. B., Sakr, R., Pavlidaki, A., Delaporte, C., Riba, A., Molina, N., et al. (2020). Temporal specificity and heterogeneity of Drosophila immune cells. *EMBO J.* 39, 1–25. doi:10.15252/embj.2020104486.
- Cerenius, L., Lee, B. L., and Söderhäll, K. (2008). The proPO-system: pros and cons for its role in invertebrate immunity. *Trends Immunol.* 29, 263–271. doi:10.1016/j.it.2008.02.009.
- Chalaris, A., Rabe, B., Paliga, K., Lange, H., Laskay, T., Fielding, C. A., et al. (2007). Apoptosis is a natural stimulus of IL6R shedding and contributes to the proinflammatory trans-signaling function of neutrophils. *Blood* 110, 1748–1755. doi:10.1182/blood-2007-01-067918.
- Champion, J. A., and Mitragotri, S. (2006). Role of target geometry in phagocytosis. *Proc. Natl. Acad. Sci. U. S. A.* 103, 4930–4934. doi:10.1073/pnas.0600997103.
- Chandrasekaran, V., and Beckendorf, S. K. (2003). Senseless is necessary for the survival of embryonic salivary glands in Drosophila. *Development* 130, 4719–4728. doi:10.1242/dev.00677.
- Chekeni, F. B., Elliott, M. R., Sandilos, J. K., Walk, S. F., Kinchen, M., Lazarowski, E. R., et al. (2011). Pannexin 1 channels mediate ‘find-me’ signal release and membrane permeability during apoptosis. 467, 863–867. doi:10.1038/nature09413.Pannexin.

- Chen, L., Iijima, M., Tang, M., Landree, M. A., Huang, Y. E., Xiong, Y., et al. (2007). PLA2 and PI3K/PTEN Pathways Act in Parallel to Mediate Chemotaxis. *Dev. Cell* 12, 603–614. doi:10.1016/j.devcel.2007.03.005.
- Chen, S., So, E. C., Strome, S. E., and Zhang, X. (2015). Impact of Detachment Methods on M2 Macrophage Phenotype and Function. *J. Immunol. Methods* 426, 56–61. doi:10.1016/j.jim.2015.08.001.
- Chimini, G., and Chavrier, P. (2000). Function of Rho family proteins in actin dynamics during phagocytosis and engulfment. *Nat. Cell Biol.* 2, E191–6.
- Cho, B., Yoon, S. H., Lee, D., Koranteng, F., Tattikota, S. G., Cha, N., et al. (2020). Single-cell transcriptome maps of myeloid blood cell lineages in *Drosophila*. *Nat. Commun.* 11. doi:10.1038/s41467-020-18135-y.
- Cho, N. K., Keyes, L., Johnson, E., Heller, J., Ryner, L., Karim, F., et al. (2002). Developmental control of blood cell migration by the *Drosophila* VEGF pathway. *Cell* 108, 865–76. doi:S0092867402006761 [pii].
- Choesmel, V., Bacqueville, D., Rouquette, J., Noaillac-Depeyre, J., Fribourg, S., Crétien, A., et al. (2007). Impaired ribosome biogenesis in Diamond-Blackfan anemia. *Blood* 109, 1275–1283. doi:10.1182/blood-2006-07-038372.
- Citri, A., and Yarden, Y. (2006). EGF-ERBB signalling: Towards the systems level. *Nat. Rev. Mol. Cell Biol.* 7, 505–516. doi:10.1038/nrm1962.
- Clemens, M. J., Bushell, M., Jeffrey, I. W., Pain, V. M., and Morley, S. J. (2000). Translation initiation factor modifications and the regulation of protein synthesis in apoptotic cells. *Cell Death Differ.* 7, 603–615. doi:10.1038/sj.cdd.4400695.
- Coates, J. A., Brooks, E., Brittle, A. L., Armitage, E. L., Zeidler, M. P., and Evans, I. R. (2021). Identification of functionally distinct macrophage subpopulations in *Drosophila*. *Elife* 10, 1–39. doi:10.7554/ELIFE.58686.
- Coleman, M. L., Sahai, E. A., Yeo, M., Bosch, M., Dewar, A., and Olson, M. F. (2001). Membrane blebbing during apoptosis results from caspase-mediated activation of ROCK I. *Nat. Cell Biol.* 3, 339–45. doi:10.1038/35070009.
- Covarrubias, A. J., Aksoylar, H. I., and Horng, T. (2015). Efferocytosis as a regulator of macrophage chemokine receptor expression and polarization. 27, 286–296. doi:10.1016/j.smim.2015.08.001.Control.
- Crozatier, M., and Meister, M. (2007). *Drosophila* haematopoiesis. *Cell. Microbiol.* 9, 1117–

1126. doi:10.1111/j.1462-5822.2007.00930.x.

Czabotar, P. E., Lessene, G., Strasser, A., and Adams, J. M. (2014). Control of apoptosis by the BCL-2 protein family: implications for physiology and therapy. *Nat. Rev. Mol. Cell Biol.* 15, 49–63. doi:10.1038/nrm3722.

Daigneault, M., Preston, J. A., Marriott, H. M., Whyte, M. K. B., and Dockrell, D. H. (2010). The identification of markers of macrophage differentiation in PMA-stimulated THP-1 cells and monocyte-derived macrophages. *PLoS One* 5. doi:10.1371/journal.pone.0008668.

Davalos, D., Grutzendler, J., Yang, G., Kim, J. V, Zuo, Y., Jung, S., et al. (2005). ATP mediates rapid microglial response to local brain injury in vivo. *Nat. Neurosci.* 8, 752–758. doi:10.1038/nn1472.

Davis, J. R., Huang, C. Y., Zanet, J., Harrison, S., Rosten, E., Cox, S., et al. (2012). Emergence of embryonic pattern through contact inhibition of locomotion. *Dev.* 139, 4555–4560. doi:10.1242/dev.082248.

Davis, R. (2003). P{tubP-GAL80[ts]} construct and insertions.

Degterev, A., and Yuan, J. (2008). Expansion and evolution of cell death programmes. *Nat. Rev. Mol. Cell Biol.* 9, 378–390. doi:10.1038/nrm2393.

Dehle, F. C., Mukaro, V. R., Jurisevic, C., Moffat, D., Ahern, J., Hodge, G., et al. (2013). Defective Lung Macrophage Function in Lung Cancer±Chronic Obstructive Pulmonary Disease (COPD/Emphysema)-Mediated by Cancer Cell Production of PGE2? *PLoS One* 8, 1–6. doi:10.1371/journal.pone.0061573.

Donaldson, T., Wang, S. H., Jacobsen, T. L., Schnepf, B., Price, J., and Simcox, A. (2004). Regulation of the Drosophila epidermal growth factor-ligand vein is mediated by multiple domains. *Genetics* 167, 687–698. doi:10.1534/genetics.103.019588.

Doran, A. C., Ozcan, L., Cai, B., Zheng, Z., Fredman, G., Rymond, C. C., et al. (2017). CAMKII γ suppresses an efferocytosis pathway in macrophages and promotes atherosclerotic plaque necrosis. *J. Clin. Invest.*, 1–15. doi:10.1172/JCI94735.

Dou, Y., Wu, H. J., Li, H. Q., Qin, S., Wang, Y. E., Li, J., et al. (2012). Microglial migration mediated by ATP-induced ATP release from lysosomes. *Cell Res.* 22, 1022–1033. doi:10.1038/cr.2012.10.

Duchek, P., and Rørth, P. (2001). Guidance of cell migration by EGF receptor signaling during Drosophila oogenesis. *Science (80-)*. 291, 131–3. doi:10.1126/science.291.5501.131.

Duchek, P., Somogyi, K., Jékely, G., Beccari, S., and Rorth, P. (2001). Guidance of cell

- migration by the Drosophila PDGF/VEGF receptor. *Cell* 107, 17–26. doi:10.1016/S0092-8674(01)00502-5.
- Dutta, D., Bloor, J. W., Ruiz-Gomez, M., VijayRaghavan, K., and Kiehart, D. P. (2002). Real-time imaging of morphogenetic movements in Drosophila using Gal4-UAS-driven expression of GFP fused to the actin-binding domain of moesin. *genesis* 34, 146–151. doi:10.1002/gene.10113.
- Dzeja, P. P., and Terzic, A. (2003). Phosphotransfer networks and cellular energetics. *J. Exp. Biol.* 206, 2039–2047. doi:10.1242/jeb.00426.
- Eligini, S., Cosentino, N., Fiorelli, S., Fabbicchi, F., Niccoli, G., Refaat, H., et al. (2019). Biological profile of monocyte-derived macrophages in coronary heart disease patients: implications for plaque morphology. *Sci. Rep.* 9, 1–14. doi:10.1038/s41598-019-44847-3.
- Elliott, M. R., Chekeni, F. B., Trampont, P. C., Lazarowski, E. R., Kadl, A., Walk, S. F., et al. (2009). Nucleotides released by apoptotic cells act as a find-me signal to promote phagocytic clearance. *Nature* 461, 282–286. Available at: <http://dx.doi.org/10.1038/nature08296>.
- Elliott, M. R., Chekeni, F. B., Trampont, P. C., Lazarowski, E. R., Kadl, A., Walk, S. F., et al. (2010). Nucleotides released by apoptotic cells act as a find-me signal to promote phagocytic clearance. *Nature* 461, 282–286. doi:10.1038/nature08296.
- Elmore, S. (2007). Apoptosis: A Review of Programmed Cell Death. *Toxicol. Pathol.* 35, 495–516. doi:10.1080/01926230701320337.
- Eltboli, O., Bafadhel, M., Hollins, F., Wright, A., Hargadon, B., Kulkarni, N., et al. (2014). COPD exacerbation severity and frequency is associated with impaired macrophage efferocytosis of eosinophils. *BMC Pulm. Med.* 14, 112. doi:10.1186/1471-2466-14-112.
- Elward, K., and Gasque, P. (2003). “Eat me” and “don’t eat me” signals govern the innate immune response and tissue repair in the CNS: Emphasis on the critical role of the complement system. *Mol. Immunol.* 40, 85–94. doi:10.1016/S0161-5890(03)00109-3.
- Epelman, S., Lavine, K. J., and Randolph, G. J. (2014). Origin and Functions of Tissue Macrophages. *Immunity* 41, 21–35. doi:10.1016/j.immuni.2014.06.013.
- Evans, C. J., Hartenstein, V., and Banerjee, U. (2003). Thicker than blood: Conserved mechanisms in Drosophila and vertebrate hematopoiesis. *Dev. Cell.* doi:10.1016/S1534-5807(03)00335-6.

- Evans, I., Ghai, P., Urbancic, V., Tan, K., and Wood, W. (2013). SCAR/WAVE mediated processing of apoptotic corpses is essential for effective macrophage migration in *Drosophila*. *Cell Death Differ.*, 709–720. doi:10.1038/cdd.2012.166.
- Evans, I. R., Hu, N., Skaer, H., and Wood, W. (2010a). Interdependence of macrophage migration and ventral nerve cord development in *Drosophila* embryos. *Development* 137, 1625–33. doi:10.1242/dev.046797.
- Evans, I. R., Rodrigues, F. S. L. M., Armitage, E. L., and Wood, W. (2015). Draper/CED-1 Mediates an Ancient Damage Response to Control Inflammatory Blood Cell Migration In Vivo. *Curr. Biol.* 25, 1606–1612. doi:10.1016/j.cub.2015.04.037.
- Evans, I. R., and Wood, W. (2011). *Drosophila* embryonic hemocytes. *Curr. Biol.* 21, R173–R174. doi:10.1016/j.cub.2011.01.061.
- Evans, I. R., and Wood, W. (2014). *Drosophila* blood cell chemotaxis. *Curr. Opin. Cell Biol.* 30, 1–8. doi:10.1016/j.ceb.2014.04.002.
- Evans, I. R., Zanet, J., Wood, W., and Stramer, B. M. (2010b). Live Imaging Of *Drosophila melanogaster* Embryonic Hemocyte Migrations. *J. Vis. Exp.* 700, 2–6. doi:10.3791/1696.
- Fan, Y., Wang, S., Hernandez, J., Yenigun, V. B., Hertlein, G., Fogarty, C. E., et al. (2014). Genetic Models of Apoptosis-Induced Proliferation Decipher Activation of JNK and Identify a Requirement of EGFR Signaling for Tissue Regenerative Responses in *Drosophila*. *PLoS Genet.* 10. doi:10.1371/journal.pgen.1004131.
- Fernandez-Gonzalez, R., and Zallen, J. A. (2013). Wounded cells drive rapid epidermal repair in the early *Drosophila* embryo. *Mol. Biol. Cell* 24, 3227–3237. doi:10.1091/mbc.E13-05-0228.
- Fésüs, L., and Szondy, Z. (2005). Transglutaminase 2 in the balance of cell death and survival. *FEBS Lett.* 579, 3297–3302. doi:10.1016/j.febslet.2005.03.063.
- Filip, A. M., Klug, J., Cayli, S., Fröhlich, S., Henke, T., Lacher, P., et al. (2009). Ribosomal protein S19 interacts with macrophage migration inhibitory factor and attenuates its pro-inflammatory function. *J. Biol. Chem.* 284, 7977–7985. doi:10.1074/jbc.M808620200.
- Florentin, A., and Arama, E. (2012). Caspase levels and execution efficiencies determine the apoptotic potential of the cell. *J. Cell Biol.* 196, 513–527. doi:10.1083/jcb.201107133.
- Fogarty, C. E., and Bergmann, A. (2017). Killers creating new life: caspases drive apoptosis-induced proliferation in tissue repair and disease. *Cell Death Differ.* 24, 1390–1400.

doi:10.1038/cdd.2017.47.

Foks, A. C., Engelbertsen, D., Kuperwaser, F., Alberts-Grill, N., Gonen, A., Witztum, J. L., et al. (2016). Blockade of Tim-1 and Tim-4 enhances atherosclerosis in low-density lipoprotein receptor-deficient mice. *Arterioscler. Thromb. Vasc. Biol.* 36, 456–465.

doi:10.1161/ATVBAHA.115.306860.

Foxman, E. F., Campbell, J. J., and Butcher, E. C. (1997). Multistep navigation and the combinatorial control of leukocyte chemotaxis. *J. Cell Biol.* 139, 1349–1360.

doi:10.1083/jcb.139.5.1349.

Franc, N. C., Dimarcq, J. L., Lagueux, M., Hoffmann, J., and Ezekowitz, R. A. B. (1996). Croquemort, a novel drosophila hemocyte/macrophage receptor that recognizes apoptotic cells. *Immunity* 4, 431–443. doi:10.1016/S1074-7613(00)80410-0.

Fransen, J. H., Hilbrands, L. B., Ruben, J., Stoffels, M., Adema, G. J., Van Der Vlag, J., et al. (2009). Mouse dendritic cells matured by ingestion of apoptotic blebs induce T cells to produce interleukin-17. *Arthritis Rheum.* 60, 2304–2313. doi:10.1002/art.24719.

Freeman, M. (1996). Reiterative use of the EGF receptor triggers differentiation of all cell types in the *Drosophila* eye. *Cell* 87, 651–660. doi:10.1016/S0092-8674(00)81385-9.

Friedl, P. (2004). Preshaping and plasticity: Shifting mechanisms of cell migration. *Curr. Opin. Cell Biol.* 16, 14–23. doi:10.1016/j.ceb.2003.11.001.

Frise, E., Hammonds, A. S., and Celniker, S. E. (2010). Systematic image-driven analysis of the spatial *Drosophila* embryonic expression landscape. *Mol. Syst. Biol.* 6, 1–15.

doi:10.1038/msb.2009.102.

Frodermann, V., van Puijvelde, G. H. M., Wierds, L., Lagrauw, H. M., Foks, A. C., van Santbrink, P. J., et al. (2015). Oxidized Low-Density Lipoprotein–Induced Apoptotic Dendritic Cells as a Novel Therapy for Atherosclerosis. *J. Immunol.* 194, 2208–2218.

doi:10.4049/jimmunol.1401843.

Fuchs, Y., and Steller, H. (2011). Programmed cell death in animal development and disease. *Cell* 147, 742–758. doi:10.1016/j.cell.2011.10.033.

Gaipl, U. S., Munoz, L. E., Grossmayer, G., Lauber, K., Franz, S., Sarter, K., et al. (2007). Clearance deficiency and systemic lupus erythematosus (SLE). *J. Autoimmun.* 28, 114–121. doi:10.1016/j.jaut.2007.02.005.

Galindo, K. A., Lu, W. J., Park, J. H., and Abrams, J. M. (2009). The Bax/Bak ortholog in *Drosophila*, Debcl, exerts limited control over programmed cell death. *Development* 136,

275–283. doi:10.1242/dev.019042.

- Galluzzi, L., Vitale, I., Abrams, J. M., Alnemri, E. S., Baehrecke, E. H., Blagosklonny, M. V., et al. (2012). Molecular definitions of cell death subroutines: recommendations of the Nomenclature Committee on Cell Death 2012. *Cell Death Differ.* 19, 107–120. doi:10.1038/cdd.2011.96.
- Garton, K. J., Gough, P. J., Blobel, C. P., Murphy, G., Greaves, D. R., Dempsey, P. J., et al. (2001). Tumor Necrosis Factor- α -converting Enzyme (ADAM17) Mediates the Cleavage and Shedding of Fractalkine (CX3CL1). *J. Biol. Chem.* 276, 37993–38001. doi:10.1074/jbc.m106434200.
- Gdynia, G., Grund, K., Eckert, A., Böck, B. C., Funke, B., Macher-Goeppinger, S., et al. (2007). Basal caspase activity promotes migration and invasiveness in glioblastoma cells. *Mol. Cancer Res.* 5, 1232–1240. doi:10.1158/1541-7786.MCR-07-0343.
- Gevrey, J.-C., Isaac, B. M., and Cox, D. (2005). Syk is required for monocyte/macrophage chemotaxis to CX3CL1 (Fractalkine). *J. Immunol.* 175, 3737–45. doi:10.4049/jimmunol.175.6.3737.
- Ghiglione, C., Bach, E. A., Paraiso, Y., Carraway, K. L., Noselli, S., and Perrimon, N. (2002). Mechanism of activation of the Drosophila EGF Receptor by the TGF α ligand Gurken during oogenesis. *Development* 129, 175–86. Available at: <http://www.ncbi.nlm.nih.gov/pubmed/11782411>.
- Goldschneider, D., and Mehlen, P. (2010). Dependence receptors: A new paradigm in cell signaling and cancer therapy. *Oncogene* 29, 1865–1882. doi:10.1038/onc.2010.13.
- Golembo, M., Raz, E., and Shilo, B. Z. (1996). The Drosophila embryonic midline is the site of Spitz processing, and induces activation of the EGF receptor in the ventral ectoderm. *Development* 122, 3363–3370.
- Gordon, S. (2002). Pattern recognition receptors: Doubling up for the innate immune response. *Cell* 111, 927–930. doi:10.1016/S0092-8674(02)01201-1.
- Gordon, S., and Martinez, F. O. (2010). Alternative activation of macrophages: Mechanism and functions. *Immunity* 32, 593–604. doi:10.1016/j.immuni.2010.05.007.
- Gramates, L. S., Marygold, S. J., Dos Santos, G., Urbano, J. M., Antonazzo, G., Matthews, B. B., et al. (2017). FlyBase at 25: Looking to the future. *Nucleic Acids Res.* 45, D663–D671. doi:10.1093/nar/gkw1016.
- Green, D. R., and Llambi, F. (2015). Cell Death Signaling. *Cold Spring Harb. Perspect. Biol.* 7,

a006080. doi:10.1101/cshperspect.a006080.

- Grether, M. E., Abrams, J. M., and Agapite, J. (1995). The head involution defective gene of *Drosophila melanogaster* functions in programmed cell death. *Genes Dev.* 9, 1694–1708. doi:10.1101/gad.9.14.1694.
- Griffith, J. W., Sokol, C. L., and Luster, A. D. (2014). Chemokines and chemokine receptors: Positioning cells for host defense and immunity. *Annu. Rev. Immunol.* 32, 659–702. doi:10.1146/annurev-immunol-032713-120145.
- Grimshaw, M. J., and Balkwill, F. R. (2001). Inhibition of monocyte and macrophage chemotaxis by hypoxia and inflammation - A potential mechanism. *Eur. J. Immunol.* 31, 480–489. doi:10.1002/1521-4141(200102)31:2<480::AID-IMMU480>3.0.CO;2-L.
- Guardiola-Serrano, F., Rossin, A., Cahuzac, N., Lücknerath, K., Melzer, I., Mailfert, S., et al. (2010). Palmitoylation of human FasL modulates its cell death-inducing function. *Cell Death Dis.* 1, e88–e88. doi:10.1038/cddis.2010.62.
- Gude, D. R., Alvarez, S. E., Paugh, S. W., Mitra, P., Yu, J., Griffiths, R., et al. (2008). Apoptosis induces expression of sphingosine kinase 1 to release sphingosine-1-phosphate as a “come-and-get-me” signal. *FASEB J.* 22, 2629–2638. doi:10.1096/fj.08-107169.
- Gyoergy, A., Roblek, M., Ratheesh, A., Valoskova, K., Belyaeva, V., Wachner, S., et al. (2018). Tools Allowing Independent Visualization and Genetic Manipulation of *Drosophila melanogaster* Macrophages and Surrounding Tissues. *G3 & Genes/Genomes/Genetics* 8, g3.300452.2017. doi:10.1534/g3.117.300452.
- Halder, G., Callaerts, P., Flister, S., Walldorf, U., Kloter, U., and Gehring, W. J. (1998). Eyeless initiates the expression of both sine oculis and eyes absent during *Drosophila* compound eye development. *Development* 125, 2181–91. Available at: <http://www.ncbi.nlm.nih.gov/pubmed/9584118>.
- Hall, P. a, Coates, P. J., Ansari, B., and Hopwood, D. (1994). Regulation of cell number in the mammalian gastrointestinal tract: the importance of apoptosis. *J. Cell Sci.* 107 (Pt 1, 3569–3577. doi:10.1002/path.1711670106.
- Hamon, R., Homan, C. C., Tran, H. B., Mukaro, V. R., Lester, S. E., Roscioli, E., et al. (2014). Zinc and zinc transporters in macrophages and their roles in efferocytosis in COPD. *PLoS One* 9, 1–9. doi:10.1371/journal.pone.0110056.
- Han, C., Song, Y., Xiao, H., Wang, D., Franc, N. C., Jan, L. Y., et al. (2014). Epidermal Cells Are the Primary Phagocytes in the Fragmentation and Clearance of Degenerating Dendrites

- in *Drosophila*. *Neuron* 81, 544–560. doi:10.1016/j.neuron.2013.11.021.
- Hanahan, D., and Weinberg, R. A. (2011). Hallmarks of cancer: The next generation. *Cell* 144, 646–674. doi:10.1016/j.cell.2011.02.013.
- Hanson, M. A., and Lemaitre, B. (2020). New insights on *Drosophila* antimicrobial peptide function in host defense and beyond. *Curr. Opin. Immunol.* 62, 22–30. doi:10.1016/j.coi.2019.11.008.
- Hatan, M., Shinder, V., Israeli, D., Schnorrer, F., and Volk, T. (2011). The *Drosophila* blood brain barrier is maintained by GPCR-dependent dynamic actin structures. *J. Cell Biol.* 192, 307–319. doi:10.1083/jcb.201007095.
- Hayes, P., and Solon, J. (2017). *Drosophila* dorsal closure: An orchestra of forces to zip shut the embryo. *Mech. Dev.* 144, 2–10. doi:10.1016/j.mod.2016.12.005.
- Hazelett, D. J., Bourouis, M., Walldorf, U., and Treisman, J. E. (1998). Decapentaplegic and Wingless Are Regulated By Eyes Absent and Eyegone and Interact To Direct the Pattern of Retinal Differentiation in the Eye Disc. *Development* 125, 3741–3751. doi:10.1242/dev.125.18.3741.
- Heino, T. I., Kärpänen, T., Wahlström, G., Pulkkinen, M., Eriksson, U., Alitalo, K., et al. (2001). The *Drosophila* VEGF receptor homolog is expressed in hemocytes. *Mech. Dev.* 109, 69–77. doi:10.1016/S0925-4773(01)00510-X.
- Heit, B., Robbins, S. M., Downey, C. M., Guan, Z., Colarusso, P., Miller, J. B., et al. (2008). PTEN functions to “prioritize” chemotactic cues and prevent “distraction” in migrating neutrophils. *Nat. Immunol.* 9, 743–752. doi:10.1038/ni.1623.
- Heit, B., Tavener, S., Raharjo, E., and Kubes, P. (2002). An intracellular signaling hierarchy determines direction of migration in opposing chemotactic gradients. *J. Cell Biol.* 159, 91–102. doi:10.1083/jcb.200202114.
- Henderson, K. D., and Andrew, D. J. (2000). Regulation and function of Scr, exd, and hth in the *Drosophila* salivary gland. *Dev. Biol.* 217, 362–374. doi:10.1006/dbio.1999.9560.
- Henson, E. S., and Gibson, S. B. (2006). Surviving cell death through epidermal growth factor (EGF) signal transduction pathways: Implications for cancer therapy. *Cell. Signal.* 18, 2089–2097. doi:10.1016/j.cellsig.2006.05.015.
- Herrmann, M., Voll, R. E., Zoller, O. M., Hagenhofer, M., Ponner, B. B., and Kalden, J. R. (1998). Impaired phagocytosis of apoptotic cell material by monocyte-derived macrophages from patients with systemic lupus erythematosus. *Arthritis Rheum.* 41,

- 1241–1250. doi:10.1002/1529-0131(199807)41:7<1241::AID-ART15>3.0.CO;2-H.
- Hiraizumi, Y. (1971). Spontaneous recombination in *Drosophila melanogaster* males. *Proc. Natl. Acad. Sci. U. S. A.* 68, 268–270. doi:10.1073/pnas.68.2.268.
- Holley, C. L., Olson, M. R., Colón-Ramos, D. A., and Kornbluth, S. (2002). Reaper eliminates IAP proteins through stimulated IAP degradation and generalized translational inhibition. *Nat. Cell Biol.* 4, 439–444. doi:10.1038/ncb798.
- Hou, Y., Plett, P. A., Ingram, D. A., Rajashekhar, G., Orschell, C. M., Yoder, M. C., et al. (2006). Endothelial-monocyte-activating polypeptide II induces migration of endothelial progenitor cells via the chemokine receptor CXCR3. *Exp. Hematol.* 34, 1125–1132. doi:10.1016/j.exphem.2006.05.021.
- Hsiao, H. M., Sapinoro, R. E., Thatcher, T. H., Croasdell, A., Levy, E. P., Fulton, R. A., et al. (2013). A Novel Anti-Inflammatory and Pro-Resolving Role for Resolvin D1 in Acute Cigarette Smoke-Induced Lung Inflammation. *PLoS One* 8. doi:10.1371/journal.pone.0058258.
- Hsiung, F., Griffis, E. R., Pickup, A., Powers, M. A., and Moses, K. (2001). Function of the *Drosophila* TGF- α homolog Spitz is controlled by Star and interacts directly with Star. *Mech. Dev.* 107, 13–23. doi:10.1016/S0925-4773(01)00432-4.
- Hui, K. P. Y., Lee, S. M. Y., Cheung, C., Ng, I. H. Y., Poon, L. L. M., Guan, Y., et al. (2009). Induction of Proinflammatory Cytokines in Primary Human Macrophages by Influenza A Virus (H5N1) Is Selectively Regulated by IFN Regulatory Factor 3 and p38 MAPK. *J. Immunol.* 182, 1088–1098. doi:10.4049/jimmunol.182.2.1088.
- Hunter, M. V., Willoughby, P. M., Bruce, A. E. E., and Fernandez-Gonzalez, R. (2018). Oxidative Stress Orchestrates Cell Polarity to Promote Embryonic Wound Healing. *Dev. Cell* 47, 377–387.e4. doi:10.1016/j.devcel.2018.10.013.
- Igaki, T. (2009). Correcting developmental errors by apoptosis: lessons from *Drosophila* JNK signaling. *Apoptosis* 14, 1021–1028. doi:10.1007/s10495-009-0361-7.
- Igaki, T., and Miura, M. (2004). Role of Bcl-2 family members in invertebrates. *Biochim. Biophys. Acta - Mol. Cell Res.* 1644, 73–81. doi:10.1016/j.bbamcr.2003.09.007.
- Igaki, T., and Miura, M. (2014). The *Drosophila* TNF ortholog Eiger: Emerging physiological roles and evolution of the TNF system. *Semin. Immunol.* 26, 267–274. doi:10.1016/j.smim.2014.05.003.
- Iglesias, P. A., and Devreotes, P. N. (2008). Navigating through models of chemotaxis. *Curr.*

- Opin. Cell Biol.* 20, 35–40. doi:10.1016/j.ceb.2007.11.011.
- Imai, T., Hieshima, K., Haskell, C., Baba, M., Nagira, M., Nishimura, M., et al. (1997). Identification and molecular characterization of fractalkine receptor CX3CR1, which mediates both leukocyte migration and adhesion. *Cell* 91, 521–530. doi:10.1016/S0092-8674(00)80438-9.
- Imamoto, N. (2000). Diversity in Nucleocytoplasmic Transport Pathways. *Cell Struct. Funct.* 25, 207–216. doi:10.1247/csf.25.207.
- Irimia, D., and Ellett, F. (2016). Big insights from small volumes: deciphering complex leukocyte behaviors using microfluidics. *J. Leukoc. Biol.* 100, 291–304. doi:10.1189/jlb.5ru0216-056r.
- Ito, K., Awano, W., Suzuki, K., Hiromi, Y., and Yamamoto, D. (1997). The Drosophila mushroom body is a quadruple structure of clonal units each of which contains a virtually identical set of neurones and glial cells. *Development* 124, 761–771. doi:10.1093/dev/124.12.761.
- Iyadurai, S. J. P., Robinson, J. T., Ma, L., He, Y., Mische, S., Li, M.-G., et al. (2008). Dynein and Star interact in EGFR signaling and ligand trafficking. *J. Cell Sci.* 121, 2643–2651. doi:10.1242/jcs.027144.
- Jakubzick, C. V., Randolph, G. J., and Henson, P. M. (2017). Monocyte differentiation and antigen-presenting functions. *Nat. Rev. Immunol.* 17, 349–362. doi:10.1038/nri.2017.28.
- Jenkins, V. K., Timmons, A. K., and McCall, K. (2013). Diversity of cell death pathways: Insight from the fly ovary. *Trends Cell Biol.* 23, 567–574. doi:10.1016/j.tcb.2013.07.005.
- Jin, M.-h., Sawamoto, K., Ito, M., and Okano, H. (2002). The Interaction between the Drosophila Secreted Protein Argos and the Epidermal Growth Factor Receptor Inhibits Dimerization of the Receptor and Binding of Secreted Spitz to the Receptor. *Mol. Cell Biol.* 22, 2098–2107. doi:10.1128/mcb.22.6.2098-2107.2002.
- Joller, N., Weber, S. S., and Oxenius, A. (2011). Antibody - Fc receptor interactions in protection against intracellular pathogens. *Eur. J. Immunol.* 41, 889–897. doi:10.1002/eji.201041340.
- Julien, O., and Wells, J. A. (2017). Caspases and their substrates. *Cell Death Differ.* 24, 1380–1389. doi:10.1038/cdd.2017.44.
- Kaoss, J., Ryan, J., Brett, G., Chen, J., Shen, H., Fan, Y., et al. (1992). Endothelial Monocyte-activating Polypeptide I1.
- Kaupilla, S., Maaty, W. S. A., Chen, P., Tomar, R. S., Eby, M. T., Chapo, J., et al. (2003). Eiger

- and its receptor, Wengen, comprise a TNF-like system in *Drosophila*. *Oncogene* 22, 4860–4867. doi:10.1038/sj.onc.1206715.
- Kayashima, Y., Makhanova, N., and Maeda, N. (2017). DBA/2J Haplotype on Distal Chromosome 2 Reduces Mertk Expression, Restricts Efferocytosis, and Increases Susceptibility to Atherosclerosis. *Arterioscler. Thromb. Vasc. Biol.* 37, e82–e91. doi:10.1161/ATVBAHA.117.309522.
- Kim, D., and Haynes, C. L. (2012). Neutrophil chemotaxis within a competing gradient of chemoattractants. *Anal. Chem.* 84, 6070–6078. doi:10.1021/ac3009548.
- Kim, K., Vallon-eberhard, A., Zigmond, E., Farache, J., Shezen, E., Shakhar, G., et al. (2011). In vivo structure / function and expression analysis of the CX3C chemokine fractalkine. *Blood* 118, 156–167. doi:10.1182/blood-2011-04-348946.This.
- Kim, S. J., Gershov, D., Ma, X., Brot, N., and Elkon, K. B. (2002). I-PLA₂ Activation during Apoptosis Promotes the Exposure of Membrane Lysophosphatidylcholine Leading to Binding by Natural Immunoglobulin M Antibodies and Complement Activation. *J. Exp. Med.* 196, 655–665. doi:10.1084/jem.20020542.
- Kim, S., Nahm, M., Kim, N., Kwon, Y., Kim, J., Choi, S., et al. (2017). Graf regulates hematopoiesis through geec endocytosis of EGFR. *Dev.* 144, 4159–4172. doi:10.1242/dev.153288.
- Kinchen, J. M., and Ravichandran, K. S. (2008). Phagosome maturation: Going through the acid test. *Nat. Rev. Mol. Cell Biol.* 9, 781–795. doi:10.1038/nrm2515.
- Klein, D. E., Stayrook, S. E., Shi, F., Narayan, K., and Lemmon, M. A. (2008). Structural basis for EGFR ligand sequestration by Argos. *Nature* 453, 1271–1275. doi:10.1038/nature06978.
- Knies, U. E., Behrendorf, H. A., Mitchell, C. A., Deutsch, U., Risau, W., Drexler, H. C., et al. (1998). Regulation of endothelial monocyte-activating polypeptide II release by apoptosis. *Proc. Natl. Acad. Sci. U. S. A.* 95, 12322–7. doi:10.1073/pnas.95.21.12322.
- Kocks, C., Cho, J. H., Nehme, N., Ulvila, J., Pearson, A. M., Meister, M., et al. (2005). Eater, a transmembrane protein mediating phagocytosis of bacterial pathogens in *Drosophila*. *Cell* 123, 335–346. doi:10.1016/j.cell.2005.08.034.
- Koh, T. J., and DiPietro, L. A. (2011). Inflammation and wound healing: the role of the macrophage. *Expert Rev. Mol. Med.* 13, e23. doi:10.1017/S1462399411001943.
- Koizumi, S. (2007). UDP acting at P2Y6 receptors is a mediator of microglial phagocytosis. *Nature* 446, 1091–1095. Available at: <http://dx.doi.org/10.1038/nature05704>.

- Kojima, Y., Volkmer, J.-P., McKenna, K., Civelek, M., Lusic, A. J., Miller, C. L., et al. (2016). CD47-blocking antibodies restore phagocytosis and prevent atherosclerosis. *Nature* 536, 86–90. doi:10.1038/nature18935.
- Kolb, J. P., and Martinez, J. (2016). Bon EPOtit! S1P-Mediated EPO Signaling Whets a Macrophage's Appetite for Apoptotic Cells. *Immunity* 44, 209–211. doi:10.1016/j.immuni.2016.01.023.
- Kolodkin, a L., Pickup, a T., Lin, D. M., Goodman, C. S., and Banerjee, U. (1994). Characterization of Star and its interactions with sevenless and EGF receptor during photoreceptor cell development in *Drosophila*. *Development* 120, 1731–1745.
- Kornbluth, S., and White, K. (2005). Apoptosis in *Drosophila*: Neither fish nor fowl (nor man, nor worm). *J. Cell Sci.* 118, 1779–1787. doi:10.1242/jcs.02377.
- Kotwal, G. J., and Chien, S. (2017). "Macrophage Differentiation in Normal and Accelerated Wound Healing," in *Macrophages Origin, Functions and Biointervention Results and Problems in Cell Differentiation.*, ed. M. Kloc (Cham: Springer International Publishing), 353–364. doi:10.1007/978-3-319-54090-0_14.
- Kroemer, G., Galluzzi, L., and Brenner, C. (2007). Mitochondrial membrane permeabilization in cell death. *Physiol. Rev.* 87, 99–163. doi:10.1152/physrev.00013.2006.
- Kronlage, M., Song, J., Sorokin, L., Isfort, K., Schwerdtle, T., Leipziger, J., et al. (2010). Autocrine Purinergic Receptor Signaling Is Essential for Macrophage Chemotaxis. *Sci. Signal.* 3, ra55–ra55. doi:10.1126/scisignal.2000588.
- Krump, E., Sanghera, J. S., Pelech, S. L., Furuya, W., and Grinstein, S. (1997). Chemotactic peptide N-formyl-Met-Leu-Phe activation of p38 mitogen- activated protein kinase (MAPK) and MAPK-activated protein kinase-2 in human neutrophils. *J. Biol. Chem.* 272, 937–944. doi:10.1074/jbc.272.2.937.
- Kuenkele, S., Beyer, T. D., Voll, R. E., Kalden, J. R., and Herrmann, M. (2003). Impaired clearance of apoptotic cells in systemic lupus erythematosus: challenge of T and B cell tolerance. *Curr. Rheumatol. Rep.* 5, 175–7. Available at: <http://www.ncbi.nlm.nih.gov/pubmed/12744807>.
- Küppers, R., and Hansmann, M. L. (2005). The Hodgkin and Reed/Sternberg cell. *Int. J. Biochem. Cell Biol.* 37, 511–517. doi:10.1016/j.biocel.2003.10.025.
- Kuraishi, T., Nakagawa, Y., Nagaosa, K., Hashimoto, Y., Ishimoto, T., Moki, T., et al. (2009). Pretaporter, a *Drosophila* protein serving as a ligand for Draper in the phagocytosis of

- apoptotic cells. *EMBO J.* 28, 3868–3878. doi:10.1038/emboj.2009.343.
- Kurant, E., Axelrod, S., Leaman, D., and Gaul, U. (2008). Six-Microns-Under Acts Upstream of Draper in the Glial Phagocytosis of Apoptotic Neurons. *Cell* 133, 498–509. doi:10.1016/j.cell.2008.02.052.
- Kurata, S. (2004). Recognition of infectious non-self and activation of immune responses by peptidoglycan recognition protein (PGRP)-family members in *Drosophila*. *Dev. Comp. Immunol.* 28, 89–95. doi:10.1016/S0145-305X(03)00121-6.
- Kvon, E. Z., Kazmar, T., Stampfel, G., Yáñez-Cuna, J. O., Pagani, M., Schernhuber, K., et al. (2014). Genome-scale functional characterization of *Drosophila* developmental enhancers in vivo. *Nature* 512, 91–95. doi:10.1038/nature13395.
- Lamb, D. J., Modjtahedi, H., Plant, N. J., and Ferns, G. A. A. (2004). EGF mediates monocyte chemotaxis and macrophage proliferation and EGF receptor is expressed in atherosclerotic plaques. *Atherosclerosis* 176, 21–26. doi:10.1016/j.atherosclerosis.2004.04.012.
- Lämmermann, T., and Kastenmüller, W. (2019). Concepts of GPCR-controlled navigation in the immune system. *Immunol. Rev.* 289, 205–231. doi:10.1111/imr.12752.
- Landsman, L., Liat, B. O., Zerneck, A., Kim, K. W., Krauthgamer, R., Shagdarsuren, E., et al. (2009). CX3CR1 is required for monocyte homeostasis and atherogenesis by promoting cell survival. *Blood* 113, 963–972. doi:10.1182/blood-2008-07-170787.
- Lanot, R., Zachary, D., Holder, F., and Meister, M. (2001). Postembryonic Hematopoiesis in *Drosophila*. *Dev. Biol.* 230, 243–257. doi:10.1006/dbio.2000.0123.
- Lara Rodriguez, L., and Schneider, I. C. (2013). Directed cell migration in multi-cue environments. *Integr. Biol.* 5, 1306–1323. doi:10.1039/c3ib40137e.
- Lattin, J. E., Schroder, K., Su, A. I., Walker, J. R., Zhang, J., Wiltshire, T., et al. (2008). Expression analysis of G Protein-Coupled Receptors in mouse macrophages. *Immunome Res.* 4, 1–13. doi:10.1186/1745-7580-4-5.
- Lauber, K. (2003). Apoptotic cells induce migration of phagocytes via caspase-3-mediated release of a lipid attraction signal. *Cell* 113, 717–730. Available at: [http://dx.doi.org/10.1016/S0092-8674\(03\)00422-7](http://dx.doi.org/10.1016/S0092-8674(03)00422-7).
- Lebestky, T., Chang, T., Hartenstein, V., and Banerjee, U. (2000). Specification of *Drosophila* hematopoietic lineage by conserved transcription factors. *Science (80-)*. 288, 146–149. doi:10.1126/science.288.5463.146.

- Lee, T., Feig, L., and Montell, D. J. (1996). Two distinct roles for Ras in a developmentally regulated cell migration. *Development* 122, 409–418. Available at: <http://www.ncbi.nlm.nih.gov/cgi-bin/Entrez/referer?http://www.cob.org.uk/Development/122/02/dev8300.html>.
- Leidi, M., Gotti, E., Bologna, L., Miranda, E., Rimoldi, M., Sica, A., et al. (2009). M2 Macrophages Phagocytose Rituximab-Opsonized Leukemic Targets More Efficiently than M1 Cells In Vitro. *J. Immunol.* 182, 4415–4422. doi:10.4049/jimmunol.0713732.
- Lemaitre, B., and Hoffmann, J. (2007). The Host Defense of *Drosophila melanogaster*. *Annu. Rev. Immunol.* 25, 697–743. doi:10.1146/annurev.immunol.25.022106.141615.
- Lengyel, J. A., and Iwaki, D. D. (2002). It takes guts: The *Drosophila* hindgut as a model system for organogenesis. *Dev. Biol.* 243, 1–19. doi:10.1006/dbio.2002.0577.
- Lesokhin, A. M., Yu, S., Katz, J., and Baker, N. E. (1999). Several Levels of EGF Receptor Signaling during Photoreceptor Specification in Wild-Type. *New York* 144, 129–144.
- Levayer, R., and Moreno, E. (2013). Mechanisms of cell competition: Themes and variations. *J. Cell Biol.* 200, 689–698. doi:10.1083/jcb.201301051.
- Li, J., Briehner, W. M., Scimone, M. L., Kang, S. J., Zhu, H., Yin, H., et al. (2007). Caspase-11 regulates cell migration by promoting Aip1-Cofilin-mediated actin depolymerization. *Nat. Cell Biol.* 9, 276–286. doi:10.1038/ncb1541.
- Li, S., Sun, Y., Liang, C. P., Thorp, E. B., Han, S., Jehle, A. W., et al. (2009). Defective phagocytosis of apoptotic cells by macrophages in atherosclerotic lesions of ob/ob mice and reversal by a fish oil diet. *Circ. Res.* 105, 1072–1082. doi:10.1161/CIRCRESAHA.109.199570.
- Liang, J., Balachandra, S., Ngo, S., and O'Brien, L. E. (2017). Feedback regulation of steady-state epithelial turnover and organ size. *Nature* 548, 588–591. doi:10.1038/nature23678.
- Liddiard, K., and Taylor, P. R. (2015). Understanding local macrophage phenotypes in disease: Shape-shifting macrophages. *Nat. Med.* 21, 119–120. doi:10.1038/nm.3798.
- Liesche, C., Sauer, P., Prager, I., Urlaub, D., Claus, M., Eils, R., et al. (2018). Single-fluorescent protein reporters allow parallel quantification of natural killer cell-mediated granzyme and caspase activities in single target cells. *Front. Immunol.* 9. doi:10.3389/fimmu.2018.01840.
- Lim, B., Dsilva, C. J., Levario, T. J., Lu, H., Schüpbach, T., Kevrekidis, I. G., et al. (2015).

- Dynamics of Inductive ERK Signaling in the *Drosophila* Embryo. *Curr. Biol.* 25, 1784–1790. doi:10.1016/j.cub.2015.05.039.
- Liu, L., and Parent, C. A. (2011). TOR kinase complexes and cell migration. *J. Cell Biol.* 194, 815–824. doi:10.1083/jcb.201102090.
- Lo, P. C. H., and Frasch, M. (2001). A role for the COUP-TF-related gene seven-up in the diversification of cardioblast identities in the dorsal vessel of *Drosophila*. *Mech. Dev.* 104, 49–60. doi:10.1016/S0925-4773(01)00361-6.
- Luo, B., Gan, W., Liu, Z., Shen, Z., Wang, J., Shi, R., et al. (2016). Erythropoietin Signaling in Macrophages Promotes Dying Cell Clearance and Immune Tolerance. *Immunity* 44, 287–302. doi:10.1016/j.immuni.2016.01.002.
- Lyko, F., Ramsahoye, B. H., Kashevsky, H., Tudor, M., Mastrangelo, M. A., Orr-Weaver, T. L., et al. (1999). Mammalian (cytosine-5) methyltransferases cause genomic DNA methylation and lethality in *Drosophila*. *Nat. Genet.* 23, 363–366. doi:10.1038/15551.
- MacNee, W. (2005). Pathogenesis of Chronic Obstructive Pulmonary Disease. *Proc. Am. Thorac. Soc.* 2, 258–266. doi:10.1513/pats.200504-045SR.
- Manaka, J., Kuraishi, T., Shiratsuchi, A., Nakai, Y., Higashida, H., Henson, P., et al. (2004). Draper-mediated and phosphatidylserine-independent phagocytosis of apoptotic cells by *Drosophila* hemocytes/macrophages. *J. Biol. Chem.* 279, 48466–48476. doi:10.1074/jbc.M408597200.
- Mañes, S., Gómez-Moutón, C., Lacalle, R. A., Jiménez-Baranda, S., Mira, E., and Martínez-A, C. (2005). Mastering time and space: Immune cell polarization and chemotaxis. *Semin. Immunol.* 17, 77–86. doi:10.1016/j.smim.2004.09.005.
- Marks, S. D., and Tullus, K. (2012). Autoantibodies in systemic lupus erythematosus. *Pediatr. Nephrol.* 27, 1855–1868. doi:10.1007/s00467-011-2078-4.
- Martin, S. J. (2002). Destabilizing influences in apoptosis: Sowing the seeds of IAP destruction. *Cell* 109, 793–796. doi:10.1016/S0092-8674(02)00802-4.
- Martinez, J., Almendinger, J., Oberst, A., Ness, R., Dillon, C. P., Fitzgerald, P., et al. (2011). Microtubule-associated protein 1 light chain 3 alpha (LC3)-associated phagocytosis is required for the efficient clearance of dead cells. *Proc. Natl. Acad. Sci.* 108, 17396–17401. doi:10.1073/pnas.1113421108.
- Mazzalupo, S., and Cooley, L. (2006). Illuminating the role of caspases during *Drosophila* oogenesis. *Cell Death Differ.* 13, 1950–1959. doi:10.1038/sj.cdd.4401892.

- McGuire, S. E., Le, P. T., Osborn, A. J., Matsumoto, K., and Davis, R. L. (2003). Temporal and Regional Gene Expression Targeting with the Conventional GAL4/UAS System in *Drosophila*. *Progr. Abstr. 44th Annu. Drosoph. Res. Conf. Chicago, 2003*, 153.
- McWhorter, F. Y., Wang, T., Nguyen, P., Chung, T., and Liu, W. F. (2013). Modulation of macrophage phenotype by cell shape. *Proc. Natl. Acad. Sci. U. S. A.* 110, 17253–17258. doi:10.1073/pnas.1308887110.
- Miksa, M., and Amin, D. (2007). Fractalkine-Induced MFG-E8 Leads to Enhanced Apoptotic Cell Clearance by Macrophages Michael. *Mol. Med.* 13, 1. doi:10.2119/2007-00019.Miksa.
- Miura, G. I., Buglino, J., Alvarado, D., Lemmon, M. A., Resh, M. D., and Treisman, J. E. (2006). Palmitoylation of the EGFR ligand spitz by rasp increases spitz activity by restricting its diffusion. *Dev. Cell* 10, 167–176. doi:10.1016/j.devcel.2005.11.017.
- Mondal, B. C. hara., Shim, J., Evans, C. J., and Banerjee, U. (2014). Pvr expression regulators in equilibrium signal control and maintenance of *Drosophila* blood progenitors. *Elife* 3, e03626. doi:10.7554/eLife.03626.
- Moreau, H. D., Piel, M., Voituriez, R., and Lennon-Duménil, A. M. (2018). Integrating Physical and Molecular Insights on Immune Cell Migration. *Trends Immunol.* 39, 632–643. doi:10.1016/j.it.2018.04.007.
- Moreira, S., Stramer, B., Evans, I., Wood, W., and Martin, P. (2010). Prioritization of Competing Damage and Developmental Signals by Migrating Macrophages in the *Drosophila* Embryo. *Curr. Biol.* 20, 464–470. doi:10.1016/j.cub.2010.01.047.
- Moreno, E., Yan, M., and Basler, K. (2002). Evolution of TNF Signaling Mechanisms. *Curr. Biol.* 12, 1263–1268. doi:10.1016/s0960-9822(02)00954-5.
- Morioka, S., Maueröder, C., and Ravichandran, K. S. (2019). Living on the Edge: Efferocytosis at the Interface of Homeostasis and Pathology. *Immunity* 50, 1149–1162. doi:10.1016/j.immuni.2019.04.018.
- Muinonen-Martin, A. J., Veltman, D. M., Kalna, G., and Insall, R. H. (2010). An improved chamber for direct visualisation of chemotaxis. *PLoS One* 5. doi:10.1371/journal.pone.0015309.
- Mukaro, V., Hodge, S., Mukaro, V. R. S., and Hodge, S. (2015). Airway Clearance of Apoptotic Cells in COPD Airway Clearance of Apoptotic Cells in COPD. doi:10.2174/1389210204504764501.

- Muñoz, L. E., Leppkes, M., Fuchs, T. A., Hoffmann, M., and Herrmann, M. (2017). Missing in action-The meaning of cell death in tissue damage and inflammation. *Immunol. Rev.* 280, 26–40. doi:10.1111/imr.12569.
- Murray, P. J., and Wynn, T. A. (2011). Protective and pathogenic functions of macrophage subsets. *Nat. Rev. Immunol.* 11, 723–737. doi:10.1038/nri3073.
- Myllymäki, H., Valanne, S., and Rämet, M. (2014). The Drosophila Imd Signaling Pathway . *J. Immunol.* 192, 3455–3462. doi:10.4049/jimmunol.1303309.
- Nagata, K., Ohashi, K., Nakano, T., Arita, H., Zong, C., Hanafusa, H., et al. (1996). Identification of the product of growth arrest-specific gene 6 as a common ligand for Axl, Sky, and Mer receptor tyrosine kinases. *J. Biol. Chem.* 271, 30022–30027. doi:10.1074/jbc.271.47.30022.
- Nakajima, Y. I., and Kuranaga, E. (2017). Caspase-dependent non-apoptotic processes in development. *Cell Death Differ.* 24, 1422–1430. doi:10.1038/cdd.2017.36.
- Nakano, T., Ishimoto, Y., Kishino, J., Umeda, M., Inoue, K., Nagata, K., et al. (1997). Cell adhesion to phosphatidylserine mediated by a product of growth arrest-specific gene 6. *J. Biol. Chem.* 272, 29411–29414. doi:10.1074/jbc.272.47.29411.
- Nelson, R. E., Fessler, L. I., Takagi, Y., Blumberg, B., Keene, D. R., Olson, P. F., et al. (1994). Peroxidase: A novel enzyme-matrix protein of Drosophila development. *EMBO J.* 13, 3438–3447. doi:10.1002/j.1460-2075.1994.tb06649.x.
- Neves, J., Zhu, J., Sousa-Victor, P., Konjikusic, M., Riley, R., Chew, S., et al. (2016). Immune modulation by MANF promotes tissue repair and regenerative success in the retina. *Science (80-.).* 353. doi:10.1126/science.aaf3646.
- Niethammer, P., Grabher, C., Look, A. T., and Mitchison, T. J. (2009). A tissue-scale gradient of hydrogen peroxide mediates rapid wound detection in zebrafish. *Nature* 459, 996–999. doi:10.1038/nature08119.
- Nishimura, T., Horino, K., Nishiura, H., Shibuya, Y., Hiraoka, T., Tanase, S., et al. (2001). Apoptotic cells of an epithelial cell line, AsPC-1, release monocyte chemotactic S19 ribosomal protein dimer. *J Biochem* 129, 445–454. doi:10.1093/oxfordjournals.jbchem.a002876.
- Noda, N., Matsumoto, K., Fukuyama, S., Asai, Y., Kitajima, H., Seki, N., et al. (2013). Cigarette smoke impairs phagocytosis of apoptotic neutrophils by alveolar macrophages via inhibition of the histone deacetylase/Rac/CD9 pathways. *Int. Immunol.* 25, 643–650.

doi:10.1093/intimm/dxt033.

- Norling, L. V., and Dalli, J. (2013). Microparticles are novel effectors of immunity. *Curr. Opin. Pharmacol.* 13, 570–575. doi:10.1016/j.coph.2013.05.008.
- Nowak, M. A., Boerlijst, M. C., Cooke, J., and Smith, J. M. (1997). Evolution of genetic redundancy. *Nature* 388, 167–171. doi:10.1038/40618.
- Nunes, P., and Demaurex, N. (2010). The role of calcium signaling in phagocytosis. *J. Leukoc. Biol.* 88, 57–68. doi:10.1189/jlb.0110028.
- O’Keefe, L., Dougan, S. T., Gabay, L., Raz, E., Shilo, B. Z., and Dinardo, S. (1997). Spitz and Wingless, emanating from distinct borders, cooperate to establish cell fate across the Engrailed domain in the Drosophila epidermis. *Development* 124, 4837–4845.
- Ocana-Morgner, C., Reichardt, P., Chopin, M., Braungart, S., Wahren, C., Gunzer, M., et al. (2011). Sphingosine 1-Phosphate-Induced Motility and Endocytosis of Dendritic Cells Is Regulated by SWAP-70 through RhoA. *J. Immunol.* 186, 5345–5355. doi:10.4049/jimmunol.1003461.
- Okabe, M., Sawamoto, K., and Okano, H. (1996). The function of the Drosophila *argos* gene product in the development of embryonic chordotonal organs. *Dev. Biol.* 175, 37–49. doi:10.1006/dbio.1996.0093.
- Okano, H., and Miura, M. (1999). Drob-1, a Drosophila member of the Bcl-2/CED-9 family that promotes cell death. 1–6.
- Olofsson, B., and Page, D. T. (2005). Condensation of the central nervous system in embryonic Drosophila is inhibited by blocking hemocyte migration or neural activity. *Dev. Biol.* 279, 233–243. doi:10.1016/j.ydbio.2004.12.020.
- Omachi, K., Miyakita, R., Fukuda, R., Kai, Y., Suico, M. A., Yokota, T., et al. (2017). Long-term treatment with EGFR inhibitor erlotinib attenuates renal inflammatory cytokines but not nephropathy in Alport syndrome mouse model. *Clin. Exp. Nephrol.* 21, 952–960. doi:10.1007/s10157-017-1386-9.
- Pacheco, P., White, D., and Sulchek, T. (2013). Effects of Microparticle Size and Fc Density on Macrophage Phagocytosis. *PLoS One* 8, 1–9. doi:10.1371/journal.pone.0060989.
- Page, D. T., and Olofsson, B. (2008). Multiple roles for apoptosis facilitating condensation of the Drosophila ventral nerve cord. *Genesis* 46, 61–68. doi:10.1002/dvg.20365.
- Paladi, M., and Tepass, U. (2004). Function of Rho GTPases in embryonic blood cell migration in Drosophila. *J. Cell Sci.* 117, 6313–6326. doi:10.1242/jcs.01552.

- Palmer, R. M., and Salmon, J. A. (1983). Release of leukotriene B4 from human neutrophils and its relationship to degranulation induced by N-formyl-methionyl-leucyl-phenylalanine, serum-treated zymosan and the ionophore A23187. *Immunology* 50, 65–73. Available at:
<http://www.ncbi.nlm.nih.gov/pubmed/6309653><http://www.pubmedcentral.nih.gov/articlerender.fcgi?artid=PMC1454236>.
- Palmgren, M. G. (1991). Acridine orange as a probe for measuring pH gradients across membranes: Mechanism and limitations. *Anal. Biochem.* 192, 316–321.
doi:10.1016/0003-2697(91)90542-2.
- Pang, Y., Bai, X. C., Yan, C., Hao, Q., Chen, Z., Wang, J. W., et al. (2015). Structure of the apoptosome: Mechanistic insights into activation of an initiator caspase from *Drosophila*. *Genes Dev.* 29, 277–287. doi:10.1101/gad.255877.114.
- Parnaik, R., Raff, M. C., and Scholes, J. (2000). Differences between the clearance of apoptotic cells by professional and non-professional phagocytes. *Curr. Biol.* 10, 857–860.
doi:10.1016/S0960-9822(00)00598-4.
- Pearson, A. M., Baksa, K., Rämets, M., Protas, M., McKee, M., Brown, D., et al. (2003). Identification of cytoskeletal regulatory proteins required for efficient phagocytosis in *Drosophila*. *Microbes Infect.* 5, 815–824. doi:10.1016/S1286-4579(03)00157-6.
- Penuela, S., Gehi, R., and Laird, D. W. (2013). The biochemistry and function of pannexin channels. *Biochim. Biophys. Acta - Biomembr.* 1828, 15–22.
doi:10.1016/j.bbamem.2012.01.017.
- Perdiguer, E. G., and Geissmann, F. (2016). The development and maintenance of resident macrophages. *Nat. Immunol.* 17, 2–8. doi:10.1038/ni.3341.
- Pérez, E., Lindblad, J. L., and Bergmann, A. (2017). Tumor-promoting function of apoptotic caspases by an amplification loop involving ROS, macrophages and JNK in *Drosophila*. *Elife* 6, 1–20. doi:10.7554/eLife.26747.
- Peter, C., Waibel, M., Radu, C. G., Yang, L. V., Witte, O. N., Schulze-Osthoff, K., et al. (2008). Migration to apoptotic “find-me” signals is mediated via the phagocyte receptor G2A. *J. Biol. Chem.* 283, 5296–5305. doi:10.1074/jbc.M706586200.
- Petrie, R. J., Doyle, A. D., and Yamada, K. M. (2009). Random versus directionally persistent cell migration. *Nat. Rev. Mol. Cell Biol.* 10, 538–549. doi:10.1038/nrm2729.
- Petrignani, B., Rommelaere, S., Hakim-Mishnaevski, K., Masson, F., Ramond, E., Hilu-Dadia, R.,

- et al. (2021). A secreted factor NimrodB4 promotes the elimination of apoptotic corpses by phagocytes in *Drosophila*. *EMBO Rep.*, 1–20.
doi:10.15252/embr.202052262.
- Piston, D. W., and Kremers, G. J. (2007). Fluorescent protein FRET: the good, the bad and the ugly. *Trends Biochem. Sci.* 32, 407–414. doi:10.1016/j.tibs.2007.08.003.
- Pizette, S., Rabouille, C., Cohen, S. M., and Thérond, P. (2009). Glycosphingolipids control the extracellular gradient of the *Drosophila* EGFR ligand Gurken. *Development* 136, 551–561. doi:10.1242/dev.031104.
- Pop, C., and Salvesen, G. S. (2009). Human caspases: Activation, specificity, and regulation. *J. Biol. Chem.* 284, 21777–21781. doi:10.1074/jbc.R800084200.
- Potter, C. J., Tasic, B., Russler, E. V., Liang, L., and Luo, L. (2010). The Q system: A repressible binary system for transgene expression, lineage tracing, and mosaic analysis. *Cell* 141, 536–548. doi:10.1016/j.cell.2010.02.025.
- Price, J. V., Clifford, R. J., and Schüpbach, T. (1989). The maternal ventralizing locus torpedo is allelic to faint little ball, an embryonic lethal, and encodes the *Drosophila* EGF receptor homolog. *Cell* 56, 1085–1092. doi:10.1016/0092-8674(89)90641-7.
- Qian, L., Liu, J., and Bodmer, R. (2007). Heart Development in *Drosophila*. *Adv. Dev. Biol.* 18, 1–29. doi:10.1016/S1574-3349(07)18001-7.
- Qin, X., Qiu, C., and Zhao, L. (2014). Lysophosphatidylcholine perpetuates macrophage polarization toward classically activated phenotype in inflammation. *Cell. Immunol.* 289, 185–190. doi:10.1016/j.cellimm.2014.04.010.
- Qu, W. sheng, Tian, D. shi, Guo, Z. bao, Fang, J., Zhang, Q., Yu, Z. yuan, et al. (2012). Inhibition of EGFR/MAPK signaling reduces microglial inflammatory response and the associated secondary damage in rats after spinal cord injury. *J. Neuroinflammation* 9, 1–14.
doi:10.1186/1742-2094-9-178.
- Qu, Y., Misaghi, S., Newton, K., Gilmour, L. L., Louie, S., Cupp, J. E., et al. (2011). Pannexin-1 Is Required for ATP Release during Apoptosis but Not for Inflammasome Activation. *J. Immunol.* 186, 6553–6561. doi:10.4049/jimmunol.1100478.
- Rahman, A., Henry, K. M., Herman, K. D., R Thompson, A. A., Isles, H. M., Tulotta, C., et al. (2019). Inhibition of ErbB kinase signalling promotes resolution of neutrophilic inflammation. *Elife* 8, 1–23. doi:10.7554/eLife.50990.
- Ravichandran, K. S. (2003). “Recruitment signals” from apoptotic cells: Invitation to a quiet

- meal. *Cell* 113, 817–820. doi:10.1016/S0092-8674(03)00471-9.
- Ravichandran, K. S. (2010). Find-me and eat-me signals in apoptotic cell clearance: Progress and conundrums. *J. Exp. Med.* 207, 1807–1817. doi:10.1084/jem.20101157.
- Raz, E., and Shilo, B. Z. (1992). Dissection of the faint little ball (flb) phenotype: Determination of the development of the Drosophila central nervous system by early interactions in the ectoderm. *Development* 114, 113–123.
- Razzell, W., Evans, I. R., Martin, P., and Wood, W. (2013). Calcium flashes orchestrate the wound inflammatory response through duox activation and hydrogen peroxide release. *Curr. Biol.* 23, 424–429. doi:10.1016/j.cub.2013.01.058.
- Razzell, W., Wood, W., and Martin, P. (2011). Swatting flies: Modelling wound healing and inflammation in Drosophila. *DMM Dis. Model. Mech.* 4, 569–574. doi:10.1242/dmm.006825.
- Redd, M. J., Cooper, L., Wood, W., Stramer, B., and Martin, P. (2004). Wound healing and inflammation: Embryos reveal the way to perfect repair. *Philos. Trans. R. Soc. B Biol. Sci.* 359, 777–784. doi:10.1098/rstb.2004.1466.
- Reed, B. H., Wilk, R., Schöck, F., and Lipshitz, H. D. (2004). Integrin-dependent apposition of Drosophila extraembryonic membranes promotes morphogenesis and prevents anoikis. *Curr. Biol.* 14, 372–380. doi:10.1016/j.cub.2004.02.029.
- Rehorn, K. P., Thelen, H., Michelson, A. M., and Reuter, R. (1996). A molecular aspect of hematopoiesis and endoderm development common to vertebrates and Drosophila. *Development* 122, 4023–4031. doi:10.1242/dev.122.12.4023.
- Reich, A., and Shilo, B.-Z. (2002). Keren, a New Ligand of the Epidermal Growth Factor Receptor, Undergoes Two Modes of Cleavage. *Embo J* 21, 4287–4296.
- Remijsen, Q., Kuijpers, T. W., Wirawan, E., Lippens, S., Vandenabeele, P., and Vanden Berghe, T. (2011). Dying for a cause: NETosis, mechanisms behind an antimicrobial cell death modality. *Cell Death Differ.* 18, 581–588. doi:10.1038/cdd.2011.1.
- Ren, Y., Tang, J., Mok, M. Y., Chan, A. W. K., Wu, A., and Lau, C. S. (2003). Increased Apoptotic Neutrophils and Macrophages and Impaired Macrophage Phagocytic Clearance of Apoptotic Neutrophils in Systemic Lupus Erythematosus. *Arthritis Rheum.* 48, 2888–2897. doi:10.1002/art.11237.
- Renshaw, S. A., Parmar, J. S., Singleton, V., Rowe, S. J., Dockrell, D. H., Dower, S. K., et al. (2003). Acceleration of Human Neutrophil Apoptosis by TRAIL. *J. Immunol.* 170, 1027–

1033. doi:10.4049/jimmunol.170.2.1027.
- Revaitis, N. T., Niepielko, M. G., Marmion, R. A., Klein, E. A., Piccoli, B., and Yakoby, N. (2020). Quantitative analyses of EGFR localization and trafficking dynamics in the follicular epithelium. *Development* 147. doi:10.1242/dev.183210.
- Revollo, I., Nishiura, H., Shibuya, Y., Oda, Y., Nishino, N., and Yamamoto, T. (2005). Agonist and antagonist dual effect of the cross-linked S19 ribosomal protein dimer in the C5a receptor-mediated respiratory burst reaction of phagocytic leukocytes. *Inflamm. Res.* 54, 82–90. doi:10.1007/s00011-004-1327-4.
- Richards, D. M., and Endres, R. G. (2014). The mechanism of phagocytosis: Two stages of engulfment. *Biophys. J.* 107, 1542–1553. doi:10.1016/j.bpj.2014.07.070.
- Richens, T. R., Linderman, D. J., Horstmann, S. A., Lambert, C., Xiao, Y. Q., Keith, R. L., et al. (2009). Cigarette smoke impairs clearance of apoptotic cells through oxidant-dependent activation of RhoA. *Am. J. Respir. Crit. Care Med.* 179, 1011–1021. doi:10.1164/rccm.200807-1148OC.
- Rizki, T. M., and Rizki, R. M. (1992). Lamellocyte differentiation in *Drosophila* larvae parasitized by *Leptopilina*. *Dev. Comp. Immunol.* 16, 103–110. doi:10.1016/0145-305X(92)90011-Z.
- Rizki, T. M., Rizki, R. M., and Bellotti, R. A. (1985). Genetics of a *Drosophila* phenoloxidase. *Mol. Gen. Genet. MGG* 201, 7–13. doi:10.1007/BF00397978.
- Roddie, H. G., Armitage, E. L., Coates, J. A., Johnston, S. A., and Evans, I. R. (2019). *Simu-dependent clearance of dying cells regulates macrophage function and inflammation resolution*. doi:10.1371/journal.pbio.2006741.
- Romao, S., and Münz, C. (2014). LC3-associated phagocytosis. *Autophagy* 10, 526–528. doi:10.4161/auto.27606.
- Rose-John, S. (2013). ADAM17, shedding, TACE as therapeutic targets. *Pharmacol. Res.* 71, 19–22. doi:10.1016/j.phrs.2013.01.012.
- Rougeot, J., Renard, M., Randsholt, N. B., Peronnet, F., and Mouchel-Vielh, E. (2013). The Elongin Complex Antagonizes the Chromatin Factor Corto for Vein versus Intervein Cell Identity in *Drosophila* Wings. *PLoS One* 8. doi:10.1371/journal.pone.0077592.
- Rutledge, B. J., Zhang, K., Bier, E., Jan, Y. N., and Perrimon, N. (1992). The *Drosophila* spitz gene encodes a putative EGF-like growth factor involved in dorsal-ventral axis formation and neurogenesis. *Genes Dev.* 6, 1503–1517. doi:10.1101/gad.6.8.1503.

- Ryoo, H. D., Gorenc, T., and Steller, H. (2004). Apoptotic cells can induce compensatory cell proliferation through the JNK and the wingless signaling pathways. *Dev. Cell* 7, 491–501. doi:10.1016/j.devcel.2004.08.019.
- Salaun, C., Greaves, J., and Chamberlain, L. H. (2010). The intracellular dynamic of protein palmitoylation. *J. Cell Biol.* 191, 1229–1238. doi:10.1083/jcb.201008160.
- Santabárbara-Ruiz, P., López-Santillán, M., Martínez-Rodríguez, I., Binagui-Casas, A., Pérez, L., Milán, M., et al. (2015). ROS-Induced JNK and p38 Signaling Is Required for Unpaired Cytokine Activation during *Drosophila* Regeneration. *PLoS Genet.* 11, 1–26. doi:10.1371/journal.pgen.1005595.
- Sarris, M., and Sixt, M. (2015). Navigating in tissue mazes: Chemoattractant interpretation in complex environments. *Curr. Opin. Cell Biol.* 36, 93–102. doi:10.1016/j.ceb.2015.08.001.
- Scheller, J., Chalaris, A., Garbers, C., and Rose-John, S. (2011). ADAM17: A molecular switch to control inflammation and tissue regeneration. *Trends Immunol.* 32, 380–387. doi:10.1016/j.it.2011.05.005.
- Schiffmann, E., Corcoran, B. A., and Wahl, S. M. (1975). N-formylmethionyl peptides as chemoattractants for leucocytes. *Proc. Natl. Acad. Sci.* 72, 1059–1062. doi:10.1073/pnas.72.3.1059.
- Schindelin, J., Arganda-Carreras, I., Frise, E., Kaynig, V., Longair, M., Pietzsch, T., et al. (2012). Fiji: An open-source platform for biological-image analysis. *Nat. Methods* 9, 676–682. doi:10.1038/nmeth.2019.
- Schlatter, R., Schmich, K., Vizcarra, I. A., Scheurich, P., Sauter, T., Borner, C., et al. (2009). ON/OFF and beyond - A Boolean model of apoptosis. *PLoS Comput. Biol.* 5. doi:10.1371/journal.pcbi.1000595.
- Schnepp, B., Grumbling, G., Donaldson, T., and Simcox, A. (1996). Vein is a novel component in the *Drosophila* epidermal growth factor receptor pathway with similarity to the neuregulins. *Genes Dev.* 10, 2302–2313. doi:10.1101/gad.10.18.2302.
- Schott, S., Ambrosini, A., Barbaste, A., Benassayag, C., Gracia, M., Proag, A., et al. (2017). A fluorescent toolkit for spatiotemporal tracking of apoptotic cells in living *Drosophila* tissues. *Development*, dev.149807. doi:10.1242/dev.149807.
- Schweitzer, R., Shaharabany, M., Seger, R., and Shilo, B. Z. (1995). Secreted Spitz triggers the DER signaling pathway and is a limiting component in embryonic ventral ectoderm determination. *Genes Dev.* 9, 1518–1529. doi:10.1101/gad.9.12.1518.

- Segundo, C., Medina, F., Rodríguez, C., Martínez-Palencia, R., Leyva-Cobián, F., and Brieva, J. A. (1999). Surface molecule loss and bleb formation by human germinal center B cells undergoing apoptosis: role of apoptotic blebs in monocyte chemotaxis. *Blood* 94, 1012–1020. Available at: <http://www.ncbi.nlm.nih.gov/pubmed/10419893>.
- Serizier, S. B., and McCall, K. (2017). Scrambled eggs: Apoptotic cell clearance by non-professional phagocytes in the *Drosophila* ovary. *Front. Immunol.* 8. doi:10.3389/fimmu.2017.01642.
- Sessler, T., Healy, S., Samali, A., and Szegezdi, E. (2013). Structural determinants of DISC function: New insights into death receptor-mediated apoptosis signalling. *Pharmacol. Ther.* 140, 186–199. doi:10.1016/j.pharmthera.2013.06.009.
- Shen, W., Chen, X., Cormier, O., Cheng, D. C. P., Reed, B., and Harden, N. (2013). Modulation of Morphogenesis by Egfr during Dorsal Closure in *Drosophila*. *PLoS One* 8, 1–13. doi:10.1371/journal.pone.0060180.
- Sheridan, G. K., and Murphy, K. J. (2013). Neuron-glia crosstalk in health and disease: fractalkine and CX3CR1 take centre stage. *Open Biol.* 3, 130181. doi:10.1098/rsob.130181.
- Shilo, B. Z. (2003). Signaling by the *Drosophila* epidermal growth factor receptor pathway during development. *Exp. Cell Res.* 284, 140–149. doi:10.1016/S0014-4827(02)00094-0.
- Shilo, B. Z. (2014). The regulation and functions of MAPK pathways in *Drosophila*. *Methods* 68, 151–159. doi:10.1016/j.ymeth.2014.01.020.
- Shilo, B. Z. (2016). Developmental roles of Rhomboid proteases. *Semin. Cell Dev. Biol.* 60, 5–9. doi:10.1016/j.semcdb.2016.07.014.
- Shklover, J., Levy-Adam, F., and Kurant, E. (2015). The role of *Drosophila* TNF Eiger in developmental and damage-induced neuronal apoptosis. *FEBS Lett.* 589, 871–879. doi:10.1016/j.febslet.2015.02.032.
- Sieger, D., Moritz, C., Ziegenhals, T., Prykhodzhiy, S., and Peri, F. (2012). Long-Range Ca²⁺ Waves Transmit Brain-Damage Signals to Microglia. *Dev. Cell* 22, 1138–1148. doi:10.1016/j.devcel.2012.04.012.
- Smith, A., AF Parkes, M., K Atkin-Smith, G., Tixeira, R., and KH Poon, I. (2017). Cell disassembly during apoptosis. *WikiJournal Med.* 4, 10–12. doi:10.15347/wjm/2017.008.
- Snyderman, R., Shin, H. S., and Dannenberg, A. M. (1972). Macrophage proteinase and inflammation: The production of chemoactive activity from the fifth component of

- complement by macrophage proteinase. *J Immunol* 109, 896–898.
- Sokolowski, J. D., Chabanon-Hicks, C. N., Han, C. Z., Heffron, D. S., and Mandell, J. W. (2014). Fractalkine is a "find-me" signal released by neurons undergoing ethanol-induced apoptosis. *Front. Cell. Neurosci.* 8, 1–10. doi:10.3389/fncel.2014.00360.
- Song, Z., McCall, K., and Steller, H. (1997a). DCP-1, a Drosophila cell death protease essential for development. *Science* 275, 536–40. doi:10.1126/science.275.5299.536.
- Song, Z., McCall, K., and Steller, H. (1997b). DCP-1, a Drosophila cell death protease essential for development. *Science* (80-.). 275, 536–40. doi:10.1126/science.275.5299.536.
- Sowa, G., Liu, J., Papapetropoulos, A., Rex-Haffner, M., Hughes, T. E., and Sessa, W. C. (1999). Trafficking of endothelial nitric-oxide synthase in living cells. Quantitative evidence supporting the role of palmitoylation as a kinetic trapping mechanism limiting membrane diffusion. *J. Biol. Chem.* 274, 22524–22531. doi:10.1074/jbc.274.32.22524.
- Spencer, S. A., Powell, P. A., Miller, D. T., and Cagan, R. L. (1998). Regulation of EGF receptor signaling establishes pattern across the developing Drosophila retina. *Development* 125, 4777–4790.
- Steinhauer, J., Liu, H. H., Miller, E., and Treisman, J. E. (2013). Trafficking of the EGFR ligand Spitz regulates its signaling activity in polarized tissues. *J Cell Sci* 126, 4469–4478. doi:10.1242/jcs.131169.
- Steller, H. (2008). Regulation of apoptosis in Drosophila. *Cell Death Differ.* 15, 1132–1138. doi:10.1038/cdd.2008.50.
- Stofanko, M., Kwon, S. Y., and Badenhorst, P. (2010). Lineage tracing of lamellocytes demonstrates Drosophila macrophage plasticity. *PLoS One* 5. doi:10.1371/journal.pone.0014051.
- Stramer, B., Moreira, S., Millard, T., Evans, I., Huang, C. Y., Sabet, O., et al. (2010). Clasp-mediated microtubule bundling regulates persistent motility and contact repulsion in Drosophila macrophages in vivo. *J. Cell Biol.* 189, 681–689. doi:10.1083/jcb.200912134.
- Stramer, B., Wood, W., Galko, M. J., Redd, M. J., Jacinto, A., Parkhurst, S. M., et al. (2005). Live imaging of wound inflammation in Drosophila embryos reveals key roles for small GTPases during in vivo cell migration. *J. Cell Biol.* 168, 567–573. doi:10.1083/jcb.200405120.
- Sturtevant, M. A., Roark, M., and Bier, E. (1993). The Drosophila rhomboid gene mediates the localized formation of wing veins and interacts genetically with components of the EGF-

- R signaling pathway. *Genes Dev.* 7, 961–973. doi:10.1101/gad.7.6.961.
- Summers, C., Rankin, S. M., Condliffe, A. M., Singh, N., Peters, A. M., and Chilvers, E. R. (2010). Neutrophil kinetics in health and disease. *Trends Immunol.* 31, 318–324. doi:10.1016/j.it.2010.05.006.
- Sun, G., Guzman, E., Balasanyan, V., Conner, C. M., Wong, K., Zhou, H. R., et al. (2017). A molecular signature for anastasis, recovery from the brink of apoptotic cell death. *J. Cell Biol.* 216, 3355–3368. doi:10.1083/jcb.201706134.
- Tabas, I., and Ron, D. (2011). Integrating the mechanisms of apoptosis induced by endoplasmic reticulum stress. *Nat. Cell Biol.* 13, 184–190. doi:10.1038/ncb0311-184.
- Takemoto, K., Nagai, T., Miyawaki, A., and Miura, M. (2003). Spatio-temporal activation of caspase revealed by indicator that is insensitive to environmental effects. *J. Cell Biol.* 160, 235–243. doi:10.1083/jcb.200207111.
- Tang, H. L., Tang, H. M., Fung, M. C., and Hardwick, J. M. (2015). In vivo Caspase tracker biosensor system for detecting anastasis and non-apoptotic caspase activity. *Sci. Rep.* 5, 1–7. doi:10.1038/srep09015.
- Tang, H. L., Tang, H. M., Mak, K. H., Hu, S., Wang, S. S., Wong, K. M., et al. (2012). Cell survival, DNA damage, and oncogenic transformation after a transient and reversible apoptotic response. *Mol. Biol. Cell* 23, 2240–2252. doi:10.1091/mbc.E11-11-0926.
- Tao, H., Yancey, P. G., Babaev, V. R., Blakemore, J. L., Zhang, Y., Ding, L., et al. (2015). Macrophage SR-BI mediates efferocytosis via Src/PI3K/Rac1 signaling and reduces atherosclerotic lesion necrosis. *J. Lipid Res.* 56, 1449–1460. doi:10.1194/jlr.M056689.
- Tardy, O. R., Armitage, E. L., Prince, L. R., and Evans, I. R. (2021). The Epidermal Growth Factor Ligand Spitz Modulates Macrophage Efferocytosis, Wound Responses and Migration Dynamics During Drosophila Embryogenesis. *Front. Cell Dev. Biol.* 9, 1–16. doi:10.3389/fcell.2021.636024.
- Tattikota, S. G., Cho, B., Liu, Y., Hu, Y., Barrera, V., Steinbaugh, M. J., et al. (2020). A single-cell survey of drosophila blood. *Elife* 9, 1–35. doi:10.7554/eLife.54818.
- Tedesco, S., Bolego, C., Toniolo, A., Nassi, A., Fadini, G. P., Locati, M., et al. (2015). Phenotypic activation and pharmacological outcomes of spontaneously differentiated human monocyte-derived macrophages. *Immunobiology* 220, 545–554. doi:10.1016/j.imbio.2014.12.008.
- Tepass, U., Fessler, L. I. I., Aziz, A., and Hartenstein, V. (1994). Embryonic origin of hemocytes

- and their relationship to cell death in *Drosophila*. *Development* 120, 1829–1837. doi:10.1242/dev.120.7.1829.
- Thompson, W. L., and Van Eldik, L. J. (2009). Inflammatory cytokines stimulate the chemokines CCL2/MCP-1 and CCL7/MCP-7 through NFκB and MAPK dependent pathways in rat astrocytes. *Brain Res.* 1287, 47–57. doi:10.1016/j.brainres.2009.06.081.
- Thorp, E. B. (2010). Mechanisms of failed apoptotic cell clearance by phagocyte subsets in cardiovascular disease. *Apoptosis* 15, 1124–1136. doi:10.1007/s10495-010-0516-6.
- Thorp, E., Cui, D., Schrijvers, D. M., Kuriakose, G., and Tabas, I. (2008). MERTK receptor mutation reduces efferocytosis efficiency and promotes apoptotic cell accumulation and plaque necrosis in atherosclerotic lesions of ApoE^{-/-} mice. *Arterioscler. Thromb. Vasc. Biol.* 28, 1421–1428. doi:10.1161/ATVBAHA.108.167197.
- Thorp, E., Subramanian, M., and Tabas, I. (2011). The role of macrophages and dendritic cells in the clearance of apoptotic cells in advanced atherosclerosis. *Eur. J. Immunol.* 41, 2515–2518. doi:10.1002/eji.201141719.
- Timmer, J. C., and Salvesen, G. S. (2007). Caspase substrates. *Cell Death Differ.* 14, 66–72. doi:10.1038/sj.cdd.4402059.
- To, T. L., Schepis, A., Ruiz-González, R., Zhang, Q., Yu, D., Dong, Z., et al. (2016). Rational Design of a GFP-Based Fluorogenic Caspase Reporter for Imaging Apoptosis In Vivo. *Cell Chem. Biol.* 23, 875–882. doi:10.1016/j.chembiol.2016.06.007.
- Tolwinski, N. (2017). Introduction: *Drosophila*—A Model System for Developmental Biology. *J. Dev. Biol.* 5, 9. doi:10.3390/jdb5030009.
- Tomancak, P., Beaton, A., Weiszmam, R., Kwan, E., Shu, S., Lewis, S. E., et al. (2002). Systematic determination of patterns of gene expression during *Drosophila* embryogenesis. *Genome Biol.* 3, RESEARCH0088. doi:10.1186/gb-2002-3-12-research0088.
- Tomancak, P., Berman, B. P., Beaton, A., Weiszmam, R., Kwan, E., Hartenstein, V., et al. (2007). Global analysis of patterns of gene expression during *Drosophila* embryogenesis. *Genome Biol.* 8, 1–24. doi:10.1186/gb-2007-8-7-r145.
- Trahtenberg, U., and Mevorach, D. (2017). Apoptotic Cells Induced Signaling for Immune Homeostasis in Macrophages and Dendritic Cells. *Front. Immunol.* 8. doi:10.3389/fimmu.2017.01356.
- Truman, L. A., Ford, C., Pasikowska, M., and Jd (2008). CX3CL1/fractalkine is released from

- apoptotic lymphocytes to stimulate macrophage chemotaxis. *Blood* 112, 5026–5036. doi:10.1182/blood-2008-06-162404.The.
- Tsai, W. H., Shih, C. H., Feng, S. Y., Li, I. T., Chang, S. C., Lin, Y. C., et al. (2014). CX3CL1(+) microparticles mediate the chemoattraction of alveolar macrophages toward apoptotic acute promyelocytic leukemic cells. *Cell. Physiol. Biochem.* 33, 594–604. doi:10.1159/000358637.
- Tsruya, R., Wojtalla, A., Carmon, S., Yogev, S., Reich, A., Bibi, E., et al. (2007). Rhomboid cleaves Star to regulate the levels of secreted Spitz. *EMBO J.* 26, 1211–1220. doi:10.1038/sj.emboj.7601581.
- Tsuyama, T., Kishikawa, J. I., Han, Y. W., Harada, Y., Tsubouchi, A., Noji, H., et al. (2013). In vivo fluorescent adenosine 5'-triphosphate (ATP) imaging of *Drosophila melanogaster* and *Caenorhabditis elegans* by using a genetically encoded fluorescent ATP Biosensor optimized for low temperatures. *Anal. Chem.* 85, 7889–7896. doi:10.1021/ac4015325.
- Tucker, P. K., Evans, I. R., and Wood, W. (2011). Ena drives invasive macrophage migration in *Drosophila* embryos. *DMM Dis. Model. Mech.* 4, 126–134. doi:10.1242/dmm.005694.
- Urban, S., Lee, J. R., and Freeman, M. (2002). A family of rhomboid intramembrane proteases activates all *Drosophila* membrane-tethered EGF ligands. *EMBO J.* 21, 4277–4286. doi:10.1093/emboj/cdf434.
- Uribe-Querol, E., and Rosales, C. (2020). Phagocytosis: Our Current Understanding of a Universal Biological Process. *Front. Immunol.* 11, 1–13. doi:10.3389/fimmu.2020.01066.
- Valanne, S., Wang, J.-H., and Rämetsä, M. (2011). The *Drosophila* Toll Signaling Pathway. *J. Immunol.* 186, 649–656. doi:10.4049/jimmunol.1002302.
- Valon, L., Davidović, A., Levillayer, F., Villars, A., Chouly, M., Cerqueira-Campos, F., et al. (2021). Robustness of epithelial sealing is an emerging property of local ERK feedback driven by cell elimination. *Dev. Cell*, 1–12. doi:10.1016/j.devcel.2021.05.006.
- van Doren, M. (1996). Heat shock hid transgenes.
- van Goethem, E., Silva, E. A., Xiao, H., and Franc, N. C. (2012). The *Drosophila* TRPP cation channel, PKD2 and Dmel/Ced-12 act in genetically distinct pathways during apoptotic cell clearance. *PLoS One* 7. doi:10.1371/journal.pone.0031488.
- Vancraeynest, D., Pasquet, A., Havaux, X., Gerber, B., Gisellu, G., and Vanoverschelde, J.-L. J. (2003). Time- and energy-dependent ischemic-like ECG changes during myocardial contrast echocardiography in rats. *J. Am. Coll. Cardiol.* 41, 465. doi:10.1016/s0735-

1097(03)82567-6.

- Veltman, D. M., Roelofs, J., Engel, R., Visser, A. J. W. G., and Van Haastert, P. J. M. (2005). Activation of soluble guanylyl cyclase at the leading edge during *Dictyostelium* chemotaxis. *Mol. Biol. Cell* 16, 976–983. doi:10.1091/mbc.E04-08-0701.
- Vlisidou, I., and Wood, W. (2015). *Drosophila* blood cells and their role in immune responses. *FEBS J.* 282, 1368–1382. doi:10.1111/febs.13235.
- Vogel, D. Y. S., Glim, J. E., Stavenuiter, A. W. D., Breur, M., Heijnen, P., Amor, S., et al. (2014). Human macrophage polarization in vitro: Maturation and activation methods compared. *Immunobiology* 219, 695–703. doi:10.1016/j.imbio.2014.05.002.
- Voss, A. K., and Strasser, A. (2020). The essentials of developmental apoptosis. *F1000Research* 9, 1–12. doi:10.12688/f1000research.21571.1.
- Wakasugi, K., and Schimmel, P. (1999). Two distinct cytokines released from a human aminoacyl-tRNA synthetase. *Science (80-.)*. 284, 147–151. doi:10.1126/science.284.5411.147.
- Wang, K. K. W. (2000). Calpain and caspase: Can you tell the difference? *Trends Neurosci.* 23, 20–26. doi:10.1016/S0166-2236(99)01479-4.
- Wang, L., Kounatidis, I., and Ligoxygakis, P. (2014). *Drosophila* as a model to study the role of blood cells in inflammation, innate immunity and cancer. *Front. Cell. Infect. Microbiol.* 3, 1–17. doi:10.3389/fcimb.2013.00113.
- Wang, Y., Chen, C. L., and Iijima, M. (2011). Signaling mechanisms for chemotaxis. *Dev. Growth Differ.* 53, 495–502. doi:10.1111/j.1440-169X.2011.01265.x.
- Wang, Y., Luo, G., Chen, J., Jiang, R., Zhu, J., Hu, N., et al. (2017). Cigarette smoke attenuates phagocytic ability of macrophages through down-regulating Milk fat globule-EGF factor 8 (MFG-E8) expressions. *Sci. Rep.* 7, 1–12. doi:10.1038/srep42642.
- Wasserman, J. D., and Freeman, M. (1998). An autoregulatory cascade of EGF receptor signaling patterns the *Drosophila* egg. *Cell* 95, 355–364. doi:10.1016/S0092-8674(00)81767-5.
- Weavers, H., Evans, I. R., Martin, P., and Wood, W. (2016a). Corpse Engulfment Generates a Molecular Memory that Primes the Macrophage Inflammatory Response. *Cell* 165, 1658–1671. doi:10.1016/j.cell.2016.04.049.
- Weavers, H., Liepe, J., Sim, A., Wood, W., Martin, P., and Stumpf, M. P. H. (2016b). Systems Analysis of the Dynamic Inflammatory Response to Tissue Damage Reveals

- Spatiotemporal Properties of the Wound Attractant Gradient. *Curr. Biol.* 26, 1975–1989. doi:10.1016/j.cub.2016.06.012.
- Weber, C., and Noels, H. (2011). Atherosclerosis: Current pathogenesis and therapeutic options. *Nat. Med.* 17, 1410–1422. doi:10.1038/nm.2538.
- Weichand, B., Weis, N., Weigert, A., Grossmann, N., Levkau, B., and Brüne, B. (2013). Apoptotic cells enhance sphingosine-1-phosphate receptor 1 dependent macrophage migration. *Eur. J. Immunol.* 43, 3306–3313. doi:10.1002/eji.201343441.
- Weigert, A., Cremer, S., Schmidt, M. V., Von Knethen, A., Angioni, C., Geisslinger, G., et al. (2010). Cleavage of sphingosine kinase 2 by caspase-1 provokes its release from apoptotic cells. *Blood* 115, 3531–3540. doi:10.1182/blood-2009-10-243444.
- Weigert, A., Johann, A. M., Von Knethen, A., Schmidt, H., Geisslinger, G., and Brüne, B. (2006). Apoptotic cells promote macrophage survival by releasing the antiapoptotic mediator sphingosine-1-phosphate. *Blood* 108, 1635–1642. doi:10.1182/blood-2006-04-014852.
- Wennerberg, K., and Der, C. J. (2004). Rho-family GTPases: It's not only Rac and Rho (and i like it). *J. Cell Sci.* 117, 1301–1312. doi:10.1242/jcs.01118.
- Wessells, R. J., Grumbling, G., Donaldson, T., Wang, S., and Simcox, A. (1999). Tissue-Specific Regulation of Vein / EGF Receptor Signaling in *Drosophila*. *Dev Biol* 216, 243–259.
- White, G. E., and Greaves, D. R. (2012). Fractalkine: A survivor's guide chemokines as antiapoptotic mediators. *Arterioscler. Thromb. Vasc. Biol.* 32, 589–594. doi:10.1161/ATVBAHA.111.237412.
- Wilkie, D. (1983). Rayleigh Test for Randomness of Circular Data. *Appl. Stat.* 32, 311–312. doi:10.2307/2347954.
- Wlodkowic, D., Skommer, J., and Pelkonen, J. (2007). Towards an understanding of apoptosis detection by SYTO dyes. *Cytom. Part A* 71, 61–72. doi:10.1002/cyto.a.20366.
- Wodarz, A., Hinz, U., Engelbert, M., and Knust, E. (1995). Expression of crumbs confers apical character on plasma membrane domains of ectodermal epithelia of *drosophila*. *Cell* 82, 67–76. doi:10.1016/0092-8674(95)90053-5.
- Wolf, K., te Lindert, M., Krause, M., Alexander, S., te Riet, J., Willis, A. L., et al. (2013). Physical limits of cell migration: Control by ECM space and nuclear deformation and tuning by proteolysis and traction force. *J. Cell Biol.* 201, 1069–1084. doi:10.1083/jcb.201210152.
- Wood, W., Faria, C., and Jacinto, A. (2006). Distinct mechanisms regulate hemocyte

- chemotaxis during development and wound healing in *Drosophila melanogaster*. *J. Cell Biol.* 173, 405–416. doi:10.1083/jcb.200508161.
- Wood, W., and Jacinto, A. (2007). *Drosophila melanogaster* embryonic haemocytes: masters of multitasking. *Nat. Rev. Mol. Cell Biol.* 8, 542–551. doi:10.1038/nrm2202.
- Wu, D. (2005). Signaling mechanisms for regulation of chemotaxis. *Cell Res.* 15, 52–56. doi:10.1038/sj.cr.7290265.
- Xu, H., Lu, C., Berendt, R., Jha, N., and Mandal, M. (2017). Automatic Nuclei Detection Based on Generalized Laplacian of Gaussian Filters. *IEEE J. Biomed. Heal. Informatics* 21, 826–837. doi:10.1109/JBHI.2016.2544245.
- Xu, J., Wang, T., Wu, Y., Jin, W., and Wen, Z. (2016). Microglia Colonization of Developing Zebrafish Midbrain Is Promoted by Apoptotic Neuron and Lysophosphatidylcholine. *Dev. Cell* 38, 214–222. doi:10.1016/j.devcel.2016.06.018.
- Xue, Q., Yan, Y., Zhang, R., and Xiong, H. (2018). Regulation of iNOS on immune cells and its role in diseases. *Int. J. Mol. Sci.* 19. doi:10.3390/ijms19123805.
- Yamaguchi, H., Maruyama, T., Urade, Y., and Nagata, S. (2014). Immunosuppression via adenosine receptor activation by adenosine monophosphate released from apoptotic cells. *Elife* 2014, 1–15. doi:10.7554/eLife.02172.
- Yamamoto, T. (2007). Roles of the ribosomal protein S19 dimer and the C5a receptor in pathophysiological functions of phagocytic leukocytes. *Pathol. Int.* 57, 1–11. doi:10.1111/j.1440-1827.2007.02049.x.
- Yang, L. V., Radu, C. G., Wang, L., Riedinger, M., and Witte, O. N. (2005). Gi-independent macrophage chemotaxis to lysophosphatidylcholine via the immunoregulatory GPCR G2A. *Blood* 105, 1127–1134. doi:10.1182/blood-2004-05-1916.
- Yarden, Y., and Shilo, B. Z. (2007). SnapShot: EGFR Signaling Pathway. *Cell* 131, 11–12. doi:10.1016/j.cell.2007.11.013.
- Yegutkin, G. G. (2008). Nucleotide- and nucleoside-converting ectoenzymes: Important modulators of purinergic signalling cascade. *Biochim. Biophys. Acta - Mol. Cell Res.* 1783, 673–694. doi:10.1016/j.bbamcr.2008.01.024.
- Yogev, S., Schejter, E. D., and Shilo, B. Z. (2008). *Drosophila* EGFR signalling is modulated by differential compartmentalization of Rhomboid intramembrane proteases. *EMBO J.* 27, 1219–1230. doi:10.1038/emboj.2008.58.
- Yona, S., Kim, K. W., Wolf, Y., Mildner, A., Varol, D., Breker, M., et al. (2013). Fate Mapping

- Reveals Origins and Dynamics of Monocytes and Tissue Macrophages under Homeostasis. *Immunity* 38, 79–91. doi:10.1016/j.immuni.2012.12.001.
- Yoo, S. J., Huh, J. R., Muro, I. R., Yu, H., Wang, L., Wang, S. L., et al. (2002). Hid, Rpr and Grim negatively regulate DIAP1 levels through distinct mechanisms. *Nat. Cell Biol.* 4, 416–424. doi:10.1038/ncb793.
- Yoo, S. K., Starnes, T. W., Deng, Q., and Huttenlocher, A. (2011). Lyn is a redox sensor that mediates leukocyte wound attraction in vivo. *Nature* 480, 109–112. doi:10.1038/nature10632.
- Yue, J., and López, J. M. (2020). Understanding MAPK signaling pathways in apoptosis. *Int. J. Mol. Sci.* 21. doi:10.3390/ijms21072346.
- Zanet, J., Stramer, B., Millard, T., Martin, P., Payre, F., and Plaza, S. (2009). Fascin is required for blood cell migration during Drosophila embryogenesis. *Development* 136, 2557–2565. doi:10.1242/dev.036517.
- Zengel, P., Nguyen-Hoang, A., Schildhammer, C., Zantl, R., Kahl, V., and Horn, E. (2011). μ -Slide Chemotaxis: A new chamber for long-term chemotaxis studies. *BMC Cell Biol.* 12. doi:10.1186/1471-2121-12-21.
- Zettervall, C. J. C.-J., Anderl, I., Williams, M. J., Palmer, R., Kurucz, E., Ando, I., et al. (2004). A directed screen for genes involved in Drosophila blood cell activation. *Proc. Natl. Acad. Sci. U. S. A.* 101, 14192–14197. doi:10.1073/pnas.0403789101.
- Zhang, F. R., and Schwarz, M. A. (2002). Pro-EMAP II is not primarily cleaved by caspase-3 and -7. *Am. J. Physiol. Cell. Mol. Physiol.* 282, L1239–L1244. doi:10.1152/ajplung.00141.2001.
- Zhou, L., Hashimi, H., Schwartz, L. M., and Nambu, J. R. (1995). Programmed cell death in the Drosophila central nervous system midline. *Curr. Biol.* 5, 784–790. doi:10.1016/S0960-9822(95)00155-2.
- Zhu, J., Zhou, Z., Liu, Y., and Zheng, J. (2009). Fractalkine and CX3CR1 are involved in the migration of intravenously grafted human bone marrow stromal cells toward ischemic brain lesion in rats. *Brain Res.* 1287, 173–183. doi:10.1016/j.brainres.2009.06.068.
- Zimmermann, H. (2000). Extracellular metabolism of ATP and other nucleotides. *Naunyn. Schmiedeberg's Arch. Pharmacol.* 362, 299–309. doi:10.1007/s002100000309.
- Zimmermann, H., Zebisch, M., and Sträter, N. (2012). Cellular function and molecular structure of ecto-nucleotidases. *Purinergic Signal.* 8, 437–502. doi:10.1007/s11302-012-

9309-4.

Zizzo, G., Hilliard, B. A., Monestier, M., and Cohen, P. L. (2012). Efficient Clearance of Early Apoptotic Cells by Human Macrophages Requires M2c Polarization and MerTK Induction. *J. Immunol.* 189, 3508–3520. doi:10.4049/jimmunol.1200662.

Zlobovskaya, O. A., Sergeeva, T. F., Shirmanova, M. V., Dudenkova, V. V., Sharonov, G. V., Zagaynova, E. V., et al. (2016). Genetically encoded far-red fluorescent sensors for caspase-3 activity. *Biotechniques* 60, 62–68. doi:10.2144/000114377.